MAGNETOTELLURIC INVESTIGATIONS OF THE TAMAR LINEAMENT

by

Memet Rachmat Hermanto
B.E. (Academy of Geology and Mines, Indonesia),
M.Sc. (University of Tasmania, Australia)

Submitted in fulfilment of the requirements
for the degree of
Doctor of Philosophy

University of Tasmania
Hobart, Australia
December, 1992

To my wife Tiny, and sons Adi, Aussie, Ricky
and my parents.

STATEMENT

This thesis contains the result of research carried out in the Geology Department, University of Tasmania from mid 1987 to the end of 1992. It contains no material which has been accepted for the award of any other degree or diploma in any University and, to the best of my knowledge and belief, contains no copy or paraphrase of material previously published or written by another person, except where due reference is made.

Memet Rachmat Hermanto,
University of Tasmania, Hobart, Australia.
December, 1992.

ACKNOWLEDGEMENTS

First, I record with gratitude the assistance and cooperation received from many people during the course of this research. My supervisors Drs. R.J.G. Lewis, W.D. Parkinson and D.E. Leaman are especially thanked for their advice, support, encouragement, wide-ranging assistance in all stages of the work and proof reading of this manuscript.

I wish to thank Mr. V. Jensen for the time he spent in checking and calibrating the recording unit and also developing the new data logger system. His constant willingness to help is very much appreciated.

I also acknowledge the help given by Michael Roach for writing a plotting program and plotting a residual Bouguer anomaly map. Without his help and kind assistance it would have been impossible for me to have such colourful plotting results. I am grateful to Mr. M. Bendall who allowed me to use his magnetics map and to Liddington Technology Pty. Ltd.who provided TEM software for interpretation.

I am very much indebted to the Eldridge family who, as my host family, not only offered hospitality but also looked after me and my family and gave great companionship, moral support and of course those delightful meals at their house. To Margaret Eldridge, especially, I owe my deep appreciation for her kind willingness, generous and unstinting help in proof reading of this thesis.

During the course of this research, interesting and formative discussions with a number of people have made a great contribution to the ideas and direction of the work. Some of those ideas were about field techniques, data acquisition, methods of interpretation and geological setting. Such discussions, for example, were held with Dr. J. Bishop, Dr. F.E.M. Lilley, Dr. A.J. Crawford, Mr. R. Kellet and Mr. U. Hartono.

I would like also to thank my friends S. Dwipa and S.Palgunadi and some other Indonesian colleagues for their company and great assistance in setting up the magnetometer and recording unit at some of the magnetotelluric sites. Third year geophysics student's invaluable help in DC-resistivity field work is also acknowledged. To all those farmers who kindly let me use their property for such long periods of time for recording magnetotelluric and DC-resistivity data, my grateful appreciation.

The help and assistance of Mr. P. Cornish and Mr. A. Gillon in arranging transport for field work and laboratory work are appreciated. Thanks also to all staff and postgraduate students in the Geology Department, University of Tasmania for their encouraging friendship throughout the years.

I am most grateful to my wife, Tiny, for the care and patience she showed in accompanying me and looking after the family. Her moral support and encouragement through difficult times over the past years is sincerely appreciated. My gratitude also goes to my parents and my parents-in-law for their endless prayers and moral support.

Finally, I wish to acknowledge the permission of the former and current director of the Directorate of Mineral Resources, Directorate General of Geology and Mineral Resources, and the Project Implementation Office, Department of Mines and Energy, Indonesia, to allow me to pursue a higher degree (Ph.D.) at the Geology Department, University of Tasmania. During the course of this thesis I was supported by an Indonesian Government Scholarship through the Asian Development Bank (ADB) funds ADB-LN NR. 641 INO and an Australian International Development Assistance Bureau (AIDAB) scholarship. I also received the E.M. Taylor Postgraduate Research Award in 1989.

ABSTRACT

Magnetotelluric experiments were carried out in the Tamar Lineament area of northern and central Tasmania to study subsurface electrical structure. These experiments have defined a high conductivity anomaly in the upper-middle crustal depth range and confirmed the presence of the anomaly suggested by previous authors (Buyung, 1980; Sayers, 1984; Hermanto, 1985; Parkinson, 1988).

Other geophysical techniques such as dc-resistivity, SIROTEM and two-dimensional gravity and magnetic modelling were also used. Results from these studies and other geophysical studies such as the seismic studies of Richardson (1985) and Vitesnik (1984) make a significant contribution to a better understanding of the shallow structure, nature, tectonic history and, most importantly, the setting of the conductivity anomaly.

The measured apparent resistivities are interpreted in terms of inhomogeneous electrical structure using one- and two-dimensional modelling indicating that the top of the high conductivity anomaly is located about 500 to 700 metres from the surface. This is about the level of the basal Permian cover unconformity. The resisitivity of the anomaly ranges from 1 to 8 Ohm.m with a thickness of 13.3 to 16.3 kilometres. The shape and position of the anomaly which tapers with depth is consistent with the results suggested by the current density and two-dimensional gravity and magnetic modelling. The gravity and magnetic data indicate large fault or thrust bounded blocks of Lower Palaeozoic and Upper Precambrian rocks underlie the Permian cover. The gravity and magnetic models also show that the more magnetic Cambrian volcanic sequences, may account for the upper part (at least 5 kilometres) of the anomaly. The deeper part of the conductive structure underlies the more magnetic part of the Cambrian volcanics. This suggests that the formation of the volcanic piles may be associated with high conductivities deeper in the crust. It seems likely that the boundaries of the conductive block are marked by tectonic slices of ultramafics. The conductive anomaly does not extend west beyond the Tiers Fault which marks a fundamental structural limit affecting rocks from Cambrian to Tertiary in age. This zone is marked by a strong gravity gradient which extends SSE from Devonport to Sorell across central Tasmania. No such feature occurs along the line of the Tamar River or the Tamar Lineament of previous authors.

The most likely cause of the high conductivity anomaly is a combination of the presence of high conducting fluids and graphite in pores, cracks, and or fractured rocks which provide a continuous conducting path. Geological and geophysical evidence showing a considerable tectonic history in this region support abnormal porosity and extensive fracturing of the deep crust providing an environment for deep fluid circulation and graphite precipitation. Black shales and sheared carbonates are to be expected in the Precambrian rocks implied to be present. The velocity-resistivity relation suggests that a resistivity as low as 2 Ohm.m may be obtained from the Tasmanian crust where the velocity is about 5.8 to 6.0 km s^{-1}. This is comparable with the resistivity associated with the high conductivity anomaly.

ERRATA

Magnetotelluric Investigations of the Tamar Lineament

by

Memet Rachmat Hermanto

Geology Department University of Tasmania, Australia

SITE	WRITTEN AS	CORRECTED
Page iii line 5-6	.... Parkinson, 1988).	.... Parkinson et al., 1988).
Page 2 line 7	Therefore, by measuring	Therefore, in principle by measuring ..
Page 2 line 15-16	.... Cagniard's theory was based on the assumption that the incident electromagnetic fields are uniform over any horizon tal plane.	The Tikhonov's and Cagniard's theory was based not only on the assumption that the incident electromagnetic fields may be approximated by the plane wave, but also on the assumption, that in the visinity of each site the fields change slowly in horizontal direction. Dmitriev and Berdichevsky (1979), recently, stated that the latter restriction might be weakened so as one-dimensional interpretation remains valid even if the electromagnetic fields change linearly in the horizontal plane.
Page 2 line 20	Madden and Nelson (1989)	Madden and Nelson (1964) ....
Page 8	Figure 1.6 .... (redrawn from Dr. F.E.M. Lilley, personal communication, 1992)	Figure 1.6 .... (redrawn from Barton et al., 1992)
Page 9 line 10-11	.... MT, DC resistivity, SIROTEM and 2D gravity and magnetic modelling was proposed. ...	.... MT, DC resistivity and SIROTEM was used. In addition 2D gravity and magnetic modelling was also proposed. ...
Page 13 line 6	and individual H components ...	and equation (2.1.1) can also be transformed into individual H components ..
Page 15 line 8	Zxy = - Zyx	Z'xy = -Z'yx
Page 15 line 19-22	.. The diagonal and off diagonal elements have the form : Zxx + Zyy = constant Zxy - Zyx = constant	.. The expression (Zxx + Zyy) and (Zxy - Zyx) are rotationally invariant. More over this is a property of the tensor (2 x 2) and, consequently is valid not only in 3D case.
Page 27 line 15	Data was then ...	Data were then ...
Page 37 line 24	Scalar or Cagniard and tensor apparent resistivities. ...	Cagniard and tensor apparent resistivities. ...
Page 38 line 13	The elements of tensors apparent resistivities. ...	The tensors apparent resistivities. ...
Page 40 line 13	... same direction for all frequencies.	... same direction for all frequencies. Jones (1986), on the other hand, indicates that at sufficiently high frequencies the real induction arrow may point

		away from zones of high internal conductivitiy.
Page 41 line 8 - 9	.... stations NI, CR, BW, ...	.... stations NI, CR, BC, ...
Page 44 line 20	10 | Valley Field | FF	10 | Valley Field | VF
Page 44 line 23-24	.... three other geophysical techniques were used here.These techniques were DC resistivity, SIROTEM, and gravity and magnetic modelling. ...	.... two other geophysical techniques such as DC resistivity and SIROTEM and gravity and magnetic modelling were used here. ...
Page 45 line 3	.... the E and E predicted ...	.... the Ex and Ey predicted ...
Page 50 line 9	A Shlumberger ...	A Schlumberger ...
Page 68	Figure 5.14 Shlumberger ...	Figure 5.14 Schlumberger ...
Page 88 line 8	.... decending ...	.... descending ...
Page 92 line 33	.... respectively (see Figure 5.29). ...	.... respectively. ...
Page 115	Figure 6.12 Bathimetric contour arround Tasmania and southern part of mainland of Australia.	Figure 6.12 Bathimetric contour arround Tasmania and southern part of mainland of Australia (redrawn from Dosso et al., 1985).
Page 123 line 3	Bennet and Lilley (1973). ...	Bennett and Lilley (1973). ...
Page 130 line 18	Bennet and Lilley (1973). ...	Bennett and Lilley (1973). ...
Page 130 line 20-22	Berdichevsky, M.N., and Dmitriev, V.I., 1976.	Barton, C.E., Chamalaun, F.H., and McKnight, J.D., 1992. Spatial and Diurnal variations of the Geomagnetic Field In: BMR 91 year book of the Bureau of Mineral resources, Geology and Geophysics, 1 July 1990, 30 June 1991, 114-115. Berdichevsky, M.N., and Dmitriev, V.I. ,1976. ....
Page 132 line 4	Duba, A., and Shankland, T.J., 1982. ...	Dmitriev, V.I., and Berdichevsky, M.N., 1979. The fundamental model of magnetotelluric sounding. Proc. of the IEEE, 67, 7, 1034-1044. Dosso, H.W., Nienaber, W., and Parkinson, W.D., 1985. An analogue model study of electromagnetic induction in the Tasmania region. Phys. of the Earth Plan. Int., 39, 118-133. Duba, A., and Shankland, T.J., 1982. ...
Page 132 line 22	Gough, D.I., McElhinney, M.N., and Thompson, B.R., 1974. ...	Gough, D.I., McElhinney, M.N., and Lilley, F.E.M., 1974. ...
Page 133 line 34	Jones, A.G., 1988. Static shift	Jones, A.G., 1986. Parkinson's pointers' potential perfidy. Geophys. J.R. Astr. Soc., 87, 1215-1224. Jones, A.G., 1988. Static shift ....
Page 135 line 29	Madden, T.R., and Nelson, P., 1989. ...	Madden, T.R., and Nelson, P., 1964. ...
Page 138 line 26	.... magnetotelluric using ...	.... magnetotellurics using ...

THESIS CONTENTS

LIST OF FIGURES

LIST OF TABLES

CHAPTER 1: INTRODUCTION

1.1 PREFACE

The magnetotelluric method is a geophysical technique which provides information about the deep electrical conductivity distribution within the earth beneath the site of the surface field measurements. This method responds to one of the basic physical properties of rocks and minerals - conductivity, which in most rocks, is determined by the path of ionic conduction (e.g. porosity, pore fluid salinity) or by paths of electronic conduction (e.g. carbon on grain boundaries and metallic minerals), or, in extreme cases, by high temperature or partial melting.

The method makes use of the temporal variations of the natural electromagnetic fields which originate outside the earth.These oscillating fields contain a wide spectrum of frequencies. The electromagnetic variations which are most suitable as a source field are those that are associated with magnetic storms or substorms.The current system that generates these variations is concentrated in the auroral zone and flows either through the temperate region ionosphere, or the magnetosphere (Parkinson, 1983). Electric fields produced by such variations cause eddy currents to flow in the earth.

The magnetotelluric method depends on penetration of the electromagnetic field into the earth's surface. Depth estimates depend on frequency since lower frequency waves penetrate deeper into the earth. It is this behaviour which enables geophysicists to determine structure at various depths. A useful estimate of the effective depth of penetration of the electromagnetic field into the earth, which depends on the period of the oscillations and conductivity distribution within the earth, is given by skin depth. In a uniform conducting earth the depth at which the amplitude of the electromagnetic field has decayed to 1/e of its surface value is called the skin depth (δ) (Vozoff, 1972) which is expressed as:

$$\delta = \sqrt{\frac{2}{\omega\mu\sigma}} \qquad \ldots\ldots\ldots\ldots\ldots\ldots \quad (2.1.1)$$

A convenient expression for the skin depth formula may be written as

$$\delta = 503\sqrt{\rho T} \quad \text{metre} \qquad \ldots\ldots\ldots\ldots\ldots\ldots \quad (2.1.2)$$

where T = period (seconds), $\omega = \frac{2\pi}{T}$, σ = conductivity (Siemens/m), ρ = resistivity (Ohm.m) = $\frac{1}{\sigma}$ and μ = permeabilty (Henry/m). Except for highly magnetic materials, the permeabilty of the conductor μ for most geological situations is considered equivalent to the permeabilty of free space μ_o.

In a magnetotelluric survey the two tangential (horizontal) components of both the magnetic and electric field variations are measured as functions of time. Therefore, by measuring both magnetic and electric fields over a wide range of periods, electrical conductivity structure as a function of depth within the earth can be determined.

The magnetotelluric technique as first used by Tikhonov (1950) in the USSR and Kato and Kikuchi (1950) in Japan showed that the electrical conductivity structure of the subsurface could be deduced from the measurement of a rapid fluctuation in the electric and magnetic fields at the surface of the earth. Cagniard's (1953) classic article provided a complete theory, interpretation and application of the technique. Cagniard's theory was based on the assumption that the incident electromagnetic fields are uniform over any horizontal plane. Wait (1954), Price (1962), Wait (1962) and Quon (1963), however, have questioned the validity of this assumption. They pointed out that errors would occur if the source fields were not plane waves.

Madden and Nelson (1989), on the other hand, defended Cagniard's assumption by showing numerically that the plane wave assumption is valid in the frequency range used by magnetotellurics. Vozoff (1972) also stated that, as a working theory, the signal can be treated as a plane electromagnetic wave. A similar assumption is also used in this study. Although the assumption is not true under all conditions, it holds for most situations (Madden and Nelson, 1964; Rikitake, 1966; Vozoff and Ellis, 1966). The validity of the plane wave model was also discussed in detail by Kauffman and Keller (1981).

1.2 PREVIOUS MT AND MV STUDIES

In the last three decades the underground conductivity distribution in Tasmania has been studied by a few researchers using magnetotelluric (MT) and magnetovariational (MV) techniques. Parkinson (1962) and Lewis (1965) were the pioneers in using the MV and MT techniques to study the ocean effect and the crustal structure in the Hobart area. Asten (1972) applied the MT technique in the Longford area.

Interesting and anomalous results in northern Tasmania were first noticed by Lilley (1976) from a magnetometer array across southern Victoria and Bass Strait area. He showed a reversal in the direction of the induction arrows from Devonport and Bridport (see Figure 1.1) which may be due to the presence of a high conductivity anomaly in the vicinity of the Tamar River. This discovery initiated intensive MT and MV studies in this part of Tasmania. Buyung (1980) who carried out further MV investigations south of Launceston found that the high conductivity anomaly continued beneath the Tamar River (see Figure 1.1).

Further investigation using single site MV techniques was carried out by Hermanto (1985) who confirmed the conductor near the Tamar River and suggested a continuation to the south-east (see Figure 1.2). Other induction arrow results from this investigation are given in Appendix 1. This conductivity zone has a width of approximately 40 km in the north and gradually decreases in width to the south-east. This conductor which is confined to a zone coinciding with the so called Tamar Lineament (see section 1.3) is now known as the Tamar Conductivity Anomaly (Parkinson et al., 1988; Parkinson and Hermanto,1990).

The use of MV techniques has provided a clear indication of lateral conductivity distribution across the study area. This method, however, gives less information concerning conductivity as a function of depth. MT techniques, which are used to investigate conductivity as a function of depth, were later carried out over a structure previously determined by MV studies. Seven MT stations, two in the north-east of Tasmania (Hollybank and Scottsdale), one at Epping Forest (Vaucluse) and four at Fingal Valley were established by Bindoff (1983), Sayers (1984) and Richardson (1985), respectively (see Figure 1.3). Lack of good high frequency data from Hollybank and Scottsdale hampered depth determination and limited accurate measurement of other layers (Bindoff, 1983). Instrumental problems and poor high frequency data from measurements at Fingal Valley caused uncertainty in the data interpretation of Richardson (1985). Only the MT measurements at Vaucluse gave a reasonable depth determination of the conductor. This MT analysis showed that the conductor extends from a depth of 2-3 km to perhaps 10 km with a conductivity of 0.2-1 Sm^{-1} (Sayers, 1984; Parkinson et al., 1988; Parkinson and Richardson, 1989).

Conductivity distributions in other parts of Tasmania have also been mapped recently by Archer (1989) and Dwipa (1992). Archer (1989) was the first to use both MT and MV techniques to study structural elements in the Tullah area, western Tasmania. Similar techniques were then also applied in southeastern Tasmania (Dwipa, 1992). Figure 1.3 Shows distribution of all sites of the above MT and MV studies in Tasmania.

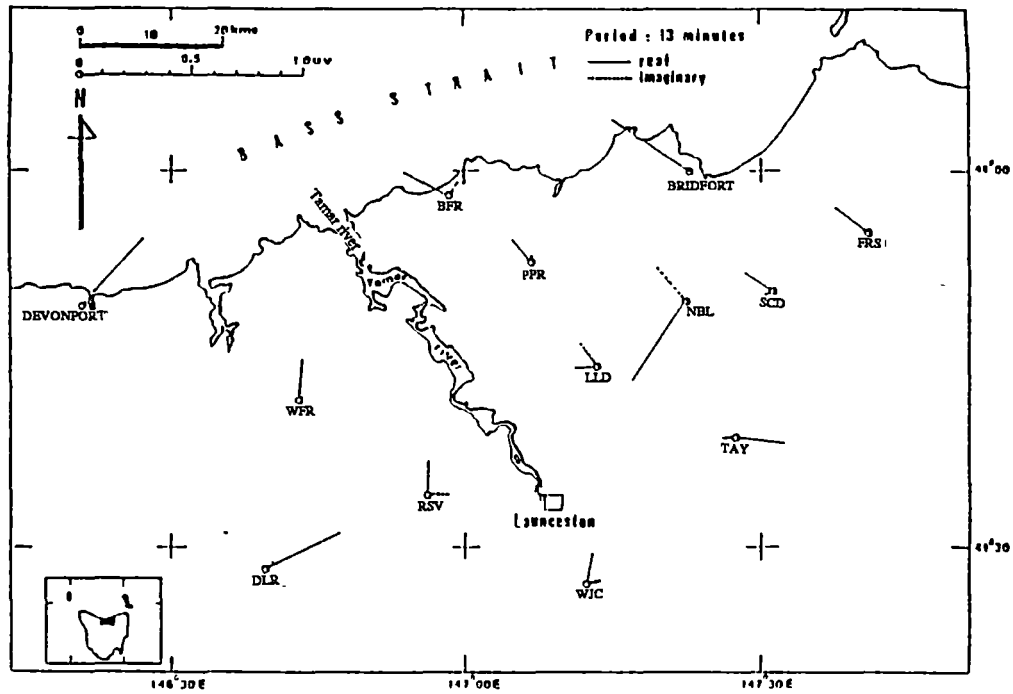

Figure 1.1 Distribution of MV sites of Lilley (1976) and Buyung (1980) in the vicinity of the Tamar River, northern Tasmania, with their induction arrows at periods of 13 minutes (after Buyung, 1980).

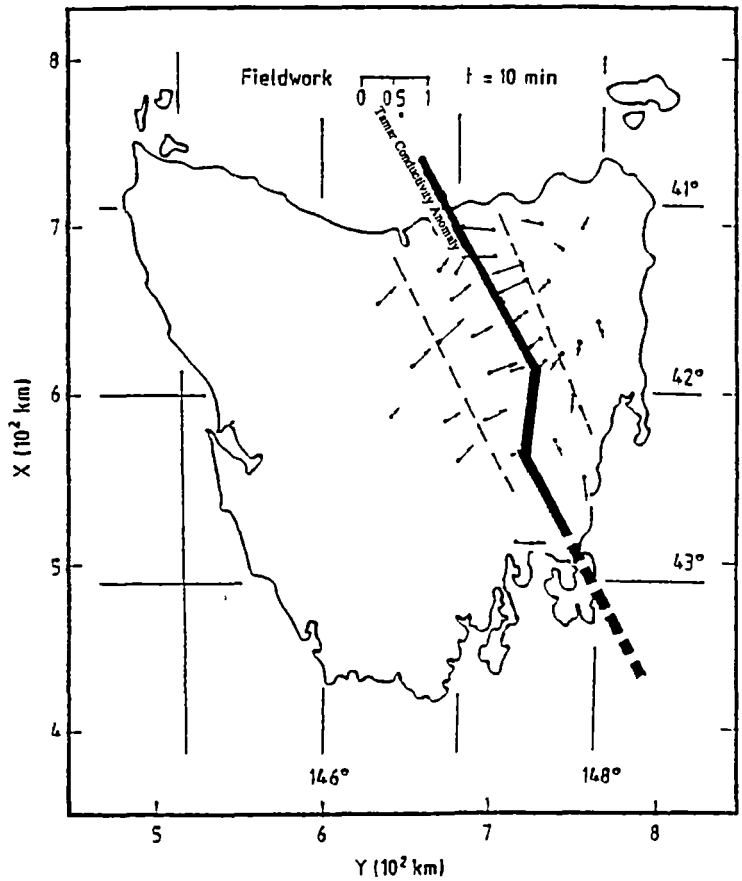

Figure 1.2 Real part induction arrows at periods of 10 minutes showing approximate centre and boundary of the Tamar Conductivity Anomaly (in thick solid and broken line, and two thin broken lines, respectively). Redrawn from Parkinson and Hermance (1986).

1.3 GEOLOGICAL AND GEOPHYSICAL FRAMEWORKS

Tasmania may be divided into two distinct terranes, namely the eastern and western Tasmania terranes of Banks and Baillie (1989). The boundary has been known for some time as the Tamar Lineament or Tamar Fracture System (Williams, 1979) (see Figure 1.4). The eastern terrane differs considerably from that of the western terrane (Corbett and Turner, 1989, Banks, 1989 and Williams, 1989). The eastern terrane consists mainly of thick folded Mathinna beds of Siluro-Devonian age consisting of interbedded turbidite, quartzwacke and mudstone, typical of a deep water facies. The western terrane, on the other hand, is mainly covered by Precambrian and Cambrian rocks. These rocks can be found starting from Beaconsfield in northern Tasmania. They extend westward and consist of dominantly quartzite-phyllite Precambrian sequences followed by largely volcanic Cambrian sequences and carbonate-dominated Ordovician section with some basal conglomerates and sandstones.

In contrast to the eastern terrane, sedimentary rocks of Siluro-Devonian age found in the western terrane (i.e. the Eldon Groups) consist of quartz sandstone and siltstone, typical of shallow marine environments (Williams, 1979). The granitic rocks found in the eastern terrane also differ slightly from those found in the western terrane. In the eastern terrane the granitic rocks are slightly older than those determined for the western province plutons (McDougall and Legge, 1965; Williams et al. 1989).

Williams (1989) postulates that the abrupt change in sedimentary rock types and structural characteristics together with different granitoid intrusion ages indicate that the Tamar river is the site of a dislocation along which possibly sinistral lateral movement brought the contrasting regions into juxtaposition. Results from seismic and gravity measurements have been interpreted to suggest that the Tamar structure, which is buried by the Permian and younger rocks, extends through the crust (Richardson, 1981). Williams (1979) also suggested that based on distribution of the contrasting rock-types both in outcrop and drill holes (e.g. Clarke and Farmer, 1983; Gulline and Clarke, 1984) the inferred Tamar Fracture System followed a line along the Tamar river continues in the direction of the Tasman Peninsula (see Figure 1.4).

Leaman et al. (1973), Leaman (1989) and Richardson (1989) also state that the Tamar Lineament follows the Tamar but may trend more north-south through the Midlands and pass into Storm Bay near Cape Raoul. This lineament concept agrees very well with the approximate strike of the conductivity anomaly known as the Tamar Conductivity anomaly (Parkinson et al., 1988) determined by Bindoff (1983), Sayers (1984) and Hermanto (1985).

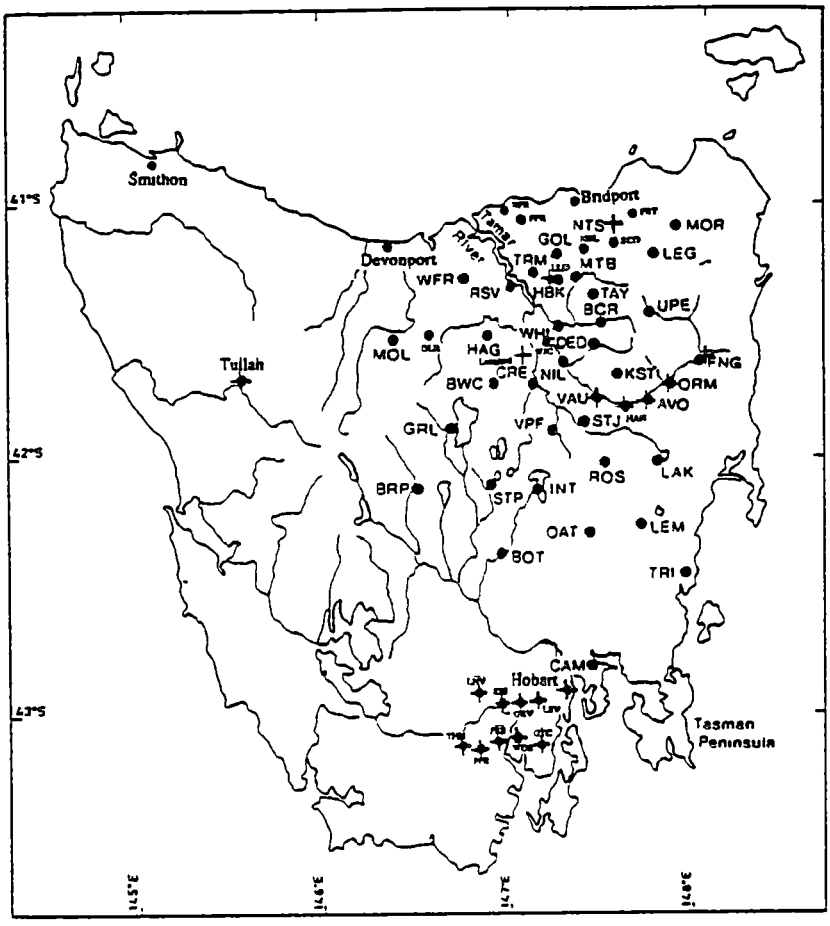

Figure 1.3 Site distribution of the MT and MV studies in Tasmania
(+) MT sites, (•) MV sites, (✚) MT and MV sites

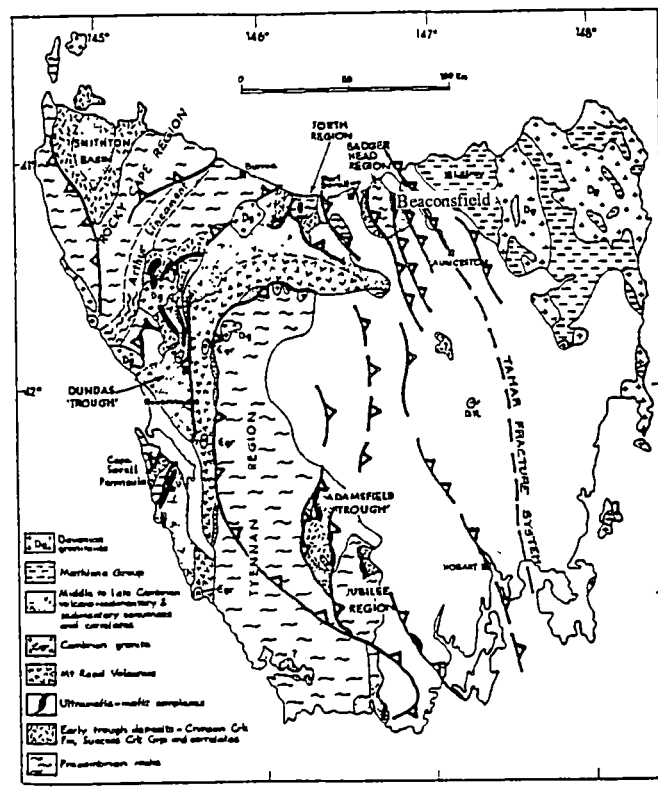

Figure 1.4 Simplified geological map of Tasmania showing tectonic elements. After Powell (1992).

Geophysically, the eastern terrane differs little from the western terrane (Wellman, 1989). This overall view contrasts with the concepts described above.

The Tasman Line (Harrington, 1974) (see Figure 1.5) extends from Cape York ridge in northern Queensland, through the Flinders Ranges, then via a transform fault (the Gambier-Beaconsfield Fracture) to Bass Strait, then to Tamania where Parkinson and Hermanto (1990) and Parkinson et al. (1988) assumed that the Tamar Fracture System may be a part of the Tasman Line. In Tasmania the Tasman Line was thought to represent the western edge of a Precambrian or Cambrian rift system, that included several large transform faults, one of which coincides with the Gambier-Beaconsfield Fracture Zone. Parkinson et al. (1988) also suggest that the Tamar Conductivity anomaly is not the only anomaly associated with the Tasman Line. The Otway anomaly (Bennet and Lilley, 1974), the Flinders Ranges anomaly (Gough et al., 1974) and the S-W Queensland anomaly (Woods and Lilley, 1979) are all spatially related to the Tasman Line (see Figure 1.6).

Based on an expanded data base and a new gravity and magnetic interpretation, Leaman (1992) strongly argues against the idea of the Tamar Fracture System as did Wellman (1989). He suggests that the difference between the eastern and western terranes is likely to be related to a major west directed thrust front and not to a crustal fracture zone. He also comments that there is no evidence for a gross crustal suture or terrane change in the Tamar region and this concept is not supported by any crustal data set. The major gravity gradient present extends SSE from Devonport, not from the Tamar, and this means that western Tasmania terrane rocks occur in the eastern terrane. The Tamar Conductivity Anomaly is bounded at its western side by this gradient and appears to correspond to the overthrust front zone.

Despite its geological and geophysical significance the nature and structure of the Tamar lineament cannot be directly assessed from the surface geology as it is overlain by dolerite and a relatively thick sequence of sediments.

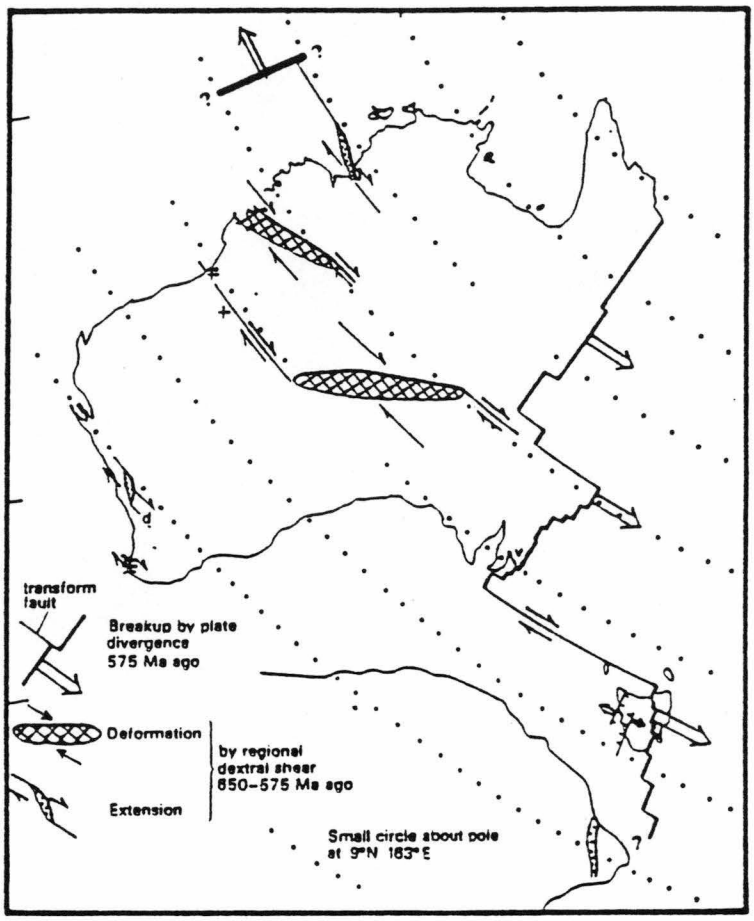

Figure 1.5 Interpretation of Epi-Adelaiden and breakup events about 650 to 575 Ma. ago related to dextral shear and then plate divergence about pole of rotation at 9° N, 163° E. After Veevers and Powell (1984).

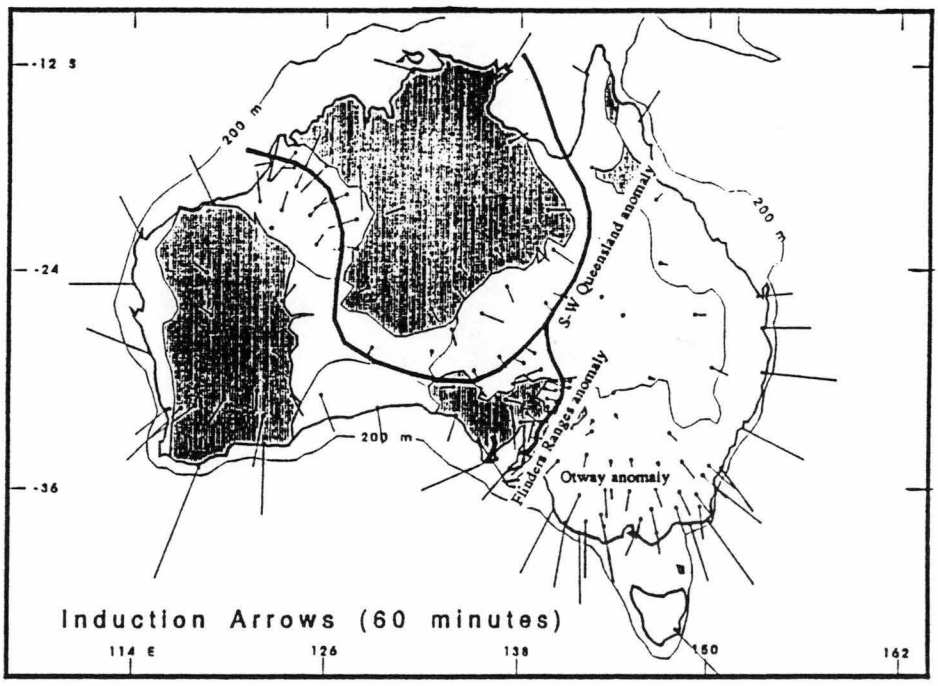

Figure 1.6 Real part induction arrows in Australia for periods of 60 minutes (redrawn from Dr. F.E.M. Lilley, personal communication, 1992).

1.4 AIMS OF THE STUDY

Previous authors have suggested that the most likely explanation of the Tamar Conductivity Anomaly is a fractured rock saturated with conducting pore fluids (Sayers, 1984; Hermanto, 1985; Parkinson and Hermanto, 1986; Parkinson et al., 1988). This explanation, however, has not resolved the nature of the source of the high conductivities or the geophysical signature of the anomaly. The main aim of the present study was, therefore, to acquire a much better understanding of the Tamar Conductivity Anomaly by determining the depth to the top and bottom of the conductor, the resistivity of the conductor and the materials responsible for the high conductivity anomaly. A combined geophysical investigation using available techniques such as MT, DC Resistivity, SIROTEM and 2D gravity and magnetic modelling was proposed. These techniques should provide detailed information on general structures over the study area and also provide much better depth control than exists at present.

1.5 SUMMARY

This thesis describes relevant theoretical considerations, data acquisition technique, analysis and a comprehensive integrated interpretation.

CHAPTER 2 : MAGNETOTELLURIC THEORY

2.1 BASIC MAGNETOTELLURIC THEORY

The basic magnetotelluric theory is derived by solving Maxwell's equations which express the relationships of electromagnetic fields. These equations when written in a standard SI form are as follows :

$$\nabla \times \vec{E} = -\frac{\partial \vec{B}}{\partial t} \qquad \text{(Faraday's law)} \qquad \ldots\ldots\ldots\ldots \quad (2.1.1)$$

$$\nabla \times \vec{H} = \vec{J} + \frac{\partial \vec{D}}{\partial t} \qquad \text{(Ampere's law)} \qquad \ldots\ldots\ldots\ldots \quad (2.1.2)$$

$$\nabla \cdot \vec{D} = q \qquad \text{(Coulomb's law)} \qquad \ldots\ldots\ldots\ldots \quad (2.1.3)$$

$$\nabla \cdot \vec{B} = 0 \qquad \ldots\ldots\ldots\ldots \quad (2.1.4)$$

Together with three other relations that concern the characteristics of the medium in which the fields exist

$$\vec{J} = \sigma \vec{E} \qquad \ldots\ldots\ldots\ldots \quad (2.1.5)$$

$$\vec{D} = \varepsilon \vec{E} \qquad \ldots\ldots\ldots\ldots \quad (2.1.6)$$

$$\vec{B} = \mu \vec{H} \qquad \ldots\ldots\ldots\ldots \quad (2.1.7)$$

where $\vec{E}$ is the electric field strength; $\vec{B}$ is the magnetic induction; $\vec{H}$ is the magnetic field strength; $\vec{D}$ is electric displacement; $\vec{J}$ is current density; q is charge density; σ is conductivity; μ is permeability and ε is permitivity.

For a homogeneous and isotropic medium and assuming a time variation of the form $e^{i\omega t}$, the first two of Maxwell's equations become

$$\nabla \times \vec{E} = -i\mu\omega \vec{H} \qquad \ldots\ldots\ldots\ldots \quad (2.1.8)$$

$$\nabla \times \vec{H} = (\sigma + i\omega\varepsilon) \vec{E} \qquad \ldots\ldots\ldots\ldots \quad (2.1.9)$$

and transform into the vector Helmholtz equations (if q = 0)

$$\nabla^2 \vec{E} = \gamma^2 \vec{E} \quad \ldots\ldots\ldots\ldots\ldots \quad (2.1.10)$$

$$\nabla^2 \vec{H} = \gamma^2 \vec{H} \quad \ldots\ldots\ldots\ldots\ldots \quad (2.1.11)$$

where $\gamma^2 = i\sigma\mu\omega - \omega^2\varepsilon\mu$, and γ is called the propagation parameter.

In rectangular cartesian coordinates these vector equations can be separated so that individual components of the $\vec{E}$ and $\vec{H}$ fields satisfy the scalar Helmholtz equations. These equations lead us to a general solution for Ex

$$E_X = E_1 e^{(\gamma_1 x + \gamma_2 y + \gamma_3 z)} + E_2 e^{-(\gamma_1 x + \gamma_2 y + \gamma_3 z)} \quad \ldots\ldots\ldots \quad (2.1.12)$$

where $E_1 = k_1 k_2 k_3$ and $E_2 = l_1 l_2 l_3$

Similar solutions can also be obtained for E_y and E_z. The equation (2.1.12) is the elementary solution to the Helmholtz equations where

$$\gamma_1^2 + \gamma_2^2 + \gamma_3^2 = \gamma^2 = i\sigma\mu\omega - \omega^2\varepsilon\mu \quad \ldots\ldots\ldots\ldots\ldots \quad (2.1.13)$$

The general solution can be obtained by summing all elementary solutions with different values of E_1, E_2, γ_1, γ_2 and γ_3 subject to constraints of equation (2.1.13).

2.2 MT RELATIONSHIPS FOR 2-D GEOMETRY

In a two dimensional structure it is normally assumed that the conductivity σ is a function of two space coordinates, the vertical or z coordinate and one horizontal, say, y coordinate. Consider the use where a vertical contact which separates the region A (conductive block) having conductivity $\sigma 1$, from the region B (resistive block) having conductivity $\sigma 2$ (see figure 2.1).

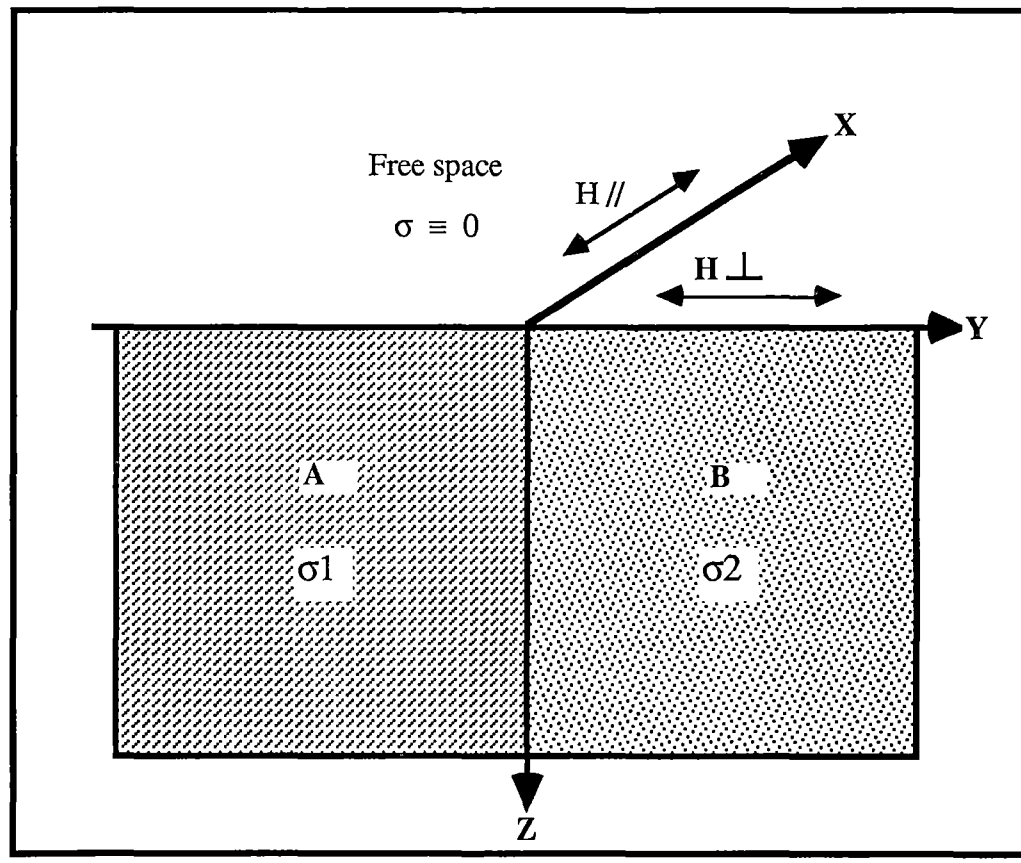

Figure 2.1 Vertical contact model and co-ordinate system

It is assumed that the conductivity $\sigma = \sigma_{(y,z)}$ and all quantities are constant along the x direction i.e. $\frac{\partial}{\partial x} = 0$. The electromagnetic fields oscillate harmonically as functions of time. It is also assumed that the oscillation of the electromagnetic field is very slow thus permitting the displacement of current $\frac{\partial D}{\partial t}$ in the right hand side of equation (2.1.2) to be ignored. Conditions under which this is valid have been specified by Price (1973). The equation (2.1.2) can now be written as :

$$\nabla \times \vec{H} = \sigma_{(y,z)} \vec{E} \qquad \ldots\ldots\ldots\ldots\ldots \quad (2.2.1)$$

this can be transformed into individual $\vec{E}$ components

$$\frac{\partial H_z}{\partial y} - \frac{\partial H_y}{\partial z} = \sigma_{(y,z)} E_x \qquad \ldots\ldots\ldots\ldots\ldots \quad (2.2.2)$$

$$\frac{\partial H_x}{\partial z} = \sigma_{(y,z)} E_y \qquad \ldots\ldots\ldots\ldots\ldots \quad (2.2.3)$$

$$-\frac{\partial H_x}{\partial y} = \sigma_{(y,z)} E_z \qquad \ldots\ldots\ldots\ldots\ldots \quad (2.2.4)$$

and individual $\vec{H}$ components

$$\frac{\partial E_z}{\partial y} - \frac{\partial E_y}{\partial z} = - i\mu\omega H_x \qquad \ldots\ldots\ldots\ldots\ldots \quad (2.2.5)$$

$$\frac{\partial E_x}{\partial z} = - i\mu\omega H_y \qquad \ldots\ldots\ldots\ldots\ldots \quad (2.2.6)$$

$$-\frac{\partial E_x}{\partial y} = - i\mu\omega H_z \qquad \ldots\ldots\ldots\ldots\ldots \quad (2.2.7)$$

The first mode of equations i.e. equations (2.2.2), (2.2.6) and (2.2.7) consists of only Ex,Hy and Hz. These equations describe a condition known as E-polarization i.e. electric field parallel to the strike direction. Similarly, the second mode of equations i.e. equations (2.2.5), (2.2.3) and (2.2.4) contains only Hx, Ey and Ez. These equations describe a condition known as H-polarization i.e. magnetic field parallel to the strike direction. Thus it is clear that the two modes decouple when one of the horizontal coordinates is aligned with the strike and the modes may be considered separately. The mode involving E_x, H_y and H_z is known as the TE mode or E polarization. The other mode involving H_x, E_y and E_z is called the TM mode or H polarization. Therefore, for the two-dimensional model, two impedances which are defined by

$$Z_{TE} = \frac{E_x}{H_y}$$

$$Z_{TM} = \frac{E_y}{H_x}$$

are required to explain the relationship between the horizontal components of the $\vec{E}$ and $\vec{H}$ fields. Analytical solutions to solve these equations in terms of $\sigma_{(y,z)}$ are very difficult. Several workers, however, have used the technique to solve some problems, for example to study the effect of faults (d'Erceville and Kunetz, 1962) and the effect of a dyke (Rankin, 1962). Other solutions to solve the equations may be obtained by using numerical methods such as the finite difference technique as applied by Jones and Price (1970) and Reddy and Rankin (1973) and the transmission line analogy which was initiated by Madden (1972) and developed by Swift (1967, 1971).

2.3 IMPEDANCE TENSORS

Impedance tensors which relate the electric to the magnetic field, as formulated by Cantwell (1960), are expressed as:

$$\begin{bmatrix} E_x \\ E_y \end{bmatrix} = \begin{bmatrix} Z_{xx} & Z_{xy} \\ Z_{yx} & Z_{yy} \end{bmatrix} \begin{bmatrix} H_x \\ H_y \end{bmatrix} \quad \ldots\ldots\ldots\ldots\ldots \quad (2.3.1)$$

where E_x, E_y and H_x, H_y are electric and magnetic field components measured along two perpendicular axes and Z_{xx}, Z_{xy}, Z_{yx} and Z_{yy} are complex unrotated impedance tensor elements. All elements in equation (2.3.1) are frequency dependent. The vectors $\vec{E}$ and $\vec{H}$ are linearly related, but they are not necessarily parallel.

For a one-dimensional earth where structure varies with depth only, as in a horizontally layered earth, the diagonal and off diagonal elements have the form :

$$Z_{xx} = Z_{yy} = 0$$

and

$$Z_{xy} = -Z_{yx}$$

Therefore upon any rotation

$$Z'_{xx} = Z'_{yy} = 0$$
$$Z'_{xy} = Z_{xy}$$
$$Z'_{yx} = Z_{yx}$$

where Z'_{xx} and Z'_{yy} are rotated impedances. These equations imply that the impedance is independent of rotation (Swift, 1967).

For a two-dimensional earth, where structure is a function of two space coordinates, the impedance tensors are rotation dependent. The diagonal and off diagonal impedances are characterized by

$$Z_{xx} + Z_{yy} = 0$$

and

$$Z_{xy} \neq -Z_{yx}$$

Impedance tensors therefore can be interpreted in terms of the geological structure and they may be rotated, thus allowing the measuring axis to be aligned to a preferred direction. In a two-dimensional structure, this would be reorienting one of the axes parallel to the strike of the structure. Upon such rotation the above equations thus become

$$Z'_{xx} = Z'_{yy} = 0$$

$$Z'_{xy} \neq Z'_{yx}$$

However, if the orientation of one of the axes is not parallel to the strike of the structure, the diagonal elements do not vanish. Vozoff (1972) states that for three-dimensional earth, where structure is a function of three space coordinates, the tensor elements are well behaved. The diagonal and off diagonal elements have the form :

$$Z_{xx} + Z_{yy} = \text{constant}$$

$$Z_{xy} - Z_{yx} = \text{constant}$$

2.4 ROTATION ANGLE

The usual method of determining the rotation angle (θ) through which axes of magnetotelluric measured values must be rotated, is by calculating an angle that minimises $(Z_{xx})^2+(Z_{yy})^2$ or by the same angle that maximises $(Z_{xy})^2+(Z_{yx})^2$. Jupp and Vozoff (1989) suggest that by maximising $(Z_{xy})^2+(Z_{yx})^2$ the rotation angle (θ) can be obtained by

$$\theta = \frac{1}{4}\arctan\frac{(Z_{xx} - Z_{yy})(Z_{xy} + Z_{yx})^* + (Z_{xx} - Z_{yy})^*(Z_{xy} + Z_{yx})}{(Z_{xx} - Z_{yy})^2 - (Z_{xy} + Z_{yx})^2} \quad \text{.... (2.4.1)}$$

where * is complex conjugate, Z_{xx}, Z_{xy}, Z_{yx} and Z_{yy} are unrotated tensor impedances. In two-dimensional structures this technique will find the true principal axes.

Another method of determining the rotation angle (θ) is that using a Mohr circle introduced by Lilley (1992).

A new simple method for derivation of the rotation angle (θ) will now be introduced here. This method which was developed by Parkinson et al. (1992) consists of determining two angles each which makes one of the diagonal elements vanish.

Consider the cartesian coordinate system in Figure 2.2. When the measuring axis (X,Y) is rotated clockwise through an angle of θ degrees to a new axis (X', Y') i.e. parallel and perpendicular to the strike of the structure then for each component of the electric and magnetic fields we have

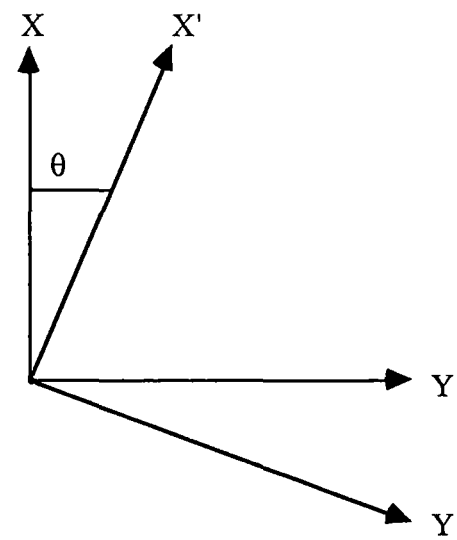

Figure 2.2 X - Y and X' - Y' coordinate system

$$E_x = E'_x \cos\theta - E'_y \sin\theta \quad \ldots\ldots\ldots\ldots \quad (2.4.2)$$

$$E_y = E'_x \sin\theta + E'_y \cos\theta \quad \ldots\ldots\ldots\ldots \quad (2.4.3)$$

$$H_x = H'_x \cos\theta - H'_y \sin\theta \quad \ldots\ldots\ldots\ldots \quad (2.4.4)$$

$$H_y = H'_x \sin\theta + H'_y \cos\theta \quad \ldots\ldots\ldots\ldots \quad (2.4.5)$$

Substituting equations (2.4.2) to (2.4.5) into similar expression for E and H as given in equations (2.3.1) leads to

$$E'_x \cos\theta - E'_y \sin\theta = Z_{xx}\left(H'_x \cos\theta - H'_y \sin\theta\right) + Z_{xy}\left(H'_x \sin\theta + H'_y \cos\theta\right) \quad \ldots\ldots\ldots\ldots \quad (2.4.6)$$

$$E'_x \sin\theta + E'_y \cos\theta = Z_{yx}\left(H'_x \cos\theta - H'_y \sin\theta\right) + Z_{yy}\left(H'_x \sin\theta + H'_y \cos\theta\right) \quad \ldots\ldots\ldots\ldots \quad (2.4.7)$$

Multiply equations (2.4.6) and (2.4.7) by cos θ and sin θ, respectively, and eliminate E'_y giving an expression for E'_x from which two tensor elements relative to rotated axes can be determined. Similarly multiplying by sin θ and cos θ and eliminating E'_x yields the other two elements. Thus :

$$Z'_{xx} = Z_{xx}\cos^2\theta + (Z_{xy} + Z_{yx})\sin\theta\cos\theta + Z_{yy}\sin^2\theta \quad \ldots\ldots (2.4.8)$$

$$Z'_{xy} = Z_{xy}\cos^2\theta + (Z_{yy} - Z_{xx})\sin\theta\cos\theta - Z_{yx}\sin^2\theta \quad \ldots\ldots (2.4.9)$$

$$Z'_{yx} = Z_{yx}\cos^2\theta + (Z_{yy} - Z_{xx})\sin\theta\cos\theta - Z_{xy}\sin^2\theta \quad \ldots\ldots (2.4.10)$$

$$Z'_{yy} = Z_{yy}\cos^2\theta - (Z_{xy} + Z_{yx})\sin\theta\cos\theta + Z_{xx}\sin^2\theta \quad \ldots\ldots (2.4.11)$$

(Swift, 1967). All variables in these equations are complex. The required rotation angle (θ) is the one that makes both Z'_{xx} and Z'_{yy} vanish. Parkinson et al. (1992) first used equations (2.4.8) to make Z'_{xx} vanish, viz:

$$Z_{xx}\cos^2\theta + (Z_{xy} + Z_{yx})\sin\theta\cos\theta + Z_{yy}\sin^2\theta = 0 \quad \ldots\ldots (2.4.12)$$

Then dividing this equation by $\cos^2\theta$ leads to a quadratic equation in tan θ with solutions

$$\tan \theta_x = \frac{\left(-S + \sqrt{S^2 - 4 Z_{xx} Z_{yy}}\right)}{2 Z_{yy}} \qquad \ldots\ldots\ldots\ldots \quad (2.4.13)$$

$$\tan \theta_x = \frac{\left(-S - \sqrt{S^2 - 4 Z_{xx} Z_{yy}}\right)}{2 Z_{yy}} \qquad \ldots\ldots\ldots\ldots \quad (2.4.14)$$

where $S = Z_{xy} + Z_{yx}$. A similar treatment to Z_{yy}' gives

$$\tan \theta_y = \frac{\left(S - \sqrt{S^2 - 4 Z_{xx} Z_{yy}}\right)}{2 Z_{xx}} \qquad \ldots\ldots\ldots\ldots \quad (2.4.15)$$

$$\tan \theta_y = \frac{\left(S + \sqrt{S^2 - 4 Z_{xx} Z_{yy}}\right)}{2 Z_{xx}} \qquad \ldots\ldots\ldots\ldots \quad (2.4.16)$$

A computer program to calculate these theta values was later developed and a test using synthetic data found that for a truly two dimensional structure tan θ becomes real. The validity of these formulae, however, depends on which root is used. Now consider equation (2.4.13). Parkinson et al. (1992) state that in the case $Z_{xx} = 0$ and $Z_{yy} \neq 0$, clearly $\theta_x = 0$ is the required solution. This is obtained when the square root is in the same quadrant as S. Similarly if $Z_{xx} \neq 0$ and $Z_{yy} = 0$ equation (2.4.15) gives $\theta_y = 0$ again, if the square root is in the same quadrant as S. All variables in these equations are complex but the physical angle through which the observed coordinates should be rotated is given by the real part of the tan θ. Average of θ_x in equation (2.4.13) and θ_y in equation (2.4.15) determines rotation angle (θ) and should rotate the observed coordinates into the direction of maximum current flow. Calculation of rotation angle (θ) using real and imaginary parts separately should be avoided as the term under the square root is not linear (Dr. W.D. Parkinson, personal communication, 1992).

Parkinson et al. (1992) also state that the other roots are not invalid. Take for example equations (2.4.13) and (2.4.16) and multiply them together then

$$\tan \theta_x \tan \theta_y = \frac{(R-S)(R+S)}{(4 Z_{xx} Z_{yy})} = -1 \qquad \ldots\ldots\ldots\ldots \quad (2.4.17)$$

where $R = \sqrt{S^2 - 4 Z_{xx} Z_{yy}}$. It can be shown here that $\theta_x - \theta_y = \frac{\pi}{2}$, thus the angles have opposite signs, so $|\theta_x|$ and $|\theta_y|$ are complementary angles. If the structure is completely two dimensional then $\theta_x = \frac{\pi}{2} + \theta_y$. This is apparent from the vanishing of $Z_{xx} + Z_{yy}$. In practice, however, this is unusual. The difference between θ_x in equation (2.4.13) and θ_y in equation (2.4.15) indicates a measure of how closely the structure approximates to two dimensions. Dr. W.D. Parkinson (personal communication, 1992) also states that rotation angle (θ) should be plotted only for

the difference between θ_x in equation (2.4.13) and θ_y in equation (2.4.15) within ± 20°. If the difference is greater than ± 20° rotation angle (θ) does not mean anything as it may not represent two-dimensionality of the structure. In other words, the closer the difference to zero degrees the better the approximation to two-dimensionality.

2.5 DIMENSIONALITY FACTOR

A skew coefficient was defined by Swift (1967) as,

$$\text{Skew} = \frac{Z_{xx} + Z_{yy}}{Z_{xy} - Z_{yx}}$$

The skew is used widely as a strong indicator of the extent to which data represents a two-dimensional model. Although there is no acceptable upper set value of skew, it is commonly agreed that values greater than 0.2 are influenced by three-dimensional structures (Kurtz, 1973). Word et al. (1970), however, state that skew may also be zero if the magnetotelluric measurements are conducted on a plane of symmetry of a three-dimensional structure. Ellipticity of the impedance ellipse defined as the ratio of the minor to major axes may also be used as a dimensionality indicator. This is given by:

$$\text{Bo} = \frac{Z_4}{Z_3}$$

where Z_4 = minor axes and Z_3 = major axes. A non zero of $|\text{Bo}|$ indicates three-dimensionality. The condition of Skew = 0 and Bo = 0 indicates a two-dimesional earth.

CHAPTER 3 :
DATA ACQUISITION

Sound data acquisition is fundamental to the success of any geophysical survey. Equipment and human factors determine data quality. It is essential that the equipment provides reliable and reproducible data.

To this end, two MT data recorders appropriately calibrated and checked, were employed during the study of the electrical conductivity structure in northern Tasmania. This eliminated undefined instrumental error which might otherwise corrupt recorded data.

3.1 INSTRUMENTATION

The MT data recorder used throughout the study consists of two main parts, namely a magnetometer and a digital data recording unit. The recording unit was designed and built by Mr. V. Jensen, a senior technical officer, at the Geology Department of the University of Tasmania. Figure 3.1 shows the block diagram of the recorder.

The magnetometer is a fluxgate EDA-FM 100B and is used to record the two orthogonal horizontal north and east components of the magnetic field. The vertical component of the magnetic field is also recorded since this component can be diagnostic of the geometry of the site. Large vertical components of the magnetic field, for example, suggest that the site is close to a lateral conductivity inhomogeneity.

The two horizontal north-south and east-west components of the electric field are measured across two nonpolarizable, Pb-$PbCl_2$, electrodes driven about 1 metre into the ground approximately 100 metres apart at a right angle to the base electrode. The voltage differences, measured between these electrodes, are fed through a fixed band pass filter, and amplified either 100 or 1000 times (see Figure 3.2). After amplification the signal is digitized by an analog-to-digital converter (ADC) and recorded on a Memodyne digital cassette recorder.

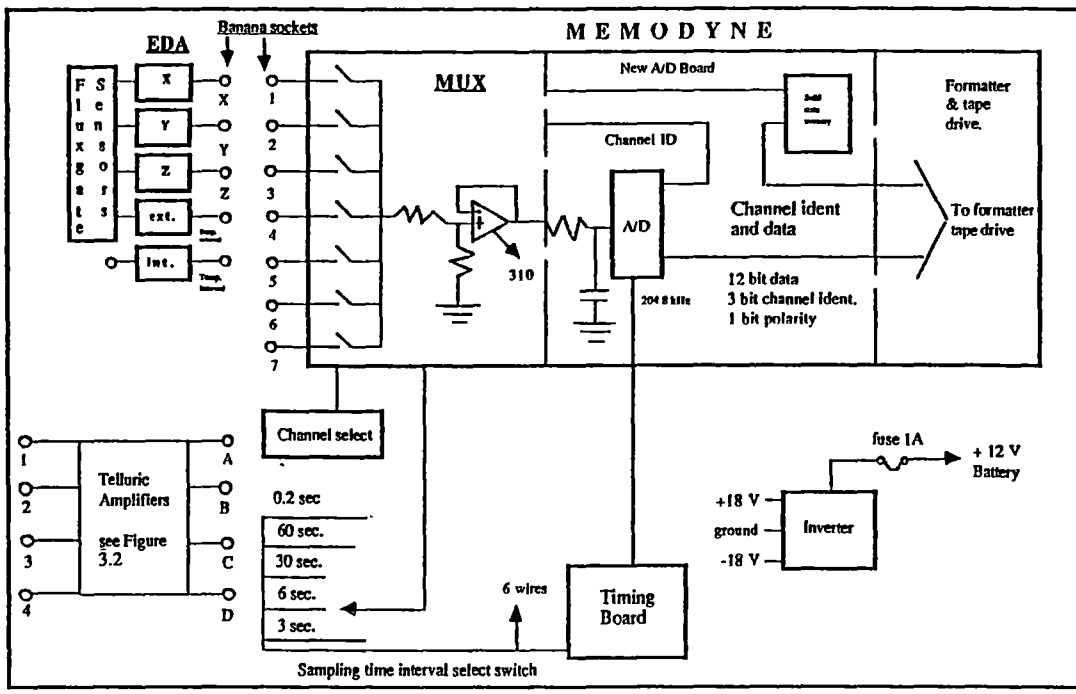

Figure 3.1 Block diagram of the EDA FM-100B Fluxgate magnetometer

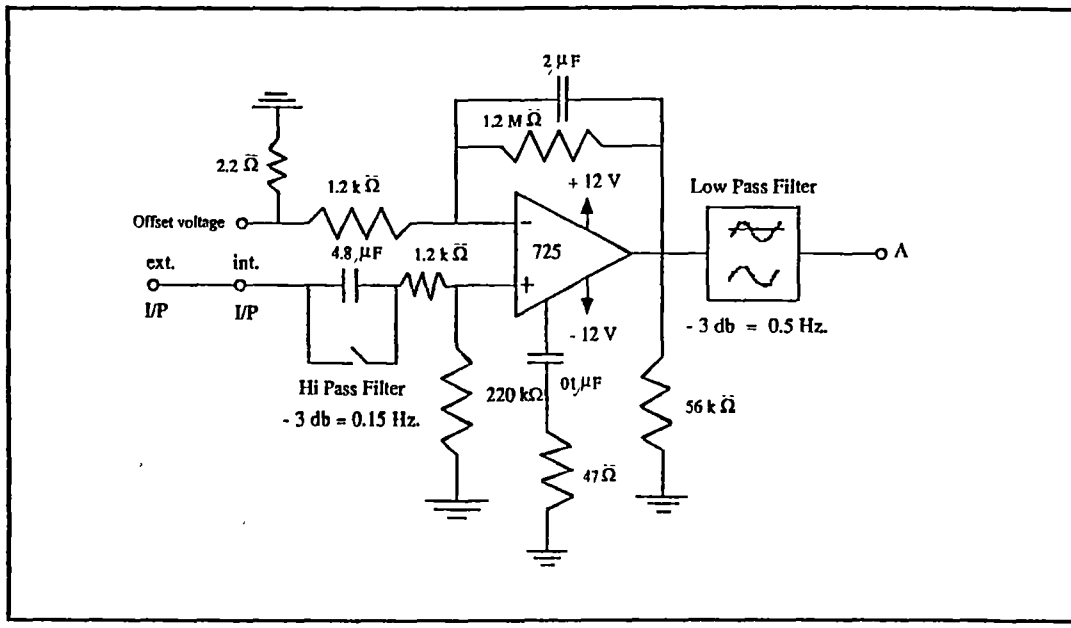

Figure 3.2 Telluric Amplifiers for A, B, C and D channels

The two recording units are similar to those used by Bindoff (1983), Sayers (1984) and Hermanto (1985). The main components of each data logger are as follows :

- detector head
- three component EDA fluxgate magnetometer
- multiplexer
- analog to digital converter (ADC)
- solid state memory
- Memodyne digital cassette recorder
- four telluric amplifiers
- four band-pass filters
- two temperature sensors
- dc-dc inverter
- channels select switch
- electrodes
- battery and solar panel

Except for the detector head, electrodes, battery and solar panel, which are separate, all components are placed together within a single water-tight box. The two recorders used have similar characteristics and sensitivities. The resolution of the magnetometer is ± 1 nT with a senstivity of 1 volt per 100 nT. The resolution of the ADC is 1 bit which is equal to 2.44 mV. Noise fluctuation in the recording unit was measured as 0.017 apparent nT hz^{-1} for magnetic channels and 0.046 apparent nT hz^{-1} for telluric channels with a gain of 1000 (fast mode) (Sayers, 1984). The EDA noise is about 0.5 nT.

The two recorders can be used to record the magnetic and the electric fields either in slow (normal) or fast (memory) mode. Micropulsations which occur normally for a short period after a magnetic storm are recorded in the fast mode.

In the slow mode, data can be sampled at intervals of 3, 6, 30 and 60 seconds. In this mode up to seven channels of data, i.e. three magnetic field components (H_x, H_y, H_z), two telluric field components (E_x, E_y), and two temperature components can be recorded. The equipment records the magnetic, electric and temperature channels sequentially. The dynamic range of the magnetic channels is ± 1000 nT and ± 100 mV for the telluric channels (assuming an amplifier gain of less than 100 for the latter).

In the fast mode data is sampled only at 0.2 seconds interval (5 Hz.). At this rate the ADC can convert a maximum of five channels i.e. H_x, H_y, H_z, E_x and E_y. As this sampling rate is too fast for the Memodyne digital cassette recorder, digital RAM (Random Access Memory) is used as a buffer to store the data temporarily. It takes about 2-3 minutes to fill the memory and about 15 minutes to transfer the data from the memory onto the Memodyne digital cassette recorder. While the stored data is transferred, sampling is stopped until the transfer is finished. Thus the data, recorded between successive readings, is discontinuous.

In the fast mode, the magnetic channels for the two orthogonal horizontal components of the magnetic field should be connected to the amplifiers. This is done to increase the recording sensitivities, as the signal amplitudes fall off rapidly with increasing frequency, over most of the frequency range used. Figure 3.3 shows typical spectral density behaviour of the magnetic and electric fields.

The disadvantage of using the fast mode, with data recorded into the memodyne digital cassete recorder, is that the length of data is limited to the capacity of the solid state memory (4096 samples). The amount of micropulsation data recorded is therefore relatively small and discontinuous.

As every channel is sampled at a 5 Hz rate in the fast mode the folding or Nyquist frequency is 2.5 Hz. The cut-off frequency of the band-pass filters is -3 dB at 0.5 Hz and attenuates to about -45 dB at the Nyquist frequency. This attenuation represents a reduction of about two hundred times that of the signal level at the input of the filter. Figure 3.4 shows the amplitude response of the telluric amplifiers. No correction was carried out to data passing through this amplifier because all variables use the same filter and results depend on ratios.

The amplifiers used in the equipment are LM725 operational amplifiers with the following specifications:

- open loop gain 3000000
- input voltage drift 0.6 uV/°C
- input noise current 0.15 pA/√Hz
- input voltage range ± 14 V
- guaranteed over a - 55 °C to + 125 °C temperature range.

The noise of these amplifiers is very small, i.e. approximately 1 μV nominal referred to input. This noise is less than 1 bit of the resolution of the ADC. The input voltage drift is also small compared to the input signal of 50 - 200 μV.

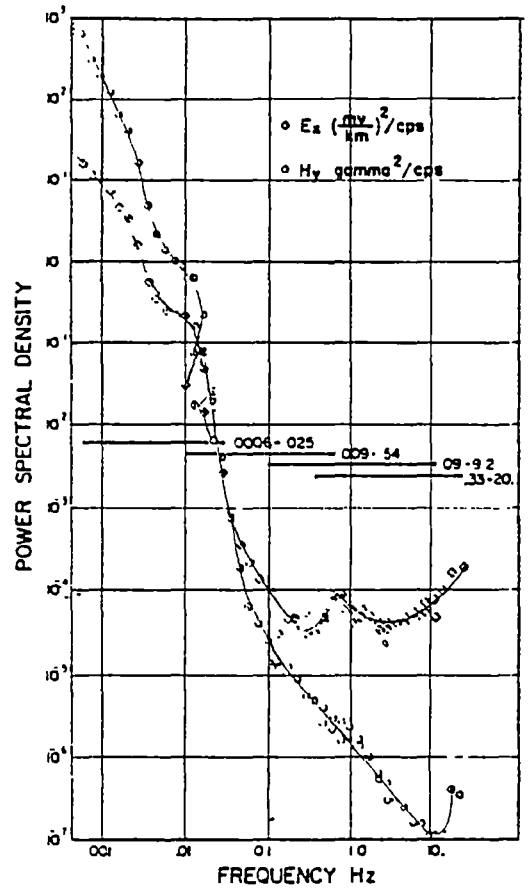

Figure 3.3 Typical spectral densities behaviour of the magnetic and electric fields (after Vozoff, 1972).

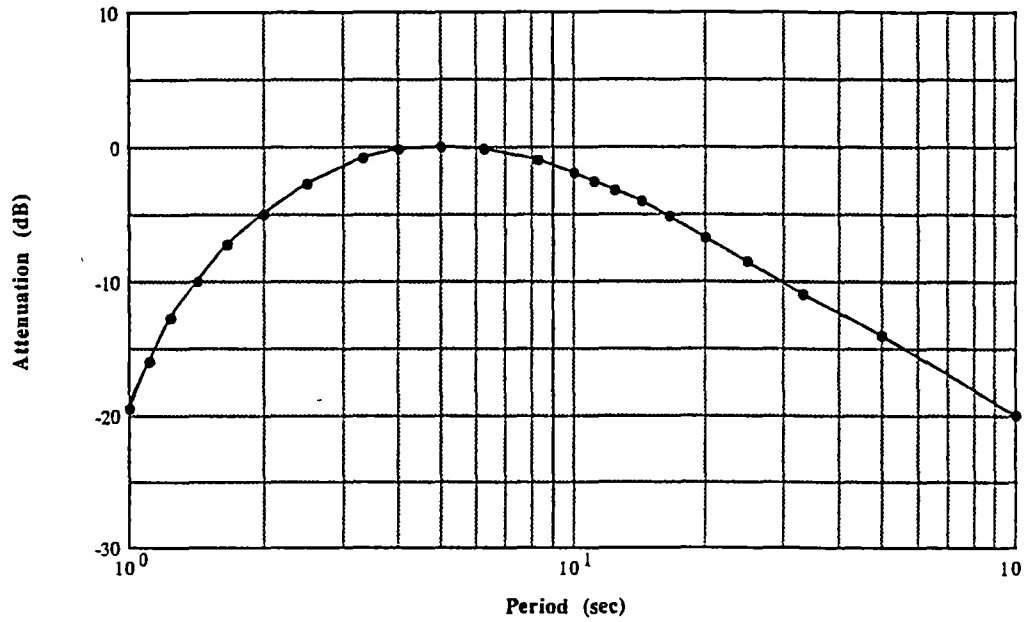

Figure 3.4 Amplitude response of telluric amplifier

3.1.1 NEW DEVELOPMENT

Since the ability of the recording unit to record data in the fast mode was limited, a new way of storing data was developed using a laptop computer. Development of a new interface between the ADC and the laptop computer was undertaken in early 1991 by Mr. V.Jensen in the Geology Department of the University of Tasmania. The laptop computer used in the new data logger system is a NEC multispeed micro-computer powered by internal rechargeable NiCad batteries that last up to eight hours. It can be connected to a car battery for a prolonged run.

With the new system, data can be recorded in either the fast or the slow recording mode, via a serial port which links the computer, RS 232 interface and the recording unit together. Figure 3.6 shows a block diagram of the interface.

This system is activated whenever the recording unit is switched to ON and to RS 232. A program called MTNEC1 is used to record data in the NEC.

While data is transferred onto the floppy disk the computer can keep recording and storing the data in the RAM. Recording will automatically be terminated after either the floppy disk is full or the recorded data reaches 700 kilobytes. Recording can also be halted manually at any time.

There are several advantages in recording data in the fast mode with the new system, these are:

- continuous recording.
- large amounts of data can be recorded in a short period of time.
- no data transfer is required. (In the old data logger system recorded data had to be transferred from a digital cassette into the computer first, before the data could be analysed.)
- recorded data can be examined at the recording site.
- recording is very fast (in the fast mode, it takes approximately 4 hours to fill up 700 kilobytes memory of a $3\frac{1}{4}$ inch floppy disk).

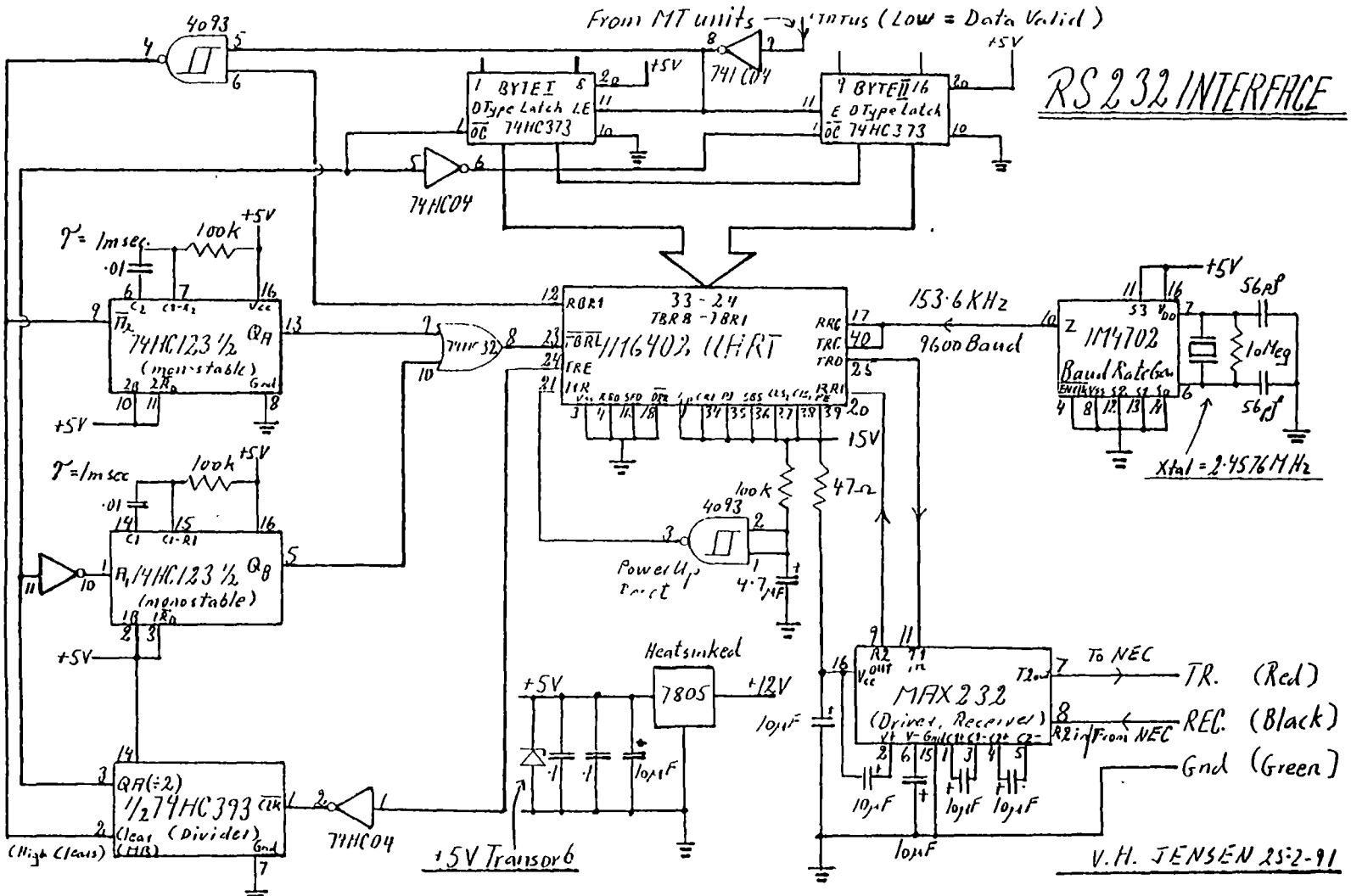

Figure 3.5 Block diagram of the RS 232 interface (drawn by V.H. Jensen)

3.2 CALIBRATION

3.2.1 MAGNETIC SENSOR CALIBRATION

Prior to the study, calibration of the magnetic sensors was carried out in the geophysics laboratory to ensure that both sensors were functioning correctly. The calibration procedure used was similar to that of Sayers (1984). X,Y and Z components of EDA I and EDA II were found to be within 2%, 3% and 2%, respectively, of the expected calibration values. Since the relation between X and Y is important in MT analysis, it is imperative that the difference between these two components be small.

3.2.2 TEMPERATURE CALIBRATION

Since experience showed that the two recorders performed well no new temperature calibration method was tried. Rather, the temperature calibration of Hermanto (1985) was used as follows :

1. The two MT units were set up as in normal observation. The control box of unit 1 was put in sunlight (unshaded) and the control box of unit 2 and the two detector heads were put in shade.
2. Data was then recorded as in normal operation.
3. It was assumed that there was no temperature differential between the shaded heads. Recorded data from both units were then compared.
4. Differences between the two recordings were plotted as a function of temperature. The slope of the line then gave the temperature correction for the control box of unit 1.
5. Similar procedures were also carried out to determine temperature correction for the detector head of unit 1, control box and detector head of unit 2, respectively, i.e. by putting each of these items in sunlight and the rest in shade.

Results from the above procedures were treated as a first approximation of the temperature correction and then used to correct instruments in the shade. By repeating the above procedure a number of times the best temperature correction was determined. Final results from this calibration are given in Appendix 2.

3.3 ELECTRODE DESIGN

Six nonpolarizable, Pb - $PbCl_2$, (after Petiau and Dupis, 1980) electrodes were made and tested prior to the MT observations. Electrodes were designed to ensure they have low noise, low amplitude drift between electrodes, low temperature coefficient, low potential drift with time and low contact resistance with the ground.

Petiau and Dupis (1980) have shown that the Pb - $PbCl_2$ electrode noise is of the order of 1.2 μV at 0.01 Hz. This noise is very small compared to noise of 10 μV or more at 0.01 Hz and 1.5 - 13 μV at 0.01 Hz for polarizable and other non-polarizable electrodes, respectively. Temperature coefficients for this electrode (- 40 μV/°C at 25 °C) are approximately one tenth of polarizable electrodes. The potential drift of 1 mV/month is also lower than other types of electrodes.

Figure 3.6 shows a schematic diagram of the non polarizable Pb - $PbCl_2$ electrode. Each was made of a lead bar 2 cm wide and 16.5 cm long. The top end of the lead bar, which was about 1 x 1 cm, was inserted into a 1 x 1 cm rectangular hole PVC washer and connected to a wire. This connection was soldered and covered by a clear silicon sealant to protect it from corrosion. The washer was then glued into a PVC tube 20 cm long by 5 cm diameter and filled with a mixture of plaster, water, 15 gr/l $PbCl_2$ and 360 gr/l NaCl (Petiau and Dupis, 1980). This electrode (lower part) was connected to another PVC tube (upper part) of 80 cm long by 5 cm diameter. This upper part of the electrode, which was sealed by a PVC cap, acted as a support or handle during placement.

Electrode resistance and variation of the potential difference between the electrodes were measured with respect to a reference electrode. During the measurement, all electrodes were placed in a large container of mud. The measurement was conducted in the laboratory for about four days using a multimeter and the Tellohm meter. Results from this measurement indicated that most electrodes stabilized very quickly i.e. within 2 hours and the potential drift between electrodes was less than 1 mV/4 days. These results are very much the same as obtained by Petiau and Dupis (1980).

3.4 SURVEY PROCEDURES

The survey procedure used to record the two orthogonal horizontal components of the magnetic and electric fields at all recording sites was relatively simple. Much time is involved, however, in planning the recording sites in advance, obtaining permission for using land from the property owner, general logistics and determining the sampling interval to be used.

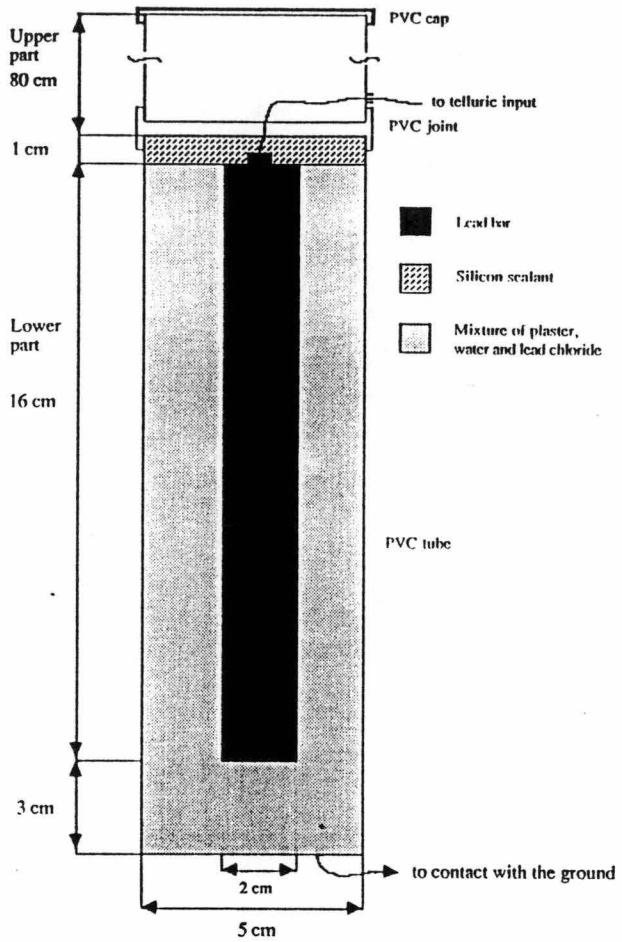

Figure 3.6 Schematic diagram of Pb-PbCl2 electrode

Power lines, railway lines, moving vehicles and electric fences are a source of noise, so recording sites were chosen free of these and distant from any artificial or man-made sources of noise. Farm land was preferred to public land to minimise vandalism and to ensure the sites were large enough to accommodate two telluric lines approximately 100 metres long at right angles.

The sampling interval was carefully considered since it determined how long the site would be occupied. Sampling intervals could be selected from 0.2, 3, 6, 30 and 60 seconds. For example, in the slow mode with 3 seconds reading intervals and a cassette length of 120 minutes, a site would be occupied for about one and a half days unattended. On the other hand, in the fast mode with the new data logger system, i.e. with 0.2 seconds sampling interval, a site would only be occupied for about 4 hours. Ultimately the longer the sampling interval chosen, the longer the site would be occupied. Throughout the survey sampling intervals of 0.2, 3 and 6 seconds were used.

CHAPTER 4 :
DATA ANALYSIS

4.1 INTRODUCTION

Magnetotelluric survey data must be reduced to produce calculated impedance tensors, dimensionality factor (skew), coherency estimate, rotation angle, and apparent resistivities.

During this study data analysis was mainly carried out using Olivetti M24 and M260 IBM compatible PC using programs MTY3 and MTYZ45. The programs were written by the author in Fortran 77 language. These programs are a modification of EMMTEE1 (Hermanto, 1985) and REDAT and MAGTEL, (Bindoff, 1983) respectively. The modification to the programs was necessary to allow them to run on a PC and to improve output presentation. Copies of the above programs and other programs used in the analysis are lodged with the curator Geology Department of the University of Tasmania.

4.2 PROGRAM TESTING

As a result of the above modifications, it was necessary for both programs to be tested to ensure a correct or reproducable test. Testing for each program was conducted separately. A program was written to generate synthetic data for the MTYZ45.

The testing procedure for the MTY3 program consisted of generating a sine wave with known amplitude and frequency using a signal generator and then feeding it to the input channels on the recording box of the MT instrument. The data was then recorded on the Memodyne cassette recorder and the laptop computer. For simplicity only two channels were used and the other channels were left grounded. This test was also used concurrently to check channel number identification and coherency between two types of recording modes. Amplitude of the input data used was 2.9 mV peak to peak at frequency of 0.01 Hz. Output of this test was then used to check the MTY3 program. The output response of the MTY3 could be predicted and compared with the input data. Figures 4.1 show plotted output of the MTY3. Results confirm correct output.

Testing of the MTYZ45 program consisted of two types of tests to check that output of unrotated and rotated tensor impedances and rotation angle were correct. The first test used purely synthetic data. Sine waves which represented the electric and magnetic fields were created by a program called SYNTEC3X.

Amplitude of the waves was determined at the beginning of the program prior to the actual calculation. Output of this program was arranged so that it matched the input required by the MTYZ45. The test, however, failed to determine the impedance tensors' values as coherency of HxHy was high i.e. greater than .8. The MTYZ45 program was set so that if coherency of HxHy is greater than .8 all calculations for data at that particular period will be by-passed until it reaches data which has coherency of HxHy less than . 8. If during the analysis of all data at all periods the coherency of HxHy is greater than .8 then all calculations for all data will be by-passed. Swift (1967) suggests that lack of random signal may produce high HxHy coherencies and therefore cause the tensor elements computed to be unstable. A few percent of random noise was then added into each data. The output result, however, still failed to determine impedance tensors values as the coherency of HxHy remained greater than .8. This test shows that purely synthetic data can give unrealistic results.

Since this test was unsuccessful another test using a combination of half synthetic and half observed MT data was considered. The half synthetic and half observed data were created by calculating E_x and E_y components of the electric field from the actual H_x and H_y components of the magnetic field data, recorded during the survey. The impedances Z_{ij} where $i = x,y$; $j = x,y$ which were taken as real, were assigned as : $Z_{xx} = .394$; $Z_{xy} = .669$; $Z_{yx} = -.531$ and $Z_{yy} = -.394$. These impedance values were also used to check the calculated rotation angle which should give 50 degrees (with clockwise rotation).

The determination of the E_x and E_y components was carried out in a program called SYNTEC. Output of the SYNTEC which consists of the actual data of the magnetic field components and synthetic (calculated) data of the electric field components is given in Appendix 3. This output was modified so that it matched the input required by the MTYZ45. The data heading on the output represents number of site, data interval, number of events and number of data points while 1, 2, 3, 4 and 5 followed by a group of numbers are the numbers of channels and data which represent H_x, H_y, H_z, E_x and E_y components of the magnetic and electric fields, respectively.

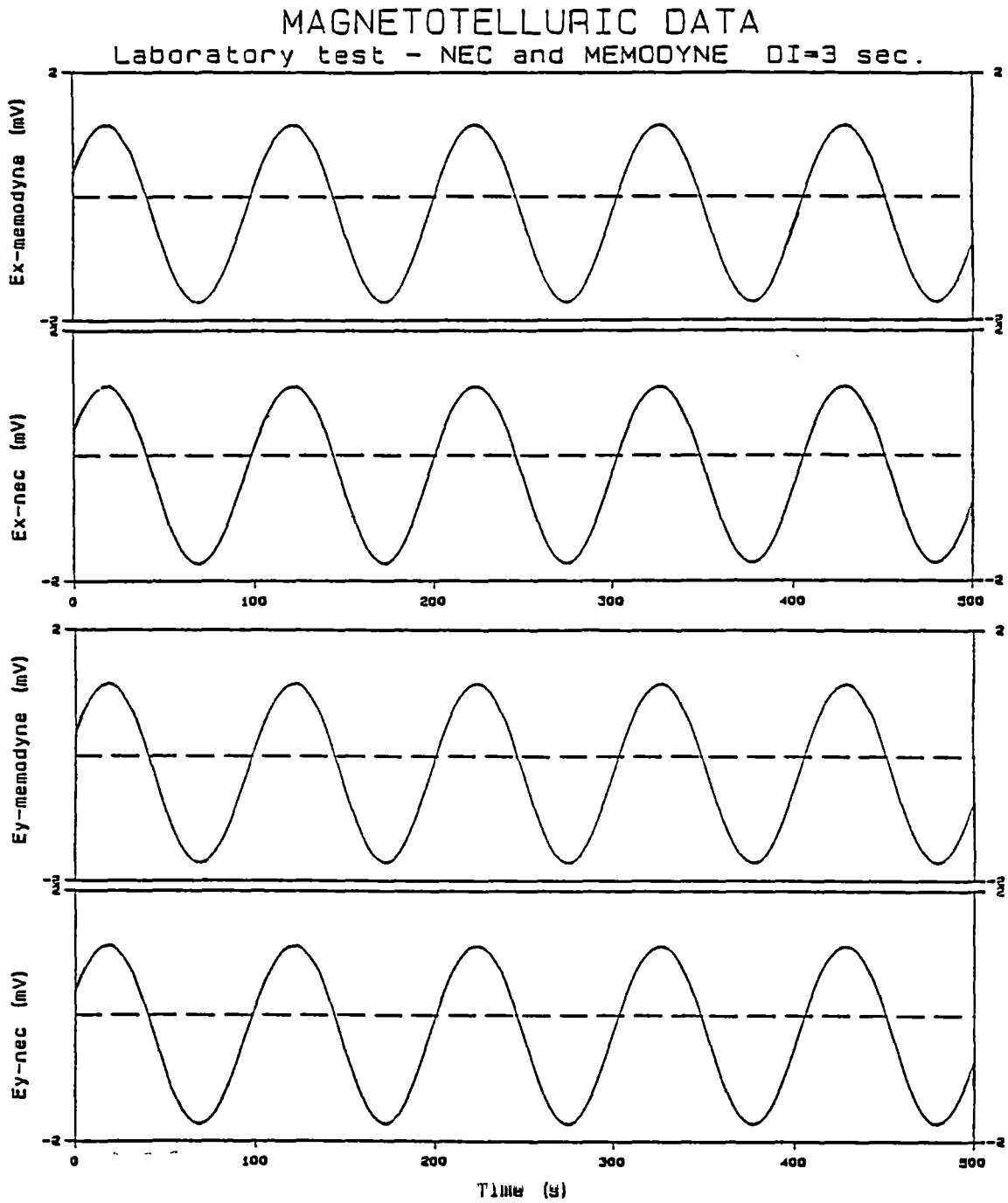

Data File: LCD1.3 Date: 01-28-1992 Time: 09: 48: 05
Figure 4.1 Plotted output of MTY3

Results from the test of the MTYZ45, which are given in Appendix 3, show that the calculated unrotated real impedances (ReZ_{ij}) and the rotation angle (THETA) are similar to the assigned values of Z_{ij} and the expected rotation angle, respectively. This test, therefore, shows that the MTYZ45 also behaves as expected.

4.3 STEPS OF ANALYSIS

4.3.1 MTY3

This program reads a block of the observed electric and magnetic field data from a file stored either in hard or floppy disk. Length of the block depends on the number typed in by the user under prompt LIMIT. Default value for LIMIT is 1024. The data is then displayed on the computer screen.

In the case of slow mode recording, the display consists of 3 magnetic field (H_x, H_y, H_z) variations, 2 telluric field (E_x, E_y) variations and 2 temperature (control box, detector head) variations. In fast mode recording, on the other hand, the display comprises only 3 magnetic field (H_x, H_y, H_z) and 2 telluric field (E_x, E_y) components. The main difference in the display of the two modes of recording lies in the capability of the analog to digital converter (ADC) in the recording unit. The ADC converts data up to seven channels in the slow mode. In the fast mode, on the other hand, it converts only five channels.

Interactive commands are used to modify the display. Occasional mis-readings occur because of a displaced bit and any such readings have been corrected. The correction is based on linear interpolation using the two adjacent points on each side of the abnormal readings. The correction is necessary as a Fourier transform of a spike would produce a broad spectrum and thus distort the frequency spectrum.

Figure 4.2 shows a plot of the observed magnetotelluric data. Any magnetotelluric events chosen from this display, are automatically corrected by instrumental gain and digital to analog converter factor (see Appendix 4). The temperature correction (see Appendix 2) is also applied here but only to the magnetic field components with sampling rate of 30 and 60 seconds. For 30 seconds sampling rate, for example, where data is recorded for about 12 days unattended, temperature variations could be appreciable. Temperature variations in the electric field components, on the other hand, are of little relevance as the telluric electrodes are normally buried in the ground to about one metre . Temperature correction for the electric field components here is therefore unnecessary.

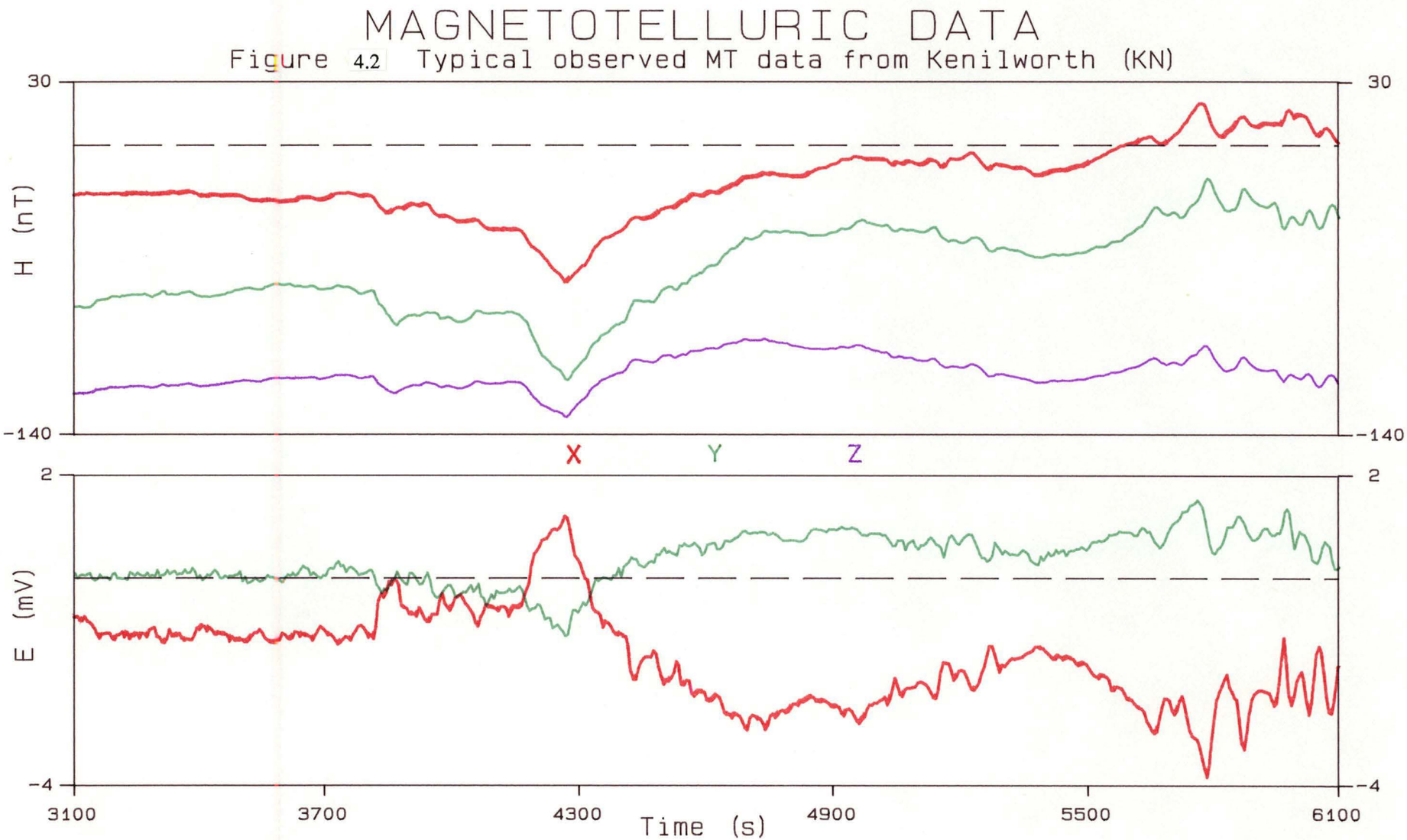

Figure 4.2 Typical observed MT data from Kenilworth (KN)

The output unit of the chosen events here is in nT for the orthogonal horizontal (H_x, H_y) and vertical (H_z) components of the magnetic field and mV for the orthogonal horizontal (E_x, E_y) components of the electric field.

4.3.2 MTYZ45

This program completes two major steps of analysis. These are (i) conversion of time to frequency domain and (ii) calculation of unrotated and rotated tensor impedances.

4.3.2.1 CONVERSION OF TIME TO FREQUENCY DOMAIN

Before a Fast Fourier Transform is carried out, linear drift which can cause distortions of power spectral estimates is first removed from the data. E_x and E_y components of the electric fields are then rotated here to coincide with H_x and H_y axes of the magnetometer. The rotation is performed using equations as follows:

$$E_x' = E_x \cos \alpha_1 + E_y \cos \alpha_2$$

$$E_y' = E_y \sin \alpha_2 + E_x \sin \alpha_1$$

where E_x' and E_y' are the rotation of Ex and Ey components; α_1 and α_2 are the angles between Hx and Ex componests and Hx and Ey components, respectively. The electric fields data is also converted automatically here from mV to mV/km.

A Fast Fourier Transform is then used to transform data from time domain into frequency domain.

4.3.2.2 CALCULATION OF IMPEDANCE TENSOR

Calculation of impedance tensors carried out by this program can be summarised as follows:

1. Spectral bands for averaging are selected. The bands overlap parameters set in the program to 0.75. The number of requested bands chosen is ten which in turn is averaged over a tenth of a decade per band to ensure normal distribution of the estimate.
2. The average powers spectra $\langle E_x E_x^* \rangle$, etc. and cross-powers spectra

$\langle E_x H_y^* \rangle$, etc. are calculated from the Fourier spectra $E_x(\omega)$, $E_y(\omega)$, $H_x(\omega)$ and $H_y(\omega)$ where E_x^* and H_y^* are complex conjugate Fourier spectra of E_x and H_x and $\langle\rangle$ represents averaging in frequency for finite band-widths. The interchannels cross-powers spectra which are determined here are: H_xH_y, H_xH_z, H_xE_x,H_xE_y, H_yH_z, H_yE_x, H_yE_y, H_zE_x, H_zE_y and E_xE_y.

The average powers spectra can be calculated by formulae similar to equations (4.3.2.3.1) and (4.3.2.3.2).

3. The average powers and the cross-powers spectra are averaged over a tenth of a decade per band using constant-Q filters section data determined in step no. 1.
4. The cross-powers are normalized here as coh = coherency.
5. The impedance tensors are calculated from the averaged powers and the normalized powers using the following equations:

$$Z_{xx} = \left|\frac{E_x}{H_x}\right| \left\langle \frac{\text{coh } E_xH_x - \text{coh } E_xH_y \text{ coh } H_yH_x}{1 - |\text{coh } H_xH_y|^2} \right\rangle$$

$$Z_{xy} = \left|\frac{E_x}{H_y}\right| \left\langle \frac{\text{coh } E_xH_y - \text{coh } E_xH_x \text{ coh } H_xH_y}{1 - |\text{coh } H_xH_y|^2} \right\rangle$$

$$Z_{yx} = \left|\frac{E_y}{H_x}\right| \left\langle \frac{\text{coh } E_yH_x - \text{coh } E_yH_y \text{ coh } H_yH_x}{1 - |\text{coh } H_xH_y|^2} \right\rangle$$

$$Z_{yy} = \left|\frac{E_y}{H_y}\right| \left\langle \frac{\text{coh } E_yH_y - \text{coh } E_yH_x \text{ coh } H_xH_y}{1 - |\text{coh } H_xH_y|^2} \right\rangle$$

6. Two rejecting criteria are applied to the coherencies. Firstly, if coherency of (H_xH_y) is greater than .8 then no calculation will be performed for data at that particular frequency. Secondly, if coherency of E_x to $E_x^{\text{predicted}}$ and E_y to $E_y^{\text{predicted}}$ is less than .8 then calculation for data at that particular frequency will also be ignored.

Step no 5. is the same expression as was used by Swift (1989) to determine the impedance tensors elements in terms of the average powers and coherencies.

Rankin and Reddy (1969) and Swift (1989) state that unstable estimates of the impedance tensor elements will be obtained when the coherency between H_x and H_y is high, which indicates a constant or nearly constant direction of incident magnetic field throughout the data sample. Swift's (1989) equations (22) to (25) are thus only valid for data when the magnetic field components are not consistently linearly polarized. Rankin and Reddy (1969) indicate that a coherency of H_xH_y of 0.8 is considered to be high.

4.3.2.3 RELIABILITY ESTIMATE

A reliability estimate calculated by MTYZ45 relates the coherency between the actually measured electric field E_x, and that predicted. These values, which are predicted from H_x and H_y, have the interesting characteristic that they must be wholly dependent on the horizontal H field. Thus any departure observed between the observed electric fields E and the $E^{predicted}$ should be due to contamination of either the E or H field by noise (Vozoff, 1972). The coherency between E_x and $E_x^{predicted}$ can be calculated from :

$$\text{coh}\left(E_x, E_x^{predicted}\right) = \frac{|H_x|\, Z_{xx}\, \text{coh}\,(H_x E_x) + |H_y|\, Z_{xy}\, \text{coh}\,(H_y E_x)}{\left[|Z_{xx}|^2 |H_x|^2 + |Z_{xy}|^2 |H_y|^2 + 2|H_x||H_y|\, \text{Re}\,(Z_{xx} Z_{xy}\, \text{coh}\, H_x H_y)\right]^{\frac{1}{2}}}$$

..... (4.3.2.3.1)

or the coherency between E_y and $E_y^{predicted}$ can be estimated from :

$$\text{coh}\left(E_y, E_y^{predicted}\right) = \frac{|H_x|\, Z_{yx}\, \text{coh}\,(H_x E_y) + |H_y|\, Z_{yy}\, \text{coh}\,(H_y E_y)}{\left[|Z_{yx}|^2 |H_x|^2 + |Z_{yy}|^2 |H_y|^2 + 2|H_x||H_y|\, \text{Re}\,(Z_{yx} Z_{yy}\, \text{coh}\, H_x H_y)\right]^{\frac{1}{2}}}$$

..... (4.3.2.3.2)

(Swift, 1967).

Theoretically with noise-free data the coherency between E and $E^{predicted}$ is equal to 1. In practice, however, a predictability coherency of 1 is rarely obtained. For noisy data, with a predictability coherency of 0.8 it can be explained by 25 % added noise power to the measured E_x or E_y electric field components (Swift, 1967). All MT data which are analysed and plotted in section 5.2 are based on a coherency estimate of greater than 0.8.

4.3.2.4 APPARENT RESISTIVITIES

Magnetotelluric techniques require the calculation of apparent resistivities and phase relationships between the measured electric and magnetic field components as function of period. In general there are two types of apparent resistivities, namely: scalar or Cagniard and tensors apparent resistivities.

The Cagniard apparent resistivities are defined as:

$$\rho_{a,\,xy} = \frac{1}{\mu\omega}\left|\frac{E_x}{H_y}\right|^2 \qquad \text{..... (4.3.2.4.1)}$$

$$\rho_{a,\,yx} = \frac{1}{\mu\omega}\left|\frac{E_y}{H_x}\right|^2 \qquad \text{..... (4.3.2.4.2)}$$

where $\rho_{a,\,xy}$ and $\rho_{a,\,yx}$ are apparent resistivity for xy and yx in Ohm.m; $\mu = 4.0 \times 10^{-7}$ Henry/m, $\omega = \frac{2\pi}{T}$ where T is period in seconds; E_x and E_y are electric field components measured in x and y directions in V/m; H_x and H_y are magnetic induction measured in x and y directions in Amp/m.

The phase information for the Cagniard apparent resistivities can be obtained from:

$$\text{Phase}_{xy} = \arctan\left(\text{Im}\,(\text{coh}\,H_xE_y)^*, \text{Re}\,(\text{coh}\,H_xE_y)^*\right) \qquad \text{..... (4.3.2.4.3)}$$

$$\text{Phase}_{yx} = \arctan\left(\text{Im}\,(\text{coh}\,H_yE_x)^*, \text{Re}\,(\text{coh}\,H_yE_x)^*\right) \qquad \text{..... (4.3.2.4.4)}$$

where Im and Re represent imaginary and real components, respectively; coh is coherency or normalized cross-powers spectra; * is complex conjugate and Phase_{xy} and Phase_{yx} are phase relationship of xy and yx in radiants.

The elements of tensors apparent resistivities that are determined from the impedance estimate are calculated from:

$$\rho_{a,\,xx} = \frac{1}{\mu\omega}|Z_{xx}|^2$$

$$\rho_{a,\,xy} = \frac{1}{\mu\omega}|Z_{xy}|^2$$

$$\rho_{a,\,yx} = \frac{1}{\mu\omega}|Z_{yx}|^2$$

$$\rho_{a,\,yy} = \frac{1}{\mu\omega}|Z_{yy}|^2$$

Their phase information can also be determined from:

$$\text{Phase}_{xx} = \arctan\left(\frac{\text{Im}\,(Z_{xx})}{\text{Re}\,(Z_{xx})}\right)$$

$$\text{Phase}_{xy} = \arctan\left(\frac{\text{Im}\,(Z_{xy})}{\text{Re}\,(Z_{xy})}\right)$$

$$\text{Phase}_{yx} = \arctan\left(\frac{\text{Im}\,(Z_{yx})}{\text{Re}\,(Z_{yx})}\right)$$

$$\text{Phase}_{yy} = \arctan\left(\frac{\text{Im}\,(Z_{yy})}{\text{Re}\,(Z_{yy})}\right)$$

where Z_{xx}, Z_{xy}, Z_{yx} and Z_{yy} are estimated impedance tensors in Ohm. Other units are similar to units for equation (4.3.2.4.1), (4.3.2.4.2), (4.3.2.4.3) and (4.3.2.4.4). The apparent resistivities can be calculated either before or after the tensors impedances are rotated to the principal direction. In the two-dimensional case, only the anti-diagonal tensors for resistivity ($\rho_{a,\,xy}$ and $\rho_{a,\,yx}$) are of interest as they carry information about the resistivities along and across the strike of a structure. Hence only the rotated tensor resistivities are plotted here and used in the interpretation. Although the other pairs of resistivity ($\rho_{a,\,xx}$ and $\rho_{a,\,yy}$) are smaller than $\rho_{a,\,xy}$ and $\rho_{a,\,yx}$, they are never found to be zero and thus can be used to judge the degree to which the structure of a site departs from two-dimensionality (Vozoff, 1989). The unrotated tensor resistivities, like the Cagniardresistivities, are of little use in the two-dimensional case as they carry no information about the resistivity along and across the structure and thus no interpretation is made based on those resistivities.

4.4 INDUCTION ARROWS

Since Hermanto's (1985) MV sites coverage overlays the present MT study, no analysis of induction arrows was carried out during this study. The previous results have been used to aid interpretation of the conductivity structure being studied.

The induction arrow used in Hermanto' s (1985) study follows Parkinson' s convention which is known as the Parkinson arrow (Parkinson, 1962). The arrow was calculated based on the least-square method introduced by Everett and Hyndman (1967) to obtain the best fit relation between the vertical and the horizontal components of the magnetic field. A linear relationship between the three components of the magnetic field can be expressed as:

$$Z = AX + BY$$

(Parkinson, 1983) where Z, X and Y are Fourier coefficients of the vertical, north and east horizontal components, respectively, for a particular period and A and B are complex transfer function as function of period. A and B were calculated, after minimising the sum of squared residuals over an ensemble of magnetic events. Lengths of the arrow for each real (Re) and imaginary (Im) part which indicate the ratio of vertical to horizontal components and are determined by :

$$\text{Length}_{Re} = \left(A_{Re}^2 + B_{Re}^2\right)^{\frac{1}{2}}$$

$$\text{Length}_{Im} = \left(A_{Im}^2 + B_{Im}^2\right)^{\frac{1}{2}}$$

and their directions (θ) which indicate the horizontal direction that correlates positively with upward vertical component (Parkinson, 1959, 1962, 1964), are calculated from :

$$\theta_{Re} = \arctan \frac{B_{Re}}{A_{Re}}$$

and

$$\theta_{Im} = \arctan \frac{B_{Im}}{A_{Im}}$$

where θ is measured from the magnetic north. The Parkinson arrows, which are normally plotted on the map starting from the location site, should point toward a zone of anomalously high conductivity. Parkinson (1983) states that for near a truly two-dimensional structure both the real and imaginary induction arrows point to the same direction for all frequencies.

Characteristics of induction arrows in any MV investigation can be summarised as follows: for sites located far away from lateral conductivity contrast and situated over a horizontal layer earth, the length of the arrows should be small as Z is also small. Similar features should also be obtained by the sites situated close or on the middle of a good conductor. For sites located on or close to the boundary of either side of the good conductor, the length of the arrows should reach maximum and should point toward the conductor. As the location of the sites gradually moves away from the conductor, the length of the arrows should also gradually decrease.

It is apparent that the small induction arrows at sites TRM, WHL,NIL,VAU,ROS and OAT are associated with the high conductivity anomaly along the postulated Tamar Fracture System (TFS) which Leaman (1992) considers to be the frontal limit of a major overthrust belt. Solid and dashed lines which are drawn in Figure 1.2 show approximate centre and boundary of the conductor, respectively.

CHAPTER 5: MAGNETOTELLURIC EXPERIMENTS IN THE TAMAR LINEAMENT AREA

5.1 PREFACE

The magnetotelluric study of the Tamar Lineament area began in the middle of 1987. Because of problems in the fast mode data collection due to limited capacity of the solid state memory in storing recorded data, limited data collection was made in this mode. Data collection was thus focussed only to record data in the slow mode recording. It was not until 1991, when a new interface capable of recording continuous data was built that the fast mode data collection was enhanced.

Ten MT sites (see Figure 5.1) were initially proposed and set up in the Tamar Lineament area. However, mainly due to lack of good data from stations NI,CR, BW and VF, the MT study in the Tamar Lineament area was thus concentrated on traverse 3 of Hermanto's (1985) magnetovariational study in north eastern Tasmania (see Figure 5.2). Therefore, only six MT measurements will be reported here. The six MT sites were arranged so that they would coincide or be close to the MV stations for easy checking or comparison of the results. A list of the sites including their geographic coordinates is given in Table 5.1.

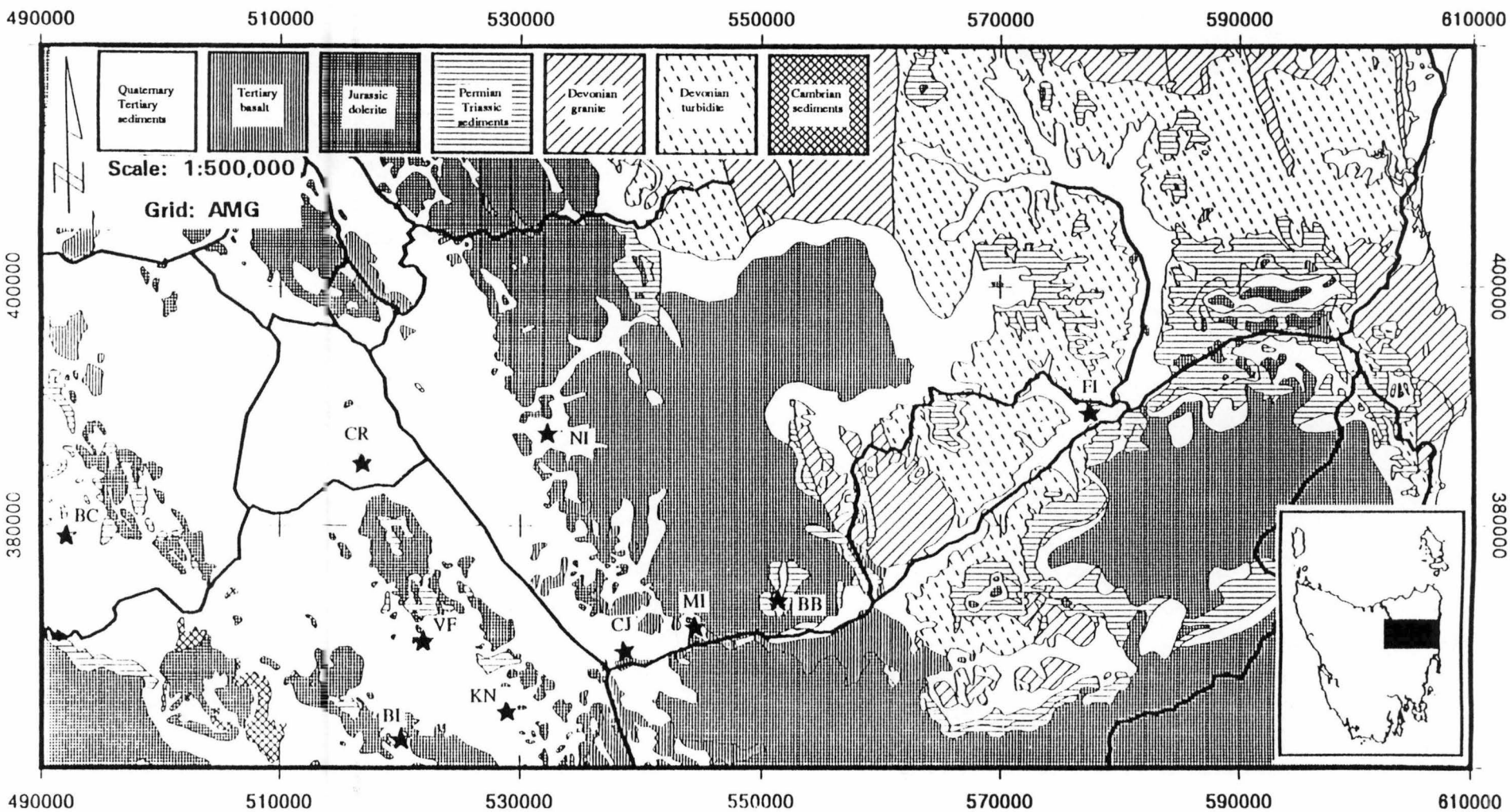

Figure 5.1 Location of MT sites across different geological contact.

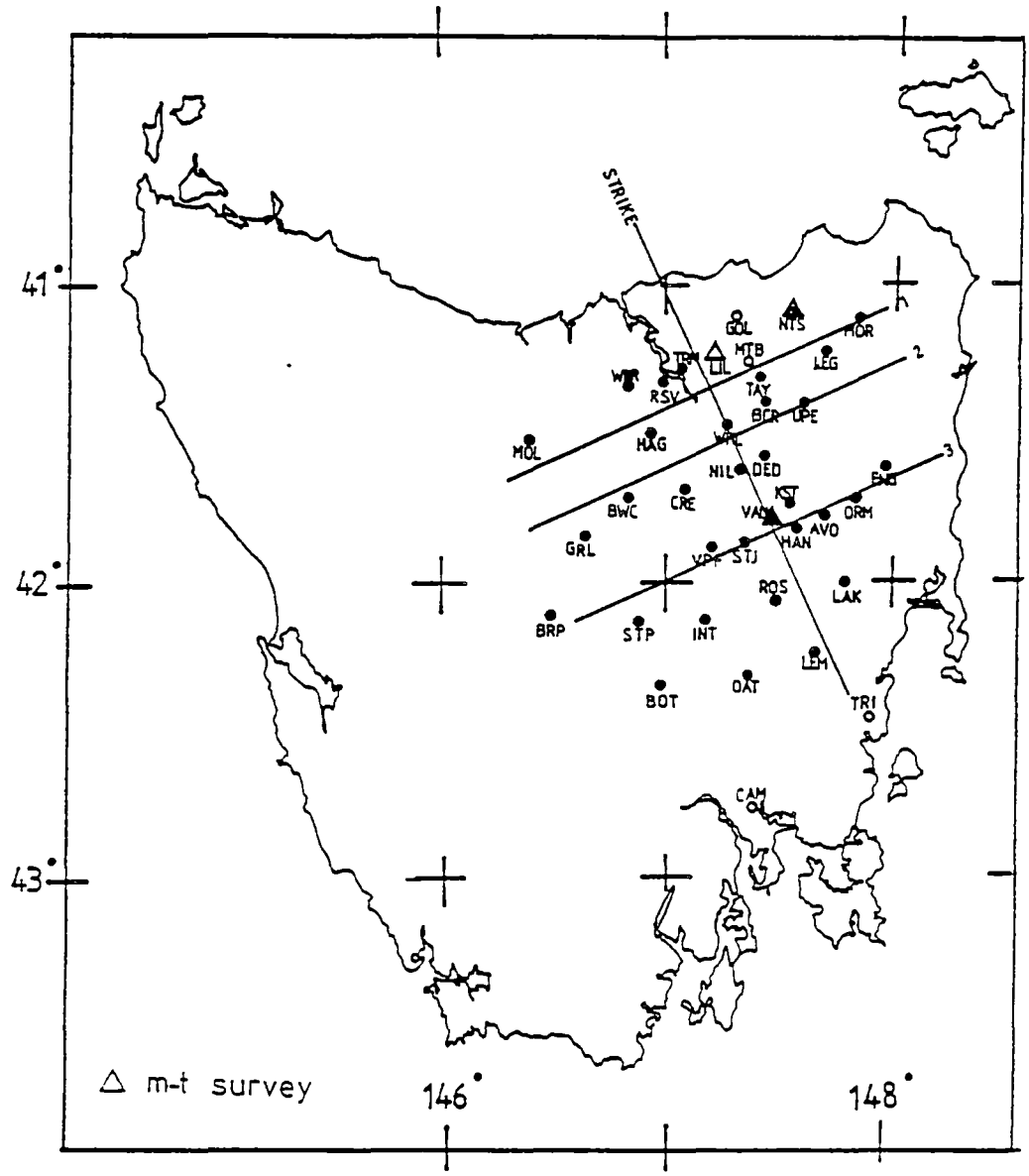

Figure 5.2 Plot of traverses 1,2 and 3 drawn perpendicular to the approximate strike of the Tamar Conductivity Anomaly. (After Hermanto (1985).

Table 5.1

List of sites and their geographical coordinates

No	Name of Station	Code	Longitude	Latitude	AMG	Remark
1	Bicton	BI	147°15'29"	41°54'02"	53619000mN 5213000mE	MT only
2	Kenilworth	KN	147°20'11"	41°52'05"	53648000mN 5273000mE	MT and TEM
3	Conara Junction	CJ	147°27'43"	41°50'00"	53888000mN 5379000mE	MT and DC Res.
4	Milford	MI	147°31'58"	41°49'04"	53711000mN 5436000mE	MT and TEM
5	Buffalo Brook	BB	147°38'16"	41°46'27"	53755000mN 5523000mE	MT only
6	Fingal	FI	147°53'36"	41°37'45"	53916000mN 5743000mE	MT only
7	Nile	NI	147°19'32"	41°39'20"	53776000mN 5172000mE	MT only
8	Cressy	CR	147°12'43"	41°41'54"	53892000mN 5264000mE	MT only
9	Blackwood Creek	BC	147°55'21"	41°45'14"	53776000mN 4926000mE	MT only
10	Valley Field	FF	147°16'22"	41°49'16"	53704000mN 5224000mE	MT only

It should also be mentioned that in conjunction with the MT technique, three other geophysical techniques were used here. These techniques were DC-resistivity, SIROTEM, and gravity and magnetic modelling. Details of these techniques, including other relevant geophysical results such as seismic and heat flow data, are described in section 5.4.

5.2 EXPERIMENTAL RESULTS

The experimental results which are presented here are the product of the analysis outlined in Chapter 4. They were all based on data which had coherency between the E and E predicted of greater than .8 and coherency between H_x and H_y of less than .8. Any data which fell outside this range of coherencies were automatically rejected.

In the tensor analysis an anticlockwise rotation angle (θ) i.e. 40° west of magnetic north, was used to rotate the observed coordinate axis at all sites to their principal axes direction. This angle (θ) which was determined from regional induction studies in northeastern Tasmania (Hermanto, 1985), represents the general strike of the conductivity anomaly in this region. This angle is also approximately similar to the principal axis direction determined by Bindoff (1983), Sayers (1984), and Richardson (1985) from their earlier MT study. The present study also indicates that rotation angle (θ) determined for Conara Junction, where this site is located approximately on the axis of the Tamar Conductivity Anomaly, is approximately similar to the angle (θ) used in the tensor analysis (as above). For other sites, for example; Kenilworth (KN) and Milford (MI), where they are close to the edges of the anomaly, the rotation angles (θ) are, however, relatively different i.e. 12° and 65° (anticlockwise rotation), respectively. The relative difference between the rotation angle (θ) at KN and MI, and the rotation angle (θ) used in this analysis may be due to the fact that KN and MI are located close to the edges of the anomaly and may therefore be affected by the shape of the edges which may not be symetrical. Detailed rotation angle results are given in section 5.3.

Error bars which are plotted on apparent resistivity, coherency, skew and phase (see Figures 5.3, 5.4, 5.5, 5.6, 5.7 and 5.8), represent quartiles from a series of data where the minimum of data calculated is four. If data at a particular period is less than four then the lower and upper limit of the error bar are determined from the lowest and highest value of those data.

5.2.1 Site 1 Bicton (BI)

Site 1 is situated approximately 4 kilometres east of the Bracknell Fault. The site, which is located on the southwestern edge of the Longford Tertiary Basin (see Figure 5.1), sits on alluvium deposits of probably Quaternary age. These deposits consist of clay, silt, sand and gravel. The thickness of these deposits under this site is unknown. Tertiary sediment, which is believed to be part of the Longford Tertiary basin occurs at this site.

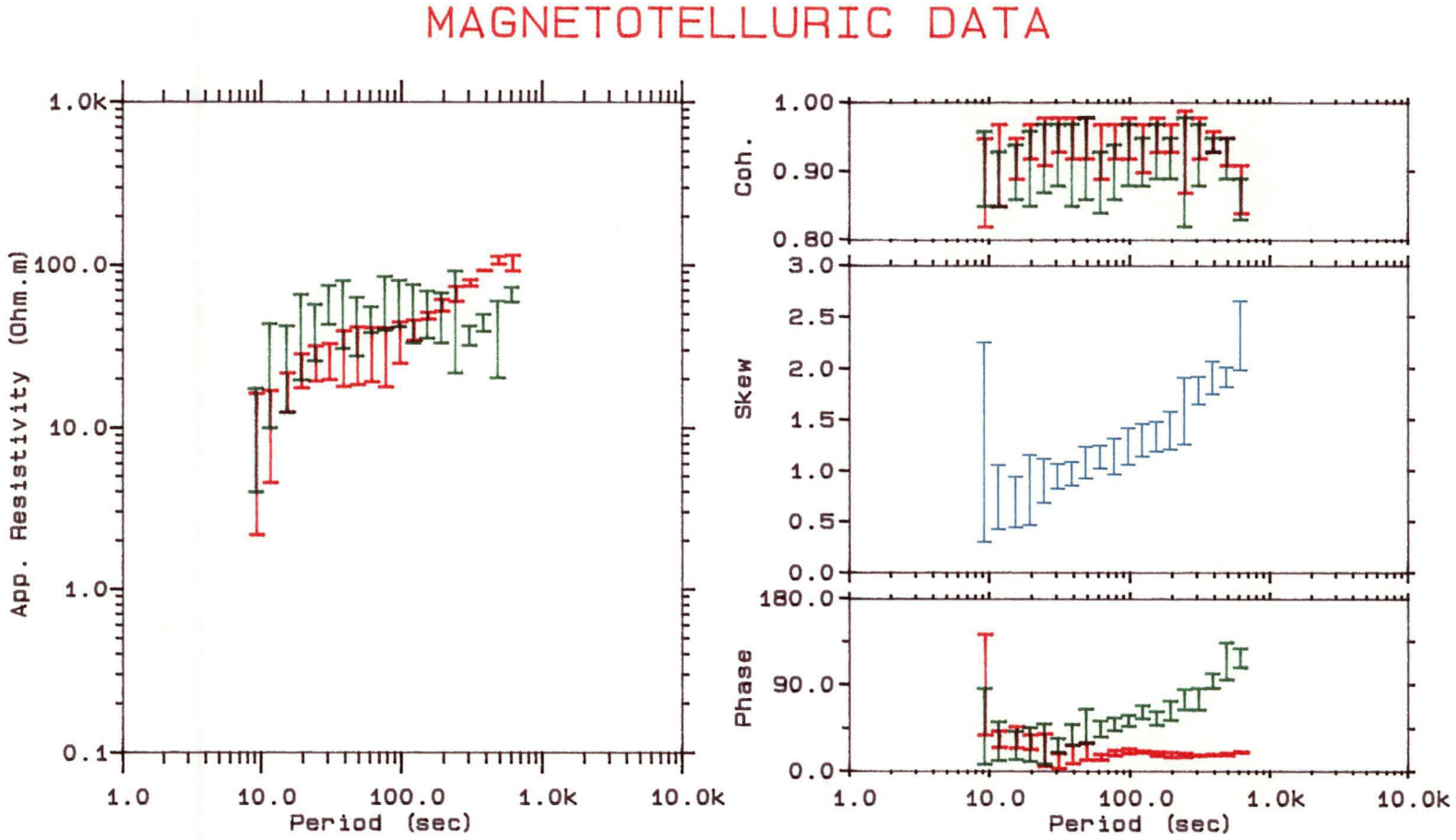

Figure 5.3 App. resistivity, coherency, phase and skew from Bicton (BI)
(red bars) E-polarization, (green bars) H-polarization

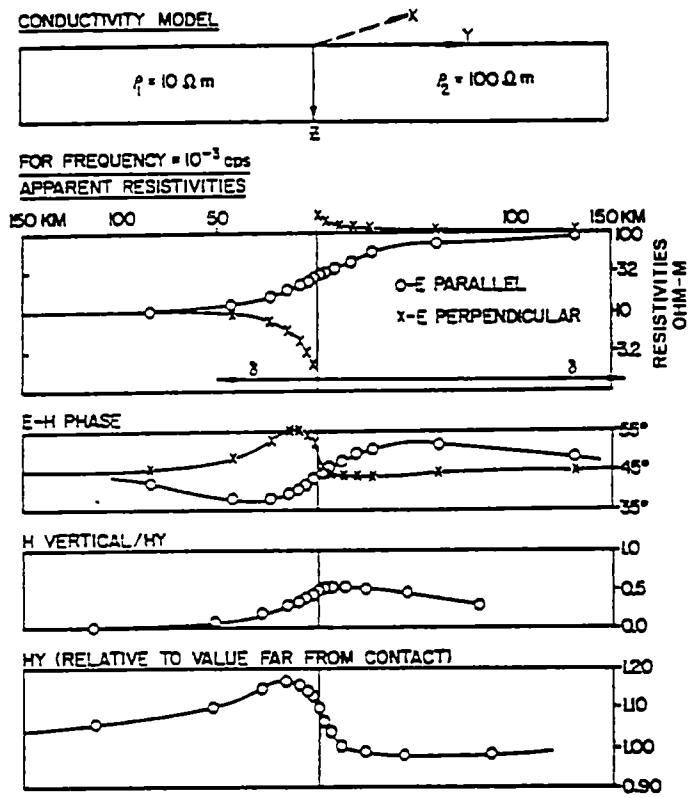

Figure 5.3a Network solution magnetotelluric field relationship over a vertical contact. After Swift (1971).

This site is located very close to Hermanto's (1985) MV site of VPF. The MV result from VPF which is shown by a long inphase induction arrow pointing to the east (see Appendix 1) suggests that the VPF site is close to or may be at the western edge of the Tamar Conductivity Anomaly (Hermanto, 1985). This result agrees very well with the MT result from this site. Apparent resistivity curves from this site, which are shown in Figure 5.3, illustrate a moderate anisotropy as period increases. The smooth increase of TE mode resistivity curve toward longer periods, for example, suggests that the resistivity gradually increases with depth. However, as this site is relatively close to the Bracknell Fault it is highly probable that the TM mode resistivity curve will be biased by the lateral inhomogeneities and thus it is doubtful whether the TM mode curve gives a true assessment of subsurface resistivity. Swift (1971) using a vertical contact model demonstrates how a vertical fault affects the TM mode resistivity. It can be seen from Figure 5.3a that the TM mode resistivity drops rapidly as it approaches the vertical contact. This effect is still seen to within 100 km from the contact. Dr. R.J.G. Lewis (personal communication, 1992) however, questions whether Swift's (1971) result can be applied to this result as this site may not be purely two-dimensional.

Skew which is normally used to determine dimensionality of a site is given in Figure 5.3. The skew which is very large, shows an increase toward longer periods. The very large skew, at all periods, confirms that this site is far from a two-dimensional structure and thus the two-dimensional tensor analysis may not be valid (Kurtz, 1973). Figure 5.3 also shows E_x-$E_x$predicted and E_y-$E_y$predicted coherencies plot for apparent resistivity curves shown in the same figure. It is shown here that most of the data has good coherency.

5.2.2 Site 2 Kenilworth (KN)

Site 2 is situated approximately 9 kilometres east of site 1. This site sits on a sandy clay of Quaternary age and possibly overlies Tertiary sediment. Underlying this sediment is dolerite of Jurassic age with a thickness about 300 metres (Dr. D.E. Leaman, personal communication, 92). The estimated thickness of the Tertiary and Jurassic rocks is in good agreement with the final model of the SIROTEM from this site (see Figure 5.20).

Hermanto's (1985) MV site of STJ (see Appendix 1) is situated only a few kilometres south east of this site. The MV result which is shown by a relatively shorter induction arrow pointing to the east than the one at VFP suggests that this site may be close to the middle of the Tamar Conductivity Anomaly (Hermanto, 1985). Apparent resistivity curves for the TE and TM modes are shown in Figure 5.4. It can be seen here that this site has much lower resistivity compared to the resistivity at site 1. This resistivity thus suggests that this site may already be inside the conductive zone and therefore supports the induction arrow analysis. Excluding the apparent resistivity curves at Fingal (FI), which are relatively large and increase toward longer period (see Figure 5.8), in general, the resistivity curves from the other MT sites seem to decrease toward the eastern site.

The resistivity curves for the TE and TM modes tend to merge at periods less than 100 seconds. The merging of both the TE and TM resistivity curves is probably due to an isotropic overburden layer. As the period increases, however, these resistivity curves strongly separate, thus showing that at a great depth the underground structure tends to demonstrate more anisotropy.

Skew plot for this site can be seen in Figure 5.4. As the site is now far from the lateral inhomogeneity contrast (i.e. the Bracknell Fault), the skew, in general, tends to be small. Except for periods greater than 500 seconds where the average skew is more than .3, other skews are less than .3. These skews indicate that dimensionality of the structure under this site is grading at depth.

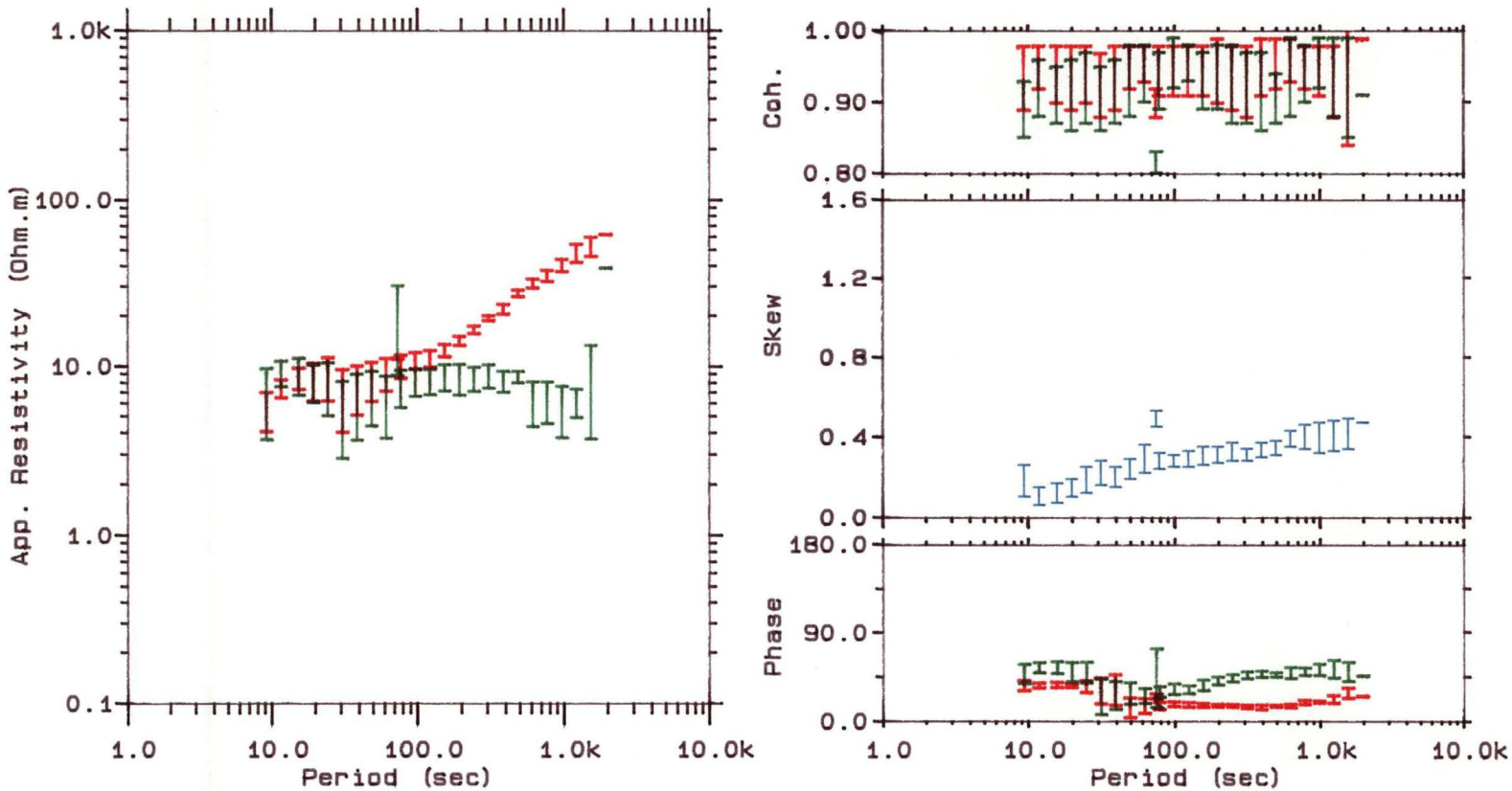

Figure 5.4 App. resistivity, coherency, phase and skew from Kenilworth (KN) (red bars) E-polarization, (green bars) H-polarization

The predicted coherency (see Figure 5.4) for both the TE and TM modes in general is above .9. Based on Swift's (1967) coherency estimation, the presence of noise in this data is therefore generally less than 10 %.

5.2.3 Site 3 Conara Junction (CJ)

This site sits on a brownish clayey sand of Tertiary-Quaternary age and probably overlies basaltic and dolerite rocks of Tertiary and Jurassic age. Boulders and gravels of the basaltic and dolerite rocks can be found scattered almost everywhere on this site. The thickness of the Tertiary-Quaternary sediments at this site is unknown.

A Shlumberger DC-resistivity sounding which was conducted on this site can be seen in Figure 5.15. It is apparent from this figure that the top layer is very resistive. The resistivity of this layer is about 1800 Ohm.m with thickness of 1.8 m. This resistive layer may be due to dolerite boulder and dry basaltic rock found on the surface. The apparent DC-resistivity curve then decreases dramatically to about 100 Ohm.m at half current electrodes spacing of about 40 metres and then drops again to about 16 Ohm.m at half current electrodes spacing of about 1000 metres. The steady decrease of the apparent DC-resistivity with increasing current electrodes spacing is likely to be due to saline Tertiary sediment. Leaman (1971) suggests that saturated Triassic rocks or dolerite could also have resistivities as low as 10 - 20 Ohm.m (see Table 5.2).

Induction arrows analysis from VAU, which is a few kilometres north east of this site, suggests that this site is situated approximately on the axis of the Tamar Conductivity Anomaly. This is shown by the very short induction arrow pointing to south east and bounded by a longer arrow at STJ and HAN, i.e. west and east of the VAU site respectively, pointing in opposite directions (see Appendix 1).

Apparent resistivity curves for both the TE and TM modes, can be seen in Figure 5.5. In general, both resistivity values are even smaller compared to the resistivity on Site 1 and Site 2 thus suggesting that this site sits on a more conducting body. These results agree very well with the result given by the induction arrows analysis. The resistivity curves for TE and TM modes which tend to separate almost at all periods, indicate a strong anisotropy. They cross over at periods of about 300 seconds indicating current flow in opposite directions at different depths.

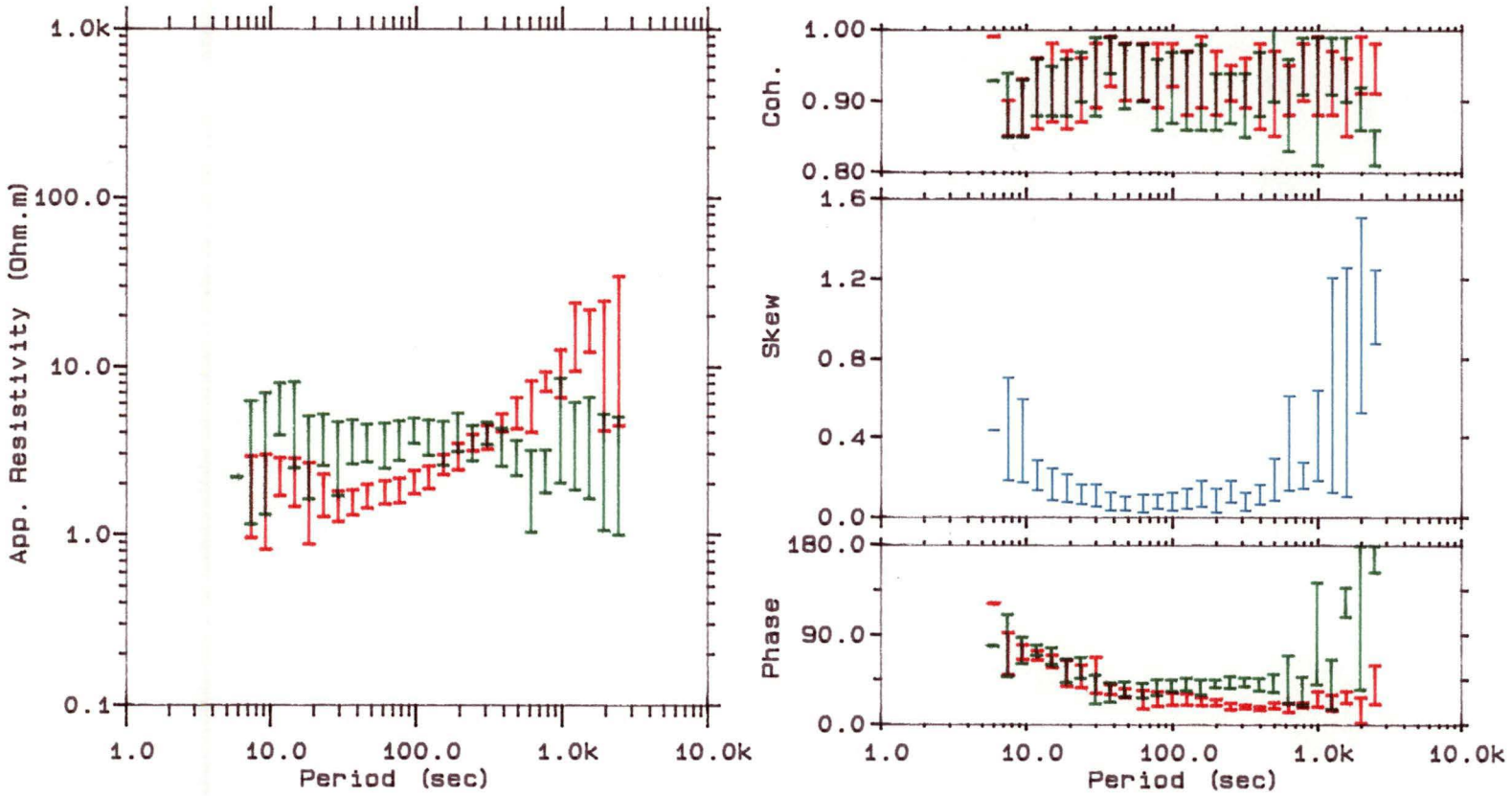

Figure 5.5 App. resistivity, coherency, phase and skew from Conara Jnc. (CJ)
(red bars) E-polarization, (green bars) H-polarization

The predicted coherencies (see Figure 5.5) of above .9 are observed at almost all periods. These coherencies also suggest that the presence of noise in the data is about or less than 10 %.

Figure 5.5 shows plot of skew from this site. In general the skew is very small at periods between 10 and 500 seconds. The skew then becomes large at periods beyond 500 seconds. Based on this skew and apparent resistivity results, it is clear that the structure under this site is approximately two-dimensional at middle depth before it changes to probably three-dimensional at greater depth.

5.2.4 Site 4 Milford (MI)

Site 4 (see Figure 5.1) is situated approximately another 8 km east of Site 3. This site which sits on a clayey sand probably of Quaternary age, is located almost at the southeastern edge of the Longford Tertiary basin. The geological map of this area which is shown in Figure 5.1 shows that to the east and north east of this site the area is mostly covered by Jurassic dolerite and Mathinna beds of Devonian-Silurian age. Granite is exposed about 15 km. north east of this site.

Induction arrows analysis from Hanleth (HAN) (see Appendix 1) which is a few kilometres east of this site suggests that the HAN site is located on the eastern side of the Tamar Conductivity Anomaly and probably close to its boundary. This is shown by a relatively long induction arrow pointing to the west. Since the granite intrusion is only a few kilometres away from the HAN site, the eastern edge of the conductivity anomaly may thus be associated with the wall of granite intrusion. Two-dimensional gravity modelling along this line (see Figure 5.26) shows that the granite is dipping gently to the west and lies beneath MI site at depth of about 7-8 kilometres.

Apparent resistivity curves which are shown in Figure 5.6 indicate that both TE and TM modes apparent resistivities are still relatively small thus suggesting that this station is still within the conductive side of the anomaly. A result from SIROTEM measurement in this site (see section 5.5) illustrates that resistivity rock to a depth of 600 metres is relatively uniform. The resistivity, however, changes dramatically below this layer. This result thus supports the MT result. The TE mode resistivity curve shows a slight variation at periods less than 100 seconds then tends to increase slightly at periods greater than 100 seconds. In general, however, the apparent resistivity curves do not show strong anisotropy. The TE and TM modes resistivity curves tend to separate at periods between 10 and 200 seconds. The curves then merge again at period greater than 300 seconds. These resistivity results

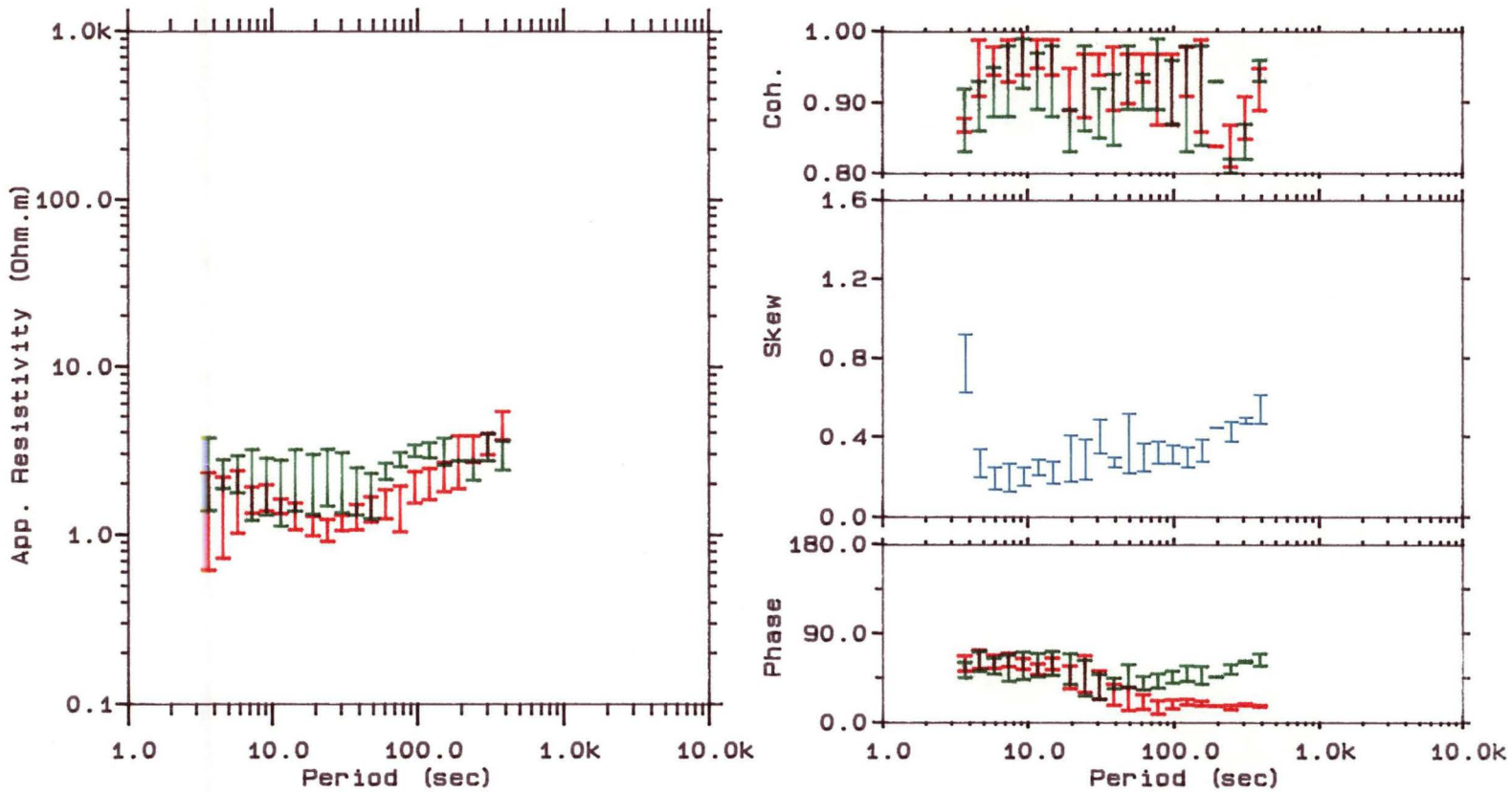

Figure 5.6 App. resistivity, coherency, phase and skew from Milford (MI) (red bars) E-polarization, (green bars) H-polarization

imply that the structure may become more anisotropic at great depth. The anisotropy may be associated with the contact between the sediment and the granite.

The coherencies and skew for all estimates on the apparent resistivities curves are shown in Figure 5.6. Both coherencies generally show good estimation. The skew is also generally low. Except for periods above 200 seconds where the skew is greater than .4, other skew is generally less than .3. The increase in skew toward longer period is also observed at all sites. This feature therefore represents general structure which is no longer two-dimensional and uniform under all sites.

5.2.5 Site 5 Buffalo Brook (BB)

This site is located approximately 7 kilometres south west of the western edge of the granite intrusion. The geological map of this region illustrates that the granite intrusion may be associated with the eastern boundary of the graben like structure. The residual Bouguer anomaly map of Tasmania (see Figure 5.24) also shows that the granite may continue to the north and south. Two-dimensional gravity modelling along this MT traverse (see Figure 5.26) indicates that the granite dips to the west and extends to about 10 km depth.

This site is situated between two MV sites AVO and HAN. Induction arrow analysis from AVO which is a few kilometres east of this site shows a relatively long induction arrow pointing to the south west. This arrow has almost the same length as the arrow at HAN which is a few kilometres west of this site. The length of the arrow tends to decrease toward the eastern MV sites (see Appendix 1). Based on these arrows it is suggested therefore that the BB site may be located very close to or at the edge of the conductivity anomaly.

Skew which is shown in part of Figure 5.7 is very large especially toward longer periods and may result from lateral inhomogeneity contrast where the subsurface structure is no longer isotropic.This skew behaviour is similar to the skew obtained at Site 1 where the site is close to the Bracknell Fault. This skew thus indicates that this site is far from two-dimensional.

Apparent resistivity curves from this site are also shown in Figure 5.7. The TE and TM modes resistivity, in general, are relatively small at all periods and therefore indicate that this site may still be within the conductive anomaly. Dr. W.D. Parkinson (personal communication, 1992), however, states that the low resistivity observed at this site may not represent its true resistivity. As this site is close to the edge of the anomaly, this resistivity may be biased by the presence of a better

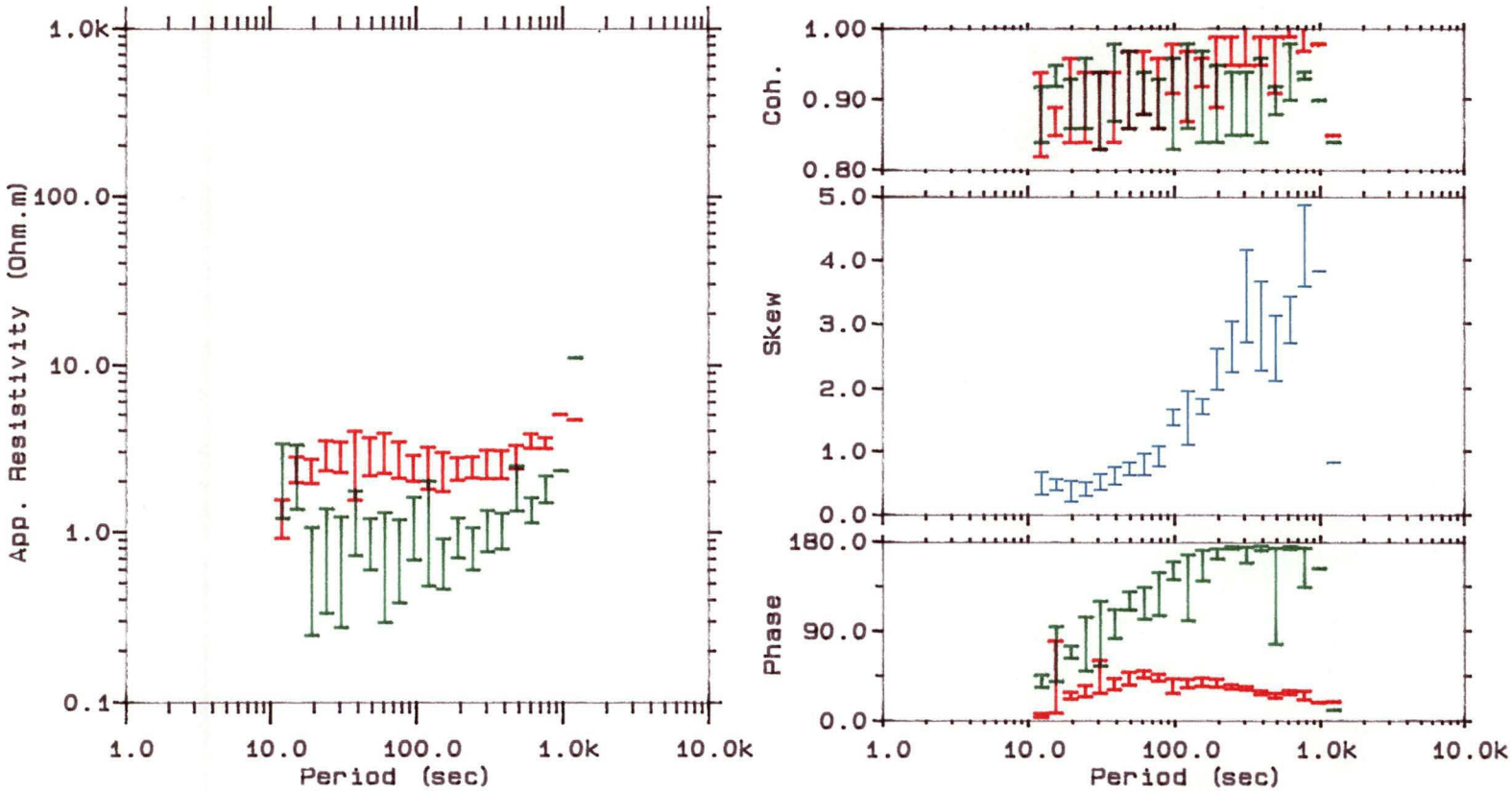

Figure 5.7 App. resistivity, coherency, phase and skew from Buffalo Brook (BB) (red bars) E-polarization, (green bars) H-polarization

conductor from the west of this site. Kurtz (1973) also states that the two-dimensional tensor analysis may not be valid for skew greater than 1.

5.2.6 Site 6 Fingal (FI)

This site, which sits on a clayey sand probably of Quaternary age, was chosen to represent the eastern end of this MT traverse. The reason for choosing this site was to see how far the Tamar Conductivity anomaly extends to the east so comparison between MV and MT results can be made.

There seems to be little known about the subsurface structure in this area except that it consists of Mathinna beds of Devonian - Silurian age whose thickness deduced from a two-dimensional gravity and magnetic model along this traverse is about 3.5 kilometres (see Figure 5.26).

Induction arrow analysis from this site (FNG) shows that the arrow now swings and points almost to the south (see Appendix 1). The direction of the arrow changes slightly to the south east as the period increases. The length of the arrow also gradually increases toward longer periods. This induction arrow clearly shows that this site is not only away from the conductivity anomaly but also experiencing a coast effect as the site gets closer to the east coast.

Apparent resistivity curves which are shown in Figure 5.8 indicate that both resistivity curves increase dramatically as period increases. The resistivity curves also show that the structure under this site seems to be very isotropic. The dramatic increase in resistivity toward longer periods suggests that the subsurface is very resistive. This resistive layer may be associated with granite body which is uniform under this area as is suggested by the two-dimensional gravity and magnetic modelling (see Figure 5.27). This result also agrees with the induction arrow analysis where this site is located well outside the Tamar Conductivity Anomaly.

Skew which is shown in Figure 5.8 is generally above .8. The large skew means that this site is no longer two-dimensional.

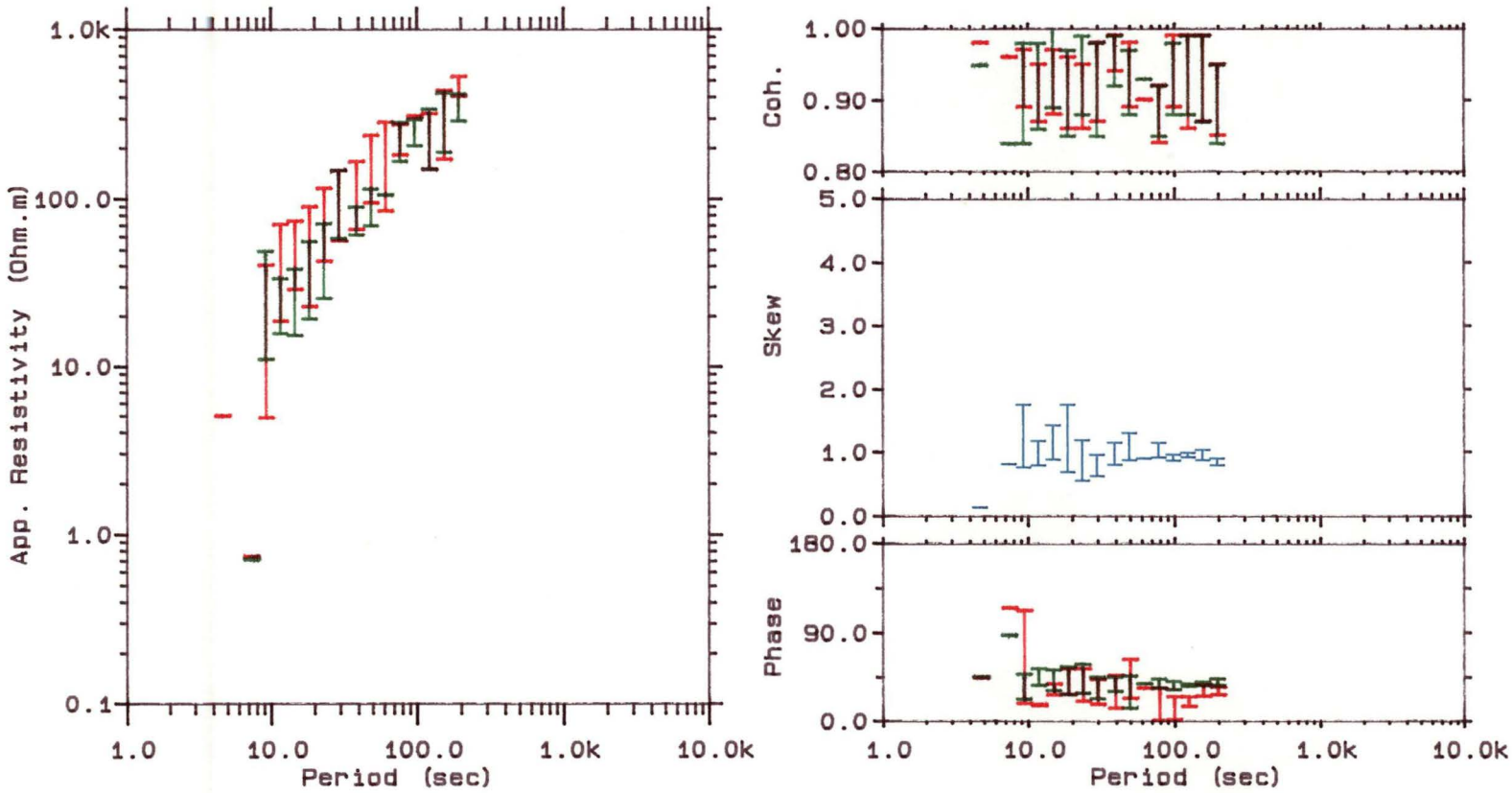

Figure 5.8 App. resistivity, coherency, phase and skew from Fingal (FI)
(red bars) E-polarization, (green bars) H-polarization

5.3 ROTATION ANGLE RESULTS

Rotation angle (θ) analysis was carried out using a program called PTH2.FOR. This program was written by the author during this study based on equations (2.4.13) to (2.4.16) and explanation as given in section 2.4. This analysis was merely conducted to test the new method of determining rotation angle (θ) described in Chapter 2.4. The result from this analysis will not be used in the apparent resistivity analysis as that analysis was carried out using an angle 40° west of magnetic north. This angle (θ) was determined from the regional induction studies in northeastern Tasmania and represents general strike of the conductivity anomaly in this region (Hermanto, 1985). Prior to any analysis the PTH2 program was tested using synthetic data. Results from the test show that the program behaves as expected.

It is apparent from the skew results given in section 5.2 that not all structures under those MT sites exhibit two-dimensionality. Three sites, for example, BI, BB and FI are believed to depart from two-dimensionality as their skews are large. Three other sites i.e. KN, CJ and MI have relatively small skew and therefore can be regarded as to have approximately two-dimensional structure. Only the rotation angle (θ) at KN, CJ and MI sites are then analysed by this new method.

Figure 5.9 shows the result from KN site. Average theta or rotation angle (θ) which is plotted on the left hand side of Figure 5.9 was determined from the average of θ_x and θ_y of equations (2.4.13) and (2.4.16). Average theta that is plotted here is based only on delta theta values, on the right hand side of Figure 5.9, within $\pm$ 20°. Although average theta plot is a little bit scattered at periods less than 200 sec., most of the data however confines within an angle of 12°. This angle represents an anticlockwise rotation. Delta theta which was derived from the difference of θ_x and θ_y of equations (2.4.13) and (2.4.16), can be used as a measure of how closely the structure approximates to two dimensions. Delta theta and average theta are also scattered here. The scattering of the average and delta theta may be due partly to noise which still presents in the data. At period less than 200 sec. most of the delta theta seems likely to peak within $\pm$ 20° and as period increases the data peaks to more than 30°. Based on these peak data the structure under this site is approximately two-dimensional at shallow depth and then changes to possible three-dimensional at great depth. This result is very similar to the result given by the skew from this site (see Figure 5.4).

Figure 5.10 illustrates rotation angle (θ) analysis results from CJ site. Rotation angle (θ) or average theta (see the left hand side of Figure 5.10) determined for this site is approximately 45° (clockwise rotation). This angle was again plotted

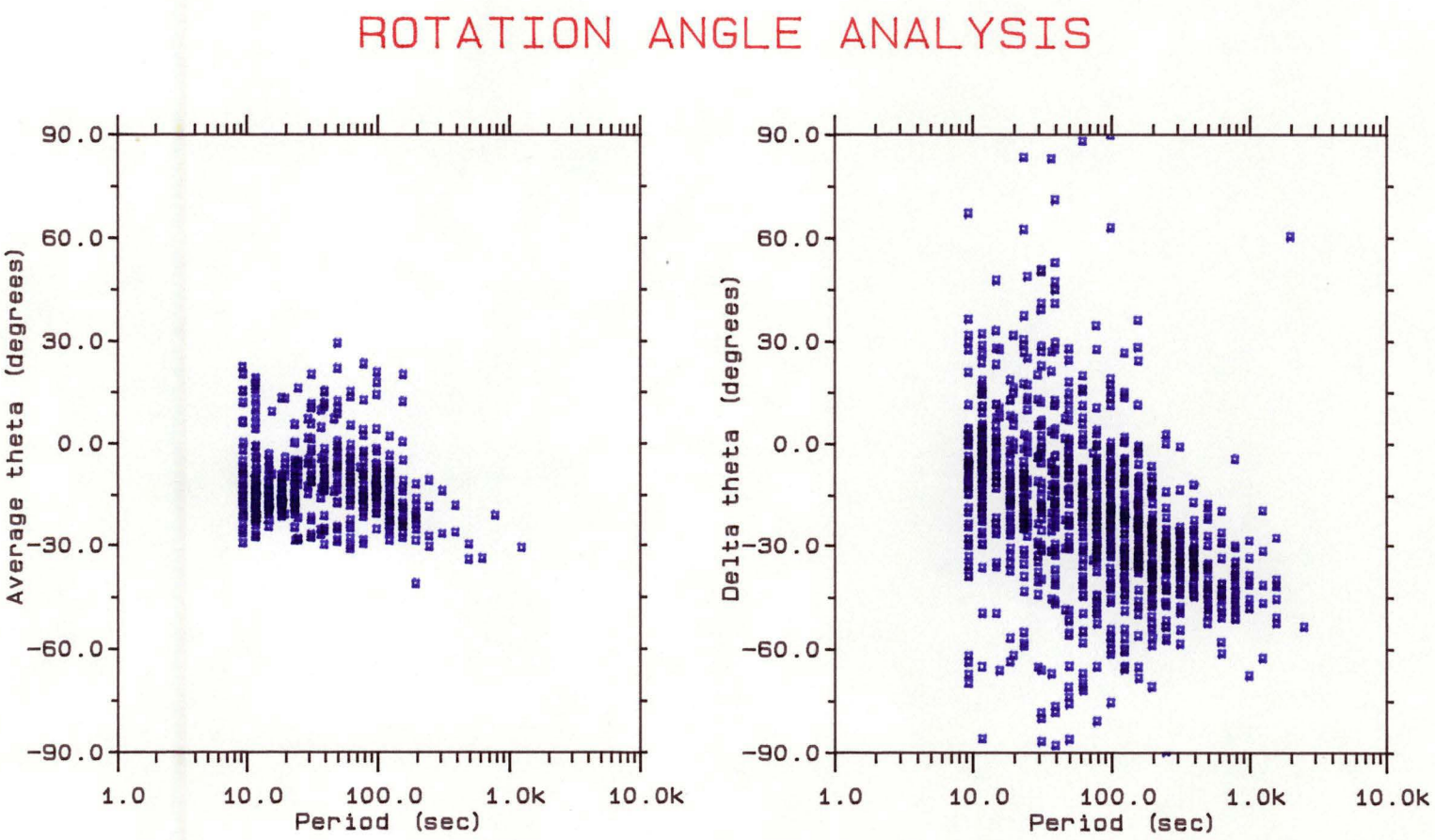

Figure 5.9 Plot of average and delta theta from Kenilworth (KN)

based on delta theta values within ± 20°. Delta theta (see the right hand side of Figure 5.10) is very scattered at periods less than 20 sec. and at periods more than 200 sec. Since noise is still present in the data, these scattered data may therefore be associated with it. At periods between 20 and 200 sec. most data , however, peak to almost zero degrees. Similar to the result given by the skew for this site (see Figure 5.5) where they are very small at periods between 20 and 200 sec., the structure under this site therefore can be approximated to have two-dimensional structure at middle depth which changes to possible three-dimensional structure at great depth.

Rotation angle (θ) analysis result from MI site can be seen in Figure 5.11. This figure shows that rotation angle (θ) or average theta determined for this site is about 25° (clockwise rotation). Delta theta (see right hand side of Figure 5.11) shows that at periods less than 200 sec. most of the data confines to an angle within ± 20°. Delta theta plot is also very similar to the skew plot for this site (see Figure 5.6). It is believed therefore that the structure under this site is also approximately two-dimensional at shallow depth and then changes to possibly three-dimensional at great depth.

5.3.1 DISCUSSION

The rotation angle (θ) determined for sites KN, CJ and MI seems to vary from one site to another and can be interpreted to be due to different structures. This is not surprising since general tectonic setting over this region seems to be very complex. This is apparent from the structural and tectonic interpretation based on the gravity and aeromagnetic data (see Figure 5.12). MT surveys conducted over this area therefore not only map the structure associated with the Tamar Lineament which is a regional tectonic feature but also map local structure due to complex faultings.

Rotation angle (θ) determined for site CJ which is about 45° (clockwise rotation) is the only angle that is very similar to the angle used in the tensor analysis i.e. 40° (anticlockwise rotation) (see section 5.2) to rotate the observed MT axes to their principal direction. Note that the angle 45° (clockwise rotation) is equivalent to the angle 45° (anticlockwise rotation) in a way that by clockwise rotation the resistivity maximum obtained is ρ_{yx} and by anticlockwise rotation the resistivity maximum obtained is ρ_{xy}. Thus these two systems of rotation will find the same maximum principal direction where maximum current flows. One of the reasons that only the CJ site finds rotation angle (θ) very similar to the one used in the tensor analysis seems to be that this site is approximately situated in the middle of the Tamar Conductivity Anomaly and seems to indicate a much broader and wider anomaly

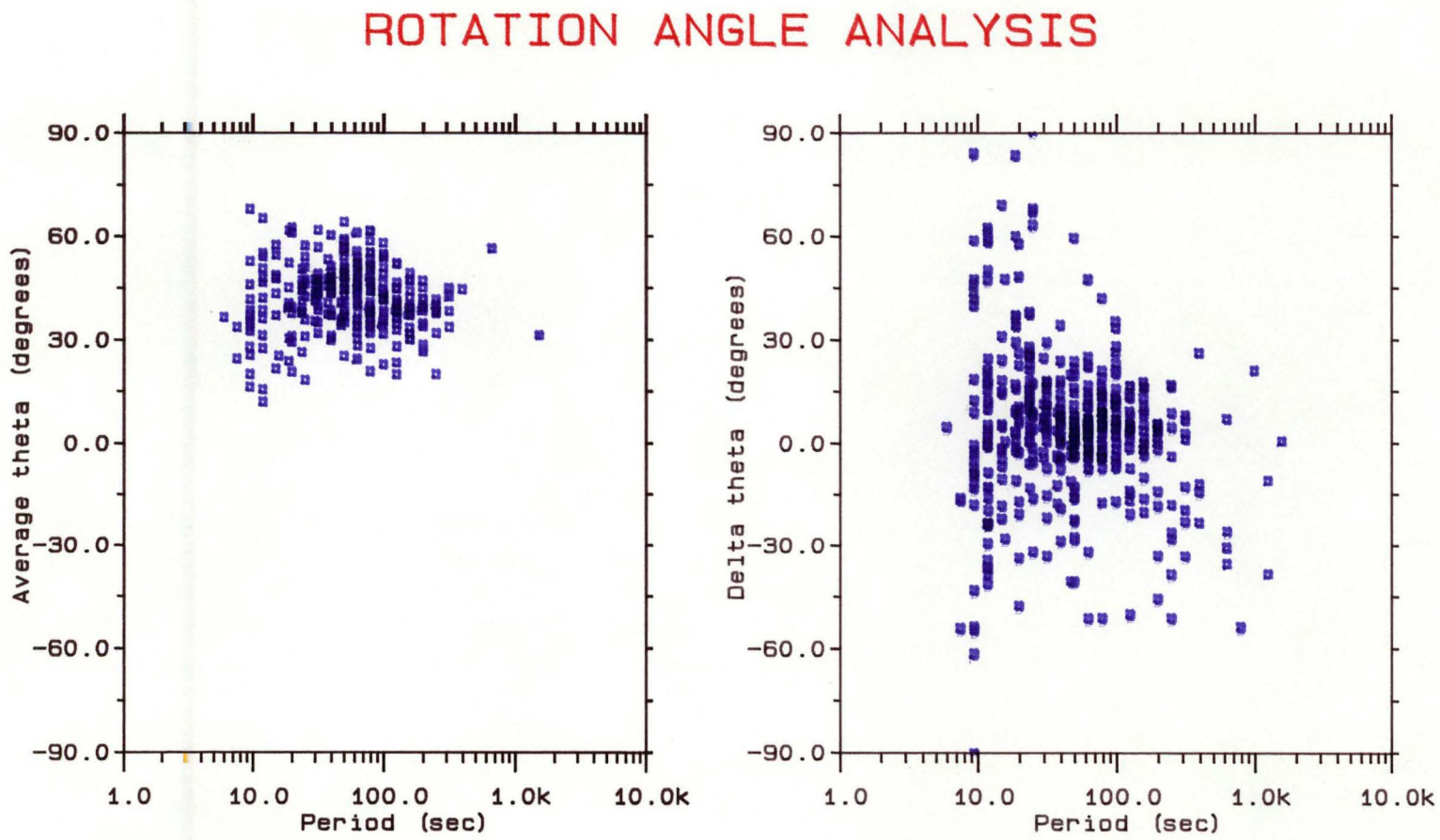

Figure 5.10 Plot of average and delta theta from Conara Jnc. (CJ)

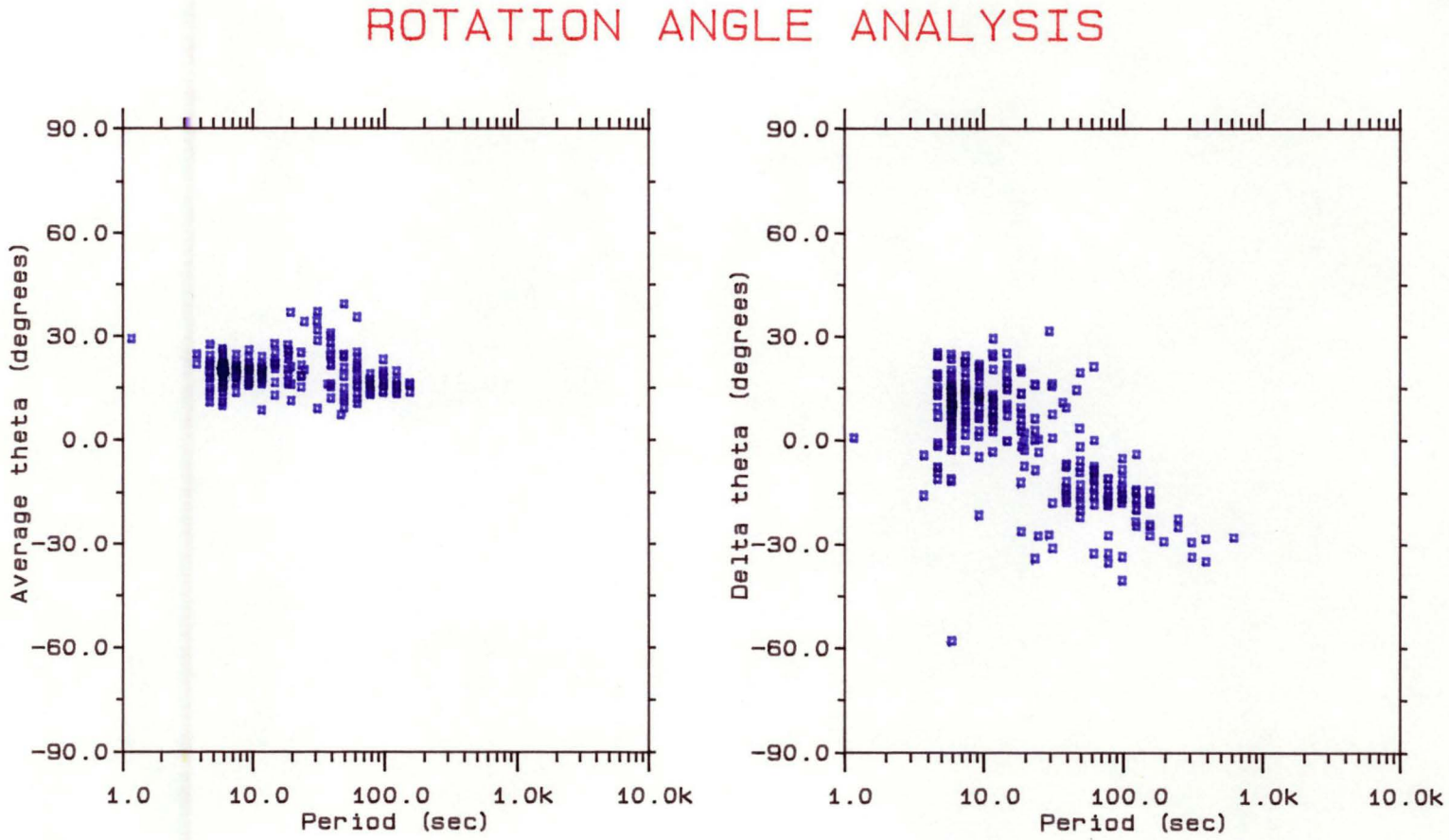

Figure 5.11 Plot of average and delta theta from Milford (MI)

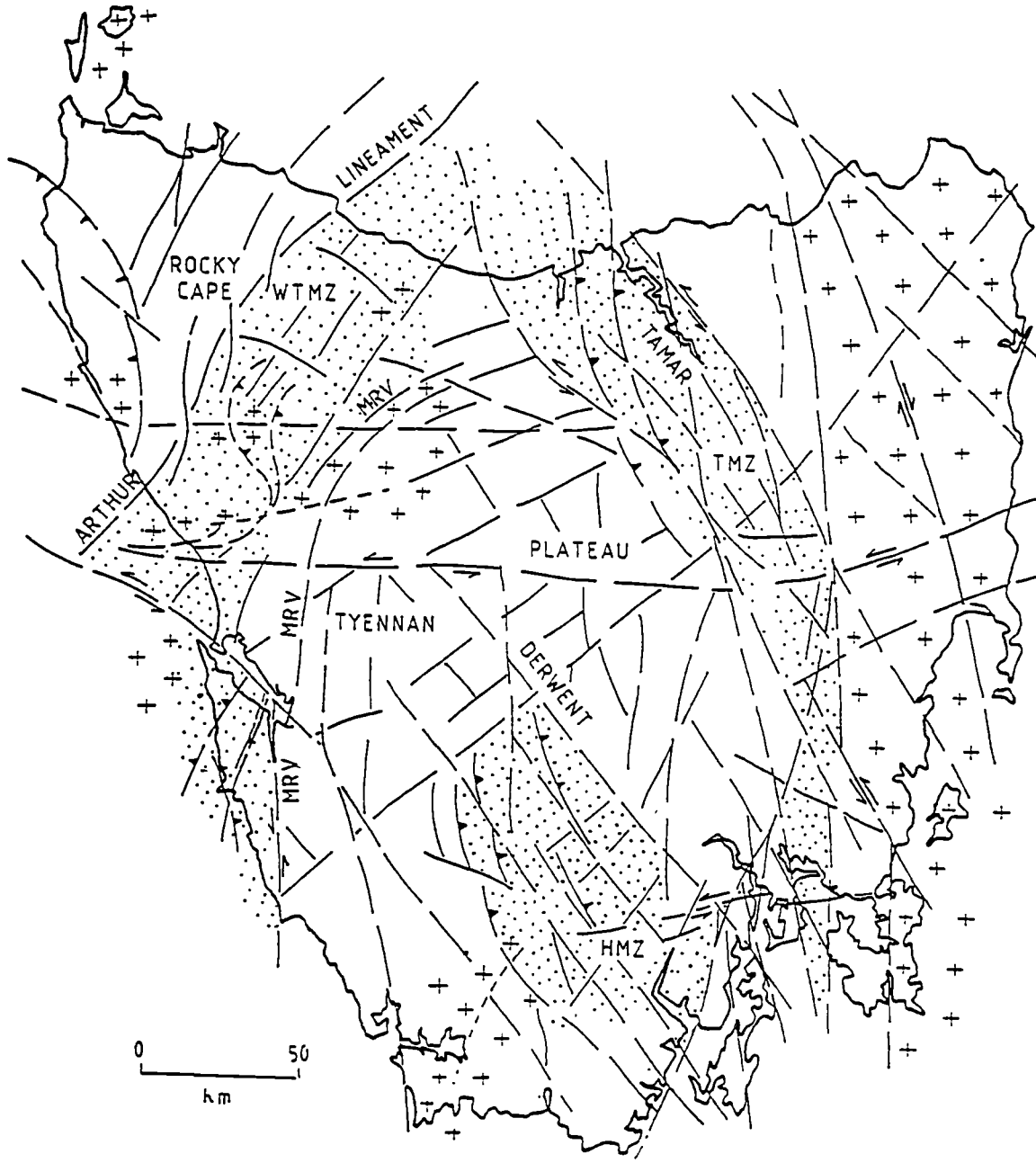

Figure 5.12 Structural and tectonic interpretation based on gravity and aeromagnetic data showing major tectonic elements. After Leaman and Richardson (1990).

compared to sites KN and MI. As the sites get closer to the east and west boundary of the anomaly they may be influenced by the shape of its boundary which may not be symetrical.

Dwipa (1992) has applied this new method to determine rotation angle (θ) at Judbury, southeast Tasmania. Figure 5.13 shows the result of that analysis. It can be seen here that both average and delta theta plot are good and very few of these data are scattered. The rotation angle (θ) or average theta determined for this site (see the left hand side of Figure 5.13) is about 45° and agrees very well with the approximate strike of the Huon Mobile Zone (HMZ) i.e. the major tectonic feature in Dwipa's region. Most of the delta theta (see the right hand side of Figure 5.13) also lies very close to zero degrees thus showing a good estimate of two-dimensionality. The Judbury (JDB) site is approximately situated on the middle of the HMZ. For other MT sites which are located close to the boundary of the HMZ, Dwipa (1992) finds different rotation angle (θ) values. These results again are similar to the results obtained in the area of this study i.e. at KN, CJ and MI and may be due to the same problem i.e. the boundary of the structure is not symetrical.

Parkinson et al. (1992) have used Lilley's (1992) Mohr circle method to determine the rotation angle at JDB and compared this result with their simple rotation angle method result at the same site. They find that the rotation angle differs by about 8°. These results, therefore, show that the new method of determining rotation angle (θ) works quite well.

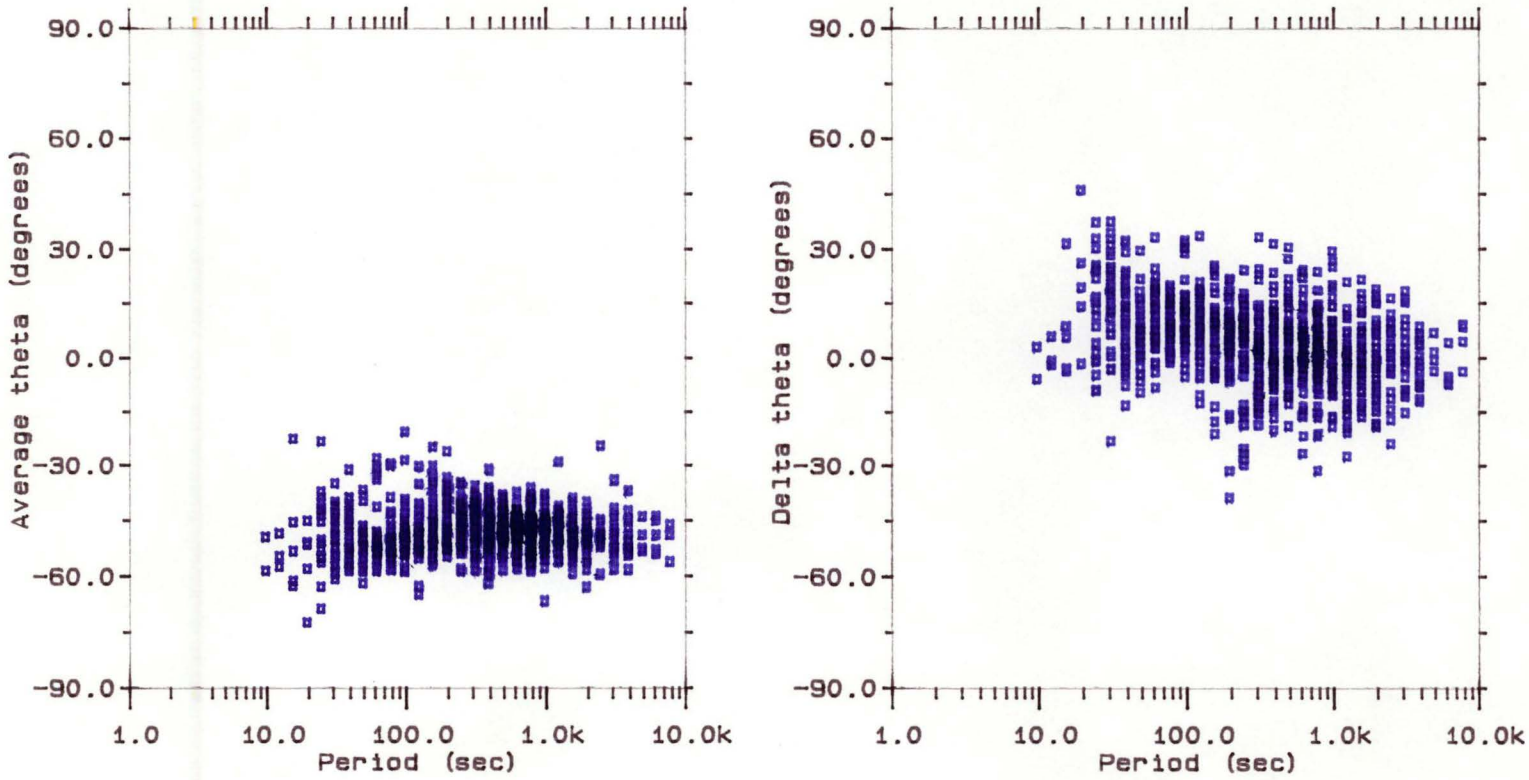

Figure 5.13 Plot of average and delta theta from Judbury (JDB)

5.4 OTHER GEOPHYSICAL STUDIES

5.4.1 DC-RESISTIVITY SOUNDING

5.4.1.1 INTRODUCTION

The use of DC-resistivity sounding to study the deep electrical structure of the earth's crust has been increasingly recognised following the development of instrumentation with high sensitivity and increased signal to noise ratio. These deep resistivity studies have been carried out by observers in many parts of the world, using either Schlumberger or dipole methods. Such studies have been reported in the USA by Cantwell et al. (1965): Keller (1968): Zohdy and Jackson (1969): Edwards (1976); in Europe and South Africa by Schlumberger & Schlumberger (1932): Blohm & Flathe (1970): van Zijl et al. (1970); and in Australasia by Henderson and Emerson (1969): Bosum and Homilius (1973): Constable et al. (1984).

The use of this technique has several advantages compared to the natural sources utilized by conventional MT and MV methods. The controlled signal source is more dependable compared to unpredictable strength and direction of the source in MT and MV and this reduces the complexity of data acquisition. Detailed information on subsurface lithology and depths can be obtained from resistivity sounding very quickly without requiring a laborious process in data reduction before interpretation can be carried out.

5.4.1.2 RESULTS AND INTERPRETATION

Two electrical sounding measurements were carried out at one of the MT sites i.e. Conara Jnc (CJ) using Schlumberger and dipole-dipole techniques. The main aims of this sounding experiment were to study the electrical structure of the upper crust in the region and in the vicinity of the Tamar Conductivity Anomaly and to obtain a better depth determination to the top of the conductor. In the Schlumberger technique a separation of up to 2000 metres between two current electrodes was used. In the dipole-dipole technique, on the other hand, a dipole separation of 200 metres was used and up to five dipole positions were measured at each array position.

The resistivity instrument used for the measurements was a home-built transmitter and a Geoscience receiver unit. Details of this instrumentation are given by Salman (1992).

Resistivity measurements are based on the fact that different rock types or formations pass different resistivity properties. In the resistivity sounding

measurement, the resistivity of rocks is measured as function of depth. In practice, it is normally conducted by applying a direct current to the ground via two current electrodes (A and B), and the resulting potential difference which occurs due to current flowing in the ground, is then measured via two potential electrodes (M and N). The distance between the current and potential electrodes is normally increased depending upon the electrode arrangement, so that potential difference as a function of depth can be measured.

In non-homogeneous earth the resistivity of rocks can be calculated by :

$$\rho_a = K \frac{\Delta V}{I}$$

where K is the geometric factor in metres; ΔV is potential difference in Volts; I is current in Amperes and ρ_a is apparent resistivity in Ohm.m. Figure 5.14 shows Schlumberger and dipole-dipole electrode arrangements together with their geometric factors.

In the Schlumberger technique, the electrical sounding curve is derived by plotting observed apparent resistivity against half distance between current electrodes or AB/2. In the dipole-dipole technique, on the other hand, the observed apparent resistivity is normally plotted as a pseudo-section.

Figure 5.15 shows the observed Schlumberger apparent resistivity result. Qualitative analysis of the Schlumberger field curve suggests that the top-most layer is thin and very resistive. This result agrees very well with the surface geology of that site which is mostly covered by dry boulders of dolerite and basaltic rocks. As current electrodes separation is gradually increased the resistivity curve decreases very rapidly suggesting that the rock just below the surface is very conductive. The resistivity which again decreases beyond the AB/2 of 50 metres suggests that at greater depth the rock becomes more conductive than the overlying layer.

The Schlumberger sounding result was interpreted using a program written by Dr. D.E. Leaman and modified by B.D. Weldon. This program is based on the method of Ghosh (1971) and the refined filter coefficients of O'Neill (1975).

Quantitative analysis of this curve is shown in Figure 5.16. The calculated curve that fits the observed curve is based on the model shown on the right hand side of Figure 5.16. The agreement between these curves is very good especially at large AB/2 spacings. The slightly misfitting curves at small AB/2 spacings may be due to near surface lateral inhomogeneities at one of the potential electrodes.

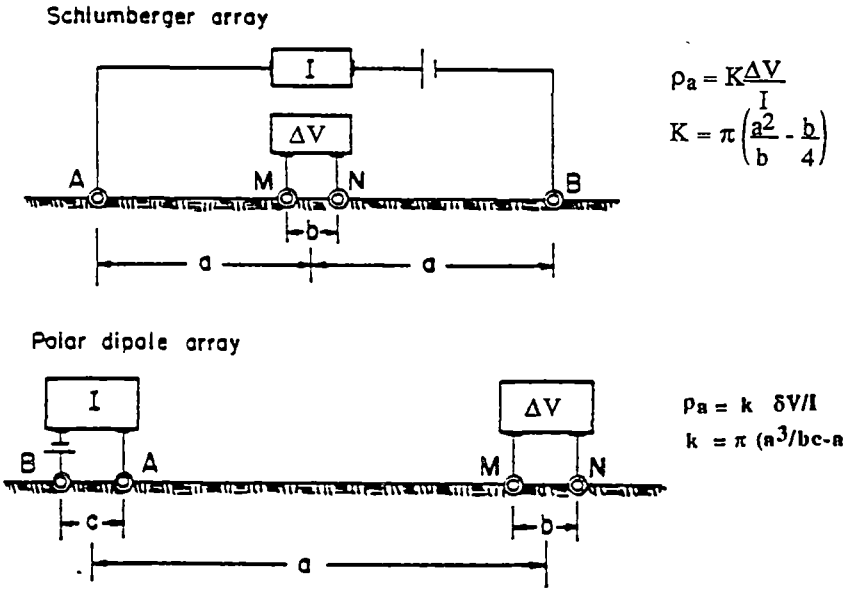

Figure 5.14 Shlumberger and dipole-dipole elctrode arrangements including their geometric factors.

Table 5.2

Field and laboratory resistivity measurements (after Leaman, 1971,1973)

Rock unit	Resistivity (Ohm.m)	
	Dry	Wet
Quaternary		
- alluvials	10 - 150	1 - 20
Tertiary		
- sediment	10 - 30	<1 - 10
Jurassic		
- dolerite	> 5000	30 - 1000
Triassic		
- sandstone	50 - 500	15 - 100
Permian		
- mudstone	100 - 5000	5 - 100
Devonian		
- granite	> 5000	100 - 1000
Devonian/Silurian		
- turbidite	50 - 600	5 - 100
Cambrian		
- volcanics	50 - 300	10 - 100
Precambrian	100 - 5000	------

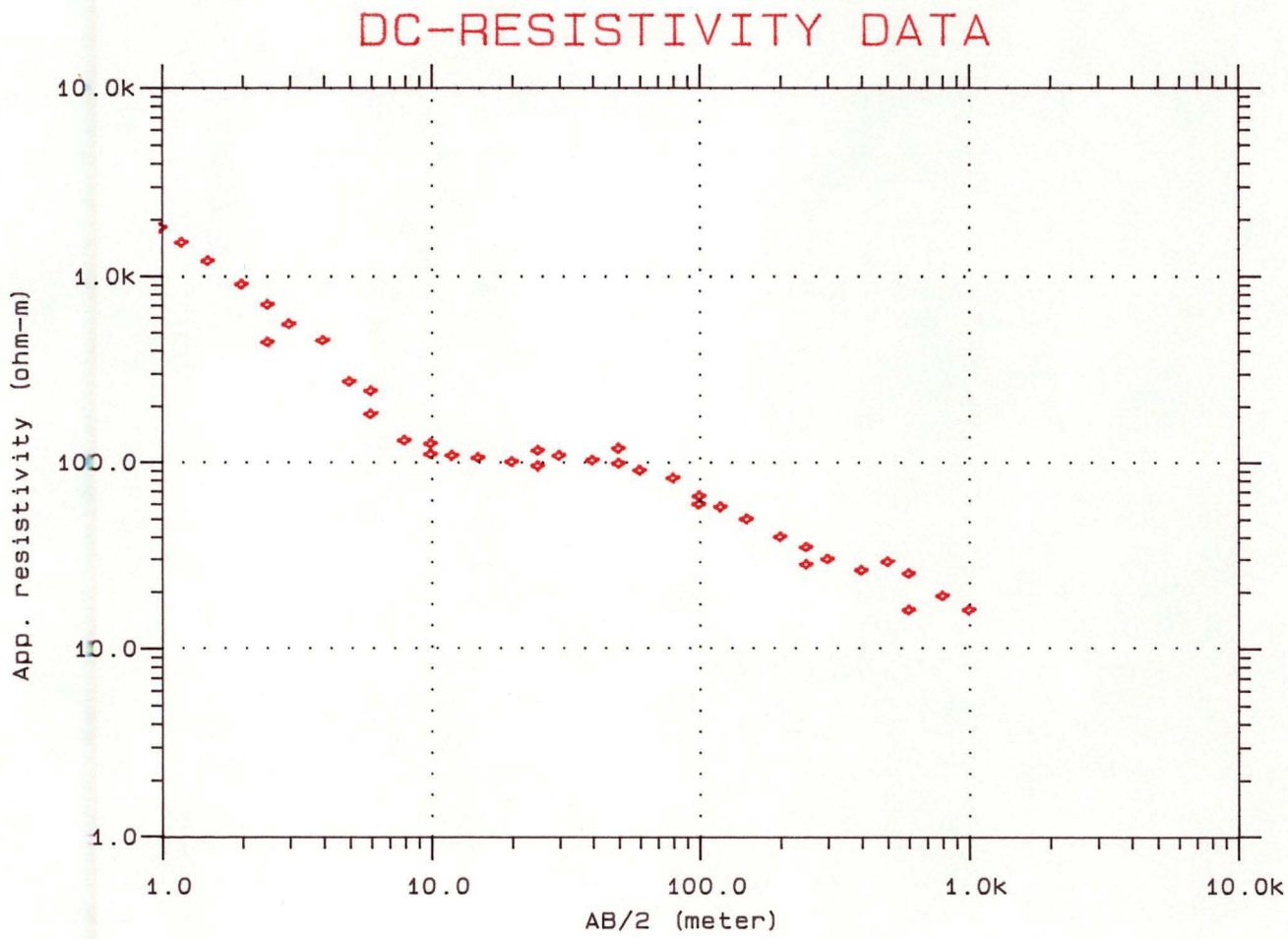

Figure 5.15 Observed Schlumberger sounding results

The model that fits the observed curve has five resistivity layers with varying thicknesses. The top 50 metres of this model can be compared with the results obtained from the shallow groundwater investigation holes 58 and 59 which are located about 3 kilometres east and north-west of this site. Although no electric log measurement was conducted to measure the resistivity from these holes, both the resistivity curve and the drilling results show good agreement. The top layer of this model, for example, has resistivity of 1800 Ohm.m with thickness of 1.8 metres. This layer may be due to dry soil on the surface. The resistivity of the second layer decreases dramatically to 150 Ohm.m at about 2 metres. Hole 59 also illustrates that this layer may consist of weathered basalt with mainly clay. The amount of clay sediment is believed to have significant impact in lowering the resistivity of this layer. The third layer has resistivity of 90 Ohm.m and thickness of 50 metres. Investigation hole 58 (Matthews, 1983) shows that this layer may consist of light grey clay and sandy clay becoming more sandy below the 50 metres depth. The resistivity of the fourth layer decreases to about 16 Ohm.m. This layer has a thickness of about 500 metres. The shallow drillings in the vicinity of this site were stopped mainly at depth of about 60 metres. Correlation to this model therefore uses resistivity results from laboratory measurements. The laboratory resistivity rock measurement was carried out in both dry and wet conditions with salinity of water used less than 500 ppm. Based on the gravity and magnetic modelling (see Figure 5.26) the fourth layer may belong to a group of Tertiary, Jurassic and Triassic rocks. Table 5.2 indicates that in wet conditions the Tertiary and Triassic rocks may have resistivity ranging from 1 to 30 Ohm.m (Leaman, 1971, 1973). This result therefore supports the fourth layer interpretation. It is very difficult to verify the thickness of this layer based only on this interpretation since the resistivity measurement stopped at AB/2 of 1000 metres. It appears from Figure 5.15, however, that the observed resistivity curve seems to continue, decreasing at AB/2 beyond 1000 metres spacings. If that is the case then the thickness of the fourth layer may also be more than the present interpretation. The basement of this model interpretation has resistivity of 5 Ohm.m. This low resistivity was also observed by the dipole-dipole technique (see Figure 5.17).

Figure 5.17 illustrates a pseudosection apparent resistivity result from a dipole-dipole resistivity measurement. It is apparent that the resistivity changes very smoothly across the traverse. This resistivity shows that the subsurface layer is uniform and very conductive. The low resistivity layer with a resistivity of less than 10 Ohm.m is observed in the middle of the traverse up to the fifth dipole measurements. This low resistivity layer, which coincides with location of MT and DC-resistivity sounding measurements, was also observed by the Schlumberger technique (see Figure 5.15). The results thus show that at large electrode spacings both techniques are compatible.

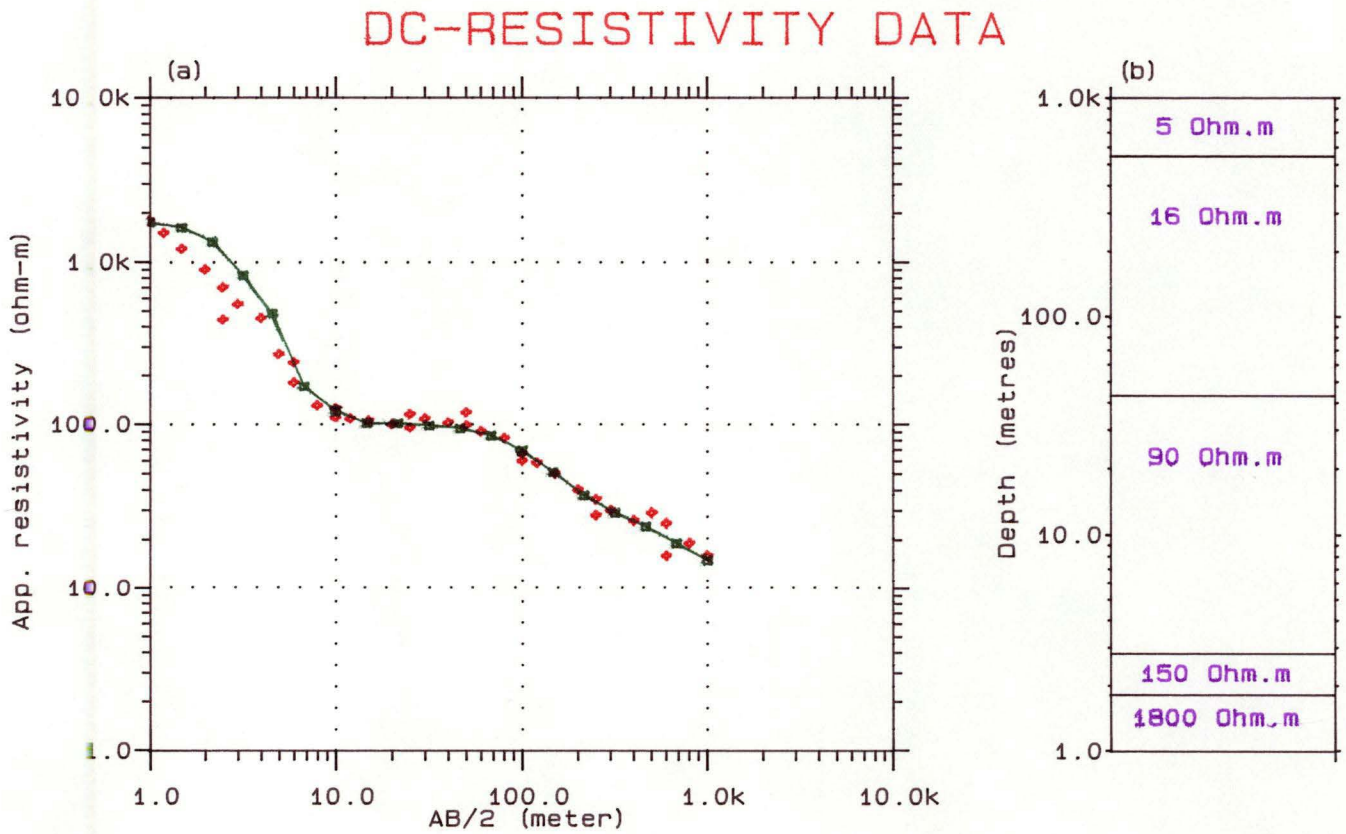

Figure 5.16 (a) Schlumberger vertical electrical sounding results
(red)-observed, (green)-calculated
(b) Layer model for (a)

Figure 5.18 shows correlation between resistivity as a function of depth determined from the pseudosection and two-dimensional MT modelling result at CJ site. It is apparent that the agreement between the two results is quite good. The resistivity and depth from the pseudosection is also similar to the resistivity and depth of the fourth layer of the Schlumberger electrical sounding interpretation. The pseudosection and the electrical sounding interpretation results thus support the one- and two-dimensional interpretation (see Figures 6.7 and 6.11a) that the depth to the top of the Tamar Conductivity Anomaly is about 700 metres. This suggests that the Tamar Conductivity Anomaly is sourced beneath the base of Permian unconformity. Drilling results some kilometres south of Conara Junction and provisional analysis of the Midlands for Conga Oil by Dr. D.E. Leaman (personal communication, 1992) indicate that the folded pre-Permian basement rocks lie between 600 and 900 metres in the centre of this region. Banks and Baillie (1989) imply that Siluro-Devonian Mathinna Beds underlie the unconformity, a view supported by Leaman (1992). The Tamar Conductivity Anomaly is thus associated, at least in part, with these rocks.

One of the objectives of these galvanic resistivity measurements was to determine a static shift correction to the MT results. The agreement shown in Figure 5.18 indicates that no static shift needs to be applied.

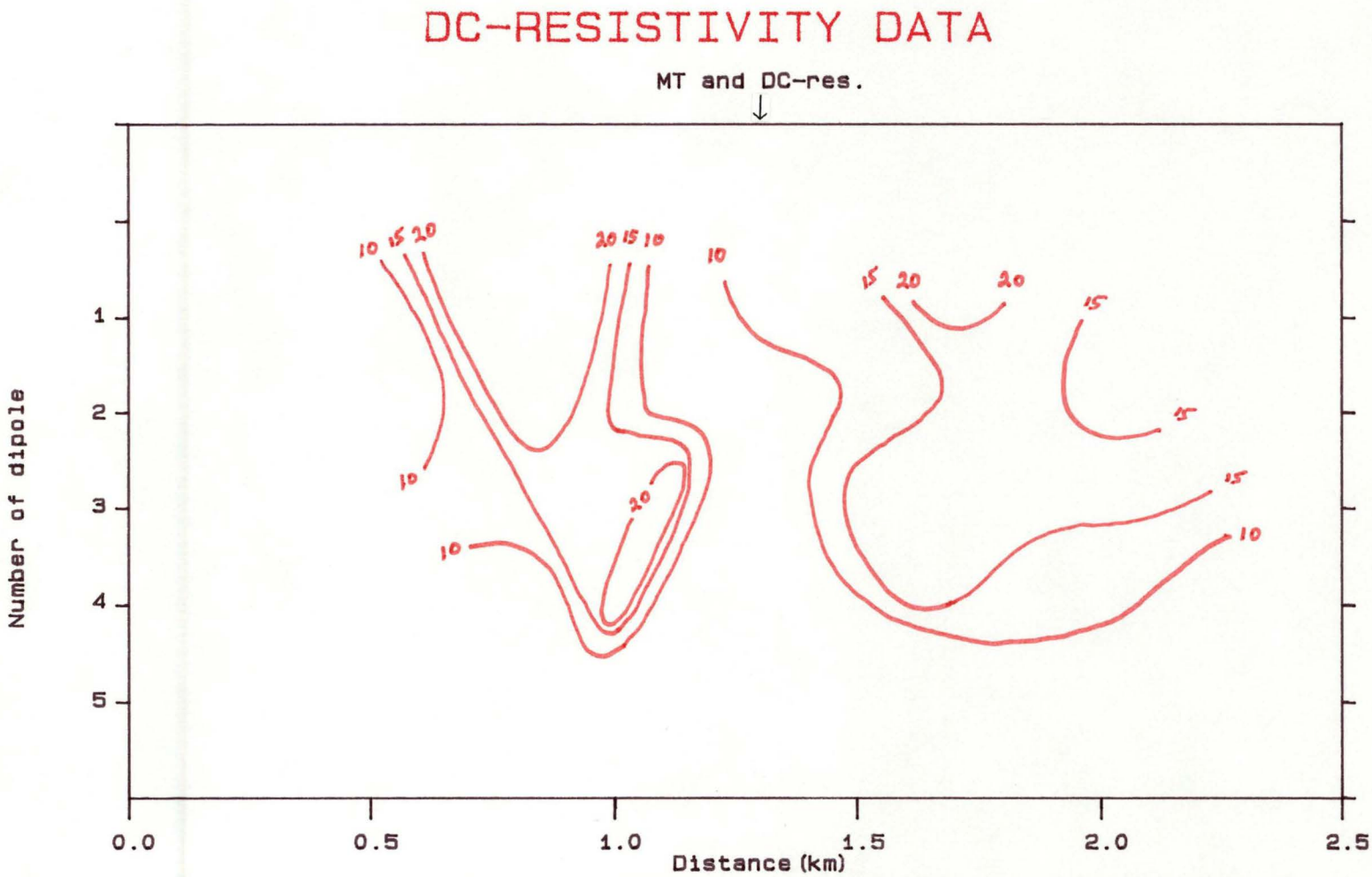

Figure 5.17 Pseudosection app. resistivity from Conara Junction (CJ)

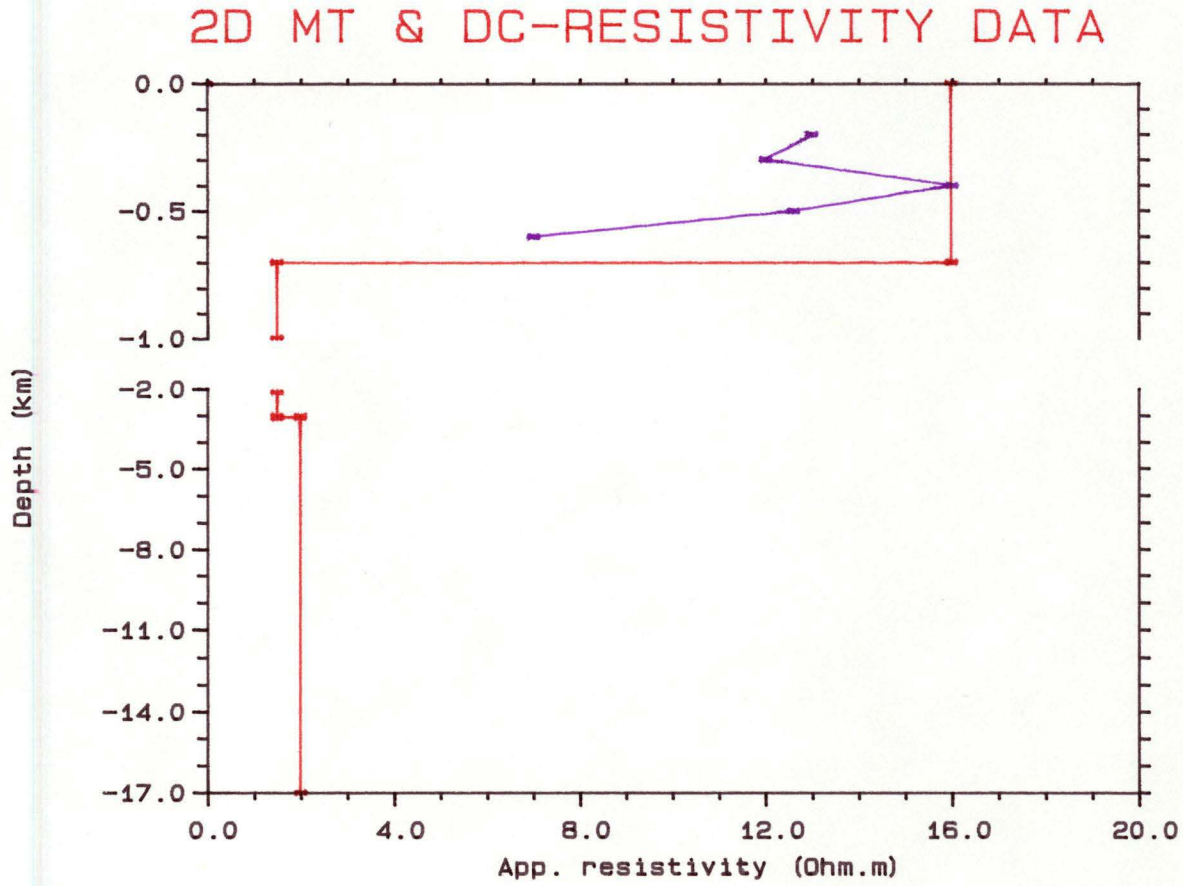

Figure 5.18 Comparison of resistivity as a fuction of depth used by the 2D MT model (red) and determined from vertical section of pseudo resistivity data (purple) at Conara Jnc. (CJ).

5.4.2 TRANSIENT ELECTROMAGNETIC SOUNDING

5.4.2.1 INTRODUCTION

Transient electromagnetic (TEM) also known as Time Domain electromagnetic (TDEM) sounding has been used widely especially in prospecting for mineral deposits. Such studies have been reported by Buselli (1977), Staltari (1986), and Macnae and Irvine (1988). Raiche and Sugeng (1989) also used the TEM response to study complex structures. Sternberg et al. (1988) and Pellerin and Hohmann (1990), on the other hand, applied this sounding technique in conjunction with magnetotelluric technique to remove static shift from magnetotelluric data.

This study used the SIROTEM system (Buselli, 1974). This technique basically operates on the same principle as any TEM sounding technique where the voltage decay is measured as a function of time induced in a receiver loop due to rapidly terminating current in a transmitter loop to provide information on the subsurface conductor. Spies (1976) discusses the principles involved.

5.4.2.2 RESULTS AND INTERPRETATION

Two SIROTEM soundings were carried out to measure the transient response at Kenilworth (KN) and Milford (MI) with the main objective to deliniate the subsurface rocks sequences in the vicinity of the Tamar Conductivity Anomaly, to obtain a better depth estimation to the top of the good conductor, and to use it as a guide for static shift correction in magnetotelluric data. The SIROTEM instrument used for this measurement was SIROTEM Mark-I. A detailed description of this instrumentation can be found in Buselli (1974), Buselli and O'Neill (1977) and van Zijl (1986). There are some different kinds of loop configurations available for the SIROTEM system. A coincident loop configuration for the transmitter and receiver (Spies,1976; Buselli, 1982), for example, with each side of the loop of 100 metres, was chosen for these measurements.

Figure 5.19 illustrates the observed transient response vs. delay time for KN and MI sites. These results were interpreted using the PANCAKE program courtesy of Liddington Technology Pty. Ltd. This interpretation was carried out on IBM-PC compatible. The PANCAKE program calculates matched transient response, calculated apparent resistivity, and final resistivity and layer thickness. The calculation takes as input data the number of layers to be calculated, an initial model, observed transient response and other parameters required by the program. The program best fits a model in a least square sense.

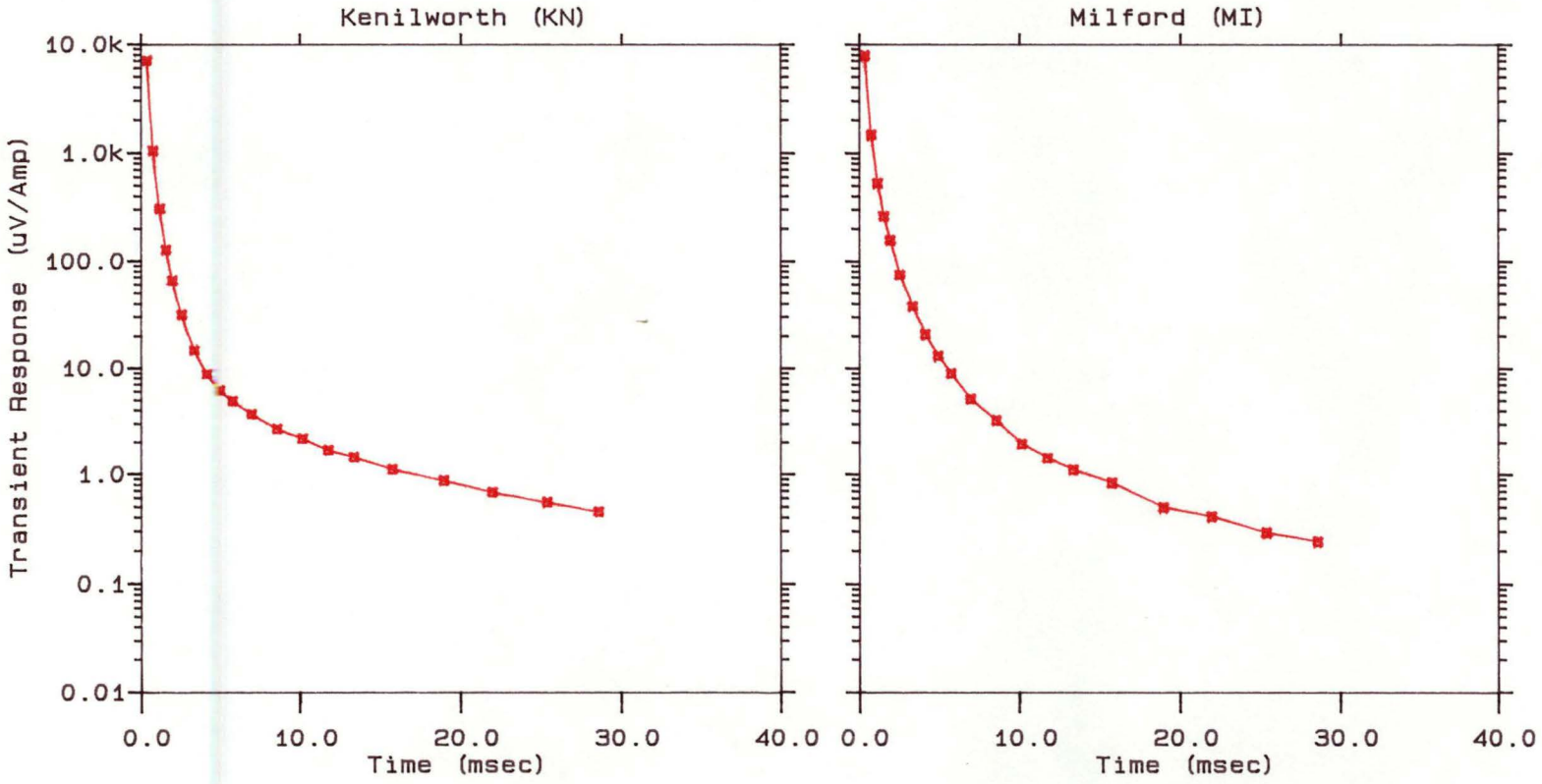

Figure 5.19 Observed transient response

Figures 5.20 and 5.21 show the best fitting results for KN and MI sites, respectively. The initial and final layer model is also included in these diagrams. The fitting between the observed and calculated curves both for the transient response and apparent resistivity are reasonably good. It can be seen here that the final models indicate consistency at both sites where they have very similar shallow and basement resistivities. The thickness of these layers tends to increase towards MI site. The resistivity of the top layer, which is between 15 and 16 Ohm.m with thickness between 50 and 200 metres, may represent the Quaternary and Tertiary rocks, whereas the resistivity of 25 to 37 Ohm.m with thickness between 300 and 400 metres for the second layer may be associated with wet dolerite. The resistivity and thickness of these layers are approximately similar to the resistivity and thickness of the fourth layer determined by the DC-resistivity sounding. The resistivity of the basement layer ranging from 2 to 3 Ohm.m is likely to be due to wet saline Triassic rocks. This resistivity is again very similar to the resistivity of the basement layer interpreted by the DC-resistivity sounding. The two sounding techniques are therefore considered to give similar results and interpretations. These resistivity values are in accord with the resistivity values of those rocks determined from the field and laboratory measurements by Leaman (1971, 1973), (see Table 5.2).

5.4.2.3 STATIC SHIFT

Berdichevsky and Dmitriev (1976), and Sternberg et al. (1988) stated that the presence of charges on local surficial or near surface, lateral inhomogeneities can produce erroneous data and hence can lead to erroneous interpretations. This phenomenon has been known for quite some time as static shift (Bahr, 1988; Jiracek, 1988; Jones, 1988; Sternberg et al. 1988; Pellerin and Hohmann, 1990). In regions where the surface layer is very resistive this problem becomes evident (Jones, 1988) and some examples concerning this problem may be found, for example, in Berdichevsky et al. (1980), and Kurtz et al. (1986).

Sternberg et al. (1988) points out that the near surface effect is easily recognised when two MT results from very close spacing, say 100 metres apart, are identical but shifted, along vertical axes, parallel to one another. They further imply that the amount of parallel shift, however, cannot be assessed directly from conventional recorded MT data at a single station. Hence, one way of measuring the amount of static shift is by employing a controlled-source technique to measure the magnetic field component only. Compared to the electric field, the magnetic field components are relatively undisturbed by near surface or lateral inhomogeneities. The controlled-source technique that is applied in this study is SIROTEM. Different ways of removing

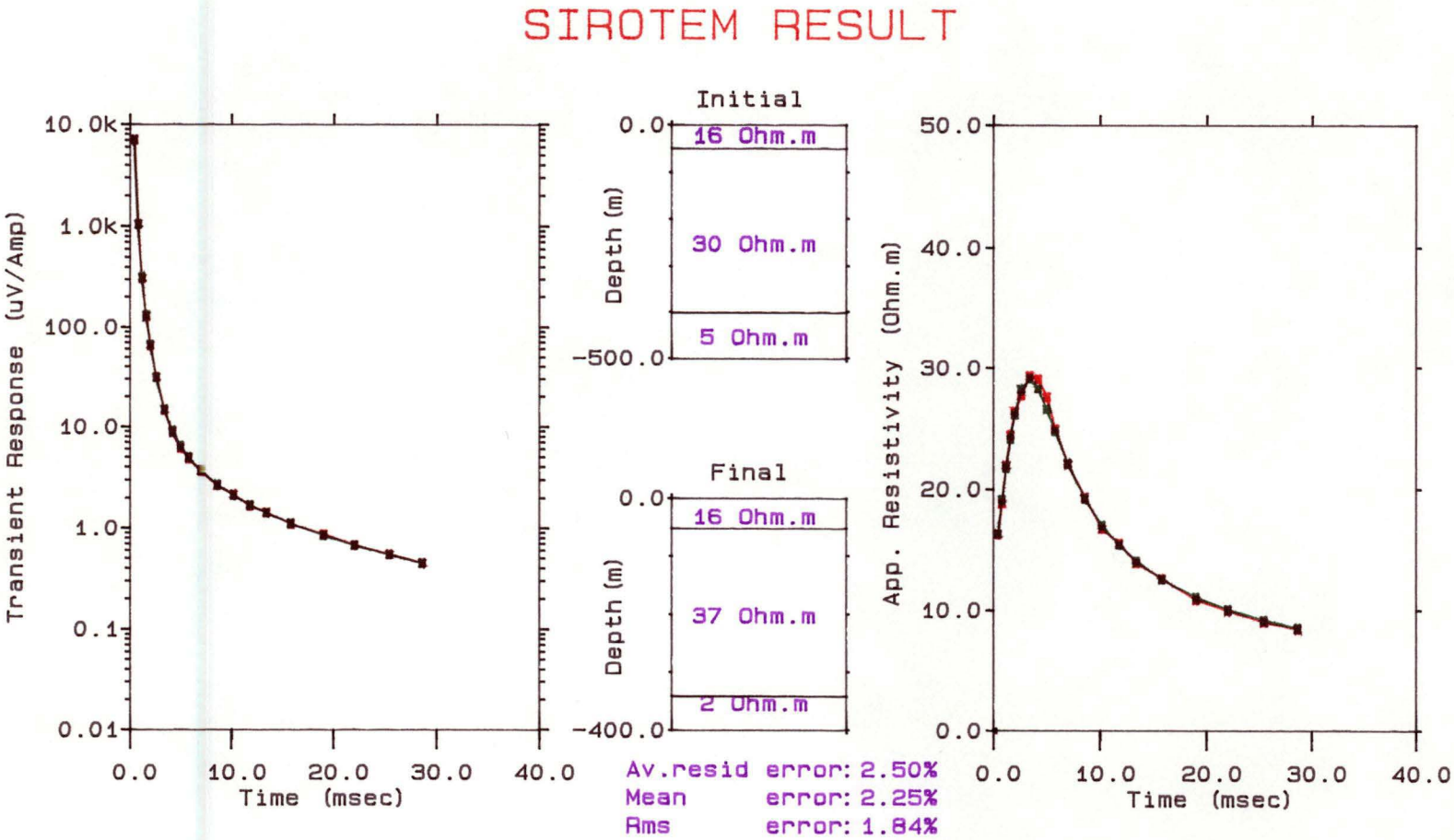

Figure 5.20 SIROTEM modelling results from Kenilworth (KN)
(red) -observed; (green) -calculated

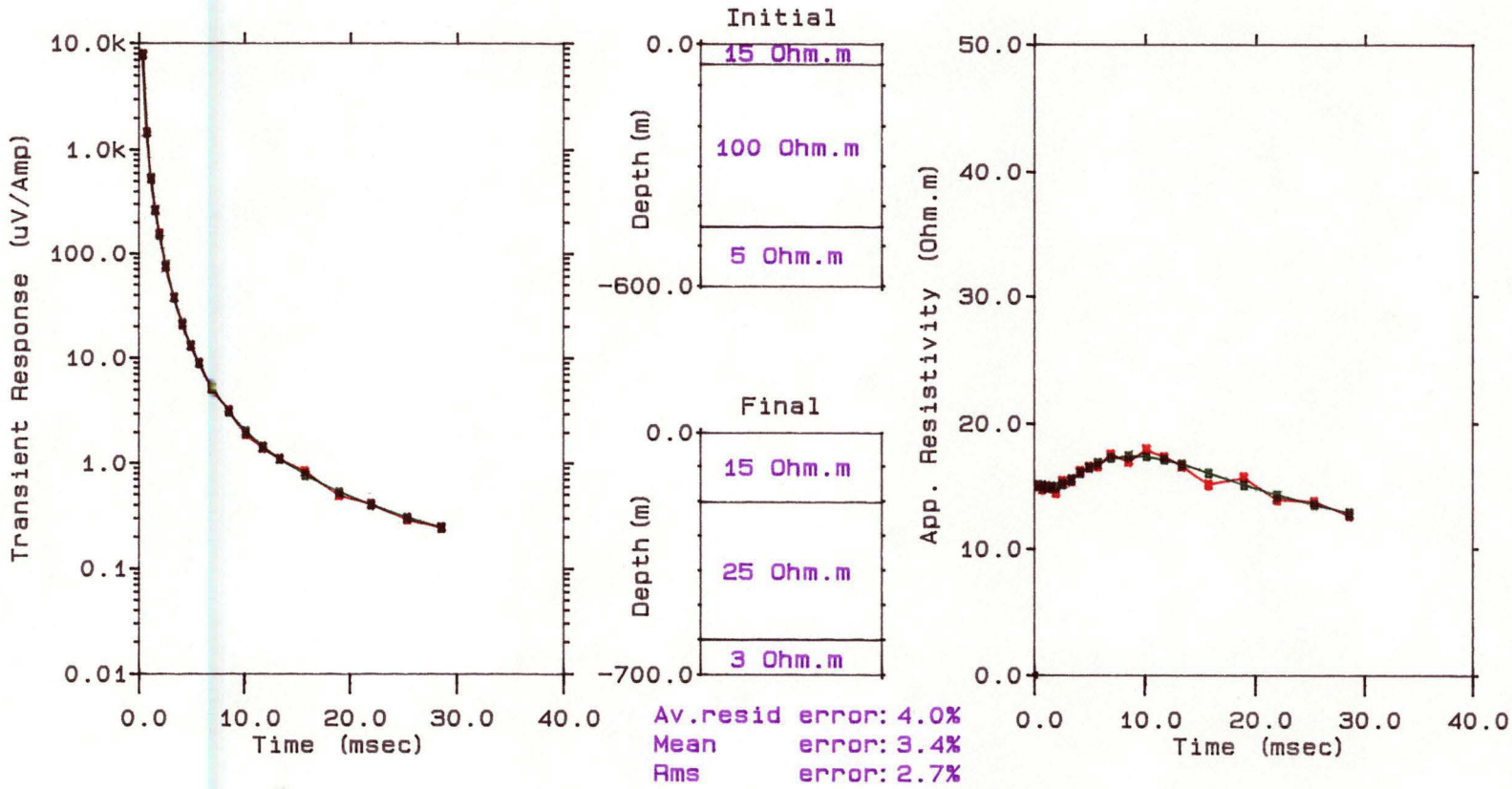

Figure 5.21 SIROTEM modelling results from Milford (MI)
(red)-observed; (green)-calculated

the unwanted distortions were discussed, for example, by Jiracek (1988), Berdichevsky et al. (1989), and Bahr and Groom (1990).

The application of the idea of Sternberg et al. (1988) suggests that by dividing the transient time scale (in ms) by 200 allowed a direct comparison between SIROTEM and MT. Figures 5.22 and 5.23 show apparent resistivity curves from SIROTEM plotted together with apparent resistivity curves from MT and one-dimensional model interpretation at KN and MI sites, respectively. At each site the SIROTEM curve is plotted on the left hand side of the diagrams. It can be seen here that both data do not overlap. Lack of short period data in MT and lack of late delay time data in SIROTEM cause a big gap between the two results, ideally they would have produced two overlapping sets of data. Although there is some absence of data between these two results it is apparent from the Figure 5.22 that both curves, at both sites, seem to conform with the one-dimensional modelling result. It is not easy to verify from these results whether there is static shift correction or not. The consistency between the DC-resistivity, SIROTEM, and one-dimensional model results, however, implies that there are no near surface inhomogeneities present in the vicinity of those sites and therefore no static shift correction to the MT data is required. Jones (1988) also stated that in a true two-dimensional surficial inhomogeneity the static shift problem can be avoided by considering the E-polarization results alone. The presumed Tamar Lineament, where the MT investigations were carried out, coincides with the Tamar Conductivity Anomaly. This anomaly is considered to have approximately two-dimensional structure (Parkinson et al. 1988). Based on Jones' (1988) assumption, no static shift correction needs to be applied to the observed MT data.

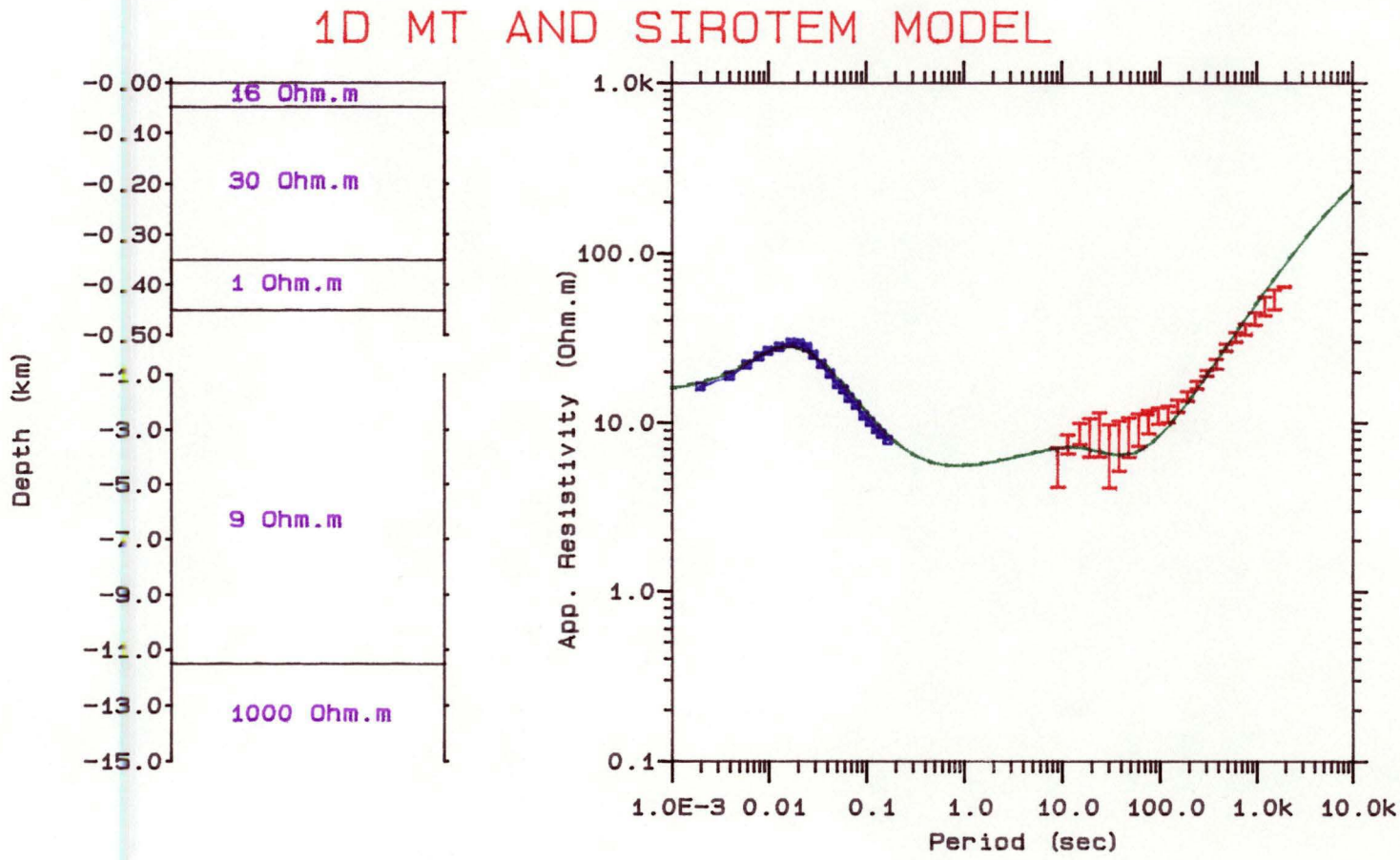

Figure 5.22 1D model based on MT and SIROTEM results from Kenilworth (KN) (red) -observed MT; (blue) -observed SIROTEM; (green) -calculated

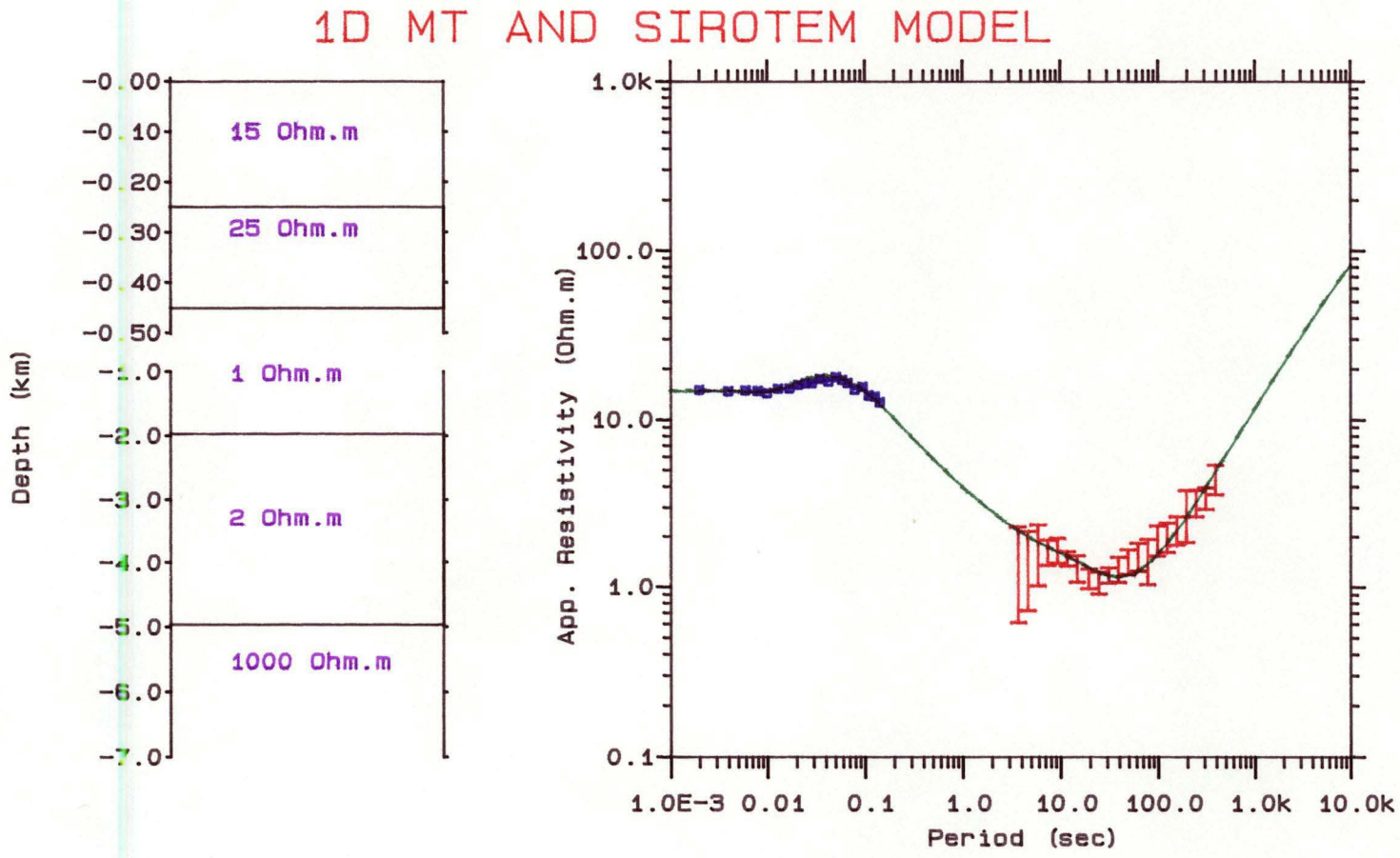

Figure 5.23 1D model based on MT and SIROTEM results from Milford (MI) (red) -observed MT; (blue) -observed SIROTEM; (green) -calculated

5.4.3 2D GRAVITY AND MAGNETIC MODELLING

5.4.3.1 INTRODUCTION

An interpretation of the gravity and magnetic data in northern Tasmania by means of two-dimensional modelling was carried out over two cross-sections (see Figure 5.24). The main aim of this modelling was to determine the shape and possible structural origin of several rock sequences associated with the Tamar Conductivity Anomaly. The gravity interpretation was based on a residual Bouguer anomaly map (see Figure 5.24). The separation process from Bouguer to residual maps is given by Leaman and Richardson (1989a). This data was obtained from the Division of Mines and Mineral Resources, Tasmanian Department of Resources and Energy. The gravity data is presently held in the combined TASGRAV and MTREAD data bases with station spacings varying from 0.8 to 7 km and fully terrain corrected to 20 km (Richardson and Leaman, 1987). The magnetic interpretation, on the other hand, was based on the total magnetic intensity aeromagnetic survey by Conga Oil aquired at an altitude of 1600 metres (see Figure 5.25). The use of this data was possible courtesy of Mr. M. Bendall (Director Conga Oil).

The two-dimensional gravity and magnetic modelling was carried out using MODEL2D program, version 2.5 written by Michael Roach based on interactive two-dimensional combined gravity and magnetic modelling using algorithms of Talwani et al. (1959) and Talwani (1965). Basic assumptions and requirements concerning the use of two-dimensional modelling have been given by Leaman and Richardson (1989b).

The surface extent of lithological units modelled along cross sections 1 and 2 were based on the geological map of Tasmania, scale 1:250.000. (Gulline, and Forsyth, 1976).

The gravity and magnetic effect can be calculated for any number of bodies and the calculated curve is compared with the observed curve. Should any discrepancy occur between these two curves, then the model along that cross-section is modified till the two curves match each other. The fit between the two curves is also determined by the vertical shift factor which must be consistent throughout the models, as the observed zero is arbitrary, whereas the calculated zero is not.

Another important aspect that needs to be taken into consideration when two-dimensional modelling is used, is the edge effect of calculated bodies at the ends of a cross-section. To avoid any errors in the calculated curve, the lithological units must be extended in a similar thickness and orientation for at least two to three times the thickness of the section in both directions (Dr. D.E. Leaman, personal communication, 1991).

The gravity models were calculated assuming a flat datum plane about 200 metres above sea level which approximates the land surface. For magnetic calculations therefore a line clearance of 1400 metres was taken. This is a reasonable approximation of the terrain east of the Great Western Tiers.

Several previous gravity surveys have been carried out in this area by Hinch, (1965), Longman and Leaman, (1971), and Leaman et al. (1973).

5.4.3.2 ROCK DENSITIES AND SUSCEPTIBILITIES

No rock density and susceptibility measurements were made for the interpretation of the residual gravity and total intensity magnetic anomalies. Instead the study uses the results of Leaman (1973) shown in Table 5.3. The density contrast was calculated with respect to the Precambrian rocks which have densities of 2.67 tm^{-3} and the star symbol represents the value used during modelling.

5.4.3.3 GRAVITY AND MAGNETIC ANOMALY MAPS

Figure 5.24 is a residual Bouguer gravity anomaly map for the northeast of Tasmania. The two model cross sections are shown on this map. The map clearly exposes several major lineaments e.g. the Tamar trough and Longford basin but the most striking feature is the lineament which coincides with the edge of the granite body in north-eastern Tasmania and the lineament associated with the Great Tiers faults. These lineaments continue very clearly to the south.

A few large negative and positive anomalies can be seen on the eastern and western side of the Tamar river with several small negative and positive anomalies occurring nearby. Two large negative anomalies with values of -24 and -14 mgal are believed to be associated with the Scottsdale batholith and the Longford basin, respectively. Other small negative anomalies of up to -8 mgal can also be seen west of Meander. These anomalies may be partly related to Permian and Triassic sediment which crop out irregularly in that area.

A broad band of positive anomalies is generally present on the western side of the Tamar river. Anomalies of up to +6 mgal which occur near Sheffield coincide with Cambrian rocks which crop out in that area. This anomaly seems to follow the axis of Cambrian rocks to almost south-west of Bracknell (probably also the axis of Cambrian and Tabberabberan folding (?) (Longman and Leaman, 1971)).

Table 5.3

List of density contrasts and susceptibilities

Rock unit	Density contrast (g/cm)	Susceptibility (cgs)
Tertiary		
- sediment	-0.60*	0.0*
- basalt	0.21, 0.35 (0.25*)	0.01*
Jurassic		
- dolerite	0.20, 0.35 (0.25*)	0.005*
Triassic		
- sandstone/mudstone	-0.15, -0.32 (-0.25*)	0.0*
Permian		
- mudstone/sandstone siltstone/limestone	-0.12, -0.25 (-0.15*)	0.0*
Ordovician		
- limestone	0.07*	0.0*
Devonian granites		
- adamellite	-0.05*	0.00005*
- granodiorite	0.03*	0.0003*
Devonian		
- turbidite	0.08*	0.0*
Cambrian		
- volcanics - acid	0.07*	0.0001*
- mafic	0.07*, 0.12	0.001*
- ultramafic	-0.25, 0.32 (0.07*)	0.02*
Precambrian		
- silicious	- 0.02, 0.0*	0.0*
- pelitic - dolomitic	0.05, 0.08 (0.07*)	0.0*

Figure 5.25 shows a total intensity magnetic map of the same region as the gravity map, with two cross sections marked. The total intensity values range from 62040 nT in the Beaconsfield area to 63200 nT near Campbeltown. In general the anomaly shows a strong N-S trend. The most obvious feature is that the lineament coincides with the Bracknell fault. The corresponding line of anomalies seems to break at Longford and then fork into two lines; it is not impossible that the other line is due to the same source. These anomalies seem to be associated with the ultramafic rocks that crop out at Beaconsfield.

Other large anomalies in the south-west and north-east corner and in the middle of the region shown on the map may be related to the exposed dolerite bodies, and the Cambrian sediments which crop out near Poatina. The low anomaly on the eastern corner of the region, on the other hand, may be related to the Tertiary

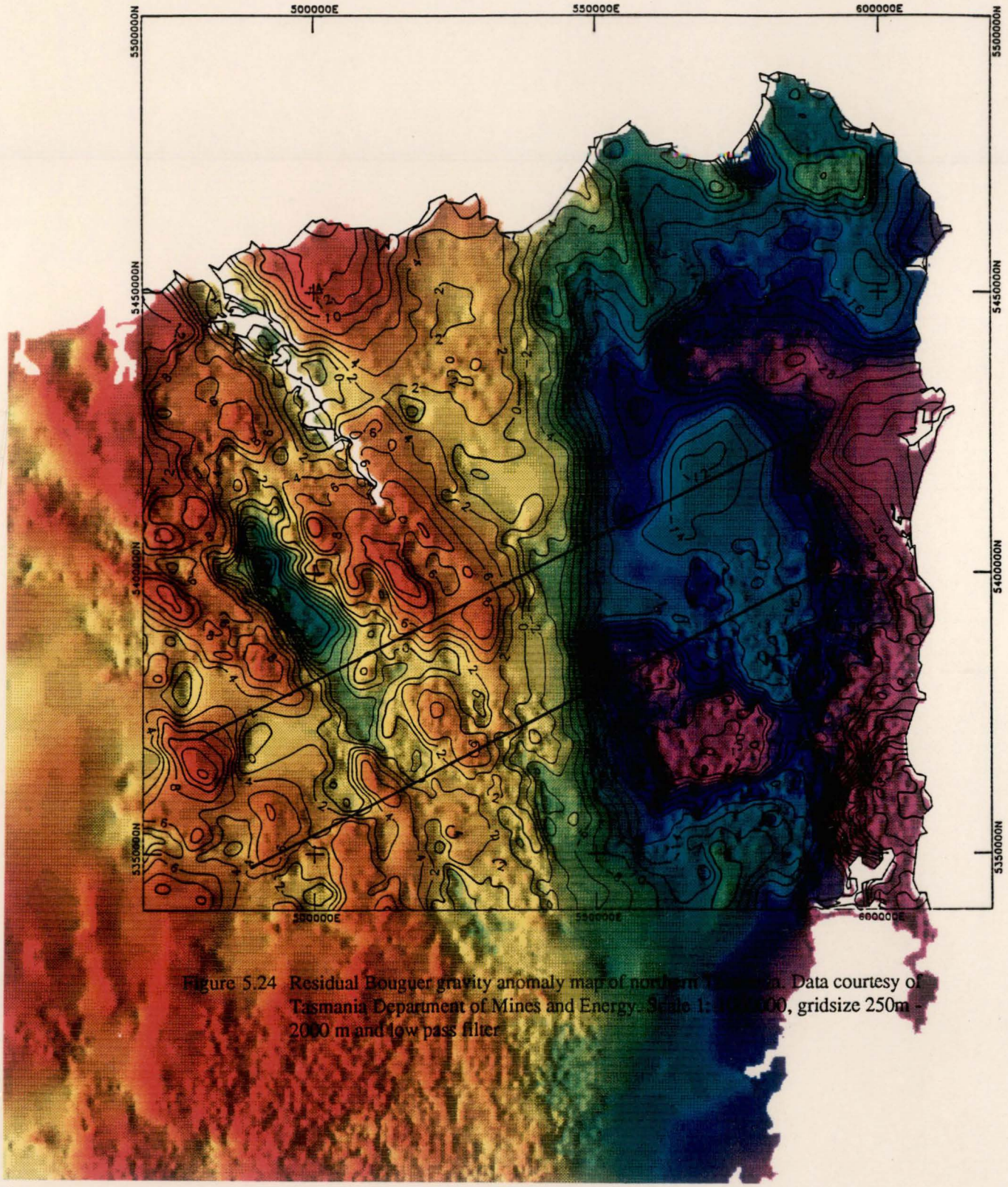

Figure 5.24 Residual Bouguer gravity anomaly map of northern Tasmania. Data courtesy of Tasmania Department of Mines and Energy. Scale 1: [illegible]000, gridsize 250m - 2000 m and low pass filter.

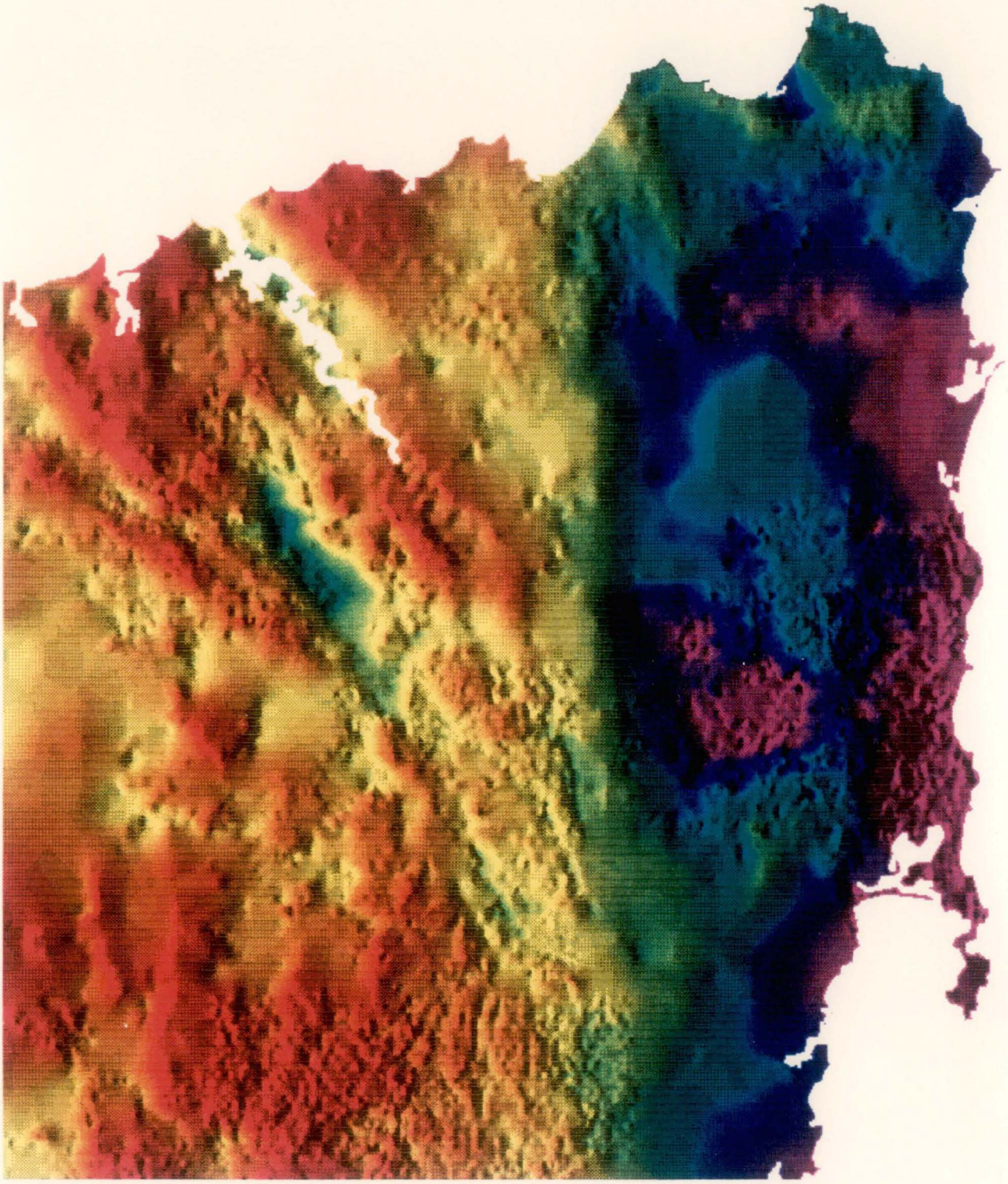

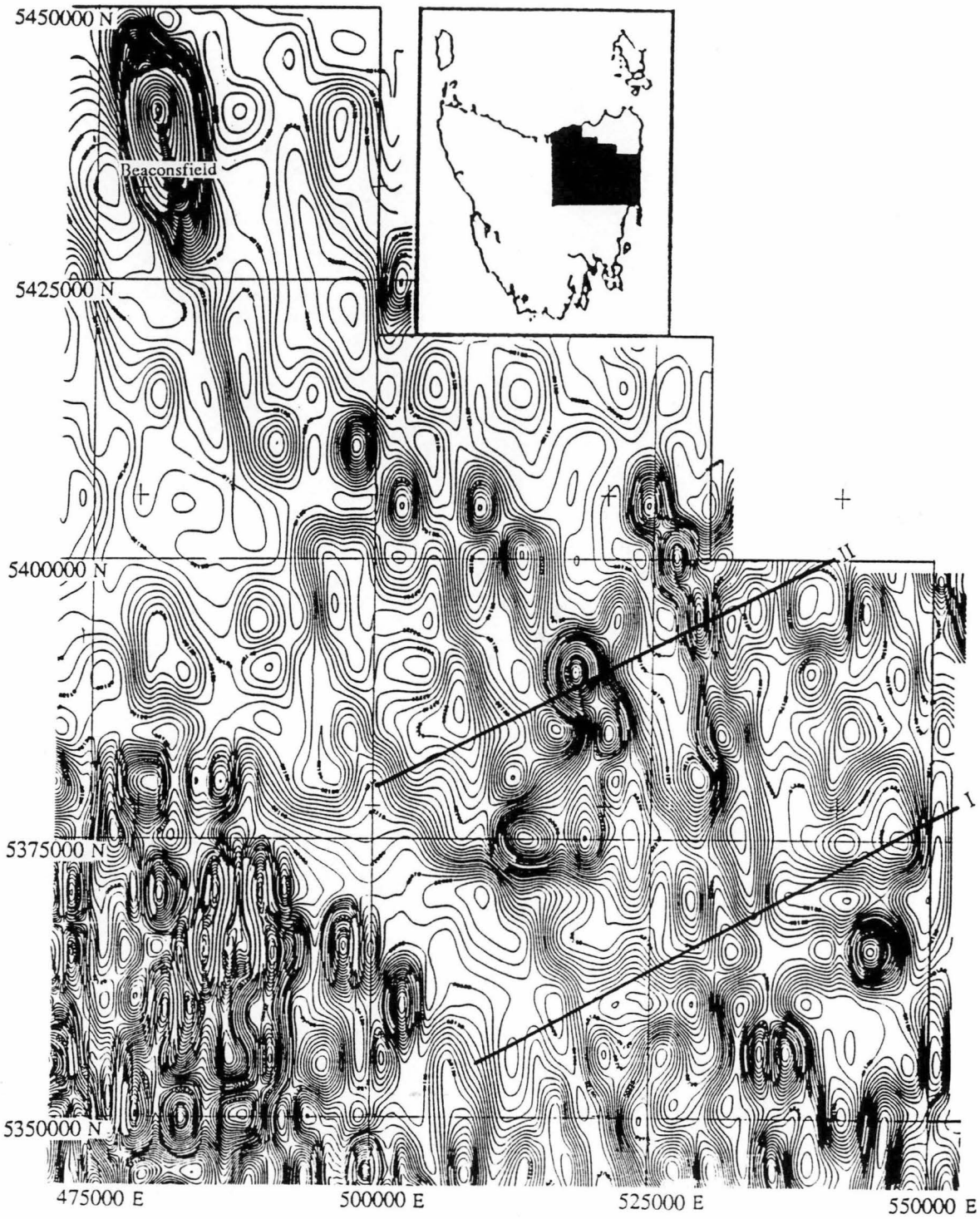

Figure 5.25 Total magnetic intensity map of north-east Tasmania. Data courtesy of Conga Oil Pty. Ltd. Grid AMG. Scale 1 : 600000.

sediment that fills the Tamar and Cressy graben. This low anomaly also coincides with the approximate centre and axis of the Tamar Conductivity Anomaly.

5.4.3.4 INTERPRETATION OF CROSS-SECTIONS

Figure 5.26 shows the observed and calculated gravity and magnetic profiles together with the likely two-dimensional model along the MT traverse. MT site locations are included in the diagram for easy checking and comparison of the results. The observed gravity profile varies very smoothly along this traverse. The general eastward decending gravity trend may be attributed to the thickening of the Permo-Triassic rocks. The thickness of the Permian and younger rocks shown i.e. 1300 to 1500 metres, is consistent with the approximate thickness of dolerite, Triassic and Permian rocks suggested by Leaman, et al. (1973) and Matthews (1983). The gravity trend becomes more negative as the traverse approaches granite intrusion near Avoca. Leaman (1992) suggests that this granite body may have a thickness of approximately 10 kilometres. The gravity profile then increases again at the eastern side of the traverse as it crosses exposed Mathinna Beds. The thickness of these Mathinna Beds is about 3.5 kilometres and is consistent with the result shown by Roach (1992) from modelling north-east of this section.

The observed magnetic profile, on the other hand, shows a large variation across the traverse and the long wavelength anomaly, suggesting that this anomaly is of deep origin and may be associated with Cambrian volcanics. The magnitude of the anomaly tends to increase toward the east and indicates that the subsurface is more magnetic on the eastern than on the western side of the traverse. This proves that the western terrane extends to granite in the east (Leaman, 1992). A large drop in magnetic anomaly on the western side of the traverse which may be partly related to the Tiers fault and suggests that the rocks under the Tiers fault are less magnetic than the same rocks on the eastern side of the traverse. This rock may be composed of Precambrian dolomite, Cambrian volcanics, and or Ordovician limestone. The magnetic profile then increases again to form two large highs. The most likely explanation for these highs is that they are partly due to long and thin ultramafic bodies that intrude into the Precambrian and Cambrian rocks (see Figure 5.26). These bodies may be part of the ultramafics that crop out at Beaconsfield and the anomaly can be traced along strike to Beaconsfield. As shown in Figure 5.26, the Cambrian rocks with a thickness of about 4000 metres and susceptibilities ranging from .0001 on the western side of the traverse to .001 on the eastern side of the traverse, are consistent with observed data. This Cambrian section would be

Figure 5.26 **2D GRAVITY AND MAGNETICS MODEL**

CROSS SECTION 1 (ALONG MT TRAVERSE)

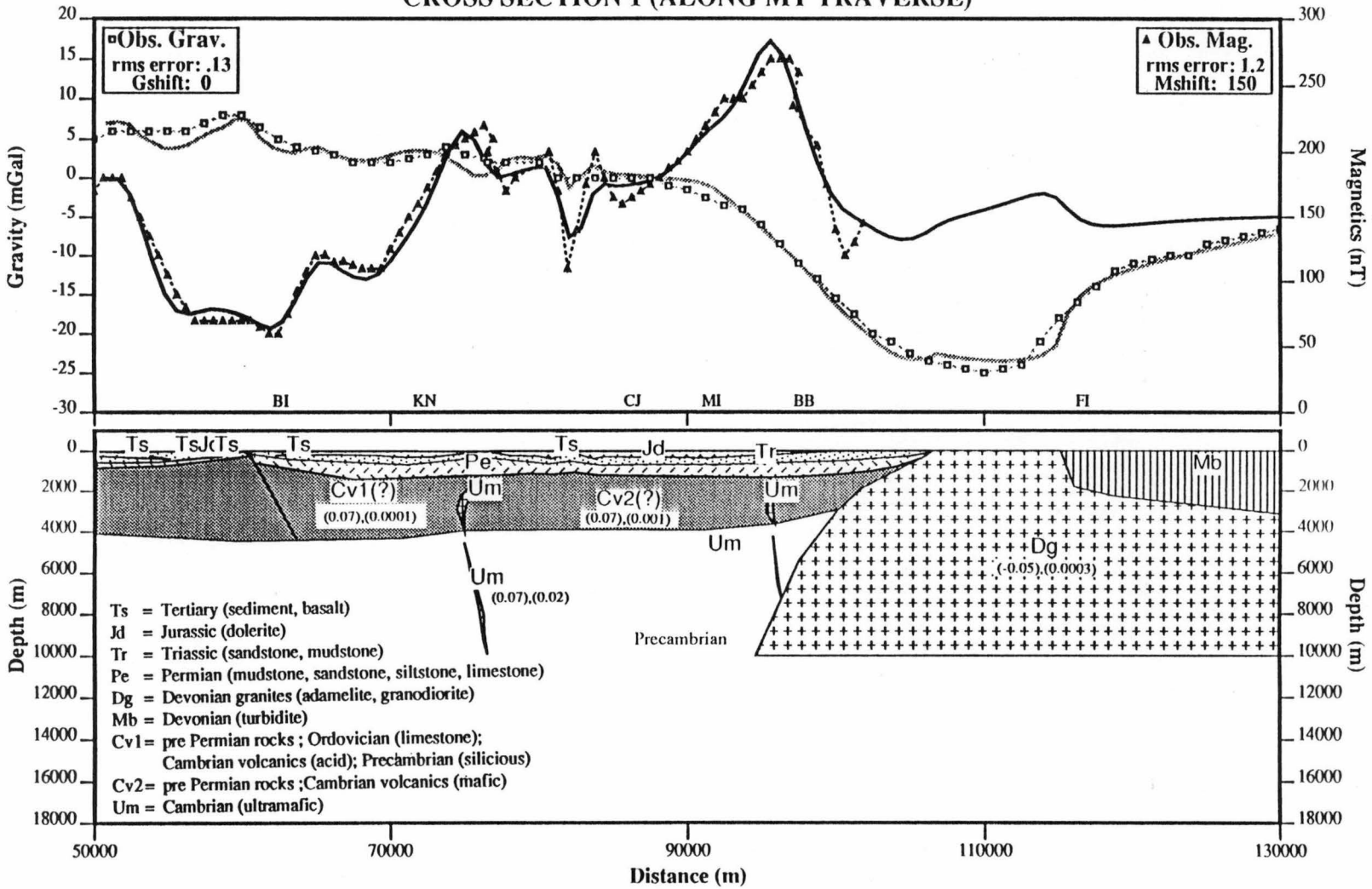

Model File:GM1BST7.MOD Obs. Gravity:GP1.OBS Obs. Magnetic:MP1.OBS Date:11-11-1992 Time:17:22:28

equivalent to the Crimson Creek and Surprise Creek formations (Brown, 1989) and may therefore be correlated with western Tasmania.

Figure 5.27 shows the observed and calculated gravity and magnetic profiles with the likely two-dimensional model for cross-section 2. It can be seen here that the gravity and magnetic profiles are slightly different compared with the profile along the MT traverse. The gravity profile begins with a small negative anomaly on the western side of the traverse then increases to form a relatively large positive anomaly in the middle, before it decreases to become a large negative anomaly on the eastern side of the traverse. The values then increase again towards the end of the traverse. The observed magnetic profile is mainly dominated by two large anomalies in the middle of the traverse. A drop in gravity and magnetic values at the beginning of the traverse is believed to be partly associated with the Tertiary sediments near the Tiers fault. The broad and large magnetic anomaly on the western side of the traverse accompanied by low gravity anomaly implies that the Cambrian rocks are more magnetic and thinner compared with the same rocks on the eastern side of the traverse. This low gravity anomaly may also be due to thickening of the Permo-Triassic rocks. The broad positive gravity anomaly in the middle of the traverse suggests that it may be due to relatively thick Cambrian volcanics. The two large magnetic anomalies, on the other hand, seem to be due to long and thin ultramafic bodies that intrude into the Precambrian and Cambrian rocks. This ultramafic rock may have the same source as the rock at cross-section 1. The large negative gravity anomaly on the eastern side of the traverse is related to the large batholith. The minimum of this anomaly is consistent with a thickness of approximately 9 kilometres of granite with a density of 2.62 tm^{-3}.

5.4.4 SEISMIC DATA

Both reflection and refraction seismic surveys have been carried out to determine the crustal structure in Tasmania and Bass Strait area (Underwood, 1969; Cameron, 1971; Johnson, 1972; Richardson, 1980 and Vitesnik, 1984). Results from these surveys show that the crustal thickness decreases near the continental margin and thickens beneath the central plateau.

Johnson (1972) for example, using P_1 (crustal) velocity of 6.0 kms^{-1} and P_n (mantle) velocity of 8.0 kms^{-1} calculated that the crustal thickness is between 20 - 25 km for the continental margin in southern Bass Strait and thickens to 30 - 35 km for central Tasmania. Richardson (1980) carried out a seismic reflection and refraction

Figure 5.27 **2D GRAVITY AND MAGNETICS MODEL**

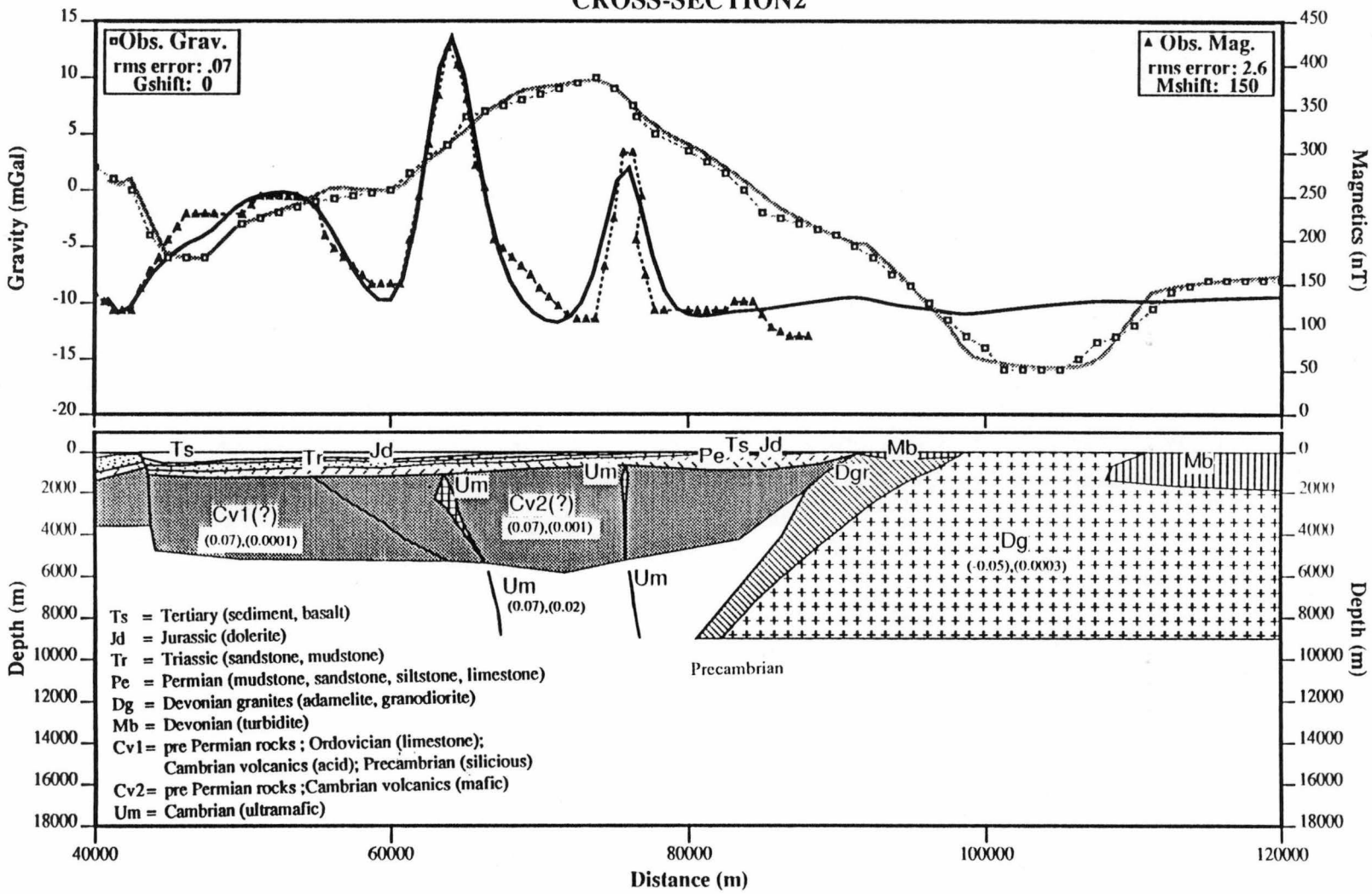

Model File:GM2BST4.MOD Obs. Gravity:GP2.OBS Obs. Magnetic:MP2.OBS Date:11-15-1992 Time:09:44:11

traverse across northern Tasmania and argued that the crustal thickness varies between 23.4 km near Savage River to 27.4 km under the postulated Tamar Fracture System (Williams, 1979) then decreases to 22.3 km at Binalong Bay. These results are based on average velocity of P_1= 5.86 kms^{-1} and P_n= 7.95 kms^{-1}.

It should be noted that Richardson (1980) recognised velocity determination problems near the Tamar axis and assumed crustal velocity set. If Leaman (1992) is correct in suggesting that this is a recent pull-apart zone at older structures then lower than normal velocities may be present in this zone and the inference of locally thicken crust may be false.

The most recent survey, by Vitesnik (1984) using both reflection and refraction techniques, also demonstrated that the crustal thickness decreases near the continental margin i.e. about 23 km at Savage River and thickens to central Tasmania (i.e. 32 km at the Central Plateau). Average velocity observed by Vitesnik is P_1= 6.0 kms^{-1} and P_n= 8.0 kms^{-1}.

The University of Tasmania Geology Department operates eight seismic stations distributed around the island. Three of these stations are located on or close to the Tamar Conductivity Anomaly. Parkinson et al. (1988) stated that from the analysis of the residual S and P arrivals, there are considerable differences in the S residual for the wave path along the Tamar Conductivity Anomaly and for the average residual for the rest of the island. These differences are generally accounted for by water saturated sheared rock, whereas Leaman (1992) would argue that a primary Devonian thrust front could also explain some of these differences (see also above).

5.4.5 HEAT FLOW DATA

The result of MT measurements is often discussed with relation to heat flow measurement conducted close or at the same site as MT. Such discussions are given, for example, by Adam (1976), Jones and Craven (1990) and Munoz et al. (1990). No heat flow measurements were carried out for this study. Instead, the heat flow results of Jaeger and Sass (1963), Wronski (1977) and Green (1989) are used in this discussion.

Green (1989) states that Tasmania has unusually high terrestial heat flux i.e. greater than 2 HFU (1 HFU = 41.86 mW m^{-2}) based on measurements at the Storey Creek mine, Glenorchy and Coles Bay, respectively (see Figure 5.29). Out

of these three measurements, Jaeger and Sass (1963) obtained very high heat flow values i.e.159 mW m^{-2} from a diamond drill hole in Mathinna beds adjacent to a Devonian alkali granite pluton, a known host for uranium mineralisation. A more recent geothermal gradient measurement in Tasmania was carried out by Green (1989) in collaboration with the Bureau of Mineral Resources. Results from measurements at Tunbridge, Coles Bay and Stanley were 41° Ckm^{-1}, 30° Ckm^{-1}, and 28° Ckm^{-1}, respectively.

Green (1989) concluded that a linear extrapolation of geothermal gradient recorded for the upper part of the lithosphere in Tasmania would imply the existence of extensive melting in the upper mantle beneath Tasmania.

CHAPTER 6 : INTERPRETATION

6.1 MAGNETOTELLURIC INTERPRETATION

6.1.1 GENERAL COMMENT

Some important information from the magnetotelluric results presented in Chapter 5 may be summarised as follows:

1. Based on the apparent resistivity curves, the structure under the BI, KN, CJ, MI and BB sites exhibits large to moderate anisotropy. The degree of anisotropy seems to decrease toward eastern sites and vanishes under the FI site.

2. Within the graben like structure, the resistivity values also tend to decrease toward the BB sites. The resistivity values then increase dramatically at the FI site.

3. The skew and delta theta values are very large at sites BI and BB where these sites are close to the Bracknell Fault and the margin of the granite intrusion. This large skew and delta theta may therefore be associated with lateral inhomogeneity contrast due to those structures. The skew and delta theta, however, tend to decrease toward the CJ site which is located approximately at the centre of the Tamar Conductivity Anomaly.

4. Induction arrow analysis from the VFP and AVO sites (see Appendix 1), which is shown by long (real part) induction arrows and point in opposite directions, suggests that those sites mark the approximate west and east boundary of the Tamar Conductivity Anomaly. The length of the arrows, which gradually decrease toward the CJ site, indicates current concentration between the VFP and AVO sites.

In view of the above results it is necessary to carry out one- and two-dimensional modelling to resolve underground conductivity structure along this MT traverse.

6.1.2 ONE-DIMENSIONAL MODELLING

There are two apparent resistivity curves calculated in the tensor analysis. They are the resistivity with electric field along the strike (ρ_{xy}) or TE mode and the resistivity with the electric field perpendicular to the strike (ρ_{yx}) or TM mode. Prior to modelling it is important to decide which resistivity is to be used. Since the TE mode has the electric field parallel to the strike, this resistivity is less affected by the lateral inhomogeneity contrast and therefore should better represent the gross structural feature of the region. TE mode resistivity has, therefore, been used throughout the modelling.

One-dimensional modelling was done to get a feel for the relation between depth and period, and as a basis for later two-dimensional modelling.

The one-dimensional modelling was carried out using a program called MT1DPLT. This program was written by the author and is based on Schmucker's algorithm (1970). This program is controlled by interactive command and can calculate up to a maximum of 15 layers. To achieve an acceptable layer model from the program, several constraints were applied i.e. local geology, resistivity rock layers and thicknesses determined by the DC-resistivity and SIROTEM, and results from shallow drilling.

There is no deep drilling in the vicinity of these MT sites and no correlation is possible to the results obtained by the DC-resistivity. The closest deep holes are at Bracknell, Westbury and Tunbridge which are about 45, 60 and 35 kilometres north west and south of Conara Junction (CJ), respectively. The first two holes are oil wildcats and the other one is a geothermal gradient measurement hole. The oil holes were drilled to a depth of 680 and 830 metres, respectively and were abandoned when they struck dolerite at those depths (Matthews, 1983). The Tunbridge hole was drilled to a depth of 780 metres and intersected the Quamby Group at a depth of about 500 metres (Green, 1989) and pre-Permian basement at hole end.

There is no indication from these holes of the thickness of the dolerite in this region. Dr. D.E. Leaman (personal communication, 1992) and Matthews (1983), however, suggest that the dolerite in some areas appears to have a thickness of about 300 to 350 metres. Based on the Longford geological map, the thickness of the Tertiary sediment along this MT traverse is less than 100 metres (Matthews, 1983). Other indications on the thickness of the Triassic and Permian rocks are given by Leaman et al. (1973) who state that the thickness of those rocks is about 300 and 600 metres, respectively. These rocks are believed to overlie basement rock of probable Cambrian and Precambrian age.

Figures 6.1 to 6.6 show one-dimensional model results from BI, KN, CJ, MI, BB and FI sites, respectively. In general, the best fit model to the observed data at each site is quite good. Except at FI site, the top resistivity layer seems to be very uniform.This layer, which has resistivity of 16 Ohm.m, has a thickness ranging from about 600 metres at MI site to about 700 metres at BI, KN, CJ, and BB sites. Based on the shallow and deep holes the 16 Ohm.m resistivity value seems likely to represent the gross resistivity value of the Tertiary and dolerite rocks. The top layer resistivity at FI, on the other hand, has resistivity of 20 Ohm.m and may represent the Mathinna Beds. The 16 Ohm.m resistivity value is similar to the resistivity value obtained by SIROTEM at KN and MI sites (see Figures 5.20 and 5.21) and the fourth layer of the DC-resistivity sounding result at Conara Junction (CJ) (see Figure 5.16). These resistivity values are also in accord with the resistivity of saturated Triassic or Mathinna Beds rocks and, sometimes, dolerite suggested by Leaman (1971). These rocks may have resistivities as low as 10-20 Ohm.m (see Table 5.2).

To fit MT data at sites BI, KN, CJ, MI and BB, the next layer needs to be more conductive than the top layer. At BI and KN , for example, this layer has resistivity of 8 Ohm.m with thickness of 1 and 11 km, respectively. Toward the eastern sites, the resistivity of this layer decreases gradually to 1.5 Ohm.m at CJ and 1 Ohm.m at MI. This resistivity then slightly increases again to 2 Ohm.m at BB. The thickness of this layer varies from 2 km at CJ, 1.5 km at MI to 10 km at BB. Another conductive layer with resistivity of 2 Ohm.m needs to be inserted under the 1.5 and 2 ohm.m layer to fit MT data at CJ and MI, respectively. This layer has a thickness of 4 km at CJ and 3 km at MI. A more resistive layer with resistivity of 30 Ohm.m and thickness of 13 km is required to fit MT data at BI. FI which lies on the Mathinna beds has top layer resistivity of 20 Ohm.m. This layer has a thickness of about 3.5 km. This thickness is based on the result of a two-dimensional gravity and magnetic model along this MT traverse (see Figure 5.27). Under all MT sites, the basement layer is assumed to be very uniform. This layer including the granite which crops out between sites BB and FI has resistivity of 1000 Ohm.m. One-dimensional model cross sections of this MT traverse can be seen in Figure 6.7.

Good fitting models to the observed data are also obtained even if a more resistive layer is inserted on the top layer. The resistivity value used for the resistive layer is 1000 Ohm.m with a thickness of about 10 metres. This resistivity is to represent the top resistive layer obtained by the DC-resistivity sounding. Appendix 5 shows the result from this modelling. It can be seen here that the difference in the results between these two models is very small. One of the reasons for this may be that the thickness of the resistive layer is too thin. But there is no evidence which

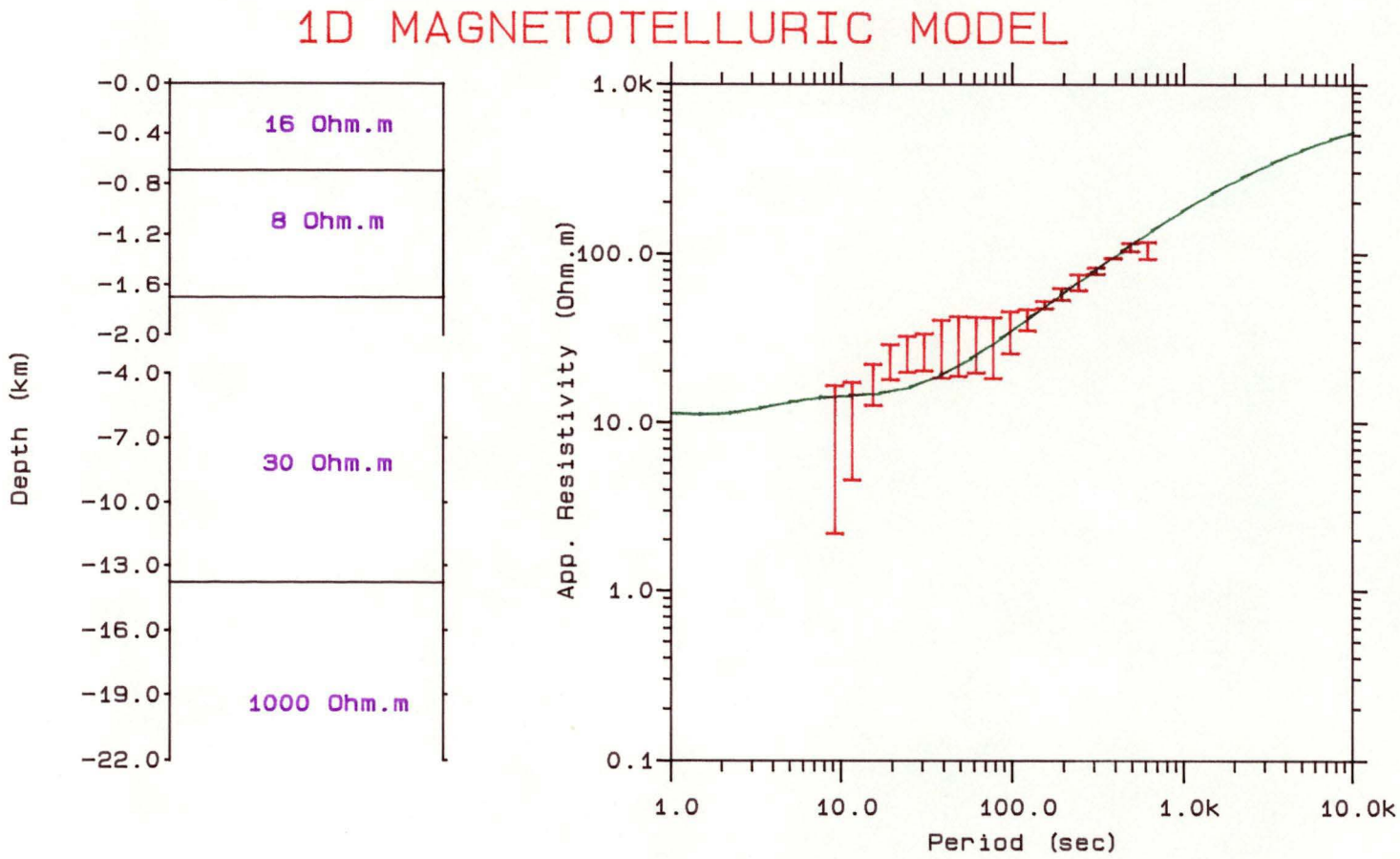

Figure 6.1 1D model results from Bicton (BI)
(red) -observed; (green) -calculated

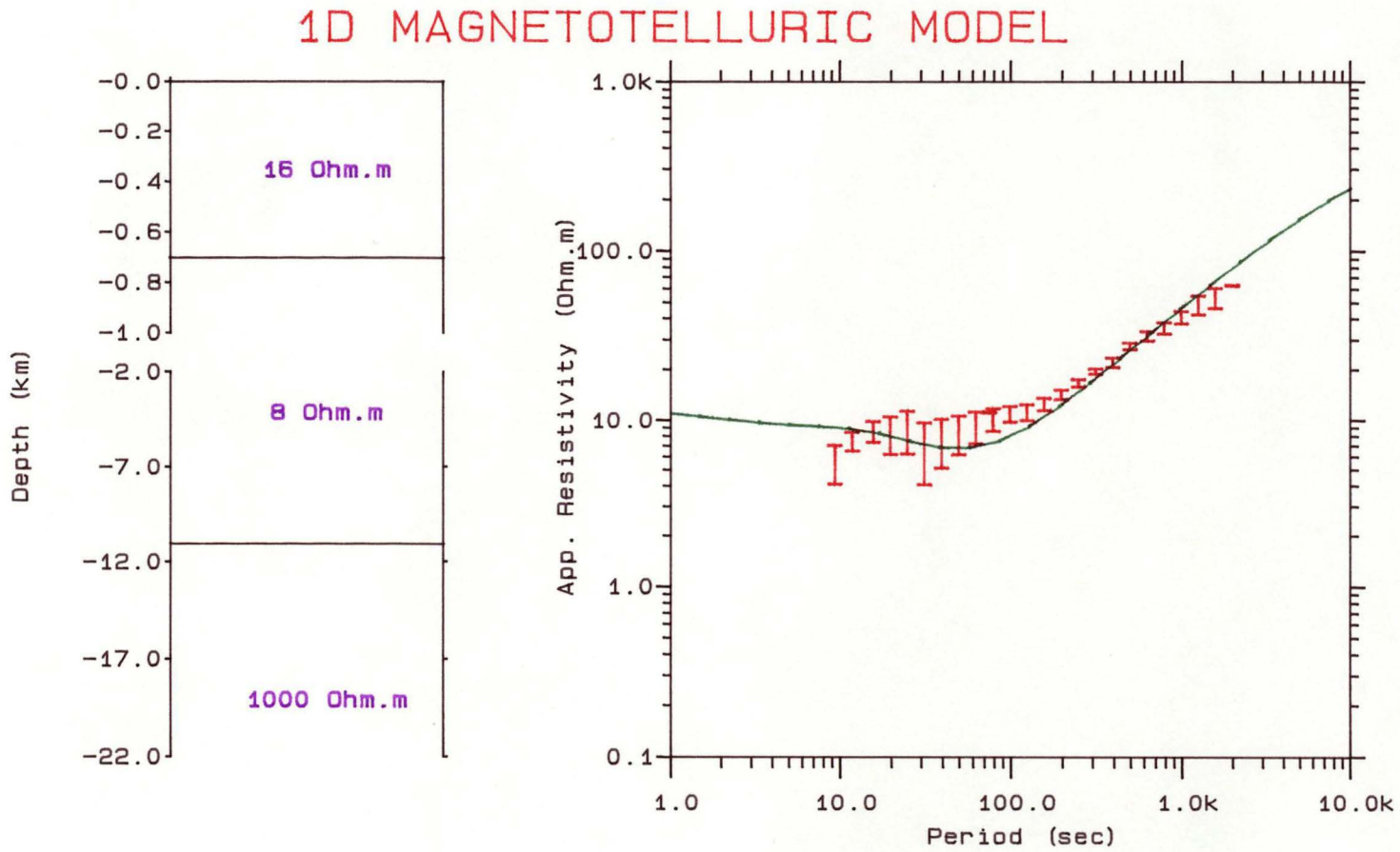

Figure 6.2 1D model results from Kenilworth (KN)
(red) -observed; (green) -calculated

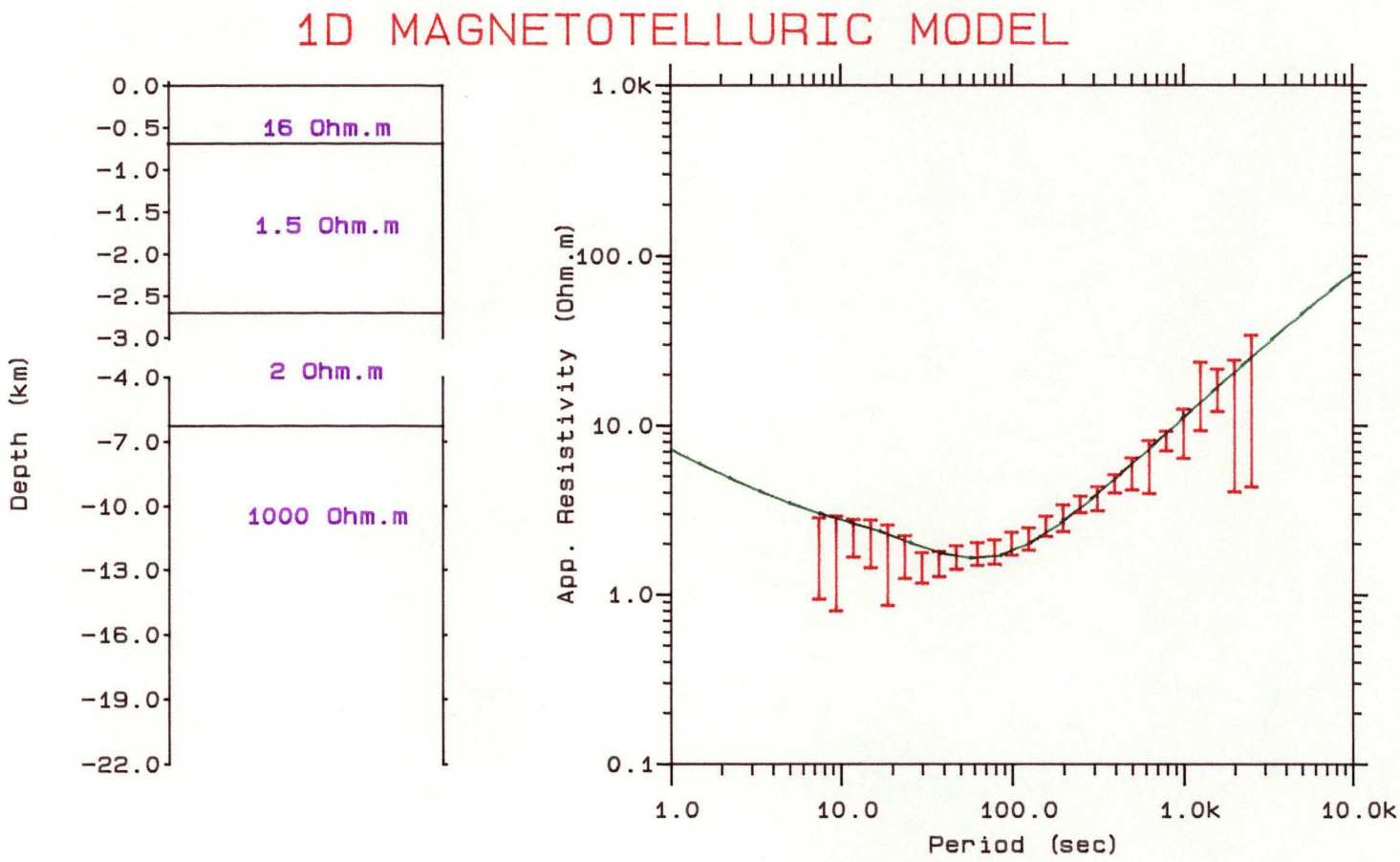

Figure 6.3 1D model results from Conara Jnc. (CJ)
(red)-observed; (green)-calculated

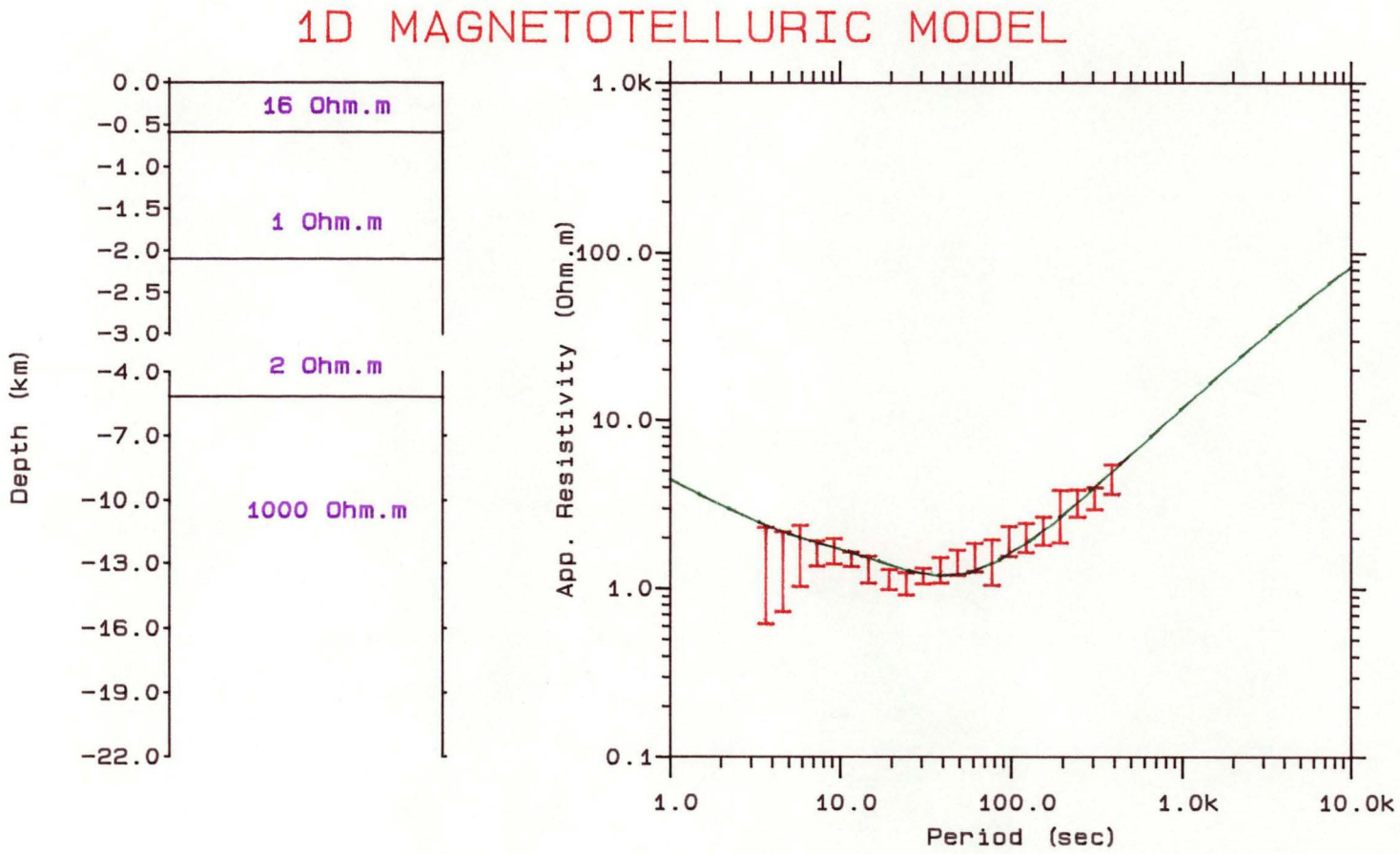

Figure 6.4 1D model results from Milford (MI)
(red) -observed; (green) -calculated

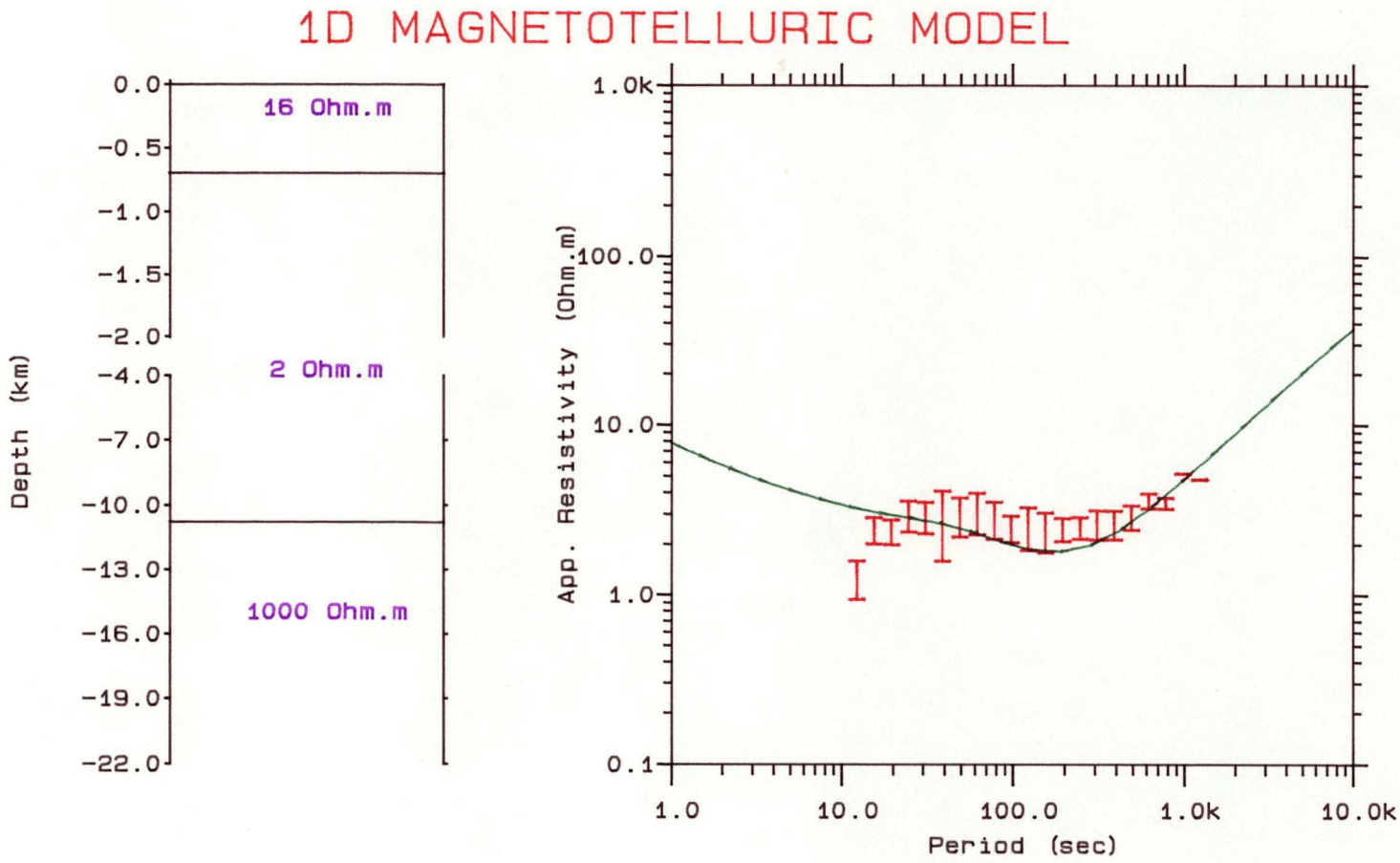

Figure 6.5 1D model results from Buffalo Brook (BB)
(red) -observed; (green) -calculated

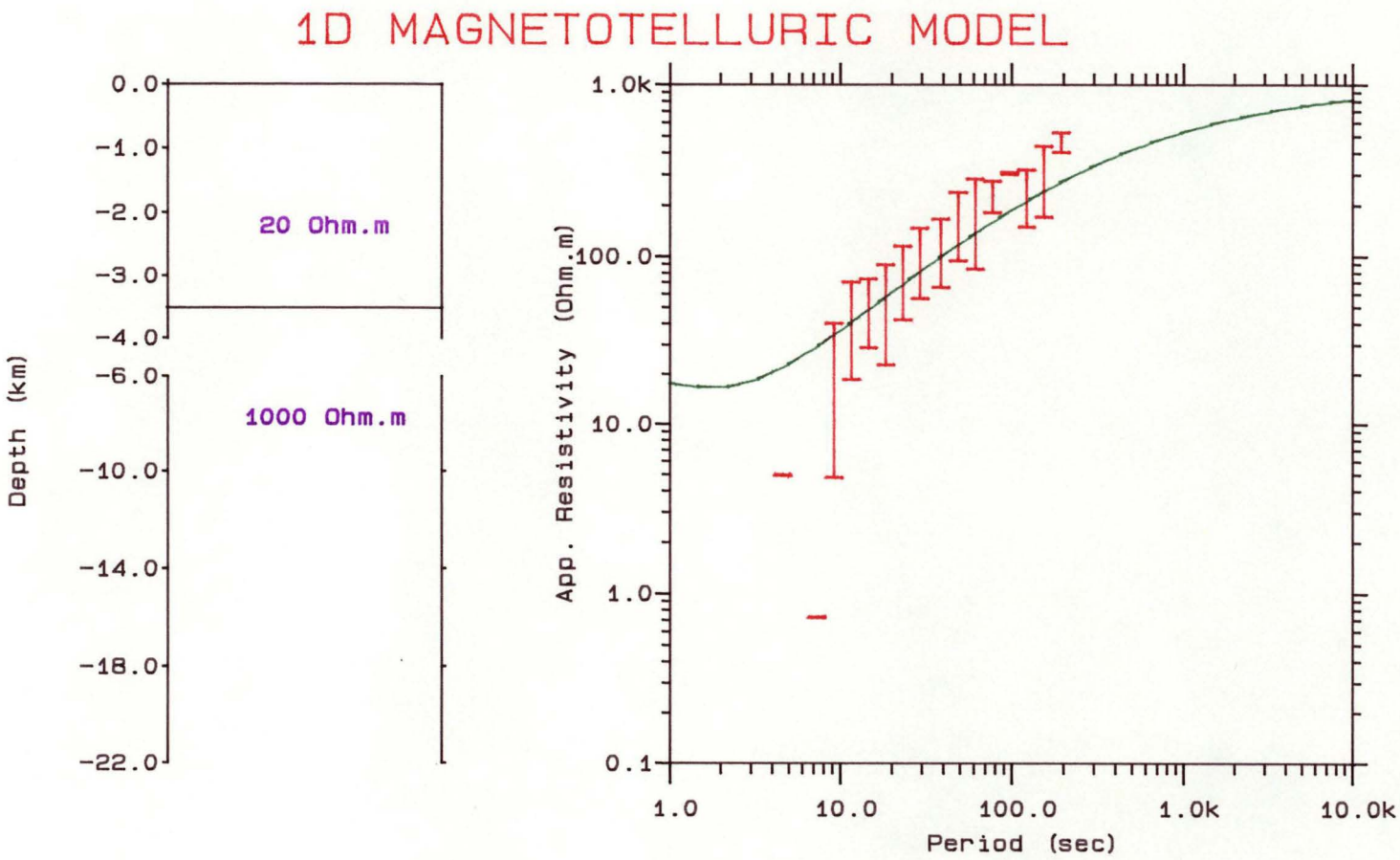

Figure 6.6 1D model results from Fingal (FI)
(red)-observed; (green)-calculated

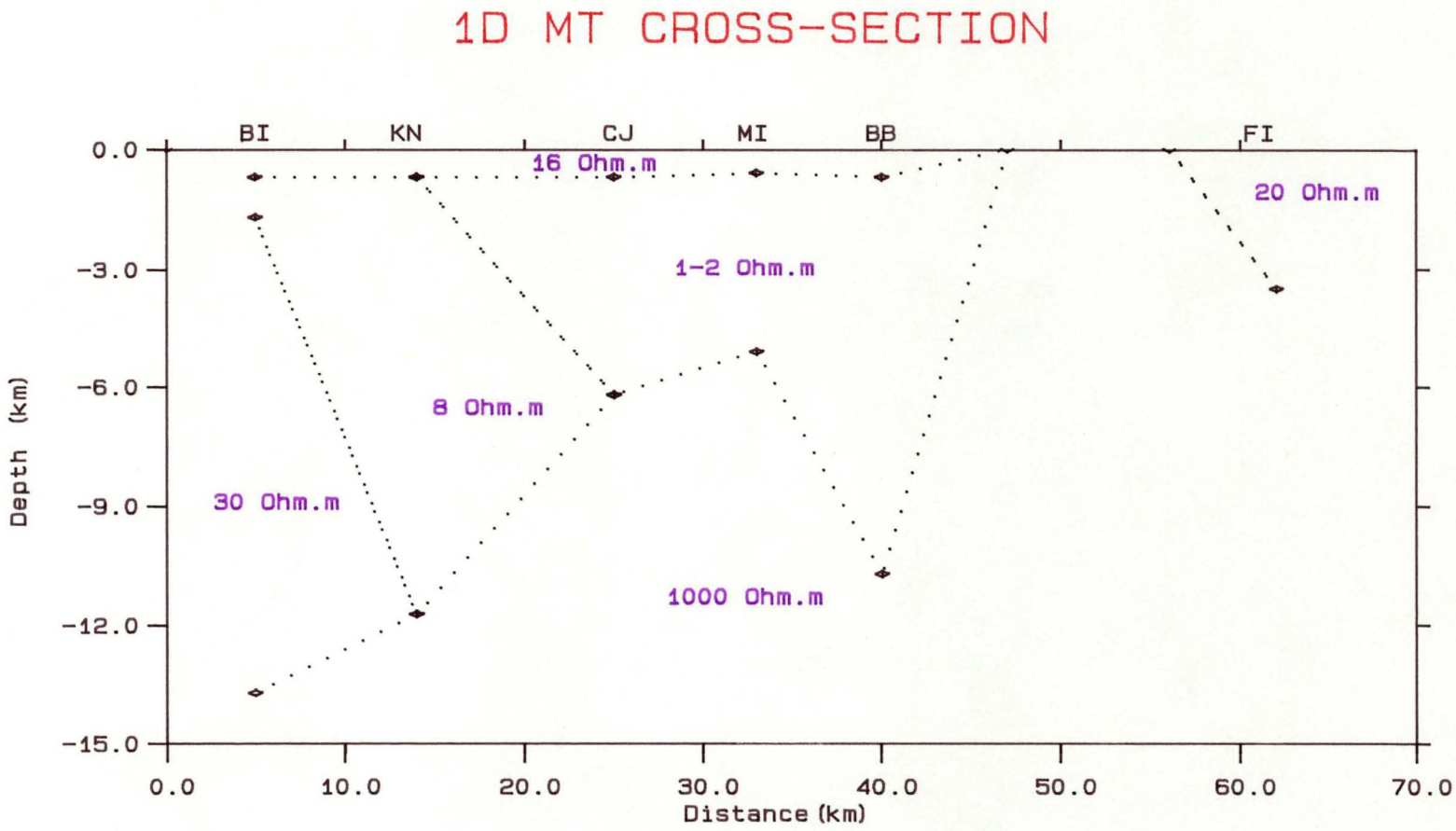

Figure 6.7 1D TE mode app. resistivity cross-section

indicates that the thickness of this resistive layer should be increased. Even with a resistive layer 100 metres thick the difference between this model result and the model shown in Figures 6.1 to 6.6 is minimal. It is concluded therefore that since the results are the same the model in Figures 6.1 to 6.6 may be used as a one-dimensional model to represent this traverse.

Based on the one-dimensional model result along this MT traverse, the Tamar Conductivity Anomaly seems to start at the BI site and is likely to terminate at the BB site. Depth to the top of the conductive body is found to be between 500 and 700 m from the surface while the thickness of the conductive body appears to vary between 4.9 and 11 km. The resistivity of the conductive body is increasing to the west. This conductive body also dips slightly to the west. Within the resolving power of MT and within the limit of frequency range over which the one-dimensional model is valid, in general, the one-dimensional interpretation resolves underground conductivity structure under this MT traverse.

6.1.3 TWO-DIMENSIONAL MODELLING

To provide more meaningful results and to support the one-dimensional model, it is necessary to carry out two-dimensional modelling. The computation was carried out using the JP2DEH1 program written by the author. This program is based on the computer programs by Jones and Pascoe (1971) and Pascoe and Jones (1972) including modifications suggested by Williamson et al. (1974), Jones and Thomson (1974).

The JP2DEH1 program is currently installed on a SUN SPARC station. This program can be run concurrently in two different modes i.e. E and H polarisations with each mode calculated for a certain number of periods given in the input. At present the program can calculate, for each mode, up to 14 periods simultaneously and takes approximately 20 minutes to do a two-dimensional model. The length of time taken generally depends on the complexity of the model.

For modelling in this project, the vertical and horizontal grid spacings chosen were as small and uniform as possible. Jones and Thompson (1974) state that large grid spacings could lead to a poor result. During the modelling the horizontal grid spacing close to MT sites was set to 1 km. Vertical grid spacing, on the other hand, was set to 100 m near the surface and gradually increased at depth. The model calculated by the program is based on 41 x 41 grid points.

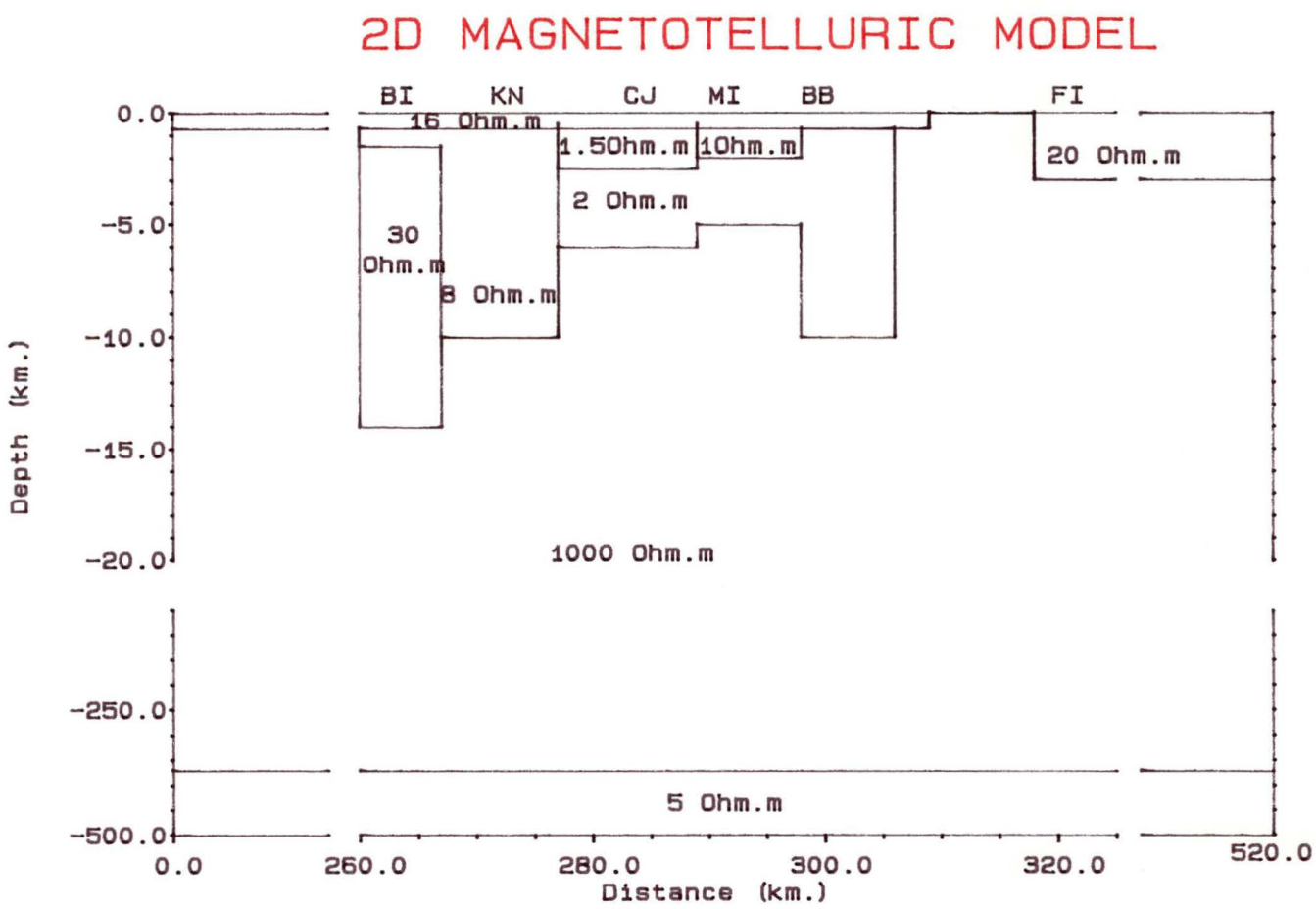

Figure 6.8 Initial 2D model configuration based on 1D results

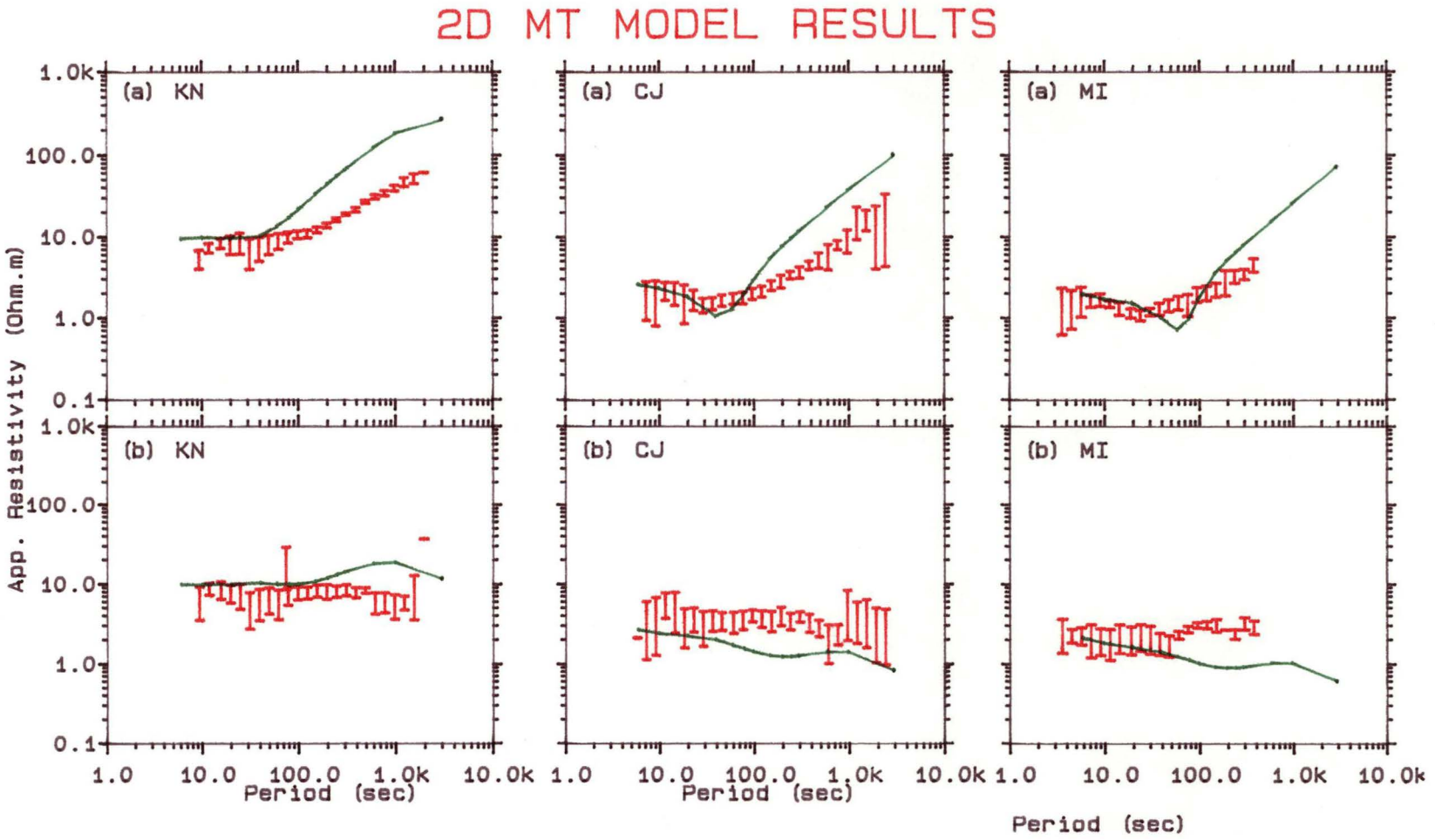

Figure 6.8a Obs. (red) and cal. (green) app. resistivity from KN, CJ, and MI sites
(a) E-polarization, (b) H-polarization

Only the sites which have approximately two-dimensional structures are modelled here. Indication of two dimensionality is given by skew values from every MT site. It is obvious from the analysis in Chapter 5 that only sites KN, CJ and MI have generally small skew i.e. less than .3. Other sites such as BI,BB and FI have large skew and therefore are assumed to depart from two-dimensionality.

Figure 6.8 shows an initial two-dimensional model configuration that was created based on one-dimensional results. For the purpose of plotting, no air layer is drawn in this configuration and other two-dimensional model configurations. Calculated data from this model for KN, CJ and MI sites in each of the TE and TM modes is plotted superimposed with the observed data and can be seen in Figure 6.8a. It is obvious from these figures that none of the calculated data from KN, CJ, and MI sites match their observed data. Take for example the TE mode result. The calculated resistivity from KN, CJ and MI, especially for periods greater than 100 seconds, is very large. The large resistivity seems to be due to too resistive a basement or too thin a conductive body.

Since the above model does not fit the observed data another model based on the one-dimensional result but with a basement resistivity of 500 Ohm.m and conductive body of 13.5 km thick was tested. The result, however, still does not fit the observed data. This model thus confirms that the large calculated TE mode resistivity for periods beyond 100 seconds, from KN, CJ and MI sites, is not due to resistive basement. Figure 6.9a, which shows calculated data for the model given in Figure 6.9, shows better results. Except for the KN calculated TE mode resistivity curve which is still relatively large, the CJ and MI calculated TE mode resistivity curves show a good match to their observed resistivity curves. The TM mode curves at KN, CJ, and MI sites also show better fit compared to the previous model. This model then suggests that the conductive body should have the 2 Ohm.m layer thicker rather than that suggested by the one-dimensional model. This model also indicates that to fit the TE observed curves at KN and CJ the 2 Ohm.m layer still needs to be thicker than the present thickness.

The model configuration which is shown in Figure 6.10 produces the best fit to the TE observed data at KN, CJ and MI sites. The TM mode curves also indicate a good fit at the short periods end of data at KN and MI but misfit at the long period data. Although the shape of the TM mode curve at CJ shows a good correlation, there remains, however, misfit between them at almost all periods. This result then suggests that a more complex model is required to satisfy both the TE and TM mode data. Results from this model can be seen in Figures 6.10a.

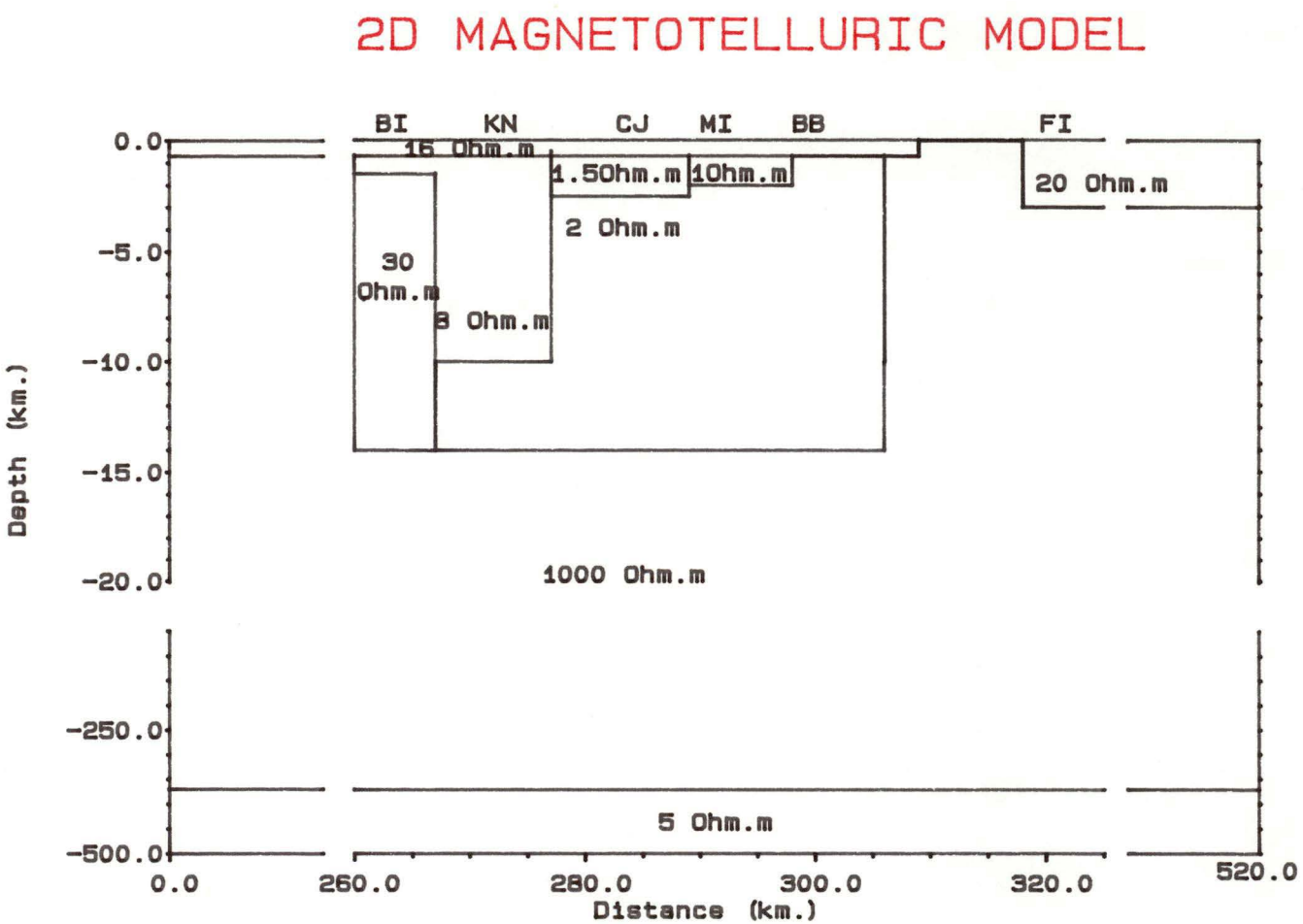

Figure 6.9 Initial 2D model configuration with a wider and thicker conducting body

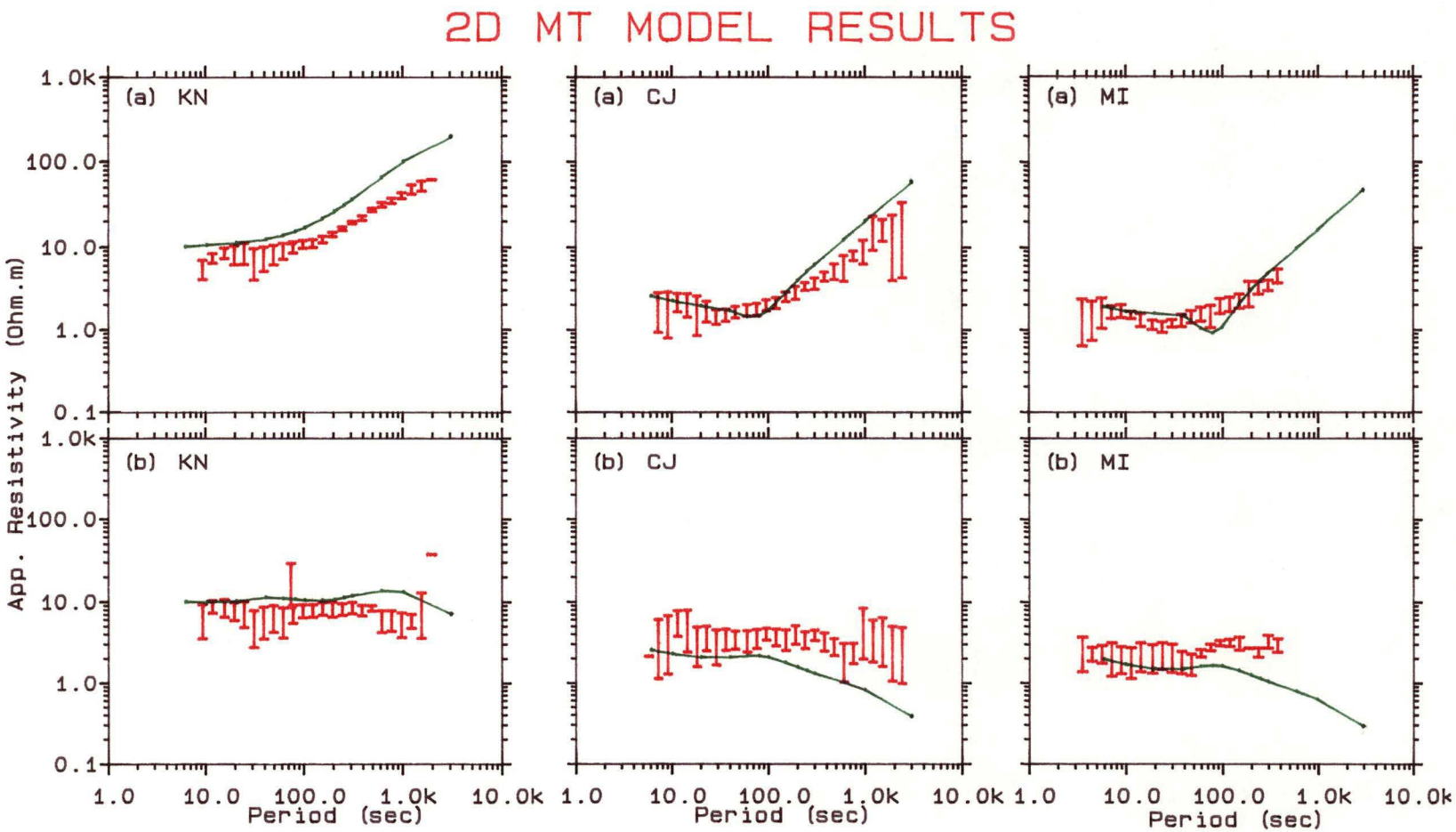

Figure 6.9a Obs. (red) and cal. (green) app. resistivity from KN, CJ, and MI sites
(a) E-polarization, (b) H-polarization

An alternative model that produces a better fit to both modes of data is shown in Figures 6.11 and 6.11a. The model configuration here is slightly different from the one shown at Figure 6.10. The insertion of a 5 Ohm.m body in between two more conducting bodies at depth seems to be useful to bring the TM curves to a better fit without affecting the TE curves. There remains, however, a misfit for the TM mode curve at CJ. Dr. W.D. Parkinson (personal communication, 1992) states that for an area having approximately two-dimensional structure the TE mode data should be used in the interpretation. This mode is less affected by the lateral inhomogeneity contrast and therefore should better represent the structural feature of the region. Gupta and Jones (1990) also imply that the TE mode data are more stable than the TM mode ones in the presence of three-dimensional structures. Skew values from all MT sites in this region, which show an increase toward longer period, indicate that at great depth the structure may no longer be two-dimensional. The misfitting TM mode data, especially at CJ, may be assumed to be due to local lateral inhomogeneity or local three-dimensional structure. It is therefore concluded that the model shown in Figure 11 is the best model configuration to represent the high conductivity anomaly in this region. This model is a culmination of about 50 different models that were tried. It has resistivity varying from 1 to 8 Ohm.m with the depth to the top of the conductor still 700 metres. The depth to the bottom conductor, on the other hand, is found to be between 14 kilometres at KN site to about 17 kilometres at CJ and MI sites. At either side of the conductor, the conductive body tapers with depth. The shape of this anomaly is consistent with the result obtained by the two-dimensional gravity and magnetic model (see Figure 5.26) and current density plot (see Figure 6.15) along this MT traverse.

Since Tasmania is an island bounded on three sides by deep oceans, it is desirable to include ocean in this two-dimensional modelling in order to see how much the ocean affects the result. Figure 6.12 shows bathimetric contours around Tasmania and the southern part of mainland Australia. The current is assumed to flow north-south on both sides of the island. As there is the mainland of Australia to the north, on the western side of the island the current will detour either to Bass Strait or to follow the south coast of the continent. On the eastern side of the island, on the other hand, the current seems to flow freely north-south. Although the margin of the east coast of Tasmania is not exactly parallel to the margin of the east coast of the mainland of Australia, it is assumed here that the ocean is approximately two-dimensional. Based on this current flow around the island, only the ocean on the eastern side of the island is included in the modelling. The ocean here has 0.3 Ohm.m resistivity and depth of about 4 km.

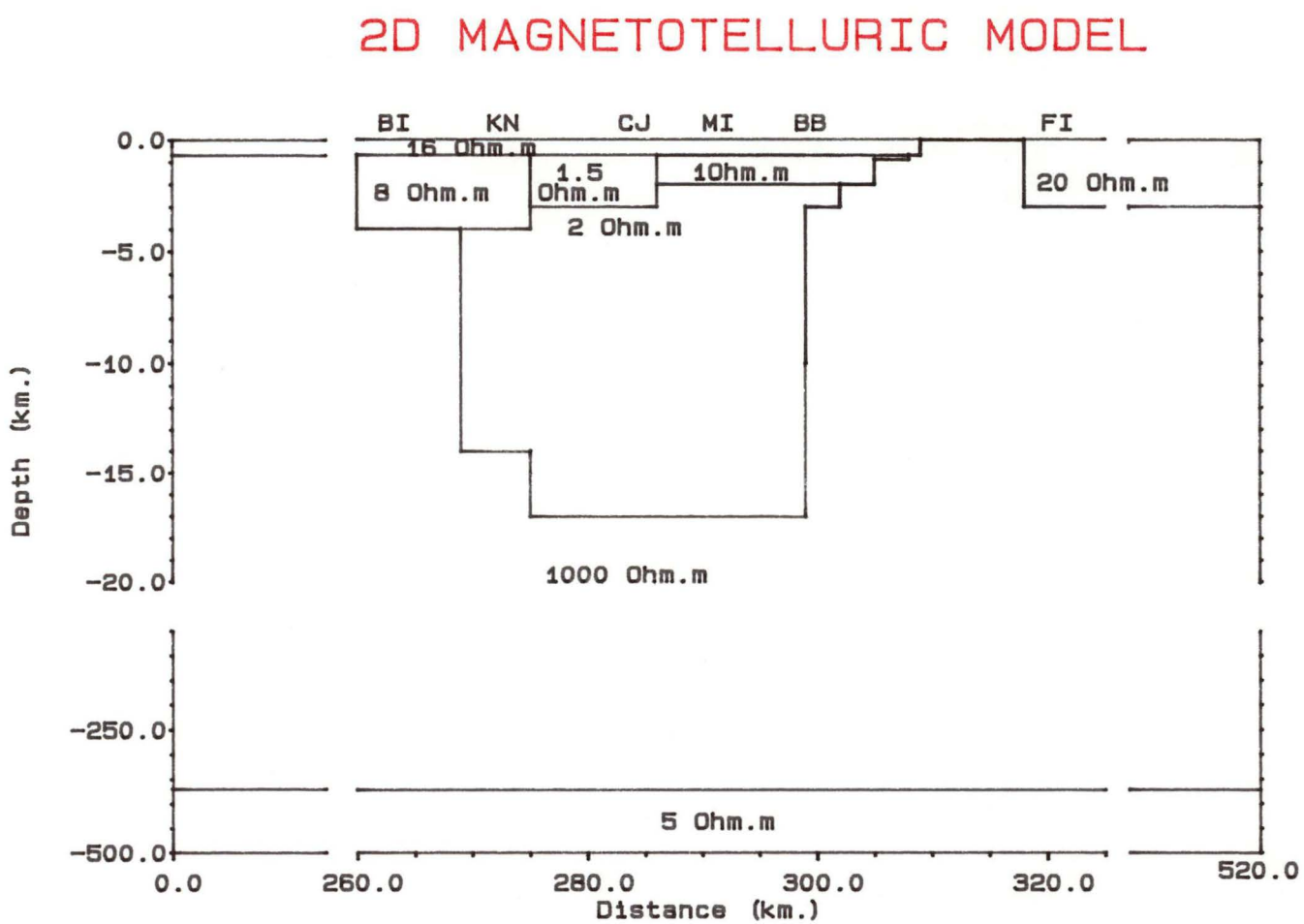

Figure 6.10 Final 2D model configuration without ocean

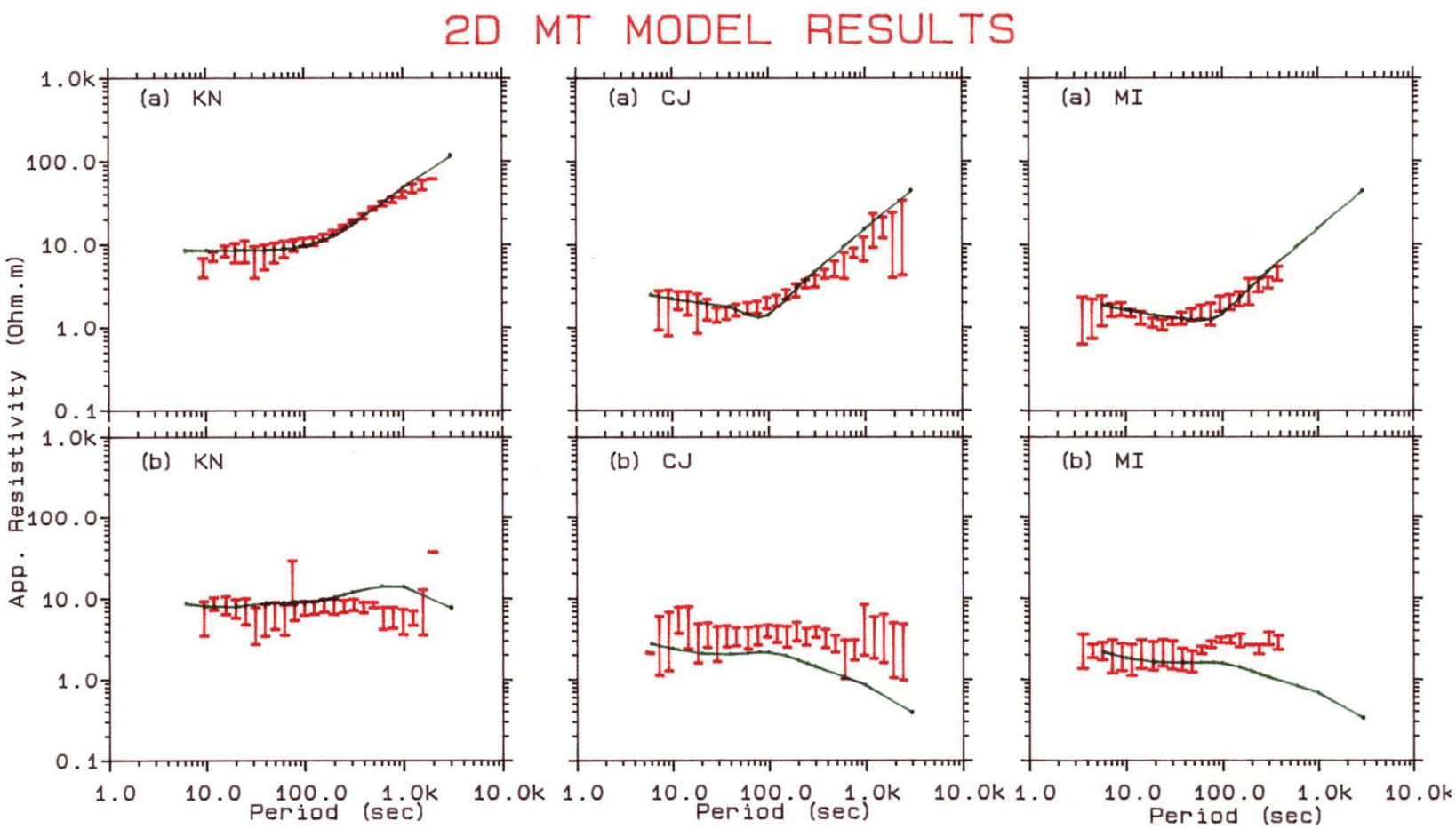

Figure 6.10a Obs. (red) and cal. (green) app. resistivity from KN, CJ, and MI sites
(a) E-polarization, (b) H-polarization

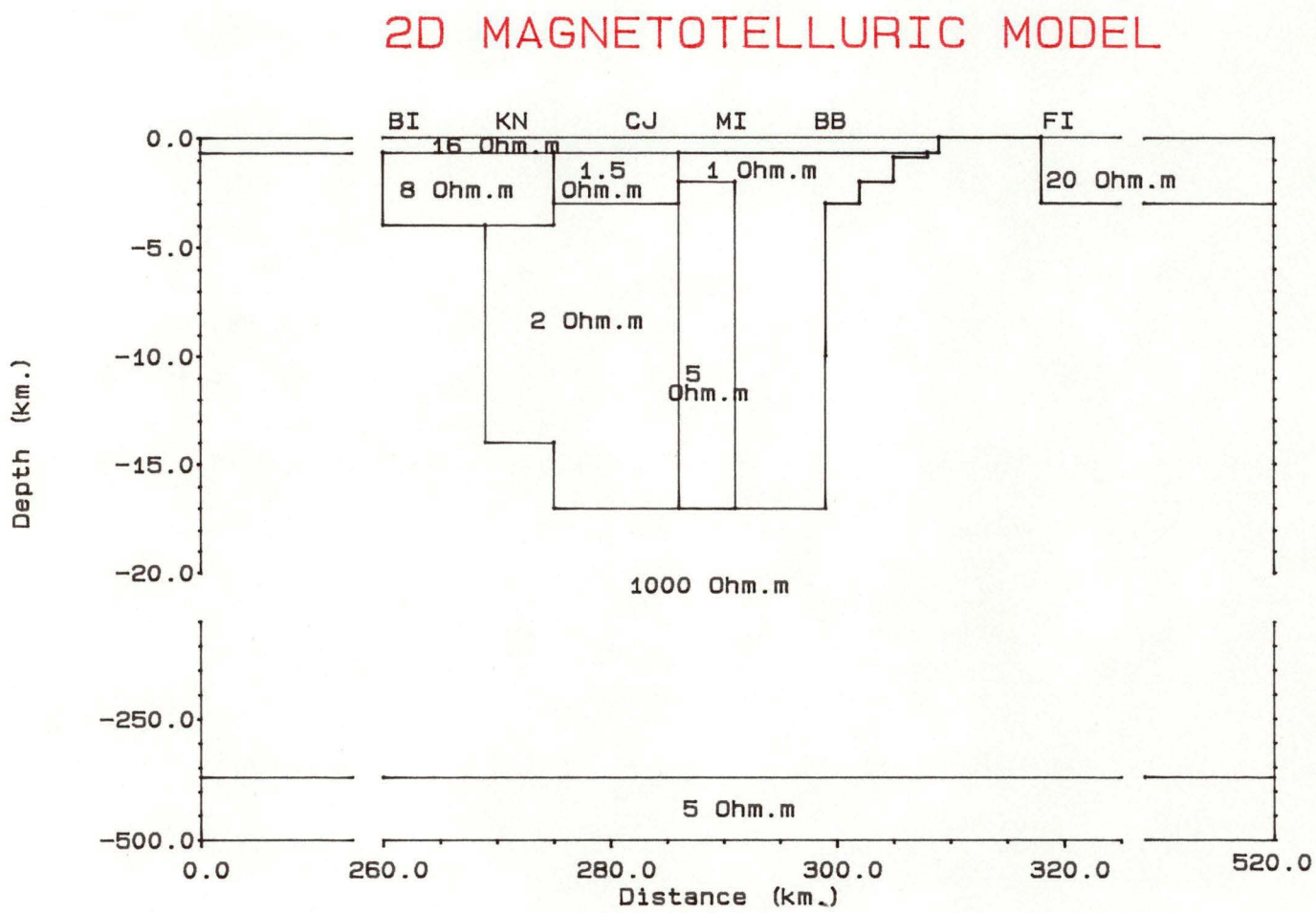

Figure 6.11 Alternative final 2D model configuration without ocean

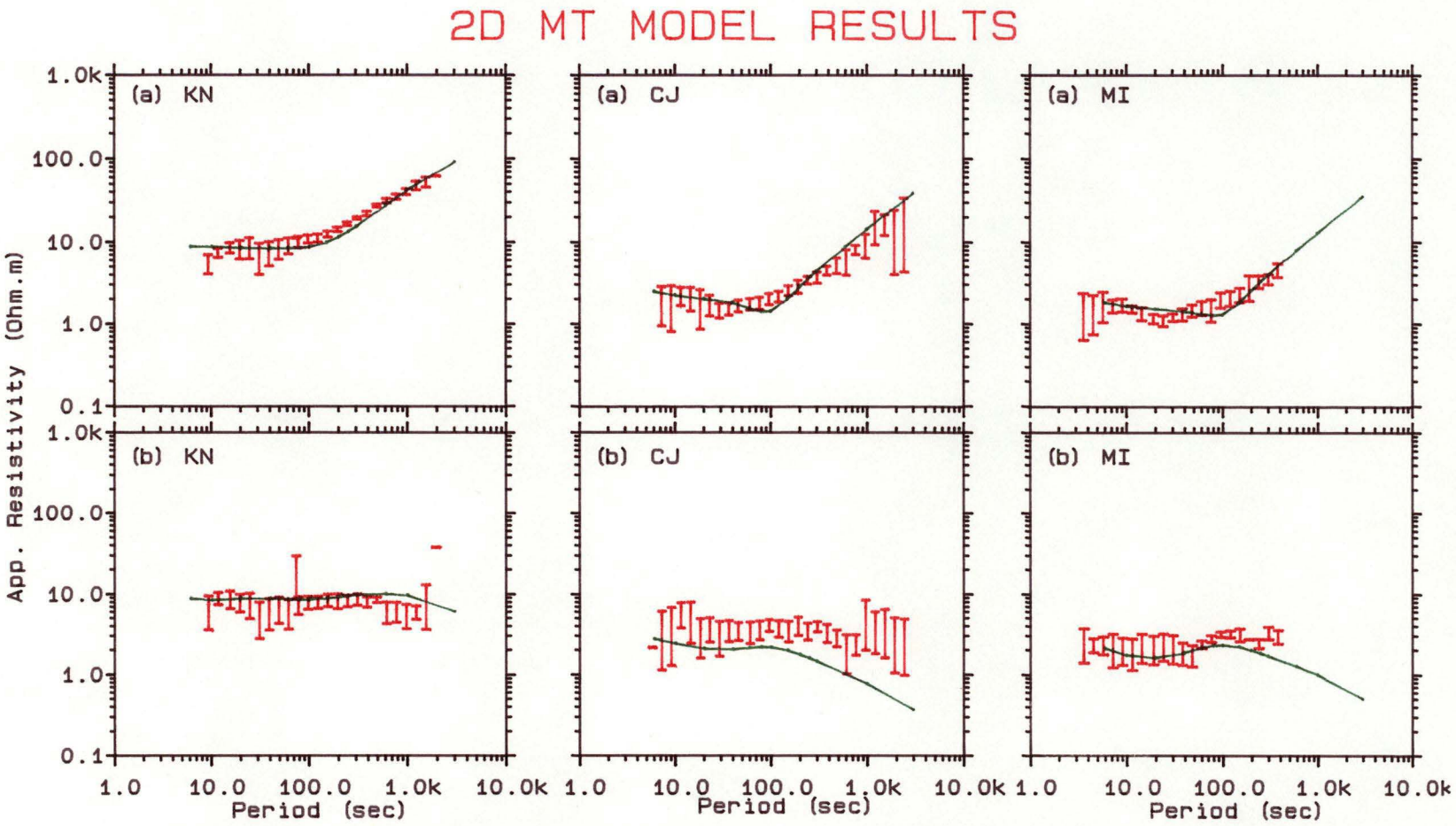

Figure 6.11a Obs. (red) and cal. (green) app. resistivity from KN, CJ, and MI sites
(a) E-polarization, (b) H-polarization

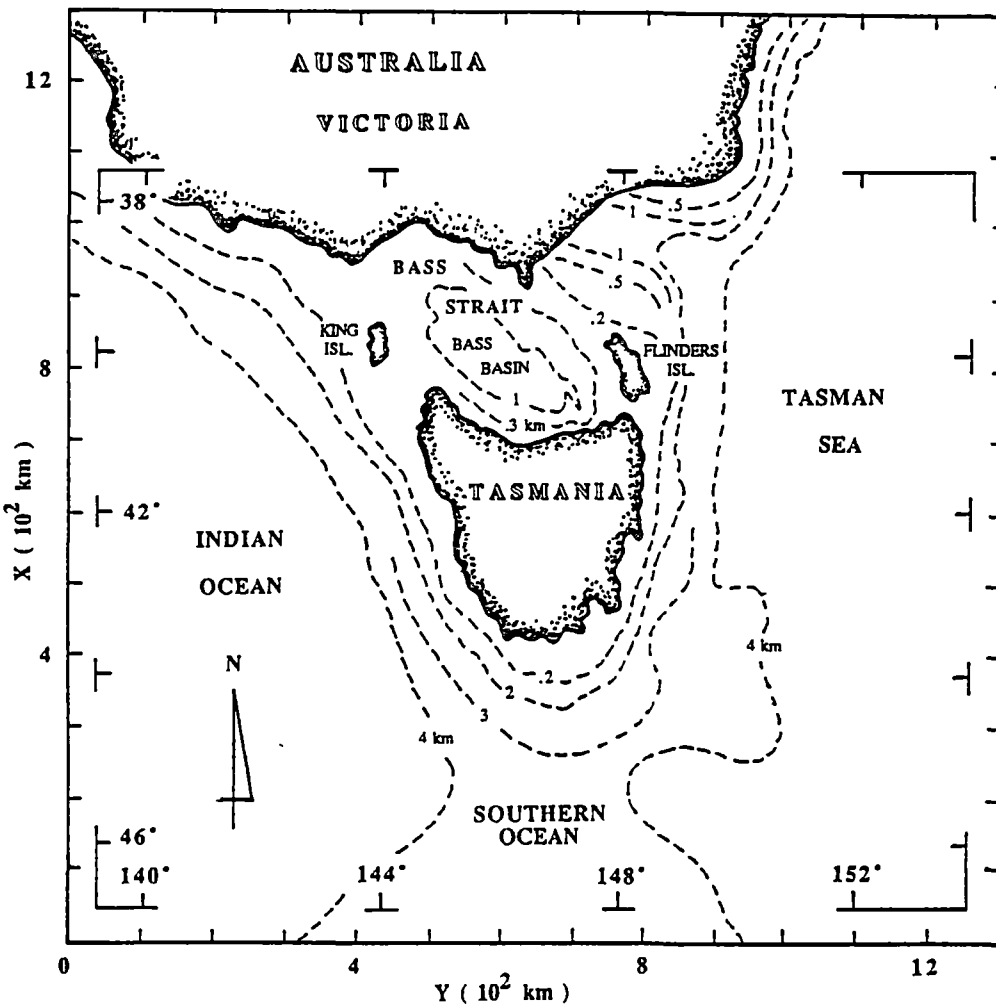

Figure 6.12 Bathimetric contour arround Tasmania and southern part of mainland of Australia.

Figure 6.13 shows two-dimensional model configuration with ocean based on the model that yields the best calculated data (i.e. Figure 6.11). The result of this modelling for KN, CJ and MI sites is given in Figure 6.13a. It is apparent here that the presence of ocean has no significant effect on the short periods end of the calculated data for both the TE and TM modes at KN, CJ and MI. In general, the ocean seems to influence only the long period end of the TE and TM modes data. This effect is seen more on the TE mode data at KI site where the calculated resistivity curve, at periods between 100 and 1000 seconds, fits the observed resistivity curve slightly less than on the TE mode data at CJ or MI sites. This is probably because KI sits on the less conductive part of the body compared to CJ and MI.

The effect of ocean on the long period end of the TM mode data at KI, CJ and MI is also very obvious. Without ocean the calculated resistivity curves at KI, CJ and MI sites (see Figure 6.11a) tend to decrease toward longer periods. With the presence of ocean, on the other hand, the calculated resistivity curves (see Figures 6.13a) tend to increase toward longer periods.

Based on the above result, it is concluded therefore that the presence of the ocean does not make the calculated resistivity curves fit any better to the observed ones. It is therefore considered that the alternative model without ocean (see Figure 6.11) is the best model to represent the two-dimensional structure along this MT traverse. Depth to the top of the conductor is about 700 metres with the thickness varying between 13.3 to 16.3 kilometres.

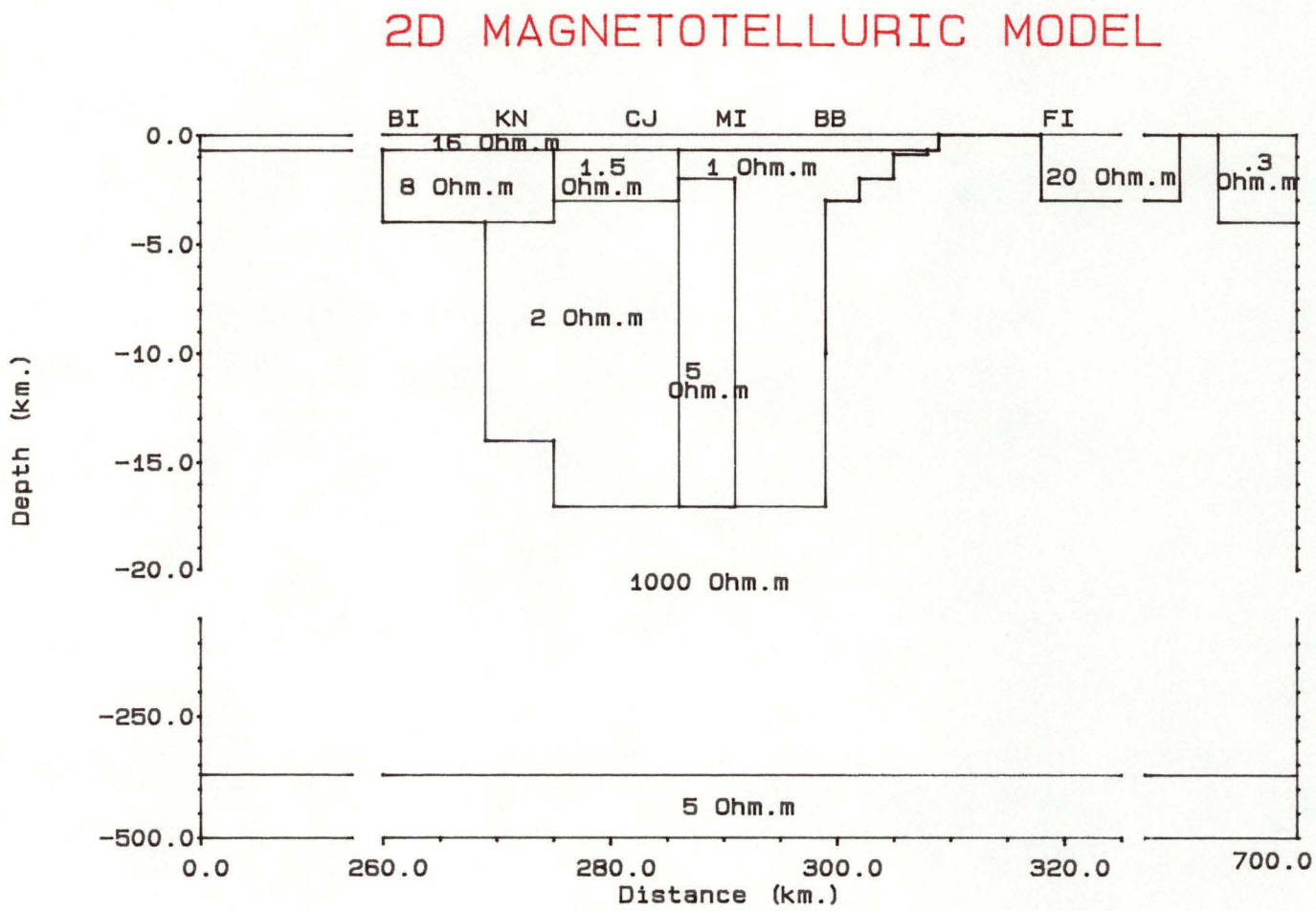

Figure 6.13 Alternative final 2D model configuration with ocean

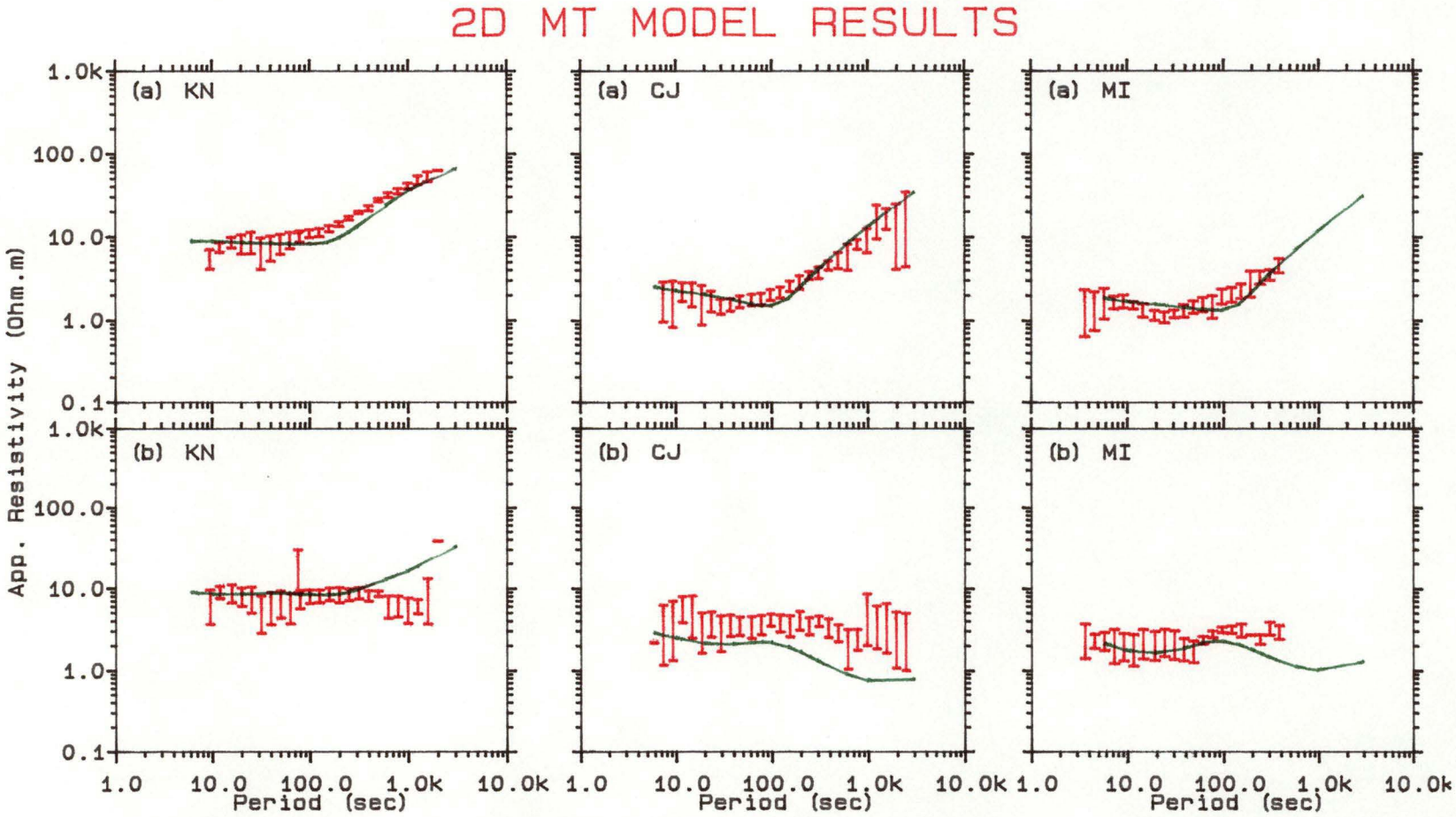

Figure 6.13a Obs. (red) and cal. (green) app. resistivity from KN, CJ, and MI sites
(a) E-polarization, (b) H-polarization

6.2 INTEGRATED INTERPRETATION

Regions of high conductivity anomaly in the upper and lower crust have been found in many parts of the world and interpreted to be associated with free fluids or free carbon, serpentinization, hydrated minerals or saline pore fluids. These findings, for example, were reported by Haak and Hutton (1984), Ritz et al. (1987), Parkinson et al. (1988), and Martinez et al. (1989).

Recent magnetotelluric experiments in the Tamar Lineament area also map a high conductivity anomaly at upper-middle crust depth. The experiments reported here confirm the presence of the high conductivity anomaly in this region suggested by the previous authors (Buyung, 1980; Sayers, 1984; Hermanto, 1985; Parkinson et al. 1988) and also give better determination on shape, thickness and resistivity of the good conductor. One- and two-dimensional MT modelling results from these experiments (see Figues 6.7 and 6.11) reveal that the high conductive body was observed at BI, KN, CJ, MI, and BB sites to a depth between 2 and 4 kilometres. Below this depth the conductive body is confined to sites between KN and BB.

The most significant result from this experiment is that the high conductivity anomaly is located relatively close to the surface i.e. at about 700 metres and extends to a depth of approximately 17 kilometres. The anomaly has resistivity ranging from 1 to 8 Ohm.m at the top 4 kilometres of the conductor and 2 Ohm.m for the rest of the conductor. These resistivity values are significantly low compared to the resistivity of the surrounding region. The resistivity of the good conductor and depth to the top of the good conductor are relatively different compared to the results obtained from the previous MT study (Sayers, 1984) which suggested that the good conductor had resistivity of 0.5 Ohm.m and was about 2 kilometres from the surface. The differences may partly be attributed to the fact that no other geophysical technique except MT was used in the previous study. Sayers' resistivity data (see Appendix 6) was a little bit scattered and contained less data in the period range below 100 seconds and therefore gave less information on the shallow structure compared to the present MT data. The use of other geophysical techniques such as DC-resistivity and SIROTEM in these experiments gave a huge advantage resulting in a better understanding of shallow subsurface structure and hence aided better estimation of resistivity of and depth to the good conductor.

Figure 6.14 shows 2D MT model results superimposed on 2D gravity and magnetic model results. There are some interesting relations between these two models. The shape of the conductive body which tapers with depth at both ends and becomes narrow at great depth, for example, is consistent with the shape of the two-dimensional gravity and magnetic modelling. The taper contacts at both sides of

Figure 6.14 Plot of 2D MT and gravity and magnetic model along MT traverse.

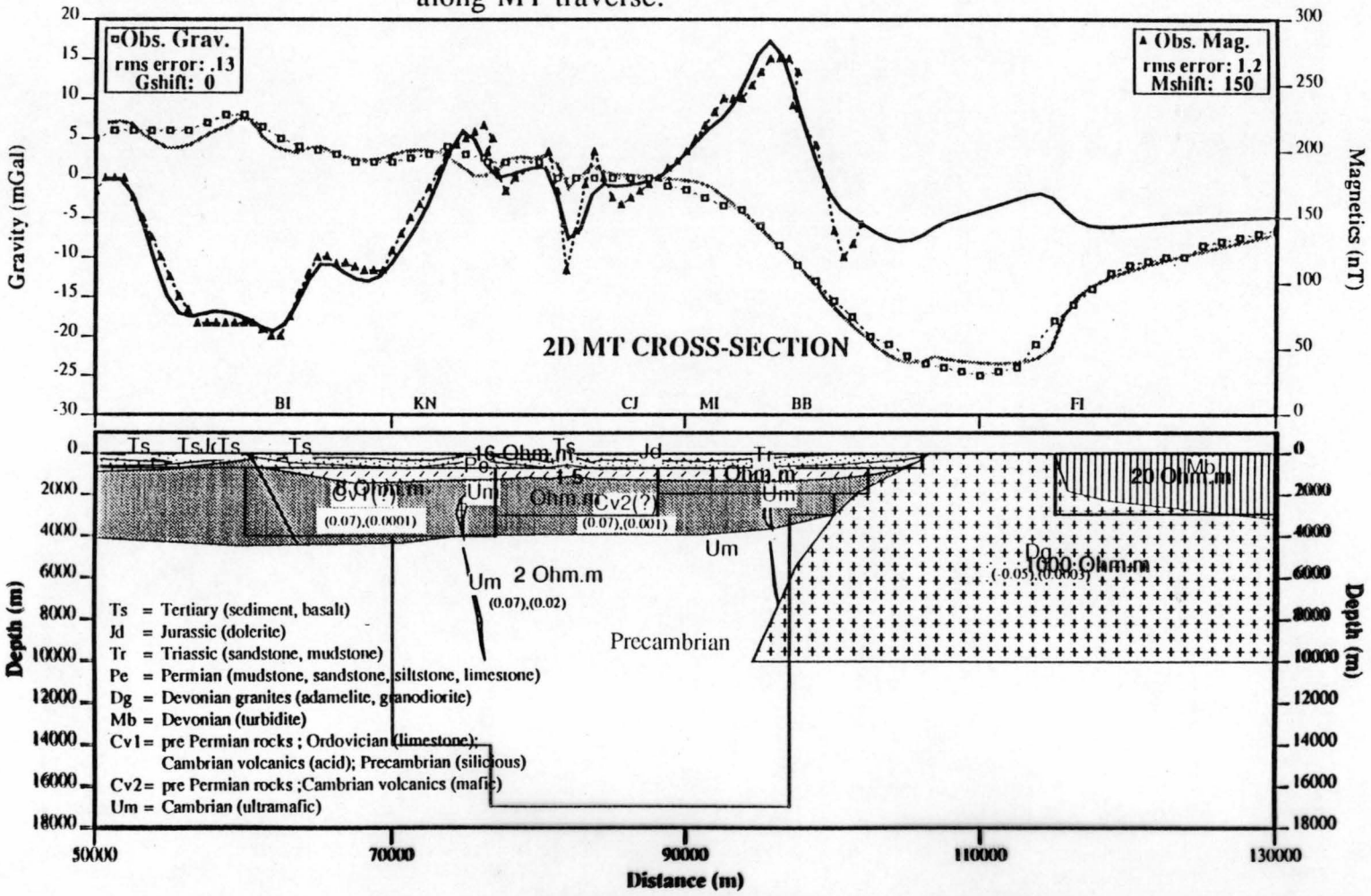

Model File:GM1BST7.MOD Date:28-11-1992 Time:17:22:28

Figure 6.14 Plot of 2D MT and gravity and magnetic model along MT traverse.

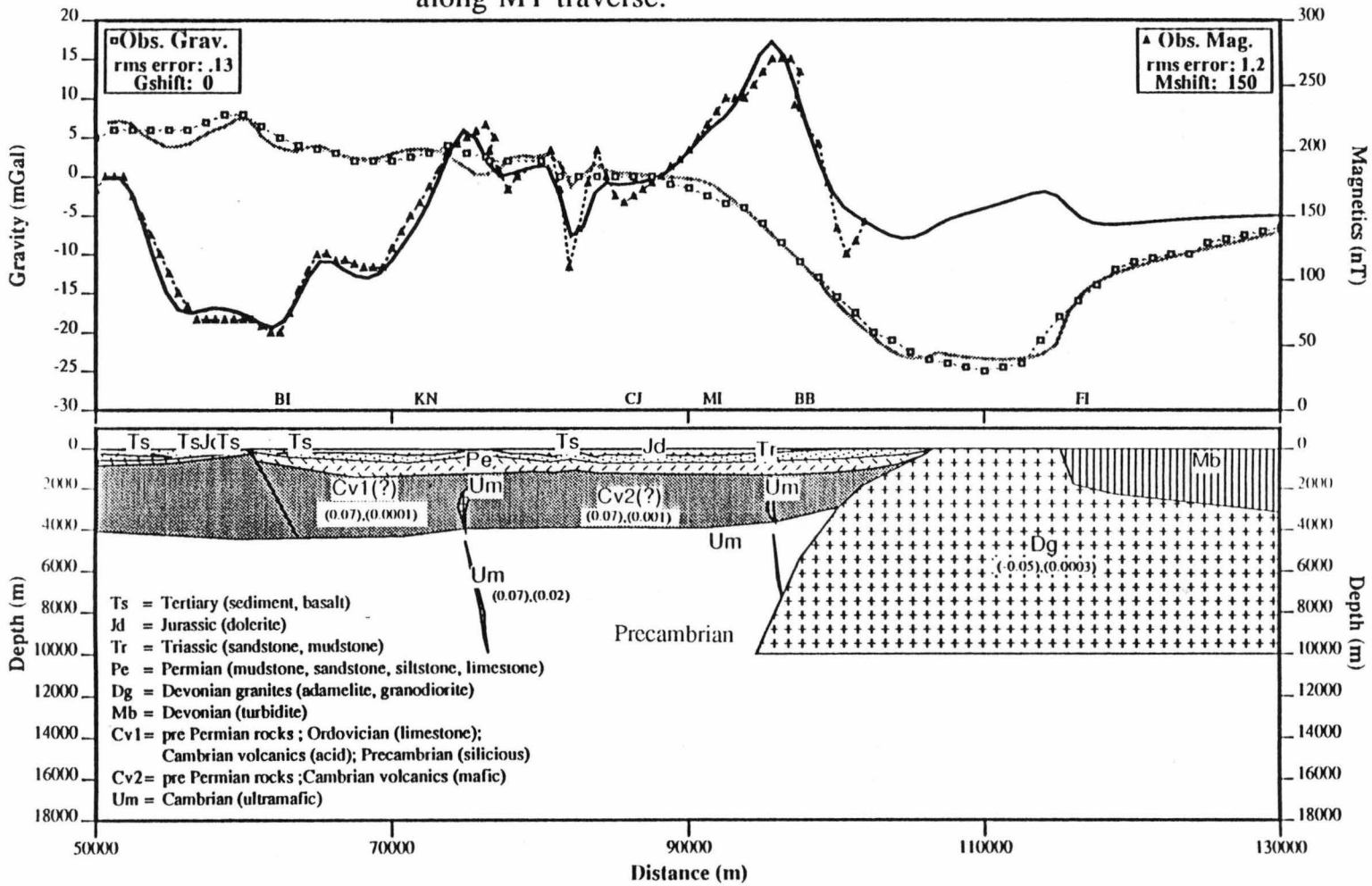

Model File:GM1BST7.MOD Obs. Gravity:GP1.OBS Obs. Magnetic:MP1.OBS Date:11-11-1992 Time:17:22:28

the conductive body seem likely to be approximately associated with the Tiers Fault and granite and ultramafic intrusions. The conductive anomaly is located coinciding with a relatively large magnetic anomaly and is interpreted to be due to ultramafic intrusions. The gravity and magnetic model indicates that the depth to the top of the conductor seems likely to be associated with the base of Permo-Triassic sediments. The depth to the bottom of the conductor, however, cannot be defined by the gravity and magnetic model. Thus the Cambrian volcanics sequences, lower Palaeozoic Mathinna Beds and dolomitic Precambrian units account for the upper part of the Tamar Conductivity Anomaly.

A good correlation between the two-dimensional MT modelling results and current densities plot, determined from the anomalous field (Parkinson et al., 1988) of the MV study along this MT traverse, is shown in Figure 6.15. The current densities, which peak between STJ and HAN sites, agree well with the position of high conductivity anomaly in this region.

Previous authors (Sayers, 1984; Hermanto, 1985; Parkinson et al. 1988) have suggested that the most likely explanation for the Tamar Conductivity Anomaly is fractured rock saturated with high conducting pore fluids. This explanation, however, requires high porosity rocks of about 12 % and very high conducting liquids of about 17 Sm^{-1} (Parkinson et al. 1988) which seem to be difficult to obtain. This is because the resistivity of the anomaly determined from previous MT study (Sayers, 1984) was too conductive i.e. about 0.5 Ohm.m. The present study, however, indicates that the conductivity anomaly has resistivity varying from 1 to 8 Ohm.m, which approximately increases by a factor of 2 to 16, and a thickness of about 13 to 17 kilometres. The possibility that the anomaly, especially at the top part, is likely to be due to electrolytic conduction in pore fluids is therefore enhanced as the effect of hydrostatic pressure on pores or cracks is relatively small. However, Leaman (1992) suggests that this is a pull-apart zone which has been inactive.

Recent geophysical results based on expanded data base and a new two-dimensional gravity and magnetic interpretation (Leaman and Richardson, 1989; Leaman, 1992), geothermal gradient, and seismic data also open new hypotheses on the likely cause of the high conductivity anomaly. Extension since the Jurassic period would support abnormal porosities and fracture permeabilities and allow better circulation at considerable depth. It should also be noted that the area is known for its surface high salinity as reported by Matthews (1983).

It has been known for some time that Tasmania is regarded as having comparatively high heat flow i.e. greater than 2 HFU (Jaeger and Sass, 1963;

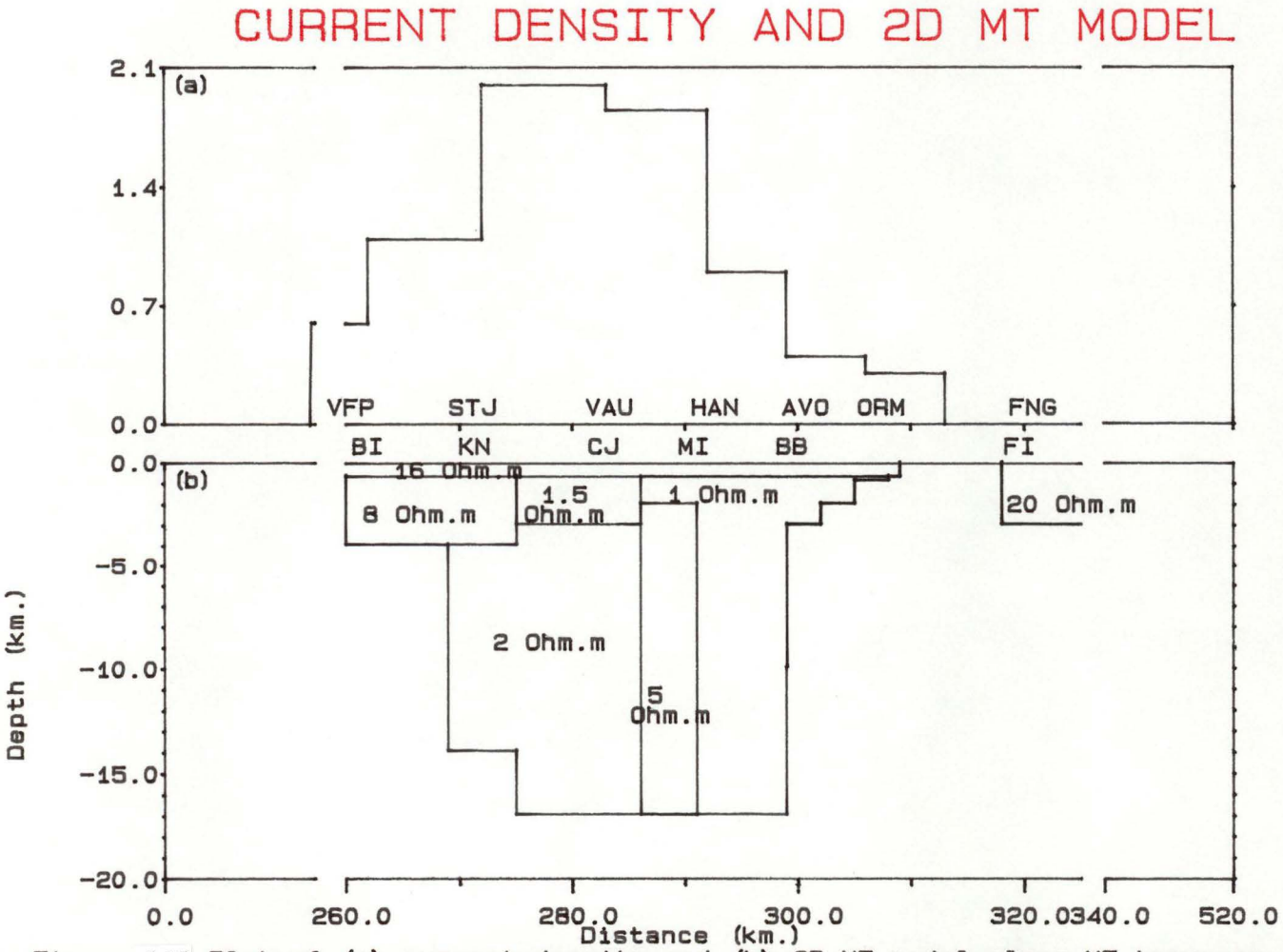

Figure 6.15 Plot of (a) current density and (b) 2D MT model along MT traverse. Current density are based on corrected for the presence of ocean. Ordinate for (a) are pure numbers being Amp.per m/Amp. per m.

Current density redrawn from Parkinson et al.(1988).

Wronski, 1977; Green, 1989). This heat flow value is consistent with the average heat flow value of 2.85 HFU observed in the south-east Australian region (Jaeger, 1970). Bennet and Lilley (1973) linked this heat flow value to the conductive anomaly observed in the same region and postulated that the anomaly was due to elevated temperature and partial melting associated with the Newer Volcanics of Victoria. Wronski (1977) and Green (1989) reported that averaged thermal gradient at Glenorchy, Stanley, Coles Bay and Tunbridge was 40.4° Ckm^{-1}, 30° Ckm^{-1}, 28° Ckm^{-1}, and 41° Ckm^{-1}, respectively, although the latter is suspect. Based on the above values the averaged thermal gradient in Tasmania is approximately 35° Ckm^{-1}. Kao (1982) suggested that at great depth a transition from resistive to conductive layers may be related to the physical condition of hydrated granites at temperature of 600° C and pressures of 3-20 kb. For a thermal gradient of 35° C/km it is expected that the 600° geotherm will be reached at depth of about 16 to 17 kilometres. Based on two-dimensional gravity and magnetic modelling the granite in north-east Tasmania, however, has a thickness of approximately 10 kilometres and since the conductivity anomaly stretches from a depth of 17 kilometres almost to the surface, it seems unlikely that the high conductivity anomaly in this region is associated with the partial melting. Magnetic anomalies along traverses 1, where some MT sites are located, and traverse 2 (see Figures 5.26 and 5.27) show quite large variations which indicates that subsurface rocks are more magnetic compared to the rest of the traverses. A long wavelength anomaly along these traverses indicates that the anomaly is of deep origin. If the conductivity anomaly is to be linked with partial melting then there should exist a magnetic quiet zone which is not observed in this case. This result also suggests that partial melting is one of the less likely hypotheses.

There is a possibility that the anomaly may be related to metallic oxides or sulphides but too large a volume would be required for this to be a realistic option. The gravity and magnetic anomaly along traverse 1 and 2 also does not support this possibility.

Another possible cause of the anomaly is that it may be due to conduction through hydrated solid rocks. Hyndman and Hyndman (1968) postulated that the presence of hydrated rocks was considered to be a possible reason for lowering resistivity in the lower crust. Hutton et al. (1980) stated that the presence of hydrated rocks with or without associated partial melting has been used to explain the conducting layer in the lower crust. Based on laboratory work Olhoef (1981), however, indicated that the hydrated minerals are not intrinsically conductive; it is the fluids released by the dehydration process that cause the high conductivity anomaly. Jones and Craven (1990) also stated that the fluids released by such reactions could become trapped beneath an impermeable layer which forms at temperatures of around 400° C. Ingham

and Hutton (1982) imply that the critical factor in controlling electrolytic conduction is porosity and based on Keller's (1966) calculation they illustrate that the conduction by pore fluids is likely to be very small below a depth of approximately 15 kilometres. It is, however, argued by Berdichevsky et al. (1972) who state that water can be released from hydrated minerals in the course of metamorphism and about 1 to 5 % water is released due to dehydration at the boundary between granulitic facies. Ingham and Hutton (1982) further state that although the electrolytic conduction in the lower crust is likely to be small due to closure of cracks and pores by pressure, it is possible that low resistivities may be produced by intergranular distribution of water of crystalization during the process of dehydration of hydrated minerals. Recent findings from the Kola 'superdeep' research well in the Soviet Arctic (Kozlovsky, 1984) revealed the presence of a large amount of mineralized water trapped at mid-crustal depth after metamorphic dehydration (Martinez, et al. 1989).

Another possibility that the anomaly is due to graphite or some amorphous kind of carbon cannot be ruled out. Duba and Shankland (1982) stated that graphite lowered resistivity values by several orders of magnitude and accounted for large-scale resistivity anomalies in the crust. Several examples relating to support for black shales as a source of high conductivity anomalies are given by Stanley (1989). Black argillites of the Pritchard Formation in the Proterozoic belt basin, Montana, for example, have resistivity of less than 1 Ohm.m (Wynn et al. 1977; Harrison et al. 1985). Massive black shales with 2 - 7 % organic carbon content have been mildly metamorphosed to argillite in Alaska and were found to have resistivity of less than 5 Ohm.m and have thickness of about 30 kilometres (Stanley, 1986). Duba et al. (1988) also reveal that black shales recovered from a 6000 metres depth well in west Germany have resistivity of 2 to 3 Ohm.m. Stanley (1989) stated that the high conductivities in black shales are most often caused by carbon films or interconnected carbon particles along fissile planes. Such thin carbon films are not accessible either to optical or electron microscopes because of their small thickness after coalification but form an efficient electrical network throughout the rocks where this process would contribute to decreased resistivity in the rocks (Duba et al. 1988). Haak et al. (1991) suggest that thin graphite films may be deposited from C-O-H fluids in the stability field of quartzs-magnetite-fayalite (QMF) buffer which have low oxygen fugacity. This C-O-H system may be generated elsewhere and then migrated through fractures and deposited by retrograde reaction. Haak et al. (1991) further suggest that such a process seems to be reasonable, as graphite coexists with chlorite - a mineral which extracts large amounts of water from C-O-H fluids so that graphite can precipitate. The importance of interconnection between carbon particles along grain boundaries in rocks is also emphasized by Haak et al. (1991) who state that the existence of graphite is not sufficient to explain the low resistivity. It is the

interconnection of graphite that is essential in lowering the resistivity. Although no graphite crops out in the vicinity of the investigation area, it is not unlikely that graphite is deposited deep in the crust under the investigation area as graphite in the form of black shales, for example, crop out in the west coast area (Dr. A.J. Crawford, personal communication, 1992). The black shale from a borehole in west Germany also crops out not in the borehole area but 80 kilometres SE of the borehole location (Duba et al. 1988). Black shales and sheared carbonates could be expected in the Precambrian rocks and implied to be present. Bishop and Lewis (1988) who conducted spectral IP measurements at several places in the west coast area, however, found that black shales from Rosebery Open Cut, Anthony Road, White Spurs, Red Hills, West Sedgwick, and Hellyer site 2 had large resistivity values ranging from about 60 Ohm.m to about 2000 Ohm.m. This resistivity seems to be too high to account for the high conductivity found in the Tamar Zone. It is, however, not surprising as it has also been pointed out by Haak et al. (1991) that most metamorphic rocks situated at the earth's surface do not illustrate such large-scale low resistivity anomalies though they may consist of significant amounts of graphite. An answer to this problem is suggested by Duba et al. (1988) that when black shale is heated to 320° C in air it becomes very resistive. A more significant view of this problem is given by Haak et al. (1991) who state that when rocks containing graphite films around their grain are moved to the earth's surface, by tectonic process, and thus to a higher oxygen fugacity, the films will become unstable and disappear resulting in high resistivity.

Out of several hypotheses suggested above a combination seems to be the most likely cause of the high conductivity anomaly in this area. Geophysical evidence shows that Tasmanian crust has relatively low seismic velocity i.e. 5.86 km s^{-1} (Richardson, 1980) compared to 6.5 km s^{-1} to 7.4 km s^{-1} (Marquis and Hyndmand, 1992) in other parts of the world. Using the velocity-porosity relationship developed by Marquis and Hyndmand, (1992) (see Figure 6.16) it is apparent that a few per cents of porosity can occur, depending on the aspect ratio used, in the Tasmanian crust. Two-dimensional gravity and magnetic modelling (see Figures 5.26 and 5.27) reveal that fractures associated with deep faults occur in the upper-middle crustal depth range. Geological evidence also indicates considerable tectonic history west of the Tamar Lineament resulting in intense fracturing or shearing (Parkinson et al. 1988) and subsequent extension (Leaman, 1992) will provide an environment for deep fluid circulation and graphite precipitation. Using the velocity-resistivity relationship generated by Marquis and Hyndman (1992) (see Figure 6.17), for aspect ratio 'a' (for velocity) of 0.03 and Archie's law exponent 'm' (for resistivity) of 2, it can be seen that a resistivity of less than 2 Ohm.m can be obtained in the crust having velocity of 5.86 km s^{-1} or 6.0 km s^{-1}. This result is thus in accord with the resistivity of the high conductive anomaly in the Tamar Lineament area.

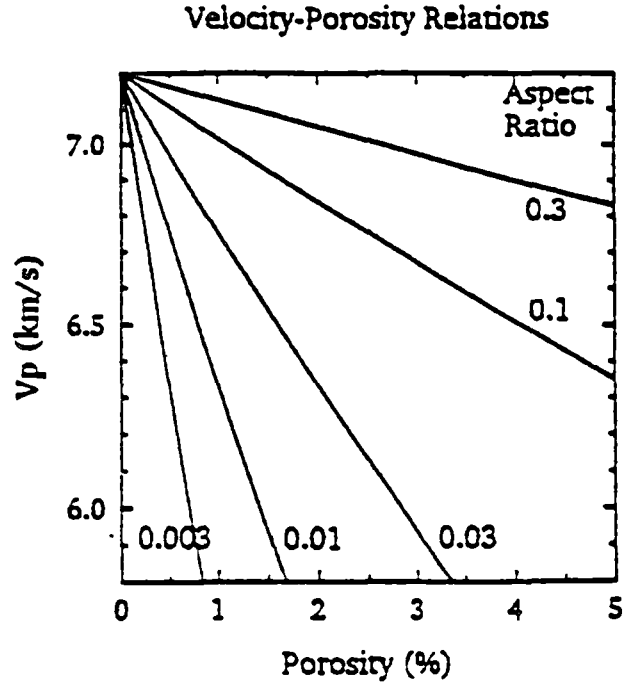

Figure 6.16 Velocity-porosity relations for a mafic rock containing ellipsoidal pores of selected aspect ratios. Zero-porosity velocity is 7.2 kms^{-1}. (After Marquis and Hyndman, 1992).

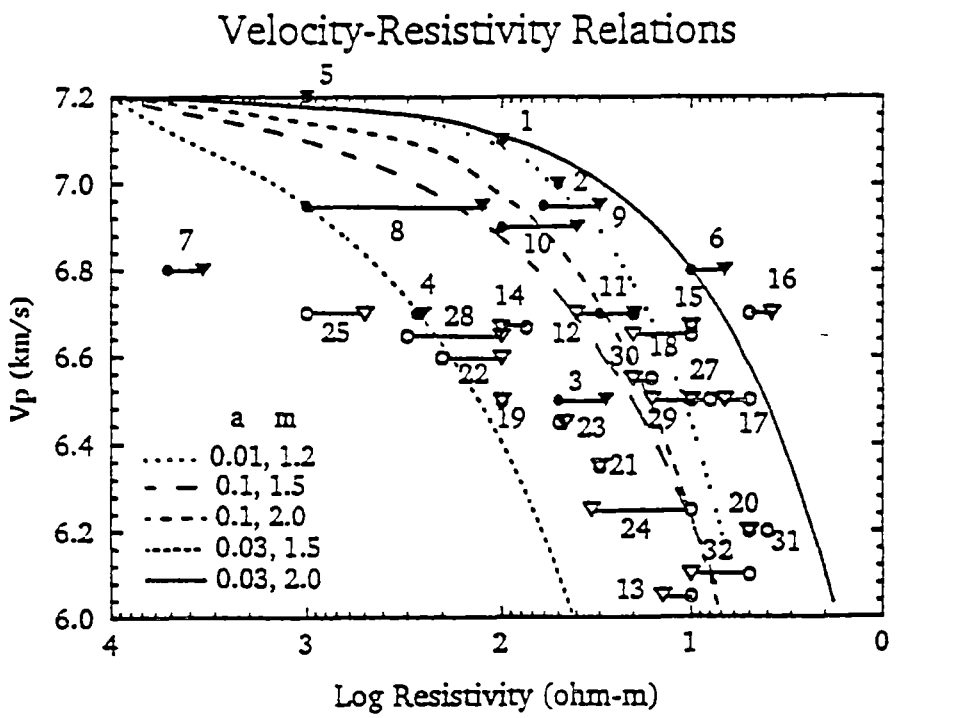

Figure 6.17 Velocity-resistivity relations. The theoretical curves represent combinations of pore aspect ratio 'a' (for velocity) and Archie's Law exponent 'm' (for resistivity). Close symbols denote Precambrian and open symbols denote Phanerozoic areas. Circles denote resistivity as reported by the original investigators, triangles denote resistivities for a 10 km thick layer of the same conductance. (After Marquis and Hyndman, 1992).

CHAPTER 7:
CONCLUSIONS

Magnetotelluric experiments conducted in the Tamar Lineament area have proved to be a useful tool in delineating subsurface electrical structure in that region. Results from these experiments have defined a high conductivity anomaly in the upper-middle crustal range and is consistent with the anomaly suggested by previous authors (Buyung, 1985; Sayers, 1984; Hermanto, 1985; Parkinson et al., 1989).

The use of other geophysical techniques such as dc-resistivity and SIROTEM add significant information on resistivity of shallow structure and aid a better determination on depth to the top of the conductor. Two-dimensional gravity and magnetic modelling carried out over two cross-sections and the results of seismic refraction and reflection of Richardson (1980) and Vitesnik (1984) are also useful in outlining the tectonic framework and, most importantly, the setting of the conductivity anomaly. The gravity and magnetic model along the MT traverse shows that the upper part (at least 5 kilometres) of the conductivity anomaly seems to be located between the granite wall on the east and the Tiers Fault on the west.

Tensor analysis of magnetotelluric data shows a consistent and marked anisotropy at almost all MT sites. The degree of anisotropy, indicated by the TE and TM mode resistivities, seems to decrease toward the eastern sites and disapears at FI site. This result suggests that the structure under the FI site may be less complex than under other MT sites. This feature, however, seems to contradict the information shown by the skew values from that site which are large at all periods implying the presence of three-dimensional structure. Apparent resistivity also tends to decrease eastward, i.e. toward BB site where it closes to the granite contact, and then changes dramatically beyond the contact. It is shown from the analysis that few sites have approximately two-dimensional structures. Indication to two-dimensionality is given by the low skew values from those sites.

Static shift effects due to local surficial or near surface lateral inhomogeneities on apparent resistivity was checked using SIROTEM data which implied that no static shift correction needs to be applied to the observed MT data. The consistency between the DC-resistivity, SIROTEM, and one-dimensional model results also indicates that there are no near surface effects present in the vicinity of the MT sites and therefore no static shift correction is required.

One-dimensional modelling offers a tentative explanation for the observed anisotropies in the apparent resistivity. It constitutes a major step towards understanding the true resistivity structure in this region. The model results suggest that the high conductivity anomaly is located about 500 to 700 metres from the surface with resistivity varying from 1 to 8 Ohm.m and thickness from 4.9 to 11 kilometres. The shape of the anomaly seems to taper with depth.

A more realistic configuration for the high conductivity anomaly in this region is probably given by the two-dimensional modelling. The overall shape, resistivity, and depth to the top of the conductor follow the one-dimensional modelling results but the conducting body has to be thicker than is suggested by the one-dimensional results in order to match the TE and TM apparent resistivity curves. The alternative final model shows that the calculated data fits better to the observed TE mode than the observed TM mode. A suggestion that the TM mode data may be affected by the presence of ocean on the eastern side of Tasmania could be dismissed since inserting ocean in that model does not improve the fit. The alternative final model without ocean is therefore considered as the best model to represent the high conductivity anomaly in this region. Based on the best fitting model the anomaly now suggests a thickness varying between 13.3 and 16.3 kilometres.

There seems to be a good correlation between the shape and position of the high conductivity anomaly determined from one- and two-dimensional MT modelling and current densities plot. A good correlation is also shown by the two-dimensional MT and gravity and magnetic modelling (see Figure 6.14). The tapering contact at both sides of the anomaly seems to follow the Tiers Fault and granite and ultramafic intrusions which mark fundamental structural limit on the west and east of the anomaly. The gravity and magnetic models indicate that the depth to the top of the conductor is likely to be associated with the basal Permo-Triassic cover unconformity. The gravity and magnetic data also show that large fault or thrust bounded blocks of Lower Palaeozoic and Upper Precambrian rocks underlie the Permian cover. The Cambrian volcanic sequences, lower Palaeozoic Mathinna Beds and dolomitic Precambrian units may therefore account for the upper part (at least 5 kilometres) of the conductive anomaly.

Comparison of the gravity and magnetic model result with the electrical structure (see Figure 6.14) shows clearly that the very conductive rocks are associated with the more magnetic part of the Cambrian sequence and that the great bulk of good conductivities lies below this sequence. Geologically this zone correlates with the region bounded by ultramafic slices which almost certainly mark fault zones which are not known at the surface. This suggests a tectonically emplaced structure

and if thrusting is involved the structure suggests transport from the east. The correlation with what is very likely a Cambrian trough at the top may indicate that the process involved in creating the volcanics is responsible for the high conductivity seen today in the lower crust. This would imply that compositional changes in the upper mantle and lower crust specific to the trough-extensional-pile zone have been defined.

A number of hypotheses have been put forward to explain the conductivity anomaly and the most likely explanation is a combination of extensive fracturing associated with the pre-Permian rocks providing an environment for deep high conductivity fluid circulation and graphite or black shales which form along grain boundaries that provide a continous conducting path. Geological and geophysical results suggest that major tectonic boundaries occur west of the Tamar Lineament resulting in extensive fracturing deep in the crust. These are marked today by the Tiers Fault system, the face of the Great Western Tiers, and a major gravity gradient. Black shales and sheared carbonates are known to exist in the Precambrian rocks implied to be present. The velocity-resistivity relation also indicates that resistivity as low as 2 Ohm.m may occur in the Tasmanian crust where the velocity is about 6.0 km s^{-1}. This possible relationship may be used to further evaluate the depth range and extent of the altered crust. It is recomended that other deeply burried, volcanics-rich, troughs present in the Tasmanian Lower Cambrian be inspected in this way. Similar results would confirm the implication of this work; that important compositional changes in the lower crust can be related to the primary structures forming at the heart of new basins and can be located using electrical methods. These methods appear to be better able to define elements at Moho depths than the potential field methods and may be more cost effective than seismic methods.

REFERENCES :

Adam, A., 1976. *In:* Adam, A., (ed), Geoelectric and Geothermal Studies. *KAPG Geophys. Monog. Akad. Kiado, Budapest.*

Archer, R., 1989. Geophysical interpretation of the Devonian Granite Complex and its relationship to mineralization on western Tasmania. *Unpublished B.Sc. Hons. thesis,* Geology Department, University of Tasmania.

Asten, M. W., 1972. Magnetotelluric Sounding in Tasmania. *Unpublished B.Sc. Hons. thesis*, Geology Department, University of Tasmania.

Bahr, K., 1988. Interpretation of magnetotelluric impedance tensor: regional induction and local telluric distortion. *J.Geophys., 62, 119-127.*

Bahr, K., and Groom, R. W., 1990. Correction for near surface effects. *Tutorial presented at Ensenada, Mexico.*

Banks, M. R., 1989. Late Cambrian to Devonian: Summary. *In* : Burrett C.F., (ed) Geology and Mineral Resources of Tasmania. *Special Publication Geol. Soc. of Aust., 15, 182-183.*

Banks, M. R., and Baillie P. W., 1989. Late Cambrian to Devonian. *In* : Burrett C.F., (ed) Geology and Mineral Resources of Tasmania. *Special Publication Geol. Soc. of Aust., 15, 182-237.*

Bennet, D. J., and Lilley, F. E. M., 1973. Electrical Conductivity Structure in South-east Australian Region. *Geophys. J. R. Astr. Soc., 37, 191-206.*

Berdichevsky, M. N., and Dmitriev, V. I., 1976. Distortion of magnetic and electrical fields by near-surface lateral inhomogeneities. *Acta Geodaet. Geophys. et Montanist. Acad. Sci. Hung. Tomus, 11, 447-483.*

Berdichevsky, M. N., Vanyan L. L., and Dmitriev, V. I., 1989. Method used in the U.S.S.R. to reduce near-surface inhomogeneity effects on deep magnetotelluric sounding. *Phys. of the Earth and Plan. Int., 53, 194-206.*

Berdichevsky, M. N., Vanyan, L. L., Feldman, I. S., and Porstendorfer, G., 1972. Conducting layers in the earth's crust and upper mantle. *Beitr. Geophys., 81, 187-196.*

Berdichevsky, M. N., Vanyan, L. L., Kuznetsov, V. A., Levadny, V. T., Mandelbaum, M. M., Nechaeva, G. P., Okulessky, B. A., Shilosky, P. P., and Shpak, I. P., 1980. Geoelectrical model of the Baikal region.*Phys.of the Earth and Plan. Inter., 22, 1-11.*

Bindoff, N. L., 1983. A preliminary magnetotelluric survey of north-eastern Tasmania.*Unpublished B.Sc. Hons. thesis*, Geology Department, University of Tasmania.

Bishop, J. R., and Lewis, R. J. G., 1988. Geophysical signatures of Western Tasmanian mineralisation volume 2. Electrical properties of Western Tasmanian materials. *Mt Read Volcanic Project, Tasmania Department of Mines, Hobart.*

Blohm, E. K., and Flathe, H., 1970. Geoelectrical deep sounding in the Rhinegraben. *In: Int. Upper Mantle Proj. Sci. Rep. No. 27, Graben Problems, 239-241.*

Bosum, W., and Homilius, J., 1973. A combined interpretation of geoelectrical and airborne-magnetic survey in Paktia, East Afghanistan. *Geophys. Prosp., 21, 46-65.*

Brown, A. V., 1989. Eo-Cambrian-Cambrian. *In* : Burrett C.F., (ed) Geology and Mineral Resources of Tasmania. *Special Publication Geol. Soc. of Aust., 15, 47-83.*

Buselli, G., 1974. Multichannel Transient Electromagnetic measurements near Cloncurry. *Bull. Aust. Soc. Explor. Geophys., 5, 31-47.*

Buselli, G., 1977. Transient Electromagnetic Measurements to Late Delay Times over the Woodlawn Ore Body. *Bull. Aust. Soc. Explor. Geophys., 8, 1-5.*

Buselli, G., 1982. The effect of near surface super paramagnetism material on electromagnetic transient. *Geophys., 47, 1315-1324.*

Buselli, G., and O'Neill, B., 1977. SIROTEM: A New Portable Instrument for Multichannel Transient Electromagnetic Measurements. *Bull. Aust. Soc. Explor. Geophys., 8, 82-87.*

Buyung, N., 1980. A Geomagnetic Induction Study in the North-east of Tasmania. *Unpublished M.Sc.thesis*, Geology Department, University of Tasmania.

Cameron, P. J., 1971. Crustal Seismic Velocities in Tasmania.*Unpublished B.Sc. Hons.thesis*, Geology Department, University of Tasmania.

Cagniard, L., 1953. Basic theory of the magnetotelluric method of geophysical prospecting. *Geophys., 18, 605-635.*

Cantwell, T., 1960. Detection and analysis of low frequency magnetotelluric signals. *Unpublished Ph.D. thesis*, M.I.T., Cambridge, Massachusetts.

Cantwell, T., Nelson, P., Webb, J., and Orange, A. S., 1965. Deep resistivity measurements in the Pacific Northwest. *J. Geophys. Res., 70, 1931-1937.*

Clarke, M. J., and Farmer, N., 1983. A diamond drill hole at the Quoin, south-east of Ross. *Tasm. Dep. Mines unpubl. rep., 18, 1-5*

Constable, S. C., McElhinny, M. W., and McFadden, P. L., 1984. Deep Schlumberger sounding and the crustal resistivity structure of central Australia. *Geophys. J. R. Astr. Soc., 79, 893-910.*

Corbett, K. D., and Turner, N. J., 1989. Early Paleozoic deformation and tectonics.*In:* Burrett, C.F., (ed) Geology and Mineral Resources of Tasmania. *Special Publication Geol. Soc. of Aust., 15, 154-181.*

Duba, A., and Shankland, T. J., 1982. Free carbon and electrical conductivity in the earth's mantle. *Geophys. Res. Lett., 9, 1271-1274.*

Duba, A., Huenges, E., Nover, G., and Will, G., 1988. Impedance of black shale from Munsterland 1 borehole: an anomalously good conductor?. *Geophys. J., 94, 413-419.*

Dwipa, S., 1992. Electrical Structures of the Crust in Southeastern Tasmania. *Unpublished Ph.D. thesis*, Geology Department, University of Tasmania.

Edwards, R. N., 1976. Electrical methods for the study of regional crustal conductivity anomalies. *Acta Geodaet., Geophys. et Montanist Acad. Sci. Hung. Tomus, 11, 399-425.*

d'Erceville, I., and Kunetz, G., 1962. The effect of a fault on the earth's natural electromagnetic field. *Geophys., 27, 651-665.*

Everett, J. E., and Hyndman, R. D., 1967. Geomagnetic variations and electrical conductivity structure in south-western Australia. *Phys. of the Earth and Plan. Inter., 1, 24-34.*

Gosh, D. P., 1971. Inverse filter coefficients for the computation of apparent resistivity standard curves for a horizontally stratified earth. *Geophys. Prosp., 19, 769-775.*

Gough, D. I., McElhinney, M. W., and Thompson, B. R., 1974. A magnetometer array study in southern Australia. *Geophys. J. R. Astr. Soc., 36, 345-362.*

Green, D.C., 1989. Heat Flow and Heat Production in Tasmania. *In:* Burrett, C.F., (ed) Geology and Mineral Resources of Tasmania. *Special Publication Geol. Soc. of Aust., 15, 461-463.*

Gulline, A. B., and Clarke, M.J., 1984. A diamond drill hole at Eaglehawk Neck, Tasman Peninsula. *Tasm. Dep. of Mines, unpubl. rep., 76, 1-5.*

Gulline, A. B., and Forsyth, S. M., 1976. Tasmanian Geological Atlas Series Sheet SK 55-4. *Launceston scale 1:250.000.* Tasmania Department of Mines, Hobart.

Gupta, J. C., and Jones, A. G., 1990. Electrical resistivity structure of the Flathead Basin in southeastern British Columbia, Canada. *Can. J. Earth Sci., 27, 1061-1073.*

Haak, V., and Hutton, R., 1984. Electrical resistivity in continental lower crust. *Paper presented at meeting on the nature of the Lower Continental Crust. Geol. Soc. London.*

Haak, V., Stoll, J., and Winter, H., 1991. Why is the electrical resistivity around the KTB hole so low?. *Phys. of the Earth and Plan. Int., 66, 12-23.*

Harrington, H. J., 1974. The Tasman Geosyncline in Australia. *In:* Denmead,A.K., Tweedale, G.W., and Wilson, A.F., (ed) the Tasman Geosyncline. *Geol. Soc. of Austr., Queensland Division, Brisbane.*

Harrison, J. E., Cressman, E. R., and Kleinkopf, M. D., 1985. Regional structure, the Atlantic Richfield-Marathon Oil No. 1 Gibbs borehole, and hydrocarbon resource potential of the Rocky Mountain trench in northwestern Montana. *U.S.G.S. Open-File rep. 85 -249, 5 pp., 3 plates.*

Henderson, R. J., and Emerson, D. W., 1969. Resistivity soundings in a petroleum prospect in the Coonabble basin, N.S.W., Australia. *Geophys., 34, 601-614.*

Hermanto, M. R., 1985. Underground conductivity structure in Tasmania. *Unpublished M.Sc. thesis*, Geology Department, University of Tasmania.

Hinch, A. J., 1965. Cressy gravity survey. *Unpublished B.Sc. Hons. thesis*, Geology Department, University of Tasmania.

Hyndman, R. D., and Hyndman, D. W., 1968. Water saturation and high electrical conductivity in the lower continental crust. *Earth Plan. Sci. Lett., 4, 427-432.*

Hutton, V. R. S., and Ingham, M. R., Mbipom, E. W., 1980. An electrical model of the crust and upper mantle in Scotland. *Nature, 287, 30-33.*

Ingham, M. R., and Hutton, V. R. S., 1982. The interpretation and tectonic implications of the geoelectric structure of southern Scotland. *Geophys. J. R. Astr. Soc., 69, 595-606.*

Jaeger, J. C., 1970. Heat flow and radio activity in Australia. *Earth Plan. Sci. Lett., 8, 285-292.*

Jaeger, J. C., and Sass, J. H., 1963. Lee's topographic corection in heat flow and the geothermal flux in Tasmania. *Geofis. Pura. Appl., 54, 53-62.*

Jiracek, G. R., 1988. Near-surface and topographic distortions in electromagnetic induction. *Review paper, 9th IAGA Workshop on Electromagnetic Induction in the Earth and Moon, Sochi, USSR.*

Johnson, B. D., 1972. Crustal structure studies in Tasmania. *Unpublished Ph.D. thesis*, Geology Department, University of Tasmania.

Jones, A. G., 1988. Static shift of magnetotelluric data and its removal in a sedimentary basin environment. *Geophys., 53, 967-978.*

Jones, A. G., and Craven, J. A., 1990. The North American Central Plains conductivity anomaly and its correlation with gravity, magnetic, seismic, and heat flow data in Saskatchewan, Canada. *Phys. of the Earth and Plan. Int., 60, 169-194.*

Jones, F. W., and Pascoe, L. J., 1971. A general computer program to determine the perturbation of alternating electric currents in a two-dimensional model of a region of uniform conductivity with an embedded inhomogeneity.*Geophys. J.R. Astr. Soc., 24, 3-30.*

Jones, F. W., and Price, A. T., 1970. The perturbation of alternating geomagnetic fields by conductivity anomalies. *Geophys. J.R. Astr. Soc., 20, 317-334.*

Jones, F. W., and Thomson, D. J., 1974. A discussion of the finite difference method in computer modelling of electrical conductivity structures: A reply to the discussion by Williamson, Hewlett and Tammemagi. *Geophys. J.R. Astr. Soc., 37, 537-544.*

Jupp, D. L. B., and Vozoff, K., 1989. Discussion on the magnetotelluric method in the exploration of sedimentary basins. *In* : Vozoff, K., (ed.) Magnetotelluric Methods.*Geophys. Reprint Series 5. Soc. of Expl. Geophys. pp. 693-696.*

Kao, D., 1982. Magnetotelluric response on vertically inhomogeneous earth having conductivity varying exponentially with depth. *Geophys., 47, 957-976.*

Kato,Y., and Kikuchi, T., 1950. Phase difference of earth currents induced by the changes of the earth's magnetic field. *Sci. Rep. Tohoku University, 2, 139-145.*

Kauffman, A. A., and Keller, G.V., 1981. The magnetotelluric sounding method. *Method in Geochemistry and Geophysics, vol. 15.* Elsevier, Amsterdam.

Keller, G. V., 1966. Electrical properties of rocks and minerals. Handbook of Physical Constant. *Mem. Geol. Soc. Am., 97, 553-577.*

Keller, G. V., 1968. Statistical study of electric fields from earth return tests in the western states compared with natural fields. *I.E.E.E. Trans. Power Appl. Sys., 87, 1050-1057.*

Kozlovsky, V. A., 1984. The world's deepest well. *Sci. Am., 251, 98-104.*

Kurtz, R. D., 1973. A Magnetotelluric investigation of eastern Canada. *Unpublished Ph.D. thesis*, Department of Physics, University of Toronto, Canada.

Kurtz, R. D., Ostrowski, J. A., and Niblett, E. R., 1986. A magnetotelluric survey over the East Bull Lake Gabbro-Anorthosite complex. *J. Geophys. Res., 91, 7403-7416.*

Leaman, D. E., 1971. Geology and Groundwater Resources of the Coal River Basin. *Undergr. Wat. Supply Pap. Tasm. 7.*

Leaman, D. E., 1973. Applied geophysics in Tasmania, Part 1 - summary of surveys and rock properties. *Aust. Soc. of Expl. Geophys. Bull., 4, 27-58.*

Leaman, D. E., 1989. The gravity field. *In:* Burrett, C.F., (ed.) Geology and Mineral Resources of Tasmania. *Special Publication Geol. Soc. of Aust., 15, 451-455.*

Leaman, D. E., 1992. Finding Cambrian Keys: An essay in controversy, prospectivity and tectonic implications. *Geol. Surv. Bull., 70, 124-128.* Tasmania Department of Mines, Hobart.

Leaman, D. E., and Richardson, B., 1989a. Production of a Residual Gravity Field Map for Tasmania and Some Implications. *Expl. Geophys., 20, 181-184.*

Leaman, D. E., and Richardson, B., 1989b. The Granite of West and North-west Tasmania - a Geophysical Interpretation. *Geol. Surv. Bull., 66.* Tasmania Department of Mines, Hobart.

Leaman, D. E., and Richardson, B., 1990. Tasmanian Crustal Features. *Geol. Soc. of Aust. Tenth Australian Geological Convention,* University of Tasmania, Hobart.

Leaman, D. E., Symonds, P. A., and Shirley, J. E., 1973. Gravity Survey of the Tamar Region Northern Tasmania. *Geol. Surv. Pap., 1.* Tasmania Department of Mines, Hobart.

Lewis, R. J. G., 1965. Conductivity of the crust in Tasmania. *Unpublished B.Sc. Hons.thesis*, Geology Department, University of Tasmania.

Lilley, F. E. M., 1976. A magnetometer array study across southern Victoria and the Bass Strait area, Australia. *Geophys. J.R. Astr. Soc., 46, 165-184.*

Lilley, F. E. M., 1992. Magnetotelluric analysis using Mohr circle. *Geophys., (in press).*

Longman, M. J., and Leaman, D. E., 1971. Gravity Survey of the Tertiary Basins in Northern Tasmania. *Geol. Surv. Bull., 51.* Tasmania Department of Mines, Hobart.

Macnae, J. C., and Irvine, R. J., 1988. Inductive Source Resistivity: A tool for outlining silicification in gold exploration. *Expl. Geophys., 19, 471-480.*

Madden, T. R., 1972. Transmission System and Network Analysis for Geophysical Forward and Inverse Problems. *Technical Report N000-14-67-A-0204-0045, 371- 401/05-01-71 M.I.T.*

Madden, T. R., and Nelson, P., 1989. A defense of Cagniard's Magnetotelluric method, *In:* Vozoff, K., (ed.) Magnetotelluric Methods. *Geophys. reprint series 5. Soc. of Expl. Geophysicists.*

Marquis, G., and Hyndman, R. D., 1992. Geophysical support for aqueous fluids in the deep crust: seismic and electrical relationships. *Geophys. J. Int., 110, 91-105.*

Martinez, M., Romo, J. M., Fernandez, R., Herrera, C., Jiracek, G. R., Weslow, V., and Miele, M. J., 1989. A magnetotelluric profile across the western boundary of the Salton Trough in northern Baja California, Mexico. *Phys. of the Earth and Plan. Int., 53, 376-383.*

Matthews, W. L., 1983. Geology and Groundwater Resources of the Longford Tertiary Basin. *Geol. Surv. Bull. 59.* Tasmania Department of Mines, Hobart.

McDougall, I., and Legge, P. J., 1965. Isotopic age determination on granitic rocks from Tasmania. *J. Geol. Soc. Aust., 12, 295-332.*

Munoz, M., Fournier, H., Mamani, M., Febrer, J., Borzotta, E., and Maidana, A., 1990. A comparative study of results obtained in magnetotelluric deep soundings in Villarica active volcano zone (Chile) with gravity interpretations, distribution of earthquake foci, heat flow empirical relationships, isotopic geochemistry $\frac{^{87}SR}{^{86}SR}$ and SB systematics. *Phys. of the Earth and Plan. Int., 60, 195-211.*

Olhoef, G. R., 1981. Electrical properties of granite with implications for the lower crust. *J. Geophys. Res., 86, 931-936.*

O'Neill, D. J., 1975. Improved linear filter coefficients for application in apparent resistivity computations. *Austr. Soc. of Expl. Geophys., 6, 104-109.*

Parkinson, W. D., 1959. Direction of rapid geomagnetic fluctuations. *Geophys. J.R. Astr. Soc., 2, 1-28.*

Parkinson, W. D., 1962. The influence of continent and oceans on geomagnetic variations. *Geophys. J.R. Astr. Soc., 6, 441-449.*

Parkinson, W. D., 1964. Conductivity anomalies in Australia and the ocean effect. J. Geomag. *Geoelect., 15, 222-226.*

Parkinson, W. D., 1969. The seismicity of Tasmania. *In: Earthquake Engineering Symposium, 1. Inst. Eng.,* Melbourne.

Parkinson, W. D., 1983. *Introduction to Geomagnetism.* Scottish Academic Press.

Parkinson, W. D., and Hermanto, R., 1986. The Tamar Conductivity Anomaly. *Expl. Geophys., 17, 34.*

Parkinson, W. D., and Hermanto, R., 1990. The Tamar Conductivity Anomaly. *Geol. Soc. of Aust., Tenth Australian Geological Convention,* University of Tasmania, Hobart.

Parkinson, W. D., Hermanto, R., and Dwipa, S., 1992. A simple method of determining rotation angle. *J. Geomag. and Geoelect. , special issue, (submitted).*

Parkinson, W. D., Hermanto, R., Sayers, J., Bindoff, N., Dosso, H. W., and Nienaber, W., 1988. The Tamar Conductivity Anomaly. *Phys. of the Earth and Plan. Inter. 52, 8-22.*

Parkinson, W. D., and Richardson, B., 1989. The Magnetic Field. *In:* Burrett, C.F., (ed.) Geology and Mineral Resources of Tasmania. *Special Publication Geol. Soc. of Aust., 15, 455-458.*

Pascoe, L. J., and Jones, F. W., 1972. Boundary conditions and calculation of surface values for the general two-dimensional electromagnetic induction problem. *Geophys. J.R. Astr. Soc., 27, 179-193.*

Pellerin, L., and Hohmann, G. W., 1990. Transient electromagnetic inversion: A remedy for magnetotelluric static shifts. *Geophys., 55, 1242-1250.*

Petiau, G., and Dupis, A., 1980. Noise, Temperature Coefficient, and Long Time Stability of Electrodes for Telluric Observation. *Geophys. Prosp., 28, 792-804.*

Powell, C. M., 1992. New Perspective on Tasmanian Geology. *Geol. Surv. Bull., 70.* Tasmania Department of Mines, Hobart.

Price, A. T., 1962. The theory of magnetotelluric methods when the source field is considered. *J. Geophys. Res., 67, 1907-1918.*

Price, A. T., 1973. The theory of geomagnetic induction. *Phys. of the Earth and Plan. Inter., 7, 227-233.*

Quon, C., 1963. Electromagnetic field of elevated dipoles on a two-layers earth. *Unpublished M.Sc. thesis,* Department of Physics, University of Alberta, Canada.

Raiche, A., and Sugeng, F., 1989. Predicting the Transient EM Response of Complex Structures using the Compact Finite-Element Method. *Expl. Geophys., 20, 51-55.*

Rankin, D., 1962. The magnetotelluric effect on a dyke. *Geophys., 27, 666-676.*

Rankin, D., and Reddy, I. K., 1969. A magnetotelluric study of resistivity anisotropy. *Geophys., 34, 438-449.*

Reddy, I. K., and Rankin, D., 1973. Magnetotelluric response of a two-dimensional sloping contact by the finite element method. *Pure and Appl. Geophys., 105, 847-857.*

Richardson, B. R. G., 1980. Crustal Seismology. *Unpublished Ph.D.thesis,* Geology Department, Universisty of Tasmania.

Richardson, B. R. G., 1989. Tasmanian Seismicity. *In:* Burrett, C.F., (ed.) Geology and Mineral Resources of Tasmania. *Special Publication Geol. Soc. of Aust., 15, 463-465.*

Richardson, B. R. G., and Leaman, D. E., 1987. The Tasmanian gravity data base. *Unpub. Rep. 1987/02, Tasmania Department of Mines, Hobart.*

Richardson, M., 1985. A magnetotelluric survey of the Fingal Valley. *Unpublished B.Sc. Hons. thesis,* Geology Department, University of Tasmania.

Rikitake, T. 1966. *Electromagnetism and the earth's interior.* Elsevier, Amsterdam.

Ritz, M., Bellion, Y., and Flicoteaux, R., 1987. Magnetotelluric soundings and the geological structure and tectonics of the Senegalo-Mauritania basin in northern Senegal, West Africa. *Tectonics, 6, 395-409.*

Roach, M. J., 1992. Geology and geophysics of the Lisle - Golconda goldfield, northeast Tasmania.*Geol. Surv. Bull., 70.* Tasmania Department of Mines, Hobart.

Salman, 1992. Electrical Geophysical Methods Applied to the Structure and Groundwater Potential of the University Farm. *Unpublished M.Sc. thesis*, Geology Department, University of Tasmania.

Sayers, J., 1984. A magnetotelluric survey of the midlands area. *Unpublished B.Sc. Hons. thesis*, Geology Department, University of Tasmania.

Schlumberger, C., and Schlumberger, M., 1932. Electrical studies of the earth's crust at great depths. *Trans. Am. Inst. Min. Metall. Engrs. Geophys. Prosp., 134-140.*

Schmucker, U., 1970. Anomalies of geomagnetic variations in the southwestern United States. *Scripps Inst. Oceanog. Bull. 13.*

Shirley, J. E., 1980. Tasmanian Seismicity - natural and reservoir induced. *Bull. Seismol. Soc. Am., 70, 2203-2220.*

Spies, B. R., 1976. The transient electromagnetic method in Australia. *Bur. Mineral Res. J. of Austral. Geol. and Geophys., 1, 23-32.*

Staltari, G., 1986. The Que River TEM Case Study. *Expl. Geophys., 17, 125-128.*

Stanley, W. D., 1986. Magnetotelluric study of a compressed flysch system in the Healy Quadrangle. *U.S.G.S. Circular 928, U.S.G.S. Field Research During 1985, 78- 91.*

Stanley, W. D., 1989. Comparison of geoelectrical/tectonic models for suture zones in the western U.S.A. and eastern Europe: are black shales a possible source of high conductivities?. *Phys. of the Earth and Plan. Int., 53, 228-238.*

Stanley, W. D., Boehl, J. E., Bostick, F. M., Smith, H. W., 1977. Geothermal significance of magnetotelluric sounding in the eastern Snake River Plain - Yellowstone region.*J. Geol. Res., 82, 2501-2514.*

Sternberg, B. K., Washburne, J. C., and Pellerin, L., 1988. Correction for the static shift in magnetotelluric using transient electromagnetic soundings. *Geophys., 53, 1459-1468.*

Swift, C. M. jr., 1967. A magnetotelluric investigation of an electrical conductivity anomaly in south-western United States. *Unpublished Ph.D. thesis*, M.I.T., Cambridge, Massachusett.

Swift, C. M. jr., 1971. Theoretical Magnetotelluric and Turam Response from Two-dimensional Inhomogeneities. *Geophys., 36, 38-52.*

Swift, C. M. jr., 1989. A magnetotelluric investigation of an electrical conductivity anomaly in south-western United States. *In:* Vozoff, K., (ed.) Magnetotelluric Methods.*Geophys. Reprint Series 5. Soc. of Expl. Geophys.*

Talwani, M., 1965. Computation with the help of a digital computer of magnetic anomalies caused by bodies of arbitrary shape. *Geophys., 30, 797-817.*

Talwani, M., Worzel, J. L., and Landisman, M., 1959. Rapid gravity computations by two-dimensional bodies with application to the Mendocino submarine fracture zone. *J. Geophys. Res., 64, 45-59.*

Tikhonov, V., 1950. Determination of the electrical characteristics of the deep strata of the earth's crust. *Dokl. Akad. Nauk., 73, 295.*

Underwood, R., 1969. A seismic refraction study of the crust and upper mantle in the vicinity of Bass Strait. *Aust. J. Phys., 22, 573-587.*

van Zijl, J. S. V., 1986 (ed). The Electromagnetic Method. *Field Manual for Technicians no. 3, pp. 83-85.* South African Geophysical Association.

van Zijl, J. S. V., Hugo, P. L. V., and deBellocq, J. H., 1970. Ultra deep Schlumberger sounding and crustal conductivity structure in South Africa. *Geophys. Prosp., 18, 615-634.*

Veevers, J. J., and Powell, C. M., 1984. Epi-Adelaiden regional shear. *In:* Veevers, J.J., (ed) Phanerozoic Earth History of Australia. Oxford University Press, Oxford.

Vitesnik, J., 1984. Crustal Seismic Survey - a traverse from Savage River to Fortescue Bay. *Unpublished B.Sc. Hons. thesis*, Geology Department, University of Tasmania.

Vozoff, K., 1972. The Magnetotelluric method in the exploration of sedimentary basins. *Geophys., 37, 98-141.*

Vozoff, K., and Ellis, R. M., 1966. Magnetotelluric measurements in southern Alberta. *Geophys., 31, 1153.*

Wait, J. R., 1954. On the relation between telluric currents and the earth's magnetic field. *Geophys., 19, 281-289.*

Wait, J. R., 1962. Theory of magnetotelluric fields. *J. Res. N.B.S., 66, 509.*

Wellman, P., 1989. Aspects of Interpretation of Aeromagnetic Data. *In:* Burrett, C.F., (ed) Geology and Mineral Resources of Tasmania. *Special Publication Geol.Soc. of Aust., 15, 459-460.*

Williams, E., 1979. Tasman Fold Belt System in Tasmania. *Explanatory notes for the 1:500.000 structural map of the pre-Carboniferous rocks of Tasmania.* Tasmania Department of Mines, Hobart.

Williams, E., 1989. Summary and synthesis. *In:* Burrett, C.F., (ed) Geology and Mineral Resources of Tasmania. *Special Publication Geol. Soc. of Aust., 15,468-499.*

Williams, E., McClenaghan, M. P., and Collins, P. L. F., 1989. Mid-Paleozoic Deformation, Granitoids and Ore Deposits. *In:* Burrett, C.F., (ed) Geology and Mineral Resources of Tasmania. *Special Publication Geol. Soc. of Aust., 15,238-292.*

Williamson, K., Hewlett, C., and Tammemagi, H. Y., 1974. Computer modelling of electrical conductivity structures: Letter to the editors. *Geophys. J.R. Astr. Soc., 37, 533-536.*

Woods, D. V., and Lilley, F. E. M., 1979. Geomagnetic induction in central Australia. *J. Geomag. Geoelectr., 31, 449-458.*

Word, D. R., Smith, H. W., and Bostick, F. X., jr., 1970. An investigation of the magnetotelluric tensor impedance method. *Tech. Rep., 82.* Electrical Geophysics Research Laboratory. University of Texas, Austin, Texas.

Wronski, E., 1977. Two heat flow values for Tasmania. *Unpublished B.Sc. Hon thesis*, Geology Department, University of Tasmania.

Wynn, J. C., Kleinkopf, M. D., and Harrison, J. E., 1977. Audio-frequency magnetotelluric and gravity traverse across the crust of the Purcell anticlinorium, northwestern Montana. *Geology, 5, 309-312.*

Zohdy, A. A., and Jackson, D. B., 1969. Application of deep electrical soundings for groundwater exploration in Hawaii. *Geophys., 34, 584-600.*

APPENDIX 1:
INDUCTION ARROWS IN NORTH-EAST TASMANIA

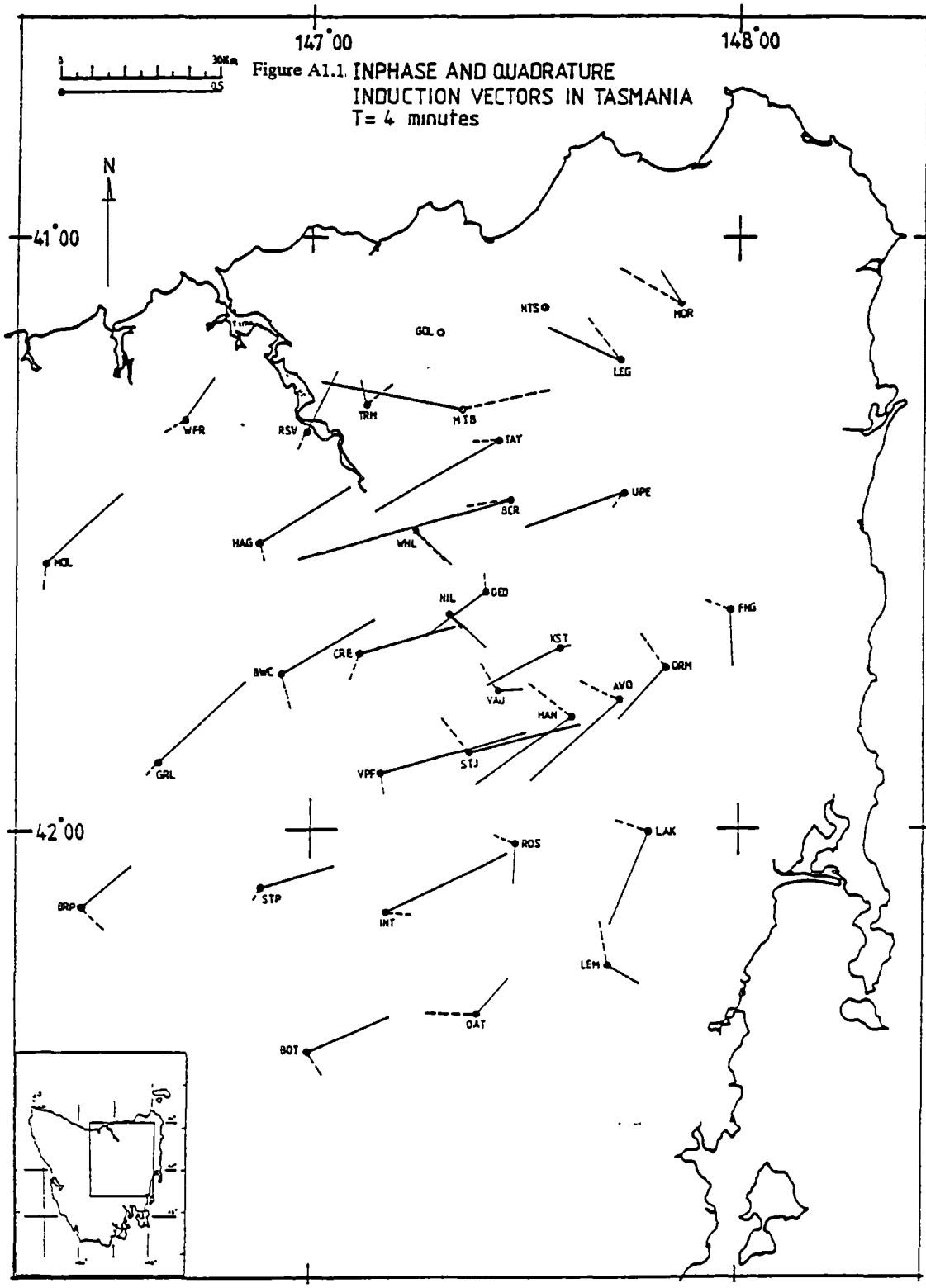
147°00
148°00
41°00
42°00
N
INPHASE AND QUADRATURE
INDUCTION VECTORS IN TASMANIA
T= 4 minutes
NTS
HOR
GOL
LEG
TRM
HTB
WFR
RSV
TAY
UPE
BCR
HAG
WHL
HOL
NIL
DED
FNG
KST
CRE
BWC
ORM
AVO
VAU
HAN
GRL
VPF
STJ
LAK
ROS
STP
BRP
INT
LEM
OAT
BOT

Figure A1.1.

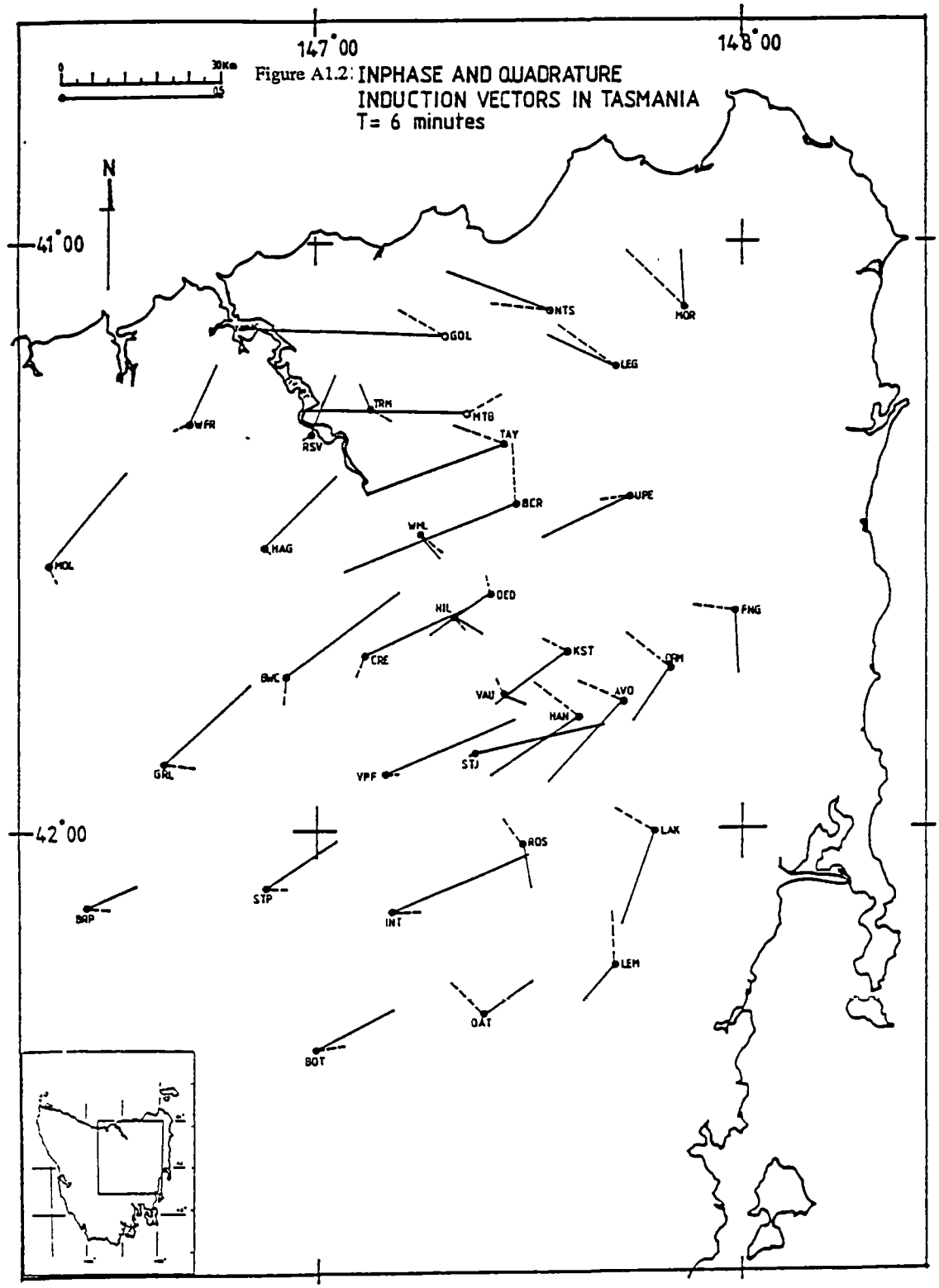
147°00
148°00
41°00
42°00
N
30Km
05
INPHASE AND QUADRATURE
INDUCTION VECTORS IN TASMANIA
T= 6 minutes
NTS
MOR
GOL
LEG
TRM
MTB
WFR
RSV
TAY
BCR
UPE
WHL
HAG
MOL
DED
HIL
FNG
CRE
KST
OPM
BWC
VAU
AVO
HAN
GRL
VPF
STJ
ROS
LAK
STP
BRP
INT
LEM
OAT
BOT

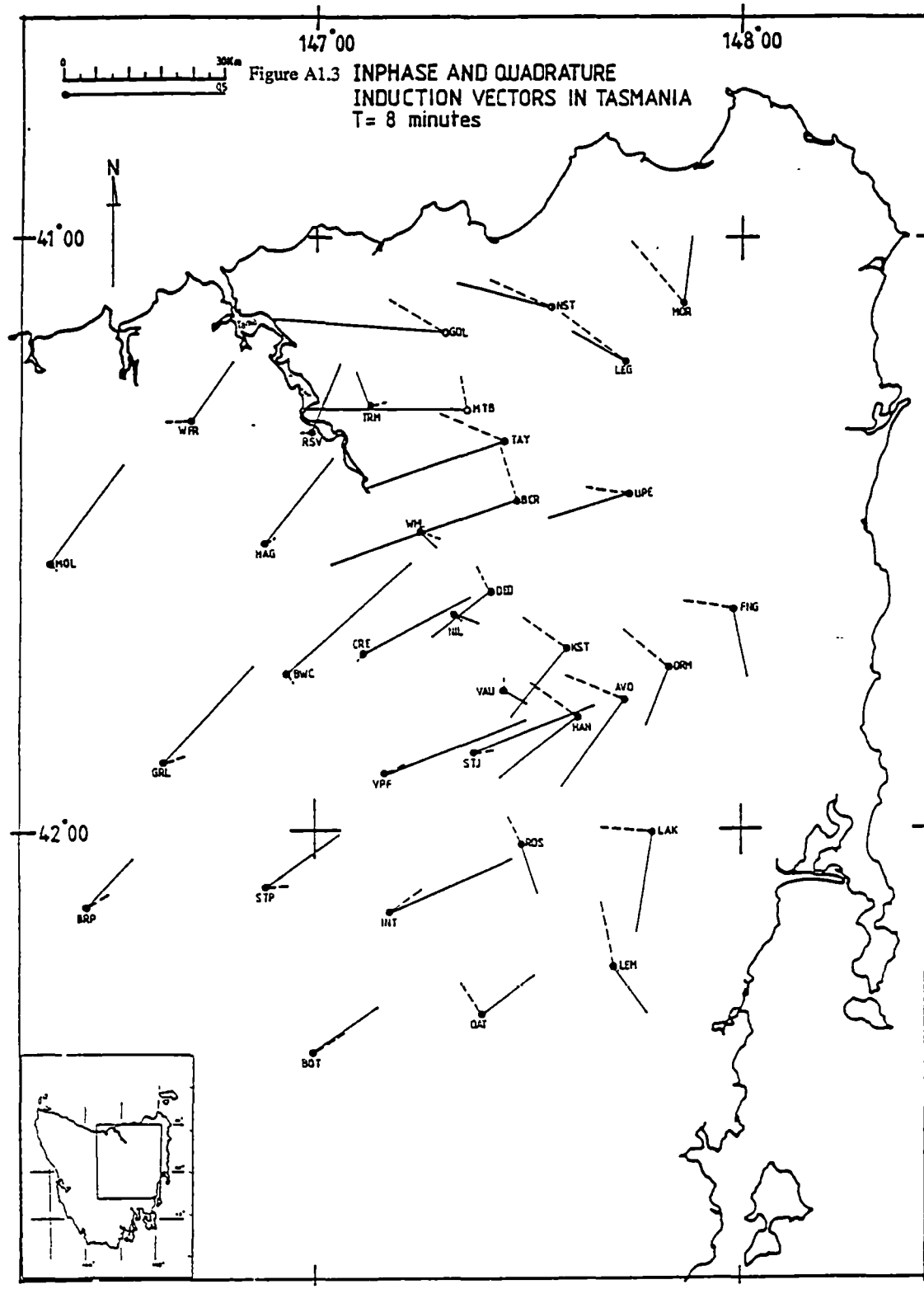
147°00
148°00
41°00
42°00
N
INPHASE AND QUADRATURE
INDUCTION VECTORS IN TASMANIA
T= 8 minutes
NST
MOR
GOL
LEG
MTB
IRM
WFR
RSV
TAY
BCR
UPE
WHI
HAG
MOL
DEO
FNG
HIL
CRE
KST
ORM
BWC
VAU
AVO
HAN
STJ
GRL
VPF
LAK
ROS
STP
BRP
INT
LEM
OAT
BOT

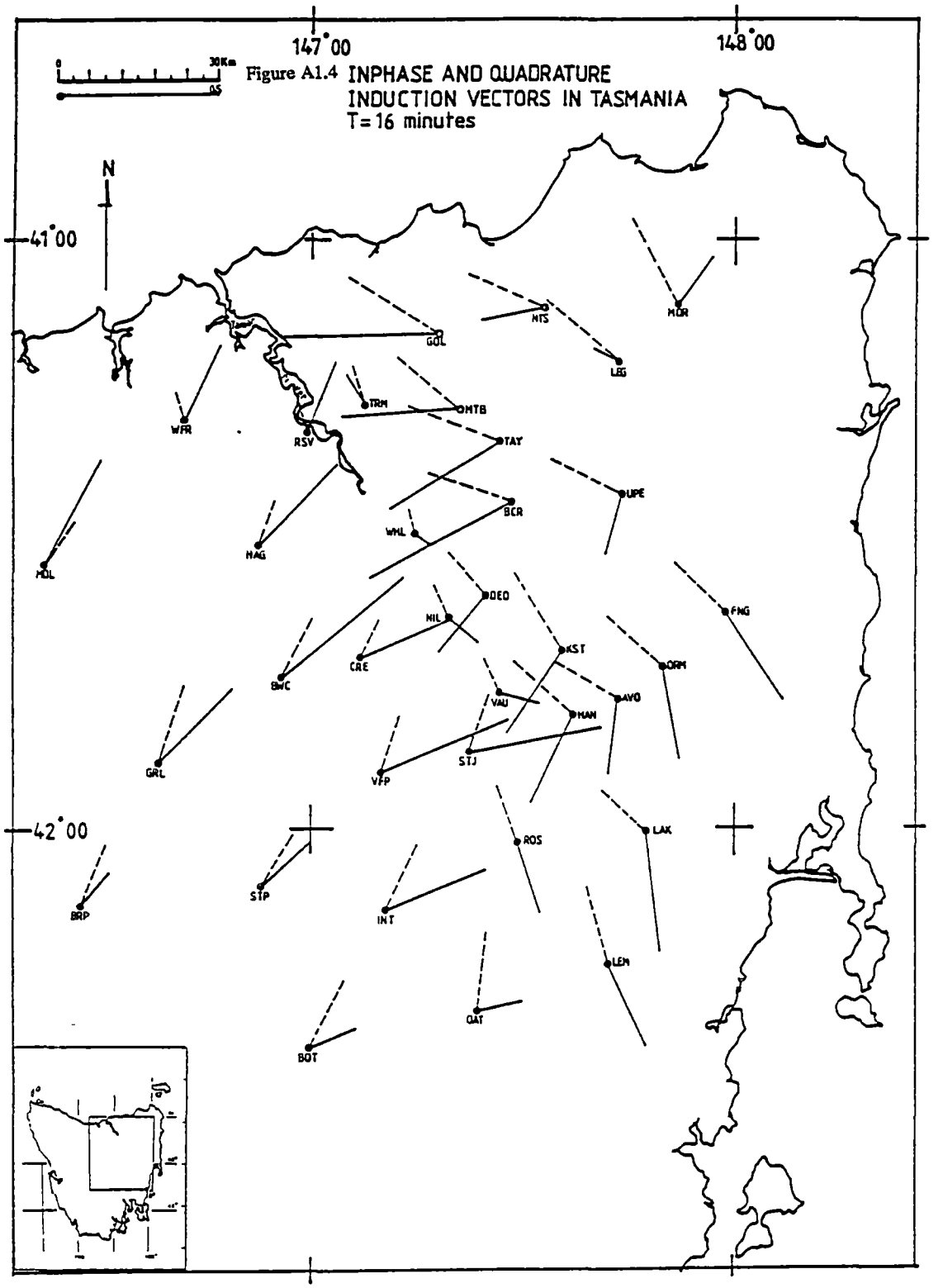
147°00
148°00
41°00
42°00
N
0
30Km
0.5
INPHASE AND QUADRATURE
INDUCTION VECTORS IN TASMANIA
T=16 minutes
GOL
NTS
MOR
LEG
TRM
MTB
WPR
RSV
TAY
UPE
BCR
WHL
HAG
HOL
DEO
NIL
FNG
KST
CRE
ORM
BWC
VAU
AVO
MAN
GRL
STJ
VFP
ROS
LAK
STP
INT
LEM
QAT
BOT
BRP

Figure A1.4

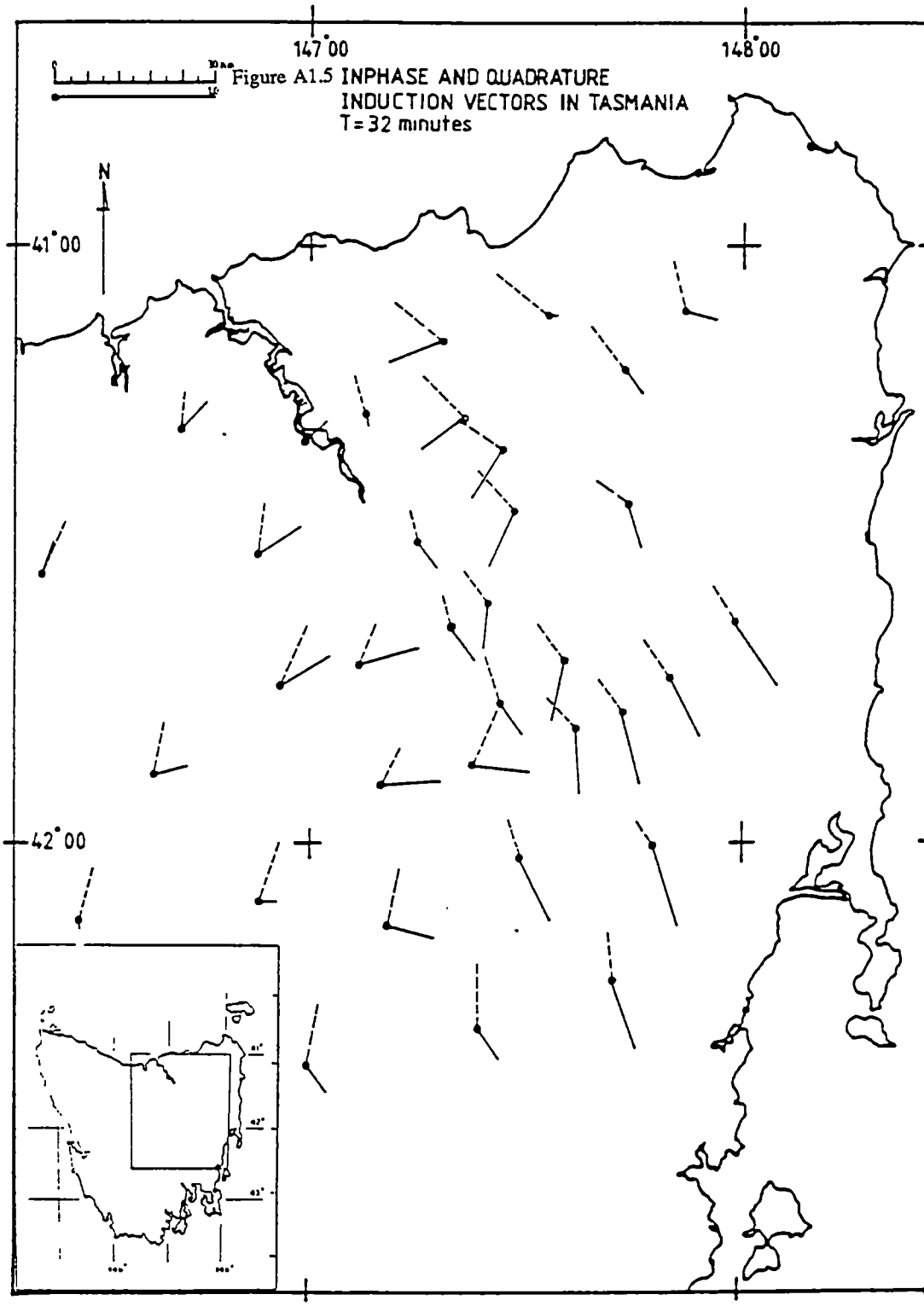
147°00
148°00
41°00
42°00
N
INPHASE AND QUADRATURE
INDUCTION VECTORS IN TASMANIA
T=32 minutes

Figure A1.5

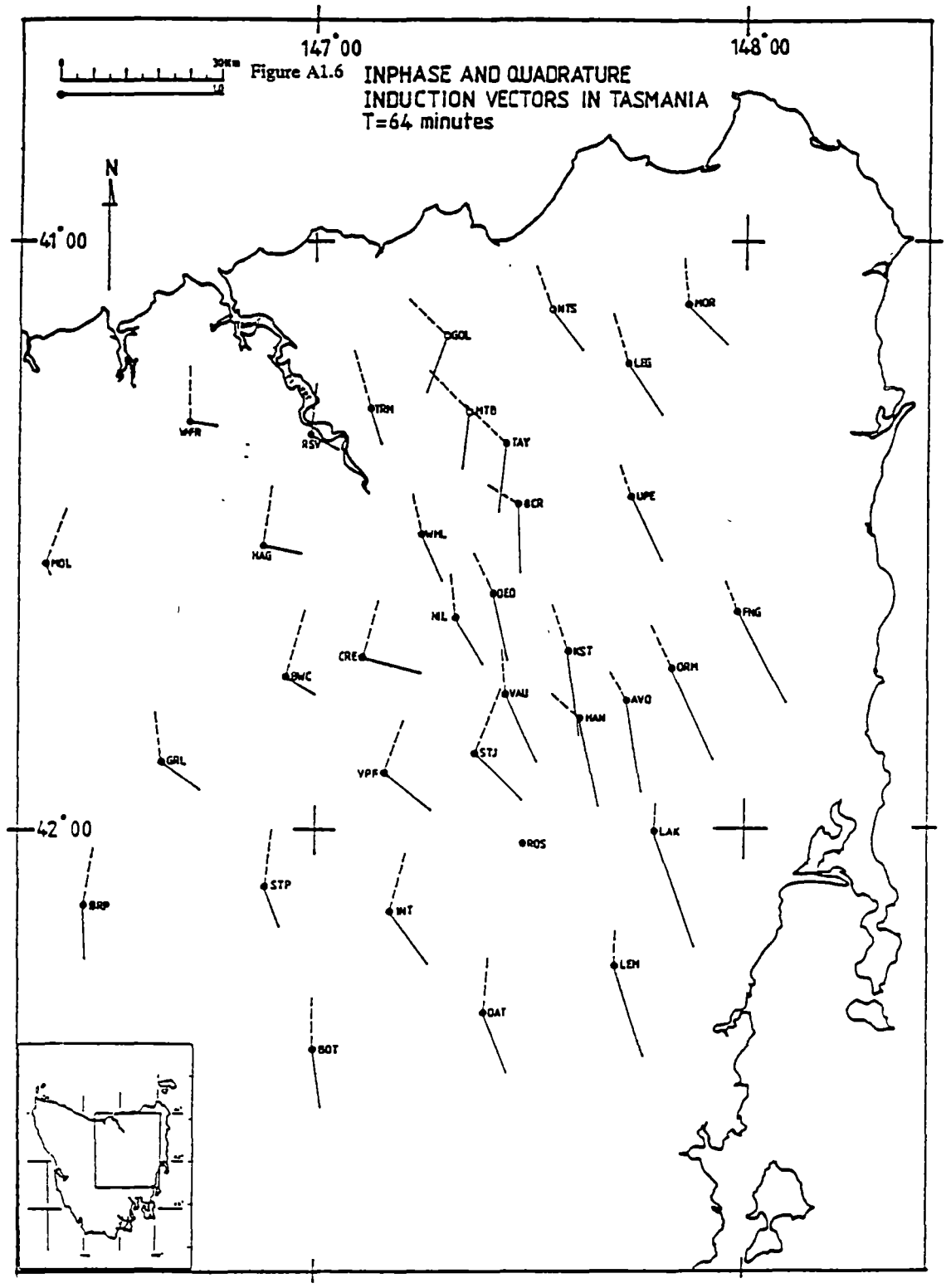
147°00
148°00
41°00
42°00
N
INPHASE AND QUADRATURE
INDUCTION VECTORS IN TASMANIA
T=64 minutes
NTS
MOR
GOL
LEG
TRM
MTB
WPR
RSV
TAY
BCR
UPE
WHL
MAG
MOL
OEO
MIL
FNG
KST
CRE
BWC
ORM
VAU
AVO
HAN
GRL
STJ
VPF
ROS
LAK
STP
BRP
INT
LEM
OAT
BOT

Figure A1.6

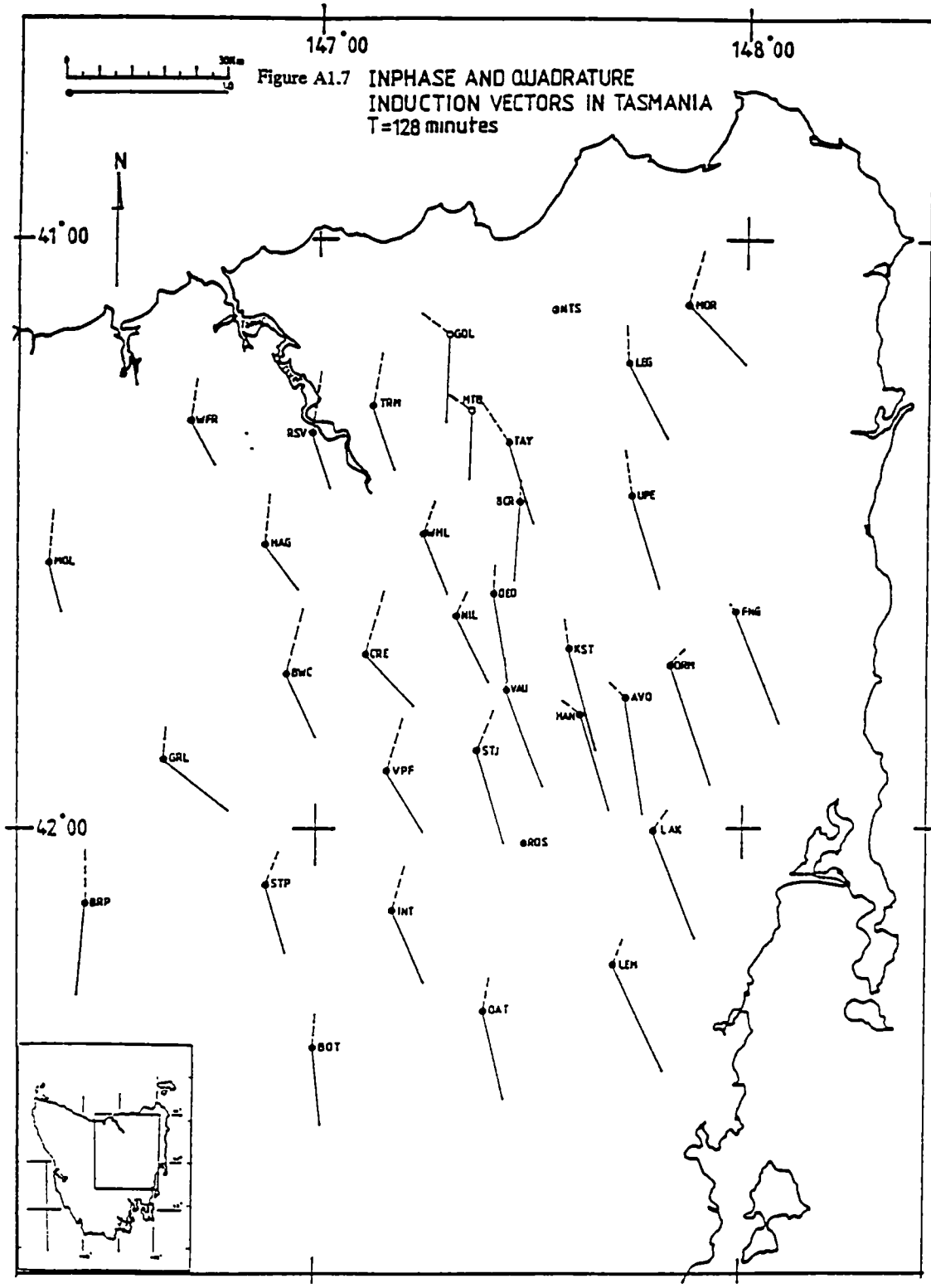
147°00
148°00
41°00
42°00
N
INPHASE AND QUADRATURE
INDUCTION VECTORS IN TASMANIA
T=128 minutes
GNTS
MOR
GOL
LEG
TRM
MTR
WFR
RSV
TAY
SCR
UPE
MAG
WHL
MOL
GED
WIL
FNG
KST
CRE
ORM
SWC
VAU
AVO
HAN
GRL
STJ
VPF
ROS
LAK
STP
BRP
INT
LEM
OAT
BOT

Figure A1.7

APPENDIX 2:
TEMPERATURE CALIBRATION

Apply temperature correction as shown below if detector head and control box temperatures are recorded on channel 4 and 5, otherwise use appropriate channel (CH) numbers.

MT UNIT I : X COMPONENT

CH	COEF	ZERO	CH	COEF	ZERO
4	-.06	200.	5	-.13	200.

MT UNIT I : Y COMPONENT

CH	COEF	ZERO	CH	COEF	ZERO
4	-.07	200.	5	.101	200.

MT UNIT I : Z COMPONENT

CH	COEF	ZERO	CH	COEF	ZERO
4	.156	200.	5	.041	200.

MT UNIT II : X COMPONENT

CH	COEF	ZERO	CH	COEF	ZERO
4	-.009	200.	5	.073	200.

MT UNIT II : Y COMPONENT

CH	COEF	ZERO	CH	COEF	ZERO
4	.007	200.	5	0.0	200.

MT UNIT II : Z COMPONENT

CH	COEF	ZERO	CH	COEF	ZERO
4	.077	200.	5	-.10	200.

APPENDIX 3:
OUTPUT OF SYNTEX AND MTYZ45 PROGRAMS

OUTPUT OF SYNTEC PROGRAM

1 .100 1 125

1

59.08 59.33 59.08 59.33 59.33 59 08 59.33 59.08 59 08 58.35 59 08 59.08 59.08 58.35 58.11 59.08
59.08 59.33 59.33 58.35 59.08 58.35 59.33 58.35 59 33 59 08 58.35 58.11 58.11 58.35 58.35 58 11
58.35 58.35 59.08 59.33 59.08 59.33 59.33 59 08 59.33 59.33 59.33 59.08 59.33 59 08 59.33 59.33
59.08 59.33 59.33 59 08 59.33 59.08 59.08 59 08 59.33 58 35 59.33 58.35 58.35 58.11 59.08 58.11
59.08 59.08 58.35 59.33 58 35 59.33 59 33 59 08 59.33 59 33 59.33 59.33 59 08 59.33 59.33 59.33
60.06 60.06 59.33 60 06 59.33 60.30 60 30 60.06 60.30 60 30 60 30 60 06 60.06 60.30 60.06 59.33
60.06 60.30 60 06 60 30 60.06 60 06 60 30 60.06 59 33 60.06 59.33 60 06 60.06 60.30 60.06 60.06
60.30 60.06 60 30 60.06 60.30 61 04 61.04 61.04 61 28 61.28 61 04 61.28 61.28

2

33.94 33.94 33.69 33.69 33.94 33.94 33.69 33 94 33.94 33.94 33 94 33.94 33.69 33.69 32.96 32.96
32.71 32 96 32.71 33.69 32 71 33.69 32.96 32 96 32.71 32 71 32.71 31.98 32.71 32.71 31 98 31.98
31.74 31.98 32.71 31.98 32.71 32.71 32.71 32 71 32.96 32 71 32.71 32 96 32.71 32.71 32 71 32.71
32.71 32.96 32.96 32.71 32.71 32.96 32.96 32.71 32.71 31.98 32.71 32.71 31.74 31 98 31.74 31.98
31.98 31 74 31.98 31 74 31 98 32.71 31 98 31 98 32.71 32 71 32.71 31.74 31.74 32.71 31 98 32 71
31.98 32.96 32.71 32.71 32.96 32 96 32.71 32 71 32.71 32.71 32.96 32.96 32 96 32.96 32.71 32 96
32.71 32.71 32 96 32.71 32.96 32.96 32.71 31 98 31 74 32.71 32.96 32.71 32 96 32.71 32.96 32.71
32.71 31.98 32 96 32.71 32.71 32 71 32.71 32.96 32 71 32.71 32.96 32.71 32 96

3

-1.71 -1.46 -1 71 -1.71 -1.46 -1 46 -1.46 -1 71 -1 46 -1.46 -1 46 -1 71 -1.71 -1 46 -1 46 -1.71
-1.71 -1.71 -1.46 -1.46 -1.71 -2.44 -1 46 -1 71 -2.44 -1 71 -2 44 -2.44 -2.44 -2 44 -2 44 -2.69
-2.44 -2 44 -1.71 -2.44 -2.44 -1.71 -2 44 -1.71 -2 44 -1.71 -1.71 -2 44 -1.71 -2.44 -2 44 -2.44
-1.71 -2.44 -2.44 -1.71 -1 46 -1.46 -1.71 -1.46 -2 44 -1 71 -1 71 -1.71 -2.44 -1.71 -1.46 -1.71
-1.71 -1.46 -1.71 -1.71 -1 71 -1.46 -1.71 -1 71 -1.71 -1 71 -1.46 -1.46 -1.71 -1.46 -1.46 -1 46
-.73 -1.46 -.73 - 49 - 73 -.49 -.73 - 49 -.49 - 49 - 49 -.49 -.49 -.73 -.73 - 73
-.49 - 73 .73 -.73 .73 - 73 .73 -.49 -.49 73 -.73 - 49 - 49 -.49 -.73 - 49
-.73 -.49 .73 .49 49 - 49 .73 49 .49 49 73 .73 73

4

45.98 46.08 45.82 45.91 46.08 45.98 45.91 45.98 45.98 45.70 45.98 45 98 45.82 45.53 44 95 45.33
45.16 45 43 45.26 45.53 45.16 45.53 45.43 45 04 45 26 45.16 44 87 44.29 44.78 44 87 44.38 44.29
44 22 44.38 45.16 44.77 45.16 45.26 45.26 45 16 45.43 45 26 45 26 45.33 45 26 45 16 45.26 45 26
45.16 45.43 45.43 45.16 45 26 45.33 45.33 45.16 45.26 44 38 45.26 44 87 44.22 44.29 44 51 44 29
44.67 44.51 44 38 44.61 44.38 45 26 44.77 44 67 45.26 45 26 45.26 44.61 44 51 45.26 44.77 45 26
45.06 45.71 45.26 45.55 45.43 45.81 45.64 45 55 45.64 45.64 45.81 45 71 45.71 45.81 45.55 45.43
45.55 45 64 45.71 45.64 45.71 45.71 45.64 45 06 44.61 45.55 45 43 45.55 45.71 45.64 45.71 45.55
45.64 45.06 45.81 45.55 45 64 45.93 45 93 46 10 46 03 46 03 46.10 46.03 46 19

5

-44.74 -44.88 -44.65 -44.78 -44.88 -44 74 -44.78 -44 74 -44.74 -44.36 -44 74 -44.74 -44 65 -44.26 -43.84 -44.36
-44.26 -44.49 -44.39 -44.26 -44.26 -44.26 -44.49 -43.97 -44 39 -44.26 -43 87 -43.46 -43.74 -43 87 -43.58 -43.46
-43.49 -43.58 -44.26 -44.10 -44.26 -44.39 -44.39 -44.26 -44 49 -44 39 -44.39 -44.36 -44.39 -44 26 -44.39 -44 39
-44.26 -44.49 -44.49 -44.26 -44.39 -44.36 -44 36 -44 26 -44.39 -43 58 -44 39 -43 87 -43.49 -43.46 -43.88 -43.46
-43.97 -43.88 -43.58 -44 01 -43.58 -44.39 -44 10 -43 97 -44 39 -44.39 -44 39 -44 01 -43.88 -44.39 -44.10 -44.39
-44.49 -44.88 -44.39 -44.78 -44 49 -45.01 -44.91 -44.78 -44.91 -44 91 -45.01 -44 88 -44.88 -45.01 -44.78 -44.49
-44.78 -44.91 -44.88 -44 91 -44.88 -44.88 -44.91 -44.49 -44 01 -44.78 -44.49 -44.78 -44.88 -44 91 -44.88 -44.78
-44.91 -44.49 -45.01 -44.78 -44.91 -45.30 -45.30 -45 40 -45.43 -45.43 -45.40 -45.43 -45.53

OUTPUT OF MTYZ45 PROGRAM

**********UNROTATED TENSORS**********

BAND	PTS	FREQUEN PERIOD	SKEW BOTL	RHO11 PHASE ECOHX ReZ11 ImZ11	RHO12 PHASE RESID1 ReZ12 ImZ12	RHO21 PHASE ECOHY ReZ21 ImZ21	RHO22 PHASE RESID2 ReZ22 ImZ22
1	5	.01026 97.44	.005 .403	.307E+01 -.022 1.000 .40 .00	.870E+01 -.064 2.225 .67 .00	.551E+01 179.885 .998 -.53 .00	.298E+01 -179.791 6.104 -.39 .00
2	6	.01292 77.40	.006 .394	.241E+01 .363 .998 .39 .00	.698E+01 -.108 6.568 .67 .00	.445E+01 -179.852 .996 -.54 .00	.235E+01 179.413 8.754 -.39 .00
3	7	.01627 61.48	.006 .902	.186E+01 .127 1.000 .39 .00	.552E+01 -.116 2.408 .67 .00	.350E+01 -179.741 .999 -.53 .00	.190E+01 179.370 5.347 -.39 .00
4	8	.02048 48.84	.006 .997	.148E+01 .089 1.000 .39 .00	.433E+01 .037 1.201 .67 .00	.275E+01 -179.817 1.000 -.53 .00	.153E+01 179.716 2.406 -.40 .00
5	10	.02578 38.79	.003 .990	.119E+01 .243 1.000 .39 .00	.346E+01 .250 .908 .67 .00	.216E+01 179.985 1.000 -.53 .00	.121E+01 179.927 1.649 -.39 .00
6	12	.03245 30.81	.001 .910	.941E+00 -.037 1.000 .39 .00	.278E+01 -.099 2.580 .67 .00	.173E+01 179.819 1.000 -.53 .00	.946E+00 179.816 1.063 -.39 .00
7	14	.04086 24.48	.004 .989	.741E+00 -.197 1.000 .39 .00	.220E+01 -.032 .428 .67 .00	.138E+01 179.895 1.000 -.53 .00	.756E+00 -179.871 .367 -.39 .00
8	17	.05144 19.44	.002 .796	.611E+00 .190 .999 .40 .00	.175E+01 -.145 3.276 .67 .00	.110E+01 179.975 .999 -.53 .00	.605E+00 -179.685 3.569 -.39 .00
9	22	.06475 15.44	.001 .973	.484E+00 .206 .999 .40 .00	.139E+01 -.033 3.457 .67 .00	.878E+00 179.937 .999 -.53 .00	.485E+00 -179.695 3.811 -.40 .00

**********ROTATED TENSORS**********

BAND	PTS	FREQUEN PERIOD	SKEW BOTL	THETA	RHO11 PHASE RESID1 ReZ11 ImZ11	RHO12 PHASE ECOHX ReZ12 ImZ12	RHO21 PHASE ECOHY ReZ21 ImZ21	RHO22 PHASE RESID2 ReZ22 ImZ22
1	5	.01026 97.44	.005 .403	49.9	.19E-03 -13.63 2.23 .00 .00	.78E+00 -.45 1.00 .20 .00	.19E+02 179.99 1.00 -1.00 .00	.19E-03 -15.42 6.10 .00 .00
2	6	.01292 77.40	.006 .394	49.9	.14E-03 44.04 6.57 .00 .00	.66E+00 .29 1.00 .21 .00	.16E+02 179.95 1.00 -1.00 .00	.37E-03 64.19 8.75 .00 .00
3	7	.01627 61.48	.006 .902	49.9	.69E-04 154.20 2.41 .00 .00	.52E+00 .71 1.00 .21 .00	.12E+02 179.91 1.00 -1.00 .00	.27E-03 117.11 5.35 .00 .00
4	8	.02048 48.84	.006 .997	49.9	.13E-03 167.92 1.20 .00 .00	.39E+00 .53 1.00 .20 .00	.97E+01 -179.98 1.00 -1.00 .00	.16E-03 153.65 2.41 .00 .00
5	10	.02578 38.79	.003 .990	50.0	.58E-04 114.82 .91 .00 .00	.30E+00 .16 1.00 .20 .00	.77E+01 -179.87 1.00 -1.00 .00	.11E-04 -164.61 1.65 .00 .00
6	12	.03245 30.81	.001 .910	50.1	.68E-05 122.08 2.58 .00 .00	.25E+00 -.20 1.00 .20 .00	.61E+01 179.88 1.00 -1.00 .00	.20E-05 168.60 1.06 .00 .00
7	14	.04086 24.48	.004 .989	50.0	.21E-04 -158.20 .43 .00 .00	.20E+00 -.14 1.00 .20 .00	.49E+01 179.95 1.00 -1.00 .00	.29E-04 -143.33 .37 .00 .00
8	17	.05144 19.44	.002 .796	50.0	.13E-04 -53.06 3.28 .00 .00	.15E+00 -.73 1.00 .20 .00	.39E+01 -179.96 1.00 -1.00 .00	.59E-05 28.90 3.57 .00 .00
9	22	.06475 15.44	.001 .973	49.9	.98E-06 -104.16 3.46 .00 .00	.12E+00 -.64 1.00 .20 .00	.31E+01 -179.93 1.00 -1.00 .00	.12E-06 -135.31 3.81 .00 .00

APPENDIX 4:
DIGITAL TO ANALOG CONVERTER FACTOR

The following factors were used to convert data from analog to digital, during data analysis, depending on the mode used during data recording. Number 1 to 7 before the factors represents channel numbers in the recording box. A detailed calculation of these factors is given by Richardson (1985).

FAST MODE FACTOR:

1. 409.600
2. 409.600
3. 4.096
4. 409.600
5. 409.600
6. 4.096
7. 4.096

SLOW MODE FACTOR:

1. 4.096
2. 4.096
3. 4.096
4. 4.096
5. 4.096
6. 409.600
7. 409.600

APPENDIX 5:
1D MODEL RESULTS

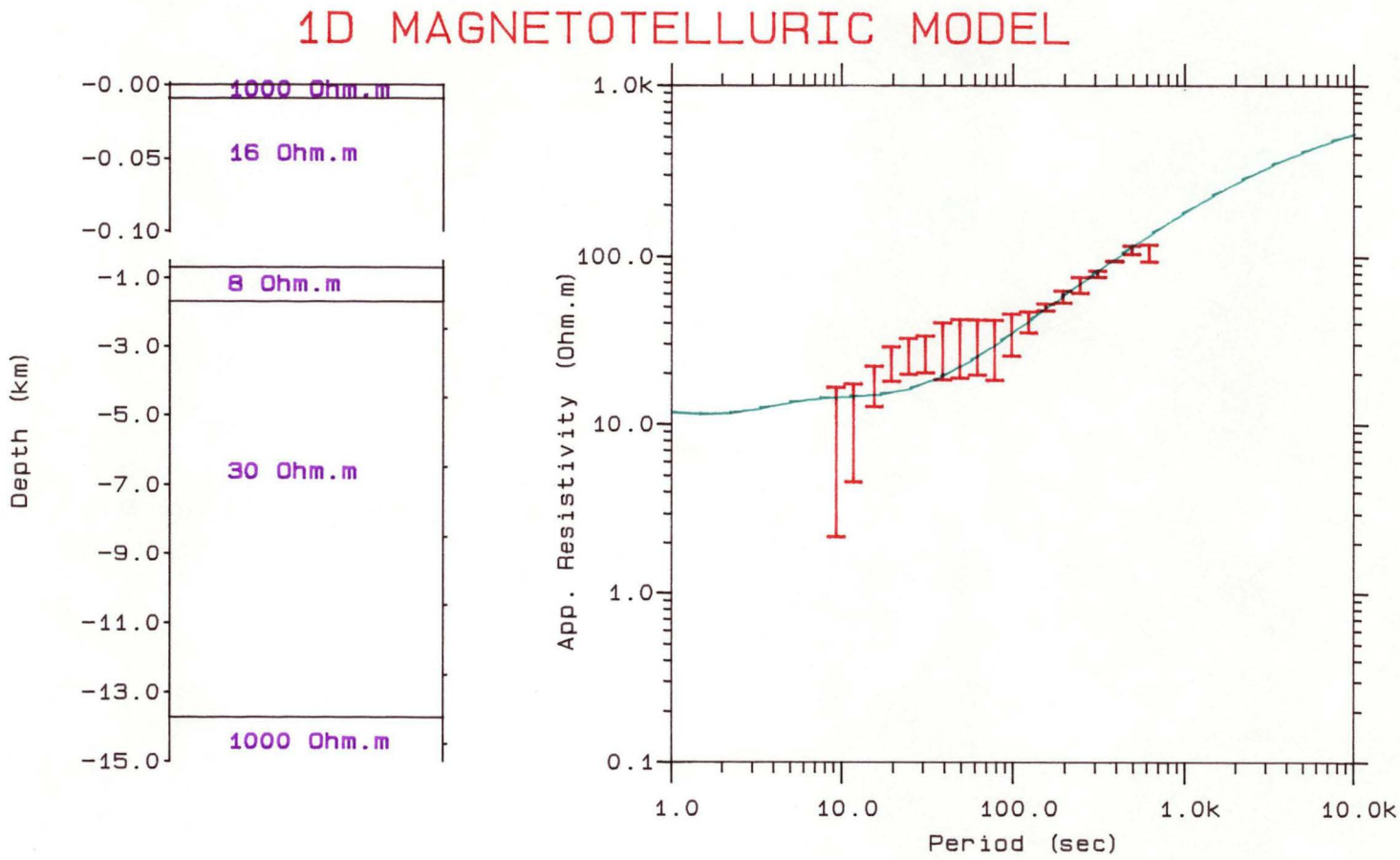

Figure A5.1 1D model results from Bicton (BI)
(red)-observed; (green)-calculated

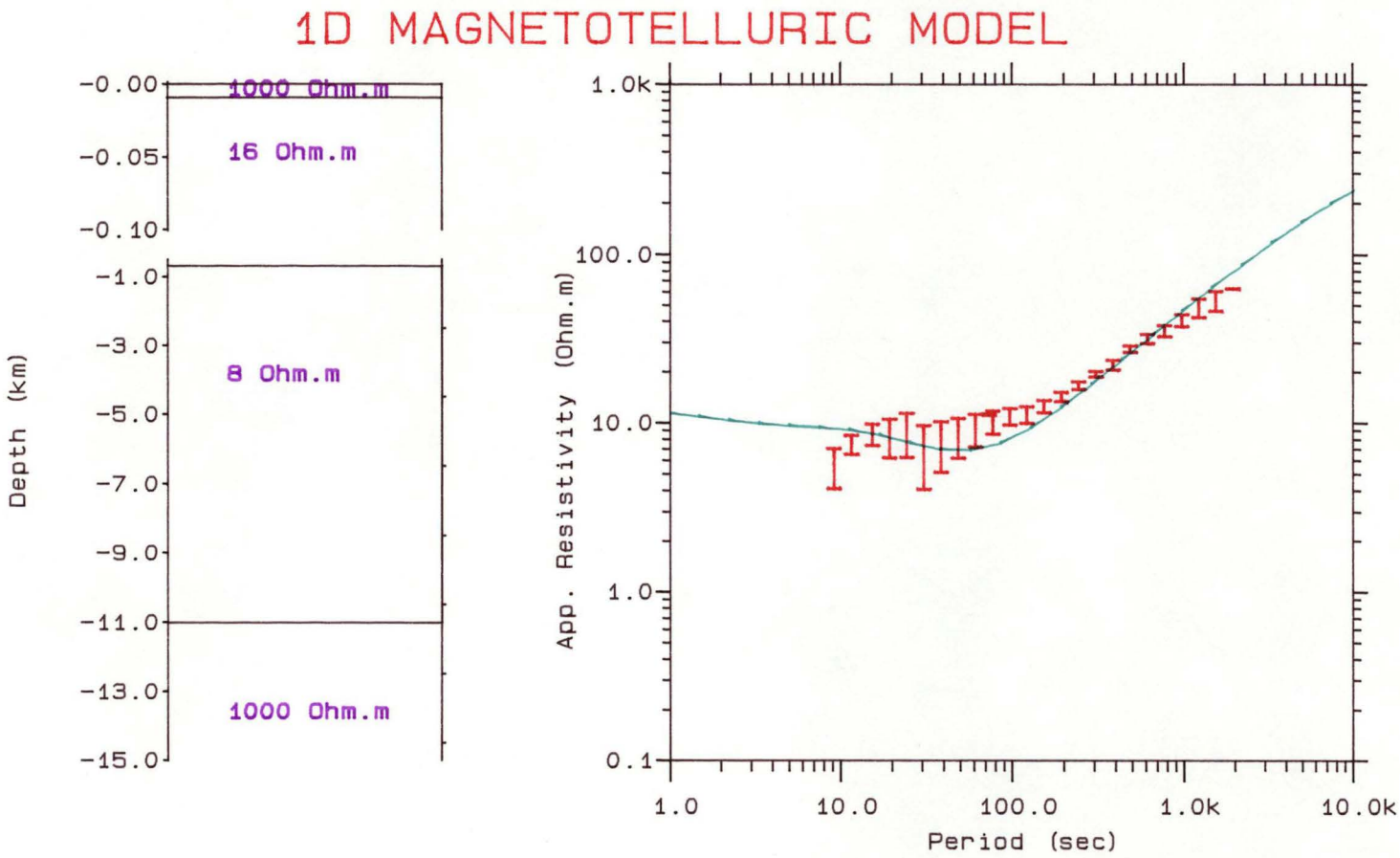

Figure A5.2 1D model results from Kenilworth (KN)
(red)-observed; (green)-calculated

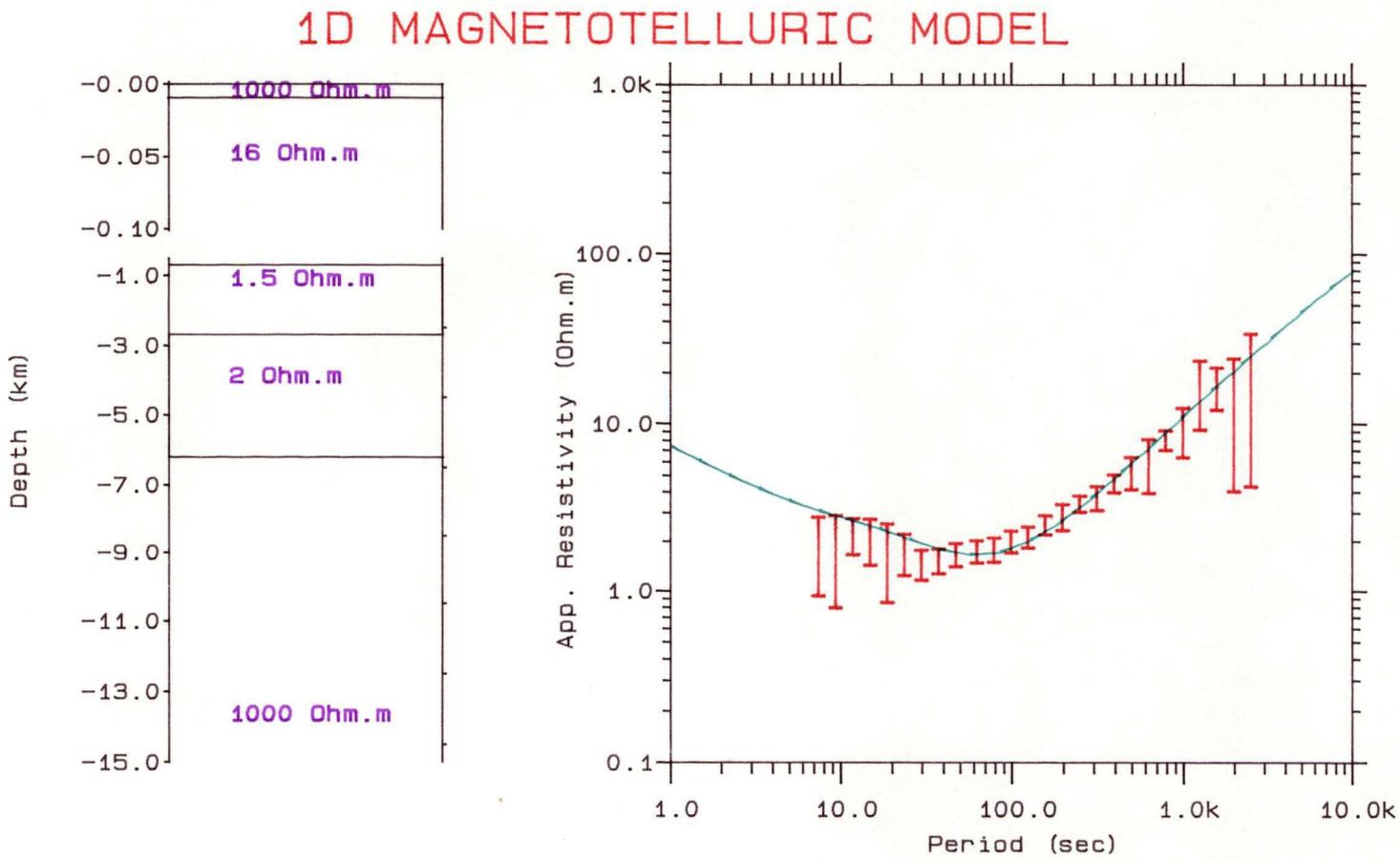

Figure A5.3 1D model results from Conara Junction (CJ)
(red)-observed; (green)-calculated

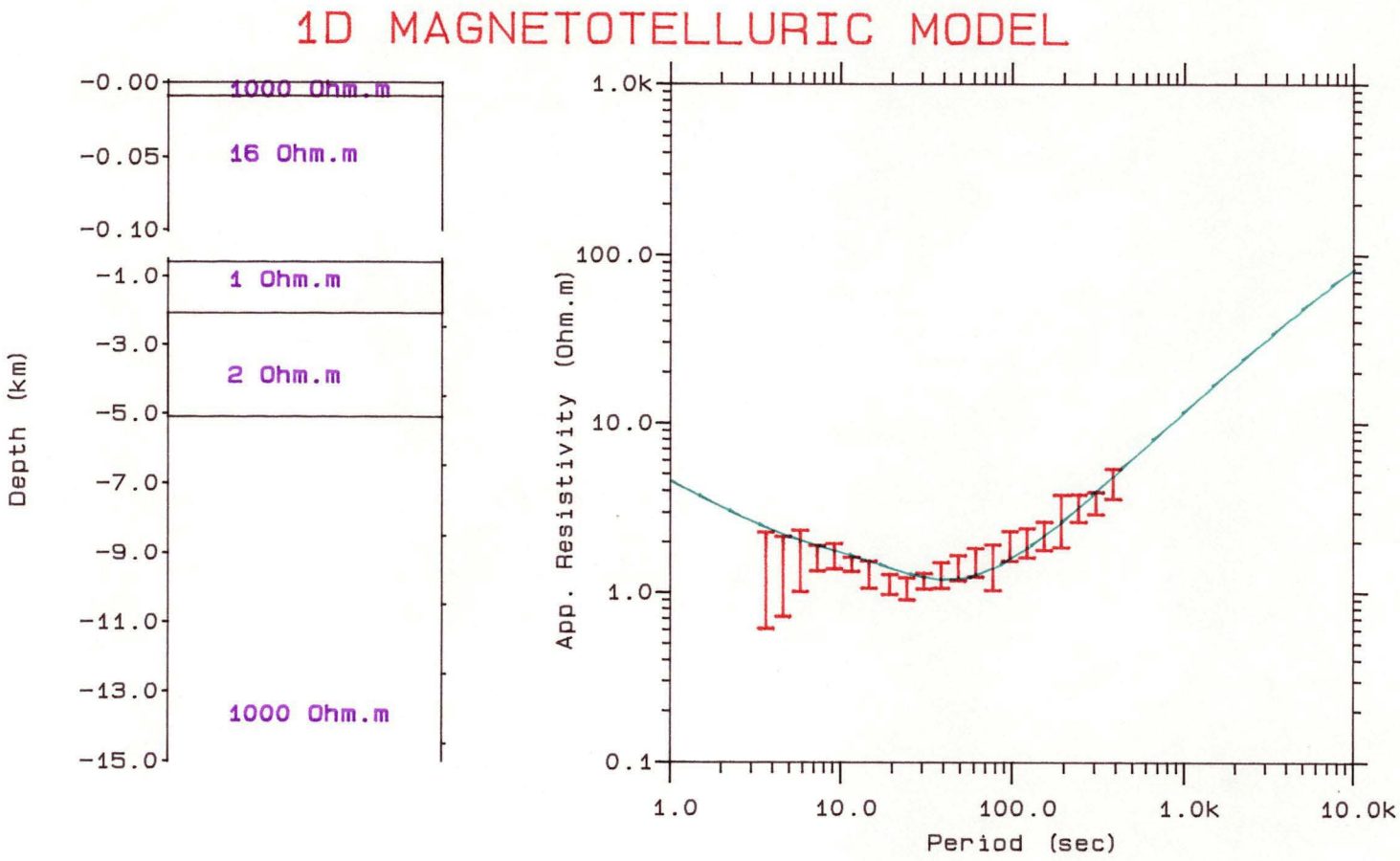

Figure A5.4 1D model results from Milford (MI)
(red)-observed; (green)-calculated

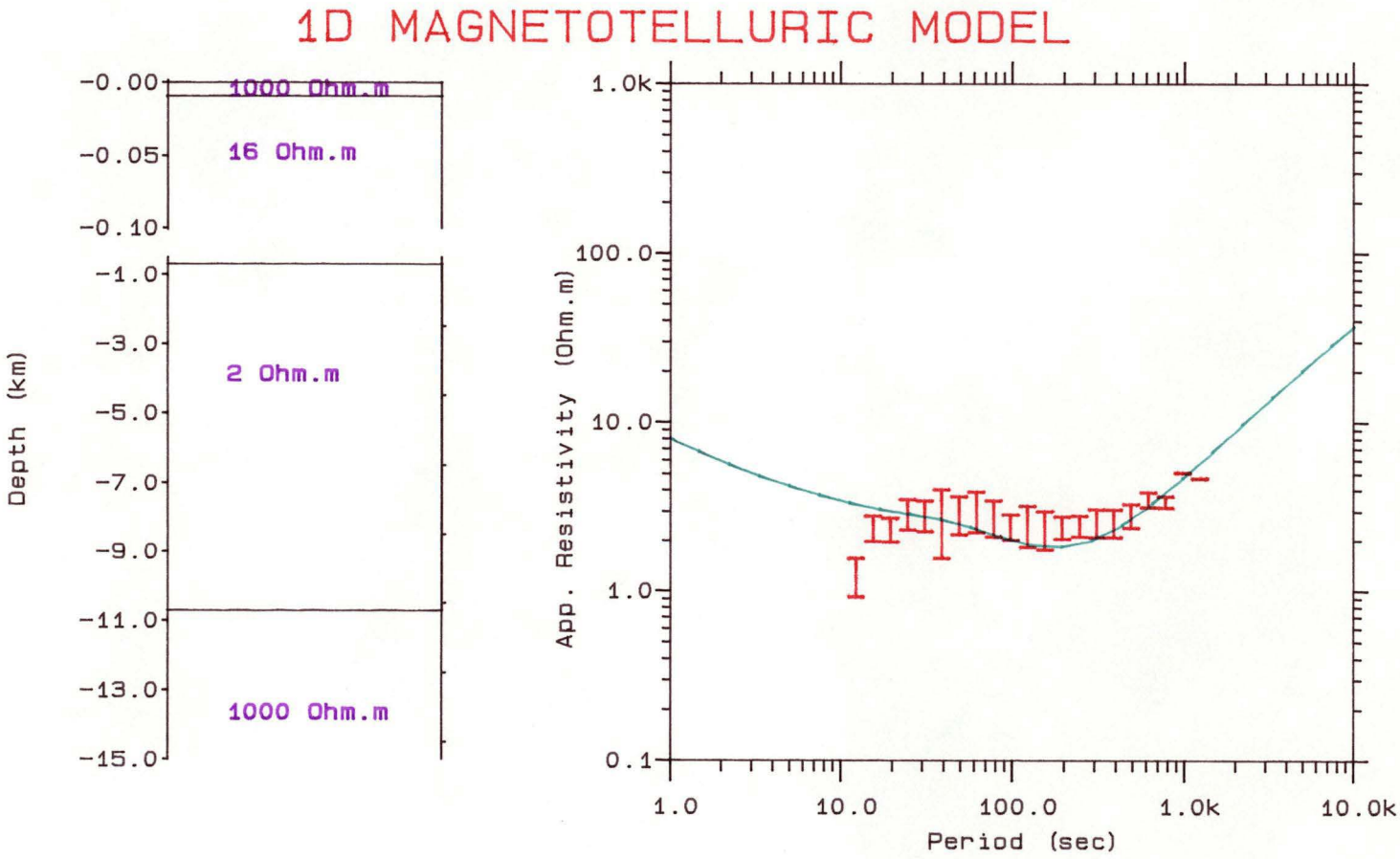

Figure A5.6 1D model results from Buffalo Brook (BB)
(red)-observed; (green)-calculated

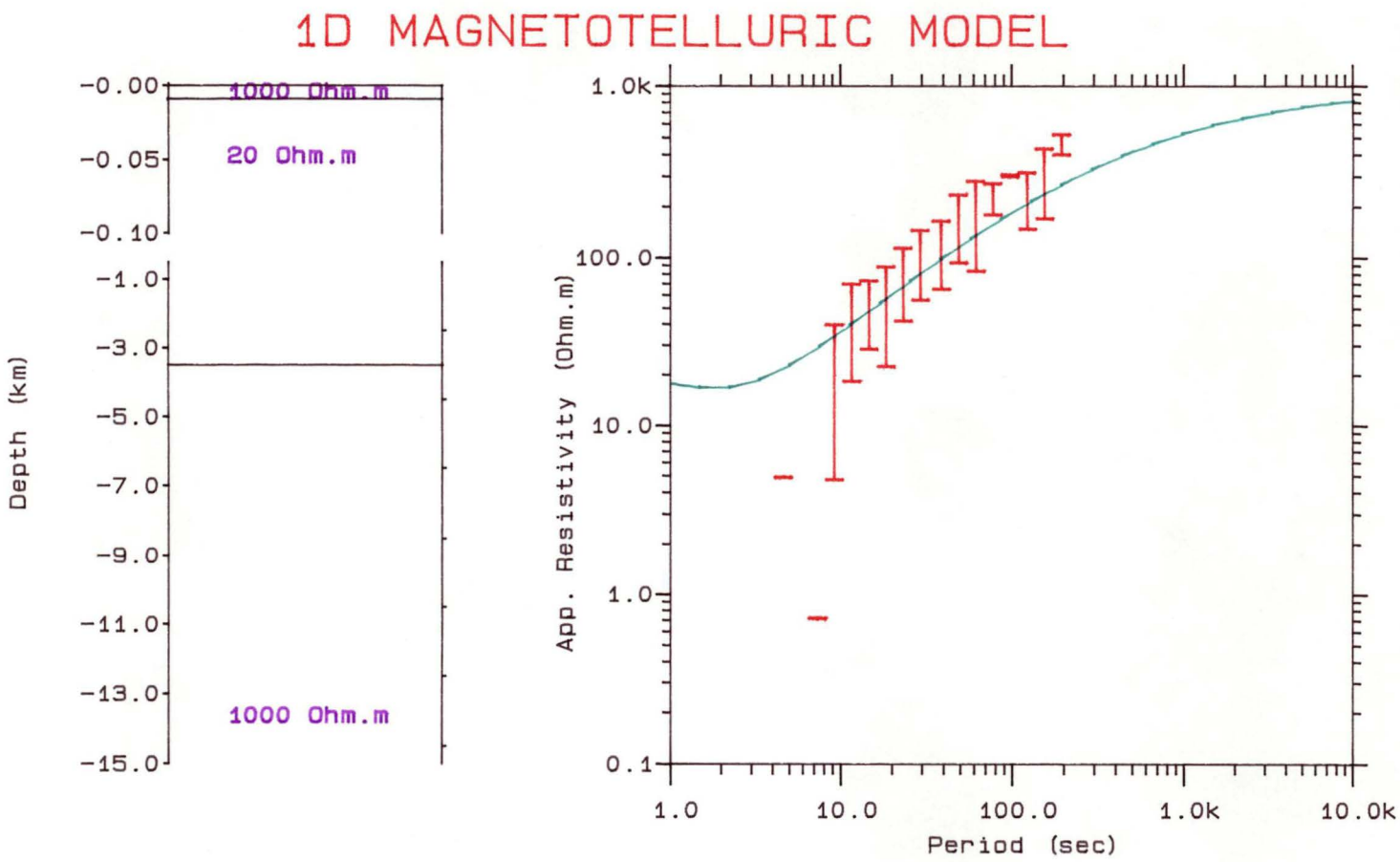

Figure A5.7 1D model results from Fingal (FI)
(red) -observed; (green) -calculated

APPENDIX 6:
APPARENT RESISTIVITY FROM VAUCLUSE